DEVELOPMENT OF A TEST DEVICE TO MEASURE THE TRIBOLOGICAL BEHAVIOUR OF SHOE-SURFACE INTERACTIONS IN TENNIS

By:

Daniel Ura Hernández

A thesis submitted in partial fulfilment of the requirements for the degree of
Doctor of Philosophy

The University of Sheffield
Department of Mechanical Engineering

March 2017

THE UNIVERSITY OF SHEFFIELD

Department of Mechanical Engineering

DEVELOPMENT OF A TEST DEVICE TO MEASURE THE TRIBOLOGICAL BEHAVIOUR OF SHOE-SURFACE INTERACTIONS IN TENNIS

Daniel Ura Hernández

Submitted for the degree of Doctor of Philosophy
March 2017

The aim of this thesis was to better understand the tribological mechanisms that occur during typical player movements, build further on this understanding and develop a robust, portable device to assess the friction characteristics of tennis surfaces that relate to playing performance and safety.

To understand the tennis player's response and adaptability to a tennis court surface, including friction in the shoe-surface interface, a series of friction experiments were carried out on three categories of tennis surface, grass, clay and hardcourt. For grass, parameters such as moisture, level of wear and height were found to have an effect on the shoe-surface friction. For clay, influence of clay particle size and the infill volume was established.

In terms of biomechanical conditions, it was found that the shoe orientation during a slide affects the friction. It was demonstrated that matching applied pressures is a useful approach for shoe friction testing and analysis. Through video analysis, shoe landing and sliding were found to be two possible 'risk' movements.

Material characterisation, combined with friction and temperature measurements have provided empirical knowledge into the manner in which shoes and surfaces behave. During a slide on hardcourts, temperature changes were found to be different along a shoe outsole. The front part experienced higher change of temperature compared to other positions.

Three types of bespoke tread samples were produced and tested, resulting a 'holed sample' the optimal to use. These samples resulted relatively easy to manufacture and generate frictional results compared to tennis shoes.

The final robust portable device resulting from this study, measures the friction characteristics of the shoe-surface interface representative of match-play tennis. The device can be used in two configurations to replicate a shoe landing and a sliding movement. The test shoe consists of a commercial rubber with a bespoke tread design with mechanical properties that match typical values to a tennis shoe.

This device will aid the International Tennis Federation (ITF) and the sports surface research community to gain understanding of player-shoe-surface frictional interactions, and allow courts to be monitored around the world.

Keywords: Tennis, Friction, Shoe, Surface, Player, test methodology.

Acknowledgments

TABLE OF CONTENTS

List of Figures

xi

List of Tables

Nomenclature

a	Acceleration (m/s^2)
A	Area (m^2)
AR	Area ratio
b	Horizontal distance between reaction force and centre of mass (m)
c	Vertical distance between F_{Ram} and centre of mass (m)
COF, μ	Coefficient of Friction
COF_u	Utilised coefficient of friction
$CONACYT$	Consejo Nacional de Ciencia y Tecnología
COT	Coefficient of traction
CPR	Court Pace Rating
$DCOF, \mu_k$	Dynamic coefficient of Friction
E'	Storage modulus
$EPSRC$	Engineering and Physical Sciences Research Council
F_d	Dynamic Friction force
F_f	Friction force
F_{fs}	Force at static peak (N)
F_H, H	Horizontal force (N)
F_N, N	Normal force (N)
F_{Ram}	Ram force (N)
F_s	Static Friction force
F_{shear}	Shear force (N)
F_v, F_z, V	Vertical force (N)
GRF	Ground Reaction Force
h	Tread height (mm)
$LVDT$	Linear Variable Differential Transformer
M	Turning moment (Nm)
NBR	Nitrile Butadiene Rubber
p	p-value

P	Pressure (kPa)
P_{peak}	Peak pressure (kPa)
PTV	Pendulum test value
r	Radius
R^2	Pearson's correlation value
R_a	Roughness arithmetic average (μm)
RMS	Root mean squared error
R_p	Roughness maximum peak square (μm)
R_{pm}	Roughness average-peak-to-mean height (μm)
R_q	Roughness root mean square (μm)
R_v	Roughness maximum valley depth (μm)
R_z	Roughness average peak-to-valley height (μm)
s	Space between treads (mm)
$SCOF\ \mu_s$	Static coefficient of Friction
T	Temperature (°C)
t	Tread height (mm)
$tan\ \delta$	Loss modulus
T_g	Transition glass temperature (°C)
$TSST$	Tennis Shoe Surface Tester
v	Velocity (m/s)
W	Weight (N)
w	width (mm)
x, d	displacement (m)
X_{ram}	Horizontal distance between Ram and centre of mass (m)
y	Vertical distance between F_f and centre of mass (m)
ϕ	Hole diameter (mm)
θ	Angle (°)
θ_s	Sliding angle (°)

Declaration, Communications and Publications

This thesis was conducted in collaboration with the sport-surfaces research group established by the International Tennis Federation (ITF). Therefore, some mechanical data collected within this thesis was collected in collaboration with the colleagues from the Instituto de Biomecanica de Valencia (IBV) and INCOTEC (Barcelona, Spain). Some perception data and biomechanical data was collected by colleagues from the University of Exeter and Sheffield Hallam University respectively. All other material within this thesis is original work conducted and written by the author. The following publications are direct consequence of this work.

Goff, J. E., Boswell, L., Ura, D. & Carré, J. M. (2016a). Critical shoe contact area ratio for sliding on a tennis hard court. Journal of Sports Engineering and Technology. (*Under review*).

Ura, D. & Carré, M. (2016). Development of a Novel Portable Test Device to Measure the Tribological Behaviour of Shoe Interactions with Tennis Courts. Procedia Engineering, 147, 550-555.

Goff, J. E., Ura, D., Boswell, L. & Carré, M. J. (2016b). Parametric Study of Simulated Tennis Shoe Treads. Procedia Engineering, 147, 443-448.

Ura, D., Conway, J., Booth, J. & Carré, M. J. (2015b). Tennis shoe outsole temperature changes during hard court sliding and their effects on friction behaviour. Procedia Engineering. 112: p. 290-295.

Ura, D., Domínguez-Caballero J., Carré, M. J. (2015a). Tennis shoe–court interactions: examining relationships between contact area, pressure and available friction. Footwear Science. 7(1): p. s87-s89.

Ura, D., Carré, M. J., Charlton, H., Capel-Davies, J., Miller, S., Almenara, M. S., Astiz, J. & Mustienes, A. D. A. (2014a). Influence of Clay Properties on Shoe-Kinematics and Friction During Tennis Movements. Procedia Engineering, 72, 889-894.

Ura, D., Carré, M. J., Starbuck, C. & Dixon, S. J. (2014b). Effect of Varying the Volume Infill Sand on Synthetic Clay Surfaces in Terms of the Shoe-surface Friction. Procedia Engineering, 72, 877-882.

Ura, D., Clarke, J. & Carré, M. (2013). Effect of shoe orientation on shoe-surface traction in tennis. Footwear Science, 5, 86-87.

This Thesis is dedicated to you Louie,

the most important project in our lives.

1. Introduction

The following chapters describe a four-year study into the design, development and validation of a portable test device to measure the tribological behaviour of shoe-surface interactions in tennis.

1.1   Study Motivation

Tennis is a popular sport that is played on a wide variety of surfaces (Fernandez et al., 2006). These surfaces influence the style of play and specific movements (ITF, 2016b). Competitive tennis events and tournaments, e.g. Grand Slams and the Olympic Tennis event, are played on a variety of court surfaces including acrylic hardcourt, grass and clay. These events are regulated by the International Tennis Federation (ITF) which is responsible for organising tournaments, in addition to setting and maintaining the standards of the sport, including player and spectator experience. The ITF's Men's Circuit provides the entry level of professional tournaments and offers over 600 tournaments across 77 countries (ITF, 2016e).

This variety of surfaces make the understanding of the mechanisms involved in the constant interactions between the court surface, ball and shoes more challenging. The study of these interactions helps the ITF in developing technological aspects to improve performance and safety of the game (ITF, 2016f). The ball-racket-surface interactions have been widely studied, resulting on rules and methodologies to assess rules and specifications of tennis to help regulate the sport. A good example is the test method used for determining the pace of a court surface, ITF CS 01/02 (ITF Court Pace Rating) which classifies the court pace in terms of ball-surface interaction (ITF, 2016a). However, current knowledge of the player-shoe-surface interaction (Figure 1.1) is limited and needs to be investigated.

Nowadays, it is well known that player movements differ between grass, clay and hardcourt surfaces. Baseline play and rallies on clay surfaces (Roland Garros) are longer compared to hardcourt surfaces (US and Australian Open). Similarly, rallies played on hardcourts are longer compared to grass (Wimbledon) (O'Donoghue and Ingram, 2001). Top-level tennis on these surfaces leads the players to perform a variety of dynamic movements dependent on each surface. Therefore, it has been suggested that the main

characteristic affecting player-surface interaction is the traction/friction coefficient (Girard et al., 2007).

1.1.1 Player-shoe-surface interaction

In previous literature, it has been shown that the traction/friction between the shoe-surface has an important role in the injury risk and performance of the player (Frederick, 1986), (Reinschmidt and Nigg, 2000). Clay has been reported to have a lower occurrence of injury, while acrylic hard court surfaces have been described to have increased injury occurrence (Nigg, 2003). Hence, there is a requirement for scientific understanding of the tribological interactions at the shoe-surface interface in tennis. Once traction/friction mechanisms are understood, surface characteristics and/or footwear can be effectively changed to maximise performance and/or minimise injury risk (Clarke et al., 2012a).
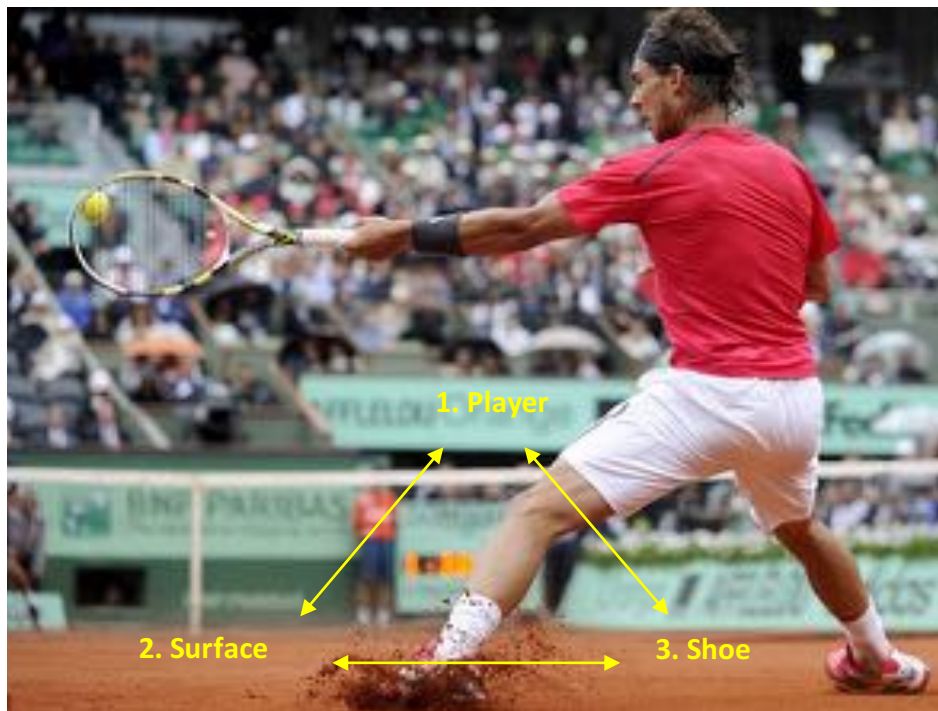
Figure 1.1 Player surface interaction

1.1.2 Mechanical friction tests

Laboratory based mechanical tests have been developed and utilised for the measurement of tennis court friction (Clarke et al., 2013). Due to the flexibility of the equipment, the interaction between commercial shoes and surfaces under match-play loading conditions have been tested successfully. For field testing, the use of portable standard test methodologies specifically for tennis is limited and could be questioned (British

Standards Institution, 2011, English, 1996), as they do not replicate the biomechanical conditions of tennis specific movements or tennis shoes materials (Stiles and Dixon, 2006, Damm et al., 2013c).

Dixon et al. (1999) and Clarke et al. (2013), have suggested that the frictional characteristics measured with mechanical tests should ideally replicate loading of specific human–shoe–surface interactions. However, due to the magnitudes of the vertical forces generated during complex dynamic movements the replication of the actual biomechanical loading using portable equipment is still a challenge.

Therefore, it is relevant to understand the tennis player interactions with different court surfaces, and quantify them through the measurement of different parameters such as friction. There are limited available tools to measure the friction characteristics between a player and tennis court surfaces. The main reason for this is that there are no available portable test devices capable of replicating the player-surface-shoe interaction under realistic match-play conditions.

In order to set the rules and maintain the standards of the sport, the ITF needs a system to quickly assess courts around the world and rate them according to expected performance during player interaction.

1.2   Aim and objectives

Aim

To take existing understanding of the tribological mechanisms that occur during typical player movements (taking into account surface type / parameters, loading conditions, contaminants etc.); build further on this understanding and develop a robust, portable device to assess the friction characteristics of tennis surfaces that relate to playing performance and safety.

Objectives

1. To review existing biomechanical data, specifically to inform the main parameters that affect the shoe-surface interaction in tennis.
2. To compare data collected from existent experimental field test methodologies on different tennis surfaces, in order to identify advantages and disadvantages of each one.

3. To carry out further laboratory/field based testing as necessary to build on understanding of tribological mechanisms and inform the design of portable test methods (e.g. effects of loading, shoe orientation, etc.).

4. To design and develop a bespoke prototype(s) for assessing the friction during shoe-surface interactions in tennis.

5. To evaluate and compare the designed prototype against lab established methodologies in order to validate it.

1.3 Format of the Thesis

The following chapters describe and address the project aim and objectives. Figure 1.2 explains how these chapters link together to deliver the main aim.
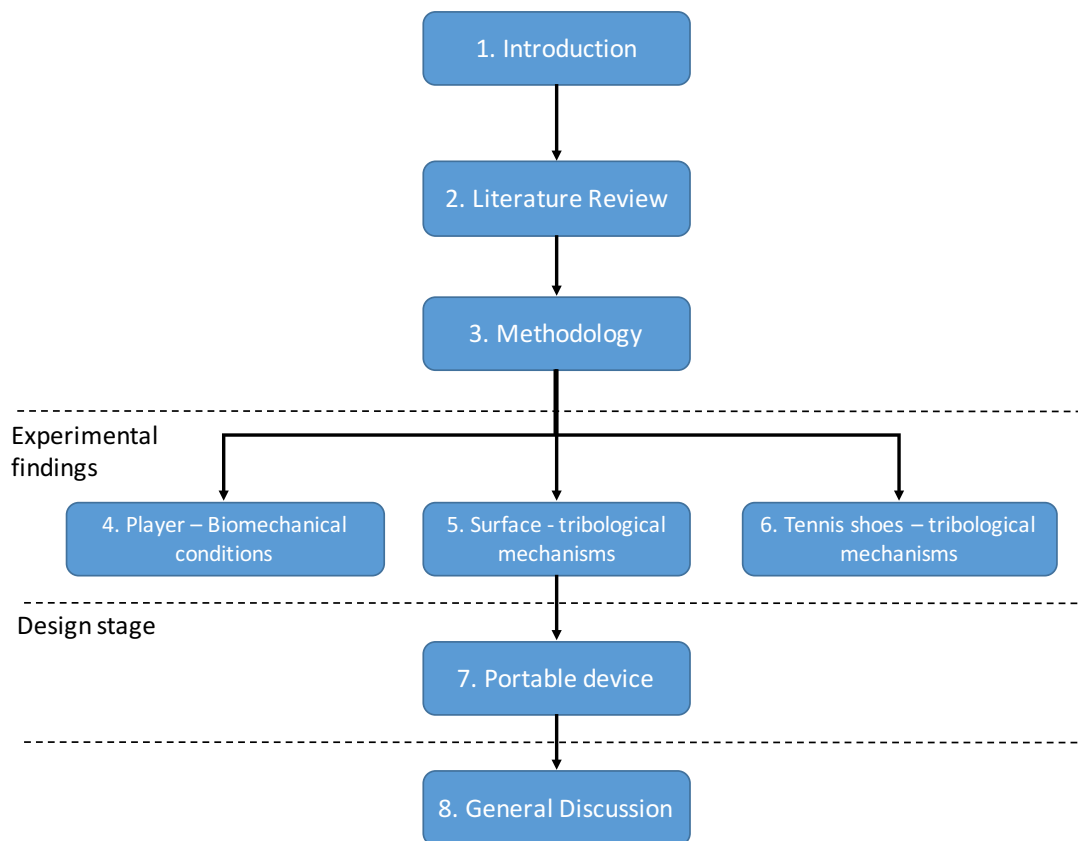
Figure 1.2 Test device stages, described within chapter

2. Literature Review

2.1 Introduction

This chapter provides a review of existing literature related to the aim and objectives identified in section 1.2. It gives an overview of the evolution of shoes and surfaces, and how the players have adapted their game style depending on the type of surface. Additionally, it reviews a variety of biomechanical studies and mechanical test methodologies used to understand and measure the friction of shoes on tennis surfaces.

2.2 Surfaces for tennis

Tennis is unique as being played professionally on a variety of surfaces. According to the ITF rules, tennis courts are 23.78 m (long) and 10.97 m (wide). Any surface levelled, uniform and with friction characteristics within a specified range, is appropriate for tennis (ITF, 2016g). Due to different climates, and maintenance requirements, different surfaces are used around the world. Based on court pace (ball speed) the ITF classifies tennis courts in 10 different categories for comparison (Table 2-1). However, the main surfaces based on their popularity are: grass, clay and acrylic hard courts (Figure 2.1).

Table 2-1 ITF surface classification

Surface code	Type	Description
A	Acrylic/Polyurethane	Textured, pigmented, resin-bound coating
B	Artificial clay	Sand-dressed and/or rubber-dressed surface
C	Artificial grass	Synthetic surface with the appearance of natural grass.
D	Asphalt	Bitumen-bound aggregate.
E	Carpet	Textile or polymeric material.
F	Clay	Unbound mineral aggregate.
G	Concrete	Cement-bound aggregate.
H	Grass	Natural grass grown from seed.
J	Hybrid clay	Clay-dressed systems supported by a carpet matrix.
K	Other	E.g. modular systems (tiles), wood, canvas.

The evolution of surfaces in tennis started with the precursor for modern tennis, the Royal Tennis or Real Tennis played over a hard court surface enclosed by walls. Subsequently, in 1874, the evolution to lawn tennis by Major Walter Clopton Wingfield marked an important chapter in the history of the sport (ITF, 2016d). In the 1940s hard courts were

used in official tournaments for the first time, and in 1956, the Gallia Tennis Club in Cannes, France, became the first place in the world to build the first modern clay court (Hickey, 2006). More recently, in the 1970's carpet surfaces were introduced mainly for indoor tennis; 'Supreme' was the first carpet surface to became widely accepted (ITF, 2016d).

Figure 2.1 Top: grass and clay; bottom: hard court tennis courts.

Nowadays, the ITF organise 600+ tournaments worldwide (ITF, 2016e) and the ATP world tour calendar is composed of 67 tournaments. The ATP tour is played over clay, grass and hard courts, and covers a range of different countries and climates through six continents. The 67 tournaments are distributed by surface: 38 tournaments over hard court (57%), 22 over clay (33%) and 7 over grass (10%) (ATP, 2016).

Tennis surfaces are structures composed with different layers and depending on their structure and characteristics, these surfaces promote different playing styles (ITF, 2016c). The following sections look in detail at the three principal types of surfaces and characteristics for playing style.

2.2.1 Grass

This was the original surface for tennis, and currently the only major tournament using this surface is the Wimbledon Championships (Great Britain). Grass courts are constructed on compacted clay over a firm base of soil or stone.

Grass courts could be a simple lawn, however, nowadays the top-class grass courts are more specialised, with careful specification of the type of grass used. An example is the grass type used for the Wimbledon Championships, *'perennial ryegrass',* cut to a specific height of 8mm shown in Figure 2.2 (AELTC, 2016).

Figure 2.2 AELTC centre court grass

Grass is characterised for a fast ball pace and low bounce compared to clay and hard courts. Due to the composition and geometry of its fibres, in terms of shoe-surface interaction, an amount of traction is needed. The cut height (McNitt et al., 2004), environmental conditions, (e.g. moisture (Wannop and Stefanyshyn, 2012) and temperature (Villwock et al., 2009), and even grass type (Orchard et al., 2005) have been demonstrated to be parameters that affect shoe-surface traction. Grass courts are very sensitive to weather and cannot be played while wet. These courts require high maintenance compared to other surfaces, which make them only playable during specific times of the year.

2.2.2 Clay

The first clay tennis courts were made from clay soil compacted to form the necessary surface to play. However, nowadays the modern clay courts are classified mainly in two kinds: red and grey clay made from different sizes of crushed brick and basalt respectively (Figure 2.3). Approximately two tons of red brick are needed to cover a clay court. A typical clay court is composed by different layers: drainage, crushed gravel, coal residue, crushed white limestone and a red brick dust (1 – 2 cm) crushed at different levels (Roland-Garros, 2016). Clay tennis courts are popular in South America and some parts of Europe where warmers climates could be found. It is the official surface used for the French Open major championships played in Paris.

Clay courts are considered to be one of the slowest surfaces, producing longer rallies compared to the other surfaces. Players on this surface rely on having enough grip to move from side to side of the court, and they need time to adapt to the surface.

Figure 2.3 Example of the different levels of crushed brick on grey and red clay tennis courts.

2.2.3 Hard courts

These surfaces are mainly made from acrylics, asphalts or concrete laid over an aggregate stone base to form a rigid surface (compared to clay or grass). The structural materials, traditionally used in civil engineering, can be porous or non-porous. Base asphalts and concrete surfaces are relatively simple to build. In contrast acrylic hard courts, asphalt or concrete surfaces coated with layers of coloured acrylic paint combining sand particles (ITF, 2016g). Examples of acrylic surfaces are Decoturf and Plexicushion, which are well known for being the official surfaces of the two major tournaments: US Open and Australian Open respectively. One of the main characteristics of these type of courts is the level of controlled surface roughness given by the size and amount of sand used in the paint. Another characteristic is the cushioned layers which helps to slow and cushion the play for greater player comfort. On hard courts, the ball pace is faster than clay but not as fast as grass. These surfaces are ideal for recreational tennis, due to the low maintenance and suitability to different environmental conditions. Figure 2.4 shows an example of a hardcourt tennis surface.
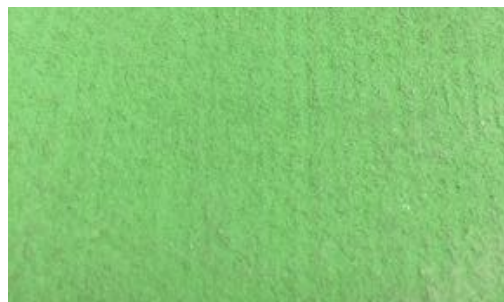
Figure 2.4 Example of hard court surface.

2.3   The Shoe

2.3.1 Early tennis shoes

The early shoes used for tennis were a flat, rubber sole, complemented with a canvas or leather upper section fastened with laces. In the 1830's the Liverpool Rubber Company founded by John Boyd Dunlop, patented a method of attaching the rubber sole to the upper in what was known as the 'plimsoll' (Keyser, 2015). These shoes became popular for grass tennis courts and sole patterns were added and patented to add grip and court adhesion. By 1884 both men and women were competing at Wimbledon wearing rubber soled shoes.

In 1933 one of the first specialised shoe for tennis, the famous *Dunlop Green Flash Lace 1555* was designed for competition, claiming quality, style and grip. The feature 'grip' is why they became the choice for the British tennis player Fred Perry (Figure 2.5), who won Wimbledon wearing them from 1934 to 1936 (Dunlop, 2016).

Figure 2.5 Fred Perry during The Wimbledon Championships.

The year 1969 saw the introduction of the first leather shoe for tennis, the adidas Haillet shoe, designed by adidas founder Horst Dassler and French tennis player Robert Haillet (adidas, 2006). Because of its rubber cup sole with herringbone profile treads (Figure 2.6-left), it was considered one of the highest performance tennis shoes on the market.

Figure 2.6 Left: the 1969 adidas Haillet shoe. Right: the 1971 adidas "Stan Smith" shoe (adidas, 2006).

In 1971, the Haillet tennis shoe evolved and took the name of the famous American tennis player "Stan Smith". The shoe was made from a vulcanised shell-shaped outsole made of compact rubber and a ridged tread. It was claimed that the different heights of the ridges on the tread of this shoe ensured a sure footing on traditional clay courts (Figure 2.6-right).

2.3.2 Contemporary Tennis shoes

Rather than focusing only on protection, nowadays, the design of modern tennis shoes involves knowledge of biomechanics, materials, textiles and sole designs to bring foot support and protection and at the same time enhance player performance. These are designed according to the mechanical properties of surface played, from hard to resilient, with different levels of friction which demand the player to have grip, cushioning and stability during complex dynamic movements on a tennis court.

Although there are specific shoes on the market developed to play tennis on the three main surfaces (e.g. grass, clay and hard courts), shown in Figure 2.7, there are few official regulations from the ITF about the shoes used on each surface. A general rule is that shoes shall not cause damage to the court other than what is expected during the normal course of a match or practice (ITF, 2016f). However, specifically for Wimbledon Championships, the tournament has detailed rules about the shoes that can be used. Characteristics such as number, diameter and height of the outsole pimples are measured for each player's shoes. The permitted maximum height for each pimple is 2 mm from

the bottom of the sole. Additionally, the hardness of any pimple shall be between 55 and 60 based on a shore "A" scale (AELTC, 2016).

The differences between the shoes designed for each surface rely mostly on the different types of treads patterns marketed for each surface. From smooth soles for indoor carpets, zig zag or herringbone pattern for clay or hard courts and pimpled treads for grass courts, the level of design has specialised according to the player-surface needs (Figure 2.7).

In a tennis shoe survey study (Sterzing et al., 2014), 1524 competitive tennis players from China, USA and Germany provided their perspective on tennis footwear by answering questionnaires. Despite the country and skill level, the most important shoe properties were fit, comfort, traction, injury protection and outsole durability. These observations have provided evidence-based guidance to shoe manufacturers about tennis footwear design in terms of the athletes' needs.

Figure 2.7 Different tread patterns for (from left to right): indoor carpet, grass, clay and hardcourts surfaces. Adapted from (ITF, 2016c).

Examples of some revolutionary and innovative designs are how some manufacturers have incorporated circular designs (Figure 2.8-right) in the tread to create pivot points where rotational friction is reduced in order to avoid injuries (Anderie, 1981). Other manufacturers have designed their outsoles by varying the geometry and orientation of the treads. A clear example is the shown in Figure 2.8-left. The sole was designed in function of the player's necessities during a tennis match. It is composed of a 'mix' of two main sections with different geometry, which allow the player to perform in a variety of ways depending on the movement and surface.

Figure 2.8 Examples of: 'Mix' sole (left) (Jara et al., 2010) and concentric circle design(right) treads outsoles.

Another example of how the specialisation of shoes for tennis has increased, is the shoe outsole presented in Figure 2.9. It comprises one main section with a sculpted pattern having recesses and solid areas. In this patent (Jara et al., 2010), the shoe manufacturer claims that the recesses and solid areas are distributed to minimise pressures to provide better adhesion and lower wear adhesion respectively. These characteristics help the player, to use the part of the shoe outsole needed, depending on the playing surface and movement. More grip at running start or sliding on clay to reach a ball faster, are examples of typical movements performed by players on a tennis court.

Figure 2.9 Left: patent of shoe outsole (taken from Jara et al., (2010); right: actual tennis shoe.

Nowadays, thanks to technological developments, tennis pace has increased (Miller, 2006, Haake et al., 2007) and players need to develop stronger and faster movements on court to react to an incoming ball (e.g. tennis serve). This implies hitting more balls and

repositioning to be ready for the next shot. As the design of shoe outsoles has been focused and mastered, it is very common to see tennis specific movements from one surface performed on other surfaces. This in conjunction with how the velocity of the ball in tennis has evolved (Miller, 2006), could explain why some players have started to slide specifically on hard courts (Pavailler and Horvais, 2014).

An example of this technological improvement is the 'Wilson glide' shoe, shown in Figure 2.10. It was developed, based on the concept of 'clay sliding', but this revolutionary design is specifically to allow players to slide on hard courts (Wilson, 2016). The upper part of the shoe is similar to a regular tennis shoe, however the difference relies in the outsole, as it integrates a strategically placed smooth plastic plate which allows players to slide. A characteristic of this shoe is that the player needs to learn the technique to use the glide plate, in order to successfully slide on hard courts. Although some disadvantages of this new shoe could be argued, it has been shown that it could help increase the performance of the players. In their study, (Pavailler and Horvais, 2014), reported that the 'Wilson glide' shoe could help reduce the players' reposition time when sliding on hard courts compared to performing traditional adjustment steps. A total of 18 male good level tennis players were filmed playing a series of ten balls, wearing the new shoes and with a regular shoe. The results showed that the time for reposition was reduced by 42% when wearing the new shoe compared to the regular one. In conclusion, this shoe could help the players to return more balls and have a tangible advantage from its rival.

Figure 2.10 Wilson Glide shoe (taken from Wilson 2016).

2.4   Player movements and biomechanical response

2.4.1 Tennis movements

In the early days of this sport, the tennis game style was characterised by being more 'technique' and 'style'. However, during the 'modern era' of tennis, considered after the introduction of the aluminium oversized racket in 1975, is mainly characterised by having powerful strokes, high spin and more athletic movements (Fernandez et al., 2006).

These movements (e.g. running, stopping, turning, sliding, side jump, etc.), typically consist of an initial split step followed by a combination of side steps to reach an incoming ball (Hughes and Meyer, 2005). Additionally, during an average rally over a three set match, players tend to cover 8 - 12 m changing direction four times, resulting in 300 – 500 high intensity efforts (Fernandez et al., 2006). This new style of tennis made an impact on the physiological demands of a tennis player, like tennis injuries.

In a review of tennis injury studies, (Pluim et al., 2006) found that the most common injuries in tennis are the lower extremities (31 – 67%), followed by upper extremities (20 – 49%) and the trunk (3 – 22%). However, there is little knowledge on how the different court surfaces impact the player-shoe-surface interactions (Miller, 2006). It could be inferred from different studies that player movement patterns are different between grass, clay and hard court tennis surfaces. O'Donoghue and Ingram (2001), identified that rallies played at Roland Garros (clay surface) consisted of more baseline play and were longer compared to Australian and US Opens (acrylic surfaces). In a similar way, the rallies played at US and Australian Opens consisted of more baseline play and were longer compared to rallies played at Wimbledon (grass surface) and shown in Table 2-2.

Table 2-2 Baseline play and rally lengths of the four Grand Slams adapted from (O'Donoghue and Ingram, 2001).

Grand Slam	Surface	% Baseline play (points)	Rally length (s)
Australian Open	Hard	46.6 ± 14.2	6.3 ± 1.8
French Open	Clay	51.9 ± 14.2*	7.7 ± 1.7*
Wimbledon Championships	Grass	19.7 ± 19.4*	4.3 ± 1.6*
US Open	Hard	35.4 ± 19.5	5.8 ± 1.9

*Significantly different ($p < 0.05$)

2.4.2 Ground reaction forces

Several laboratory research experiments have been implemented to characterise the shoe-surface interaction during tennis movements on different surfaces, (Damm et al., 2013a, Damm et al., 2013c, Damm et al., 2011b, Stiles and Dixon, 2006, Damm et al., 2014, Girard et al., 2007, Bloch et al., 1999). These studies focused their work on specific tennis movements (side jump, foot plant forehand) and tennis surfaces like hybrid clay and hard courts. Their work included the analysis of player-surface interactions and indicated the use of biomechanical assessments of court surface properties. They have provided data of ground reaction forces (*GRF*) experienced during tennis manoeuvres on different surfaces.   Table 2-3 shows the vertical reaction force (F_z) and peak pressures (P_{peak}) reported in the different studies. These forces were measured in the lab with the use of a force plate.

Table 2-3 Summarised F_z and P_{peak} with standard deviation data of different tennis movements on two surfaces.

Movement	F_z (N)		P_{peak} (kPa)	
	Hard	Clay	Hard	Clay
Forehand	1469 (583) [1] 1681 (484) [2] 1936 (484) [3]	1351 (379) [1] 1829 (393) [2]	417 (77) [5] 512 (85) [5]	379 (74) [5] 456 (112) [5]
Side Jump	1244 (100) [2]	1317 (82) [2]	428 (71) [5]	351 (73) [5]
Turn	1432 (593) [4]	1319 (500) [4]	-	-
Stop	1833 (646) [4]	1680 (713) [4]	-	-
Baseline play	-	-	381 (69) [6]	404 (137) [6]
Sliding	-	-	-	200 – 220 [7]

[1] (Damm et al., 2013a); [2] (Damm et al., 2013c); [3] (Stiles and Dixon, 2006); [4](Damm et al., 2011a); [5] (Damm et al., 2014); [6] (Girard et al., 2007); [7] (Bloch et al., 1999)

Damm et al., (2013a) studied the traction/friction demands of players on clay and hard courts. They measured three dimensional ground reaction forces, with a force platform, of tennis players performing a side jump movement and a free running forehand. No significant differences in the vertical component of the *GRF* over hybrid clay and a cushioned acrylic hard court were reported. However, there was a greater peak horizontal *GRF* on clay than on hard courts showing a clear effect of the surface on the player's ability and performance. The conclusion was that players adapt to the traction/friction characteristics of the playing surface.

The concept of 'available' and 'utilised' traction/friction has been useful to describe the shoe-surface interaction; if the ratio (available/utilised) is greater than one, then a slip

should not occur (Redfern et al., 2001). Girard et al., 2007 has suggested that the main characteristic affecting the player-surface interaction, is the coefficient of friction (COF).

Nigg (2003) reported clay surfaces to have traction/friction coefficients from 0.5 – 0.7 whereas other types of surfaces have coefficients of 0.8 - 1.2. Clay courts are associated with lower occurrence of injury, meanwhile hard court surfaces with high occurrence of injury. The difference in injury has been attributed to style of game improvements on each surface caused by the differences in ball-surface interaction (Nigg, 2003). However, this could also be due to the tractional/frictional characteristics of the playing surface changing the playing style (Dixon et al., 1999).

Stiles and Dixon (2006) found no differences in traction/friction coefficient for carpet, acrylic and artificial turf, even when they were differences in the mechanical characteristics of these surfaces. Additionally, no differences were observed in lower-limb kinematics or peak vertical or horizontal ground reaction forces (Stiles and Dixon, 2006).

2.4.3 In-shoe pressure

Several studies of in-shoe pressure data, shown in Table 2-3 have reported differences between clay and hard courts during tennis specific movements (Girard et al., 2007) (Damm et al., 2014) (Bloch et al., 1999). In their study, Girard et al. (2007), reported whole foot pressure data of 10 tennis players, to be lower on clay courts compared to hard courts during baseline and serve and volley movements. In another study Damm et al. (2014), reported similar findings during the analysis of a running forehand on artificial clay and acrylic court surfaces.

The difference in pressure between surfaces has been suggested to be due to adaptations of the players to the surface (Damm et al., 2014). An example of these adaptations is how the tennis players have mastered the sliding on clay through the tennis history.

Although there is some biomechanical evidence suggesting that the tennis surface influences the players' kinetics and kinematics, there is little research on the study of the interaction parameters between the rubber outsole and the tennis surfaces.

2.5   Friction and coefficient of friction

Solid friction is defined as the resistance to motion between two solid bodies that move relative to one another (ASM, 1992). This movement may be by sliding or rolling; the terms used are "sliding friction" and "rolling friction" respectively. Sliding friction is defined as the friction that arises when a solid body slides over another. Rolling friction is obtained as one solid body rolls over another. Normally, it is easier to roll surfaces than to slide them (ASM, 1992).

Friction has been studied since old times, and the first studies on friction belong to Leonardo da Vinci. Two hundred years later, Guillaume Amontons introduced two of the sliding friction laws:

"Friction force is directly proportional to the applied load".
"Friction force is independent of the apparent area of contact".

The concept of coefficient of friction (μ) as the ratio of the friction force F_f to normal load N was introduced by Leonardo da Vinci.

$$\mu = F_f / N$$

Equation 2-1

Johann Andreas von Segner was the first who made the distinction between static and dynamic (or kinetic) friction. Leonhard Euler proposed the easiest set-up to understand friction, which consists in a body placed on an inclined plane Figure 2.11.
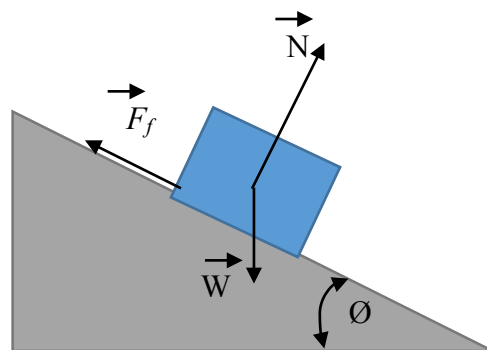
Figure 2.11 Forces acting on a body in sliding motion (friction (F_f), Normal (N) forces and weight (W) on an inclined plane (angle Ø).

The force which maintains the body at rest is the static friction force *(F_s)*. The force needed to initiate sliding is the maximum static friction force. The force required to maintain motion is the dynamic friction force *(F_d)*. The coefficient of friction (μ) could

also be defined as the tangent of the angle of the inclined plane. The body will continue in rest for an angle θ less than a certain value α and it will start moving down if the inclination angle exceeds α. The load balance equations for the body in Figure 2.11 in terms of the coefficient of static friction is given by:

$$\mu_s = {F_s}/{N} = {W\ sin\ \alpha}/{W\ cos\ \alpha} = tan\ \alpha$$

<div align="right">**Equation 2-2**</div>

Charles Coulomb conducted more experimental studies on friction and fulfilled the laws of friction with the third law:

"Dynamic friction is independent of the sliding velocity".
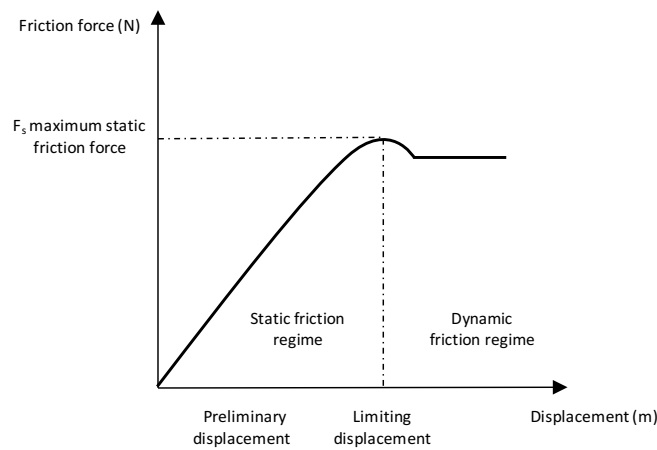
Figure 2.12 Friction force vs displacement (adapted from (Loredana, 2006)

These laws have been proved to be valid for many materials and under specific conditions. However, a condition of this classical model of friction is that it ignores the mechanical properties of the materials. This model is valid for contact between two rigid bodies of certain materials.

2.5.1 Roughness

Friction is caused by forces between the two bodies in contact. Despite the load, these forces are determined by two main factors: the properties of the materials and the area of contact. The real area of contact is usually smaller than the apparent area of the bodies because real surfaces are not smooth, having a level of roughness (ASM, 1992).

Roughness has been defined as irregularities or deviations on the surface resulted from the method of manufacture (Bharat and Bhushan, 2001). It commonly refers to the variations in height of the surface relative to a reference plane as representatively shown in Figure 2.13. The peaks of surface roughness are called asperities. These are determinant in sliding friction, because this process usually involves contact between the asperities on opposing surfaces.

Two of the most used statistical height descriptors advocated by the American National Standards Institute (ANSI) and the International Standardisation Organisation (ISO) are: (1) R_a (arithmetic average) and (2) R_q (standard deviation variance or root mean square). Other values utilised to characterise roughness include the R_p (maximum peak height), R_v (maximum valley depth), R_z (average peak-to-valley height) and R_{pm} (average-peak-to-mean height). However, in most countries the R_a is the official standard measurement (Bharat and Bhushan, 2001).
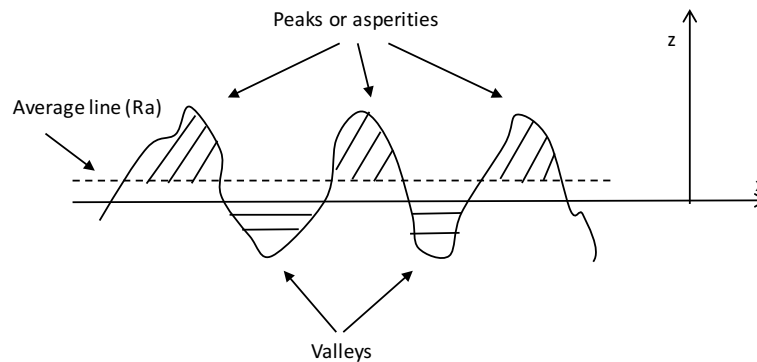
Figure 2.13 Surface roughness description, showing the Ra line.

Different measurement techniques are used to obtain surface height data. They can be classified according to the physical principle involved, being the most common: mechanical stylus, optical methods and electron microscopy methods (Bharat and Bhushan, 2001). The most common one is the mechanical stylus, which is composed by a fine diamond with a fairly sharp tip. In this method, the stylus is moved with a constant velocity across the surface. The vertical movement, due to the height of surface asperities is amplified and recorded.

2.6   Tribology of shoe-surface interaction

In sport, there is a good amount of literature about the shoe-surface interaction and its implications in performance and safety (Nigg et al. 1986, Frederick 1986, Gronqvist et al. 2001). However, there is a lack of research about the frictional mechanisms involved in this interface. For athletes, traction and friction are necessary to stop, accelerate or change of direction more rapidly to have an advantage over their opponents. In Bell et al. (1985), the term 'friction' is applied to smoothed-soled footwear and 'traction' to footwear with studs, which provide extra grip in contact with other surface.

Specifically in tennis, the friction force is dependent on the friction mechanisms developed between the shoe and the playing surface. As an example, tennis shoe outsoles are made from viscoelastic rubber, and hard tennis surfaces are characterised by having a level of roughness. In consequence, when this rubber is compressed against a hard tennis surface with some roughness, there is an interface between their asperities (Figure 2.14).

As mentioned by Chang et al., (2001a). The friction mechanisms of a shoe-floor interaction (rubber-hard substrate), during a slip, are dependent on the material properties, contact area, pressure, velocity, contact time and numerous other variables. However, many of these have never been evaluated in sports, such as tennis, which is characterised by a range of different movements.

Figure 2.14 Left: Shoe-surface interface; right: Representation of the interaction between their asperities.

2.6.1 Rubber friction mechanisms

In clean dry conditions, the friction between rubbers and rough (hard) solid substrate will result in a combination of the following mechanisms: adhesion, hysteresis and tearing (Persson, 2001, Persson, 2006, Palasantzas, 2004).

$$F_f = F_{adhesion} + F_{hysteresis} + Tearing$$

Equation 2-3

Rubber friction differs from the frictional properties of other materials. This difference is due to the low elastic modulus and the high internal friction exhibited (Persson et al., 1999). The friction of the rubber is considered to be a *bulk property* of the rubber, as in many cases it is directly related to the internal friction of the material (Persson, 1998).
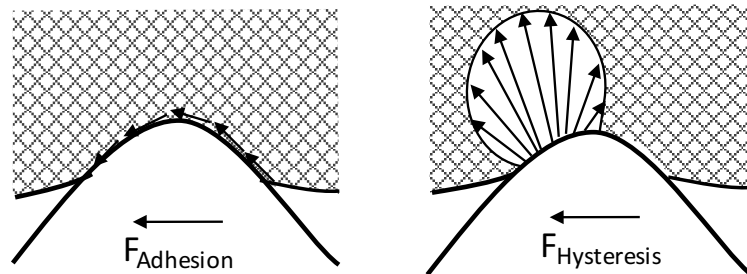
Figure 2.15 Representation of a piece of rubber on a hard surface showing the adhesion and hysteresis generated. Adapted from (Moore and Geyer, 1974)

Adhesion (Figure 2.15-left) is the process of making and breaking of bonds, due to van der Waal's interaction between surfaces and the occurring friction force is the force required for the junctions (where the raised asperities have made contact and welded together) to separate (Persson, 2001, Persson, 2006). Adhesion is stronger when rubber slides over a very smooth surface as the real contact area increases. It has been found that in general cases, when the surface roughness increases, the adhesion component decreases, caused by a reduction in asperity interaction (Persson, 2001, Persson, 2006, Palasantzas, 2004).

The hysteresis friction (Figure 2.15-right), also known as deformation component, is caused by the recovery of the deformed rubber (Loredana, 2006). Internal damping causes energy dissipation during the recovery phase (Persson, 2001, Persson, 2006, Palasantzas, 2004). If the rubber deforms more than its elastic limit, it will not recover causing potential breaking. Increased roughness of a relatively stiff surface, in contact with a rubber surface, can increase the deformation in the rubber, in turn increasing the hysteresis component.

2.6.2 Tribological system

For a mechanical system where surfaces are in relative motion, there are some characteristics that determine the behaviour. A diagram showing a general tribosystem with the parameters affecting the interaction between two material pairs, is shown in Figure 2.16. For any friction or wear test of two materials in an environment and under

the action of a certain type of motion, such as sliding or rolling, the resultant tribometric characteristics associated are grouped by:

- *Structural parameters:* physical, chemical and technological parameters of materials, lubricant and environment.
- *Operational parameters:* loading, kinematic, temperature conditions and functional duration.
- *Interaction parameters:* describing the action of the operational parameters on the structural components defining its contact and lubrication modes.
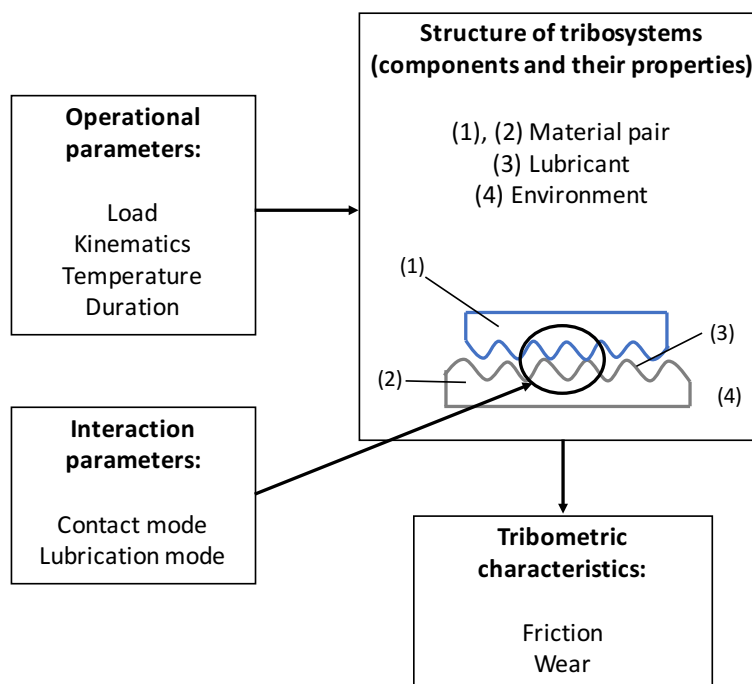
Figure 2.16 Characteristics and parameters of friction and wear tests. Adapted from (ASM, 1992).

The analysis of *structural parameters* focuses in identifying the components involved in the friction or wear scenario. Figure 2.16 illustrates the four tribocomponents involved: triboelement (1), triboelement (2), interfacial element (3) such as lubricant or particles and environmental medium (4) like air or atmosphere.

The *operational parameters* are considered independent variables that can be varied during tribological testing to obtain friction and wear data. Basic operational parameters in tribology are:

- *Type of motion:* kinematics of triboelements in terms of sliding, rolling. Could be continuous, intermittent or oscillating.

- *Load (F_N):* Total force that acts perpendicular to the contact area between triboelements.

- *Velocity (v):* specified with respect to the vector components and the absolute values of the individual motions of the objects in contact.

- *Temperature (T):* of the structural components in a specific location and time. It could be the initial (steady state) and friction-induced temperature rise.

- *Time:* dependence of the operational parameters (e.g. load cycles, heating intervals)

- *Duration:* the test overall performance or operation.

The *interaction parameters* describe the interaction between the operational parameters on the structure components of the tribosystem. They define in particular the contact mode and lubrication mode of the two materials in contact. This contact mode between two solid objects is characterised by material interactions, such as contact stresses and stress distribution at a microscopically level. Therefore, the friction and wear mechanisms are specified in terms such as adhesion, abrasion, fatigue, etc.

For this study, it is important to identify and define the tribological parameters, with the objective to analyse, measure and rank their contribution to the shoe-surface interaction. The challenge remains to identify these parameters on each surface.

2.7   Mechanical shoe-surface interaction

2.7.1   Slip-risk methodologies

Over time, numerous mechanical friction tests have been designed and used to replicate the loading conditions at the shoe-surface interface of a human in different environments and performing certain movements. As an example, pedestrian slips and falls have represented a severe problem in the health and safety field. Nowadays, the annual direct cost of injuries due to slip and falls is reasonably (Chang, 2002). For this reason, several test methodologies have been developed to assess slip resistance in different field and lab environments (Chang et al., 2001a). Additionally, the coefficient of friction has been used as a measure of slipperiness to prevent accidents (Redfern et al., 2001).

Strandberg (1985) indicated that more than 70 machines have been invented to measure slip resistance, however, many of them were not representative of the human motion

(Chang et al., 2001b). The variability in the friction measurement of all such devices, makes the comparison and validity between them difficult, and it is hard to ascertain which friction value is correct. In this literature review, some of these devices are studied, to show the variety of devices designed.

The slipmeters developed through time have different measurement characteristics, but the main operating principle is the application of normal and horizontal forces to a surface through a test foot/shoe. Key characteristics as driving force, test foot, measurement and loading conditions are presented and compared in Table 2-4. The manner in which the loading is applied in the different devices varies considerably. Common approaches of driving forces are gravity, pneumatic pressure and motors.

The Brungraber Mark II and English XL are inclined-strut slipmeters which have a similar operating principle (Chang, 2002). They measure the coefficient of friction obtained from the angle at which a non-slip to a slip occurs. The Brungraber Mark II, utilises a footwear pad which is impacted on a floor surface. In a similar way, the English XL, driven by a pneumatic pressure, indicates the angle at which the test foot sample slips on a surface. Results obtained with these devices were compared directly with studies where the coefficient of friction was obtained using a force plate (Chang et al., 2001a) and indicated good agreement over different surfaces and contaminants.

The British Pendulum Tester (British Standards Institution, 2011) shown in Table 2-4 is used to simulate contact conditions during footwear-surface interactions. When released from a set height, a rectangular spring loaded rubber slider comes into contact with the surface. The height achieved at the end of the swing, after contact (termed the Pendulum Test Value (PTV)) is measured on a scale. PTV values are related to the dynamic coefficient of friction and, in practice, are found to be approximately equal to COF x 100.

The Tortus II, is a controlled motor driven precision instrument which measures the dynamic coefficient of friction (Grönqvist et al., 1999). As the devices moves forward at a constant velocity, the deflection of the test foot is measured by strain gauges. The signal measured is then transformed to a digital value of coefficient of friction.

The Kirchberg Rolling slider, fully described in (Kirchberg et al., 1997) was constructed to determine the level of dynamic friction available in contact with a floor surface. It has three different heights where can be released, and gives three different speeds. The distance travelled by the trolley is related to the dynamic friction.

Although there are many test devices related to measure slipperiness, the large variations of loading conditions and extracted measurement of friction in the test devices presented here make difficult to compare them directly. Various studies have been completed comparing the results of the different test devices (Grönqvist et al., 1999, Ricotti et al., 2008, Grönqvist et al., 2003), however there is limited evidence demonstrating which device replicates and predicts the friction during the shoe-surface interface.

Table 2-4 Summary of portable testing devices

	Test device	Driving force	Test foot	Loading conditions	Measure	Reference
	English XL	Pneumatic Pressure (dynamic impact)	Circle with a diameter of 31.75m, Contact area of 792 mm²	Pneumatic press of 136N. The normal force should not be applied for more than 1 s	Angle at which a non-slip is changed to a slip. COF is the angle at which occurs.	(Chang, 2002)
	Brungraber Mark II	Gravity - sample is dropped 3.175 - 6.35 mm above the surface	A test footwear sample, dimension of 76.2 x 76.2 mm. Max area of 5806 mm²	4.5kg mass impacts the floor surface at an inclined angle with the vertical. The angle is increased until a slip occurs	Tangent of angle is COF. Taking an average of angle than non-slip occurs and min angle that slip occurs	(Chang, 2002)
	Tortus 2 "Sled Test"	Motor driven. Constant velocity of friction foot mounted on a spring	4S rubber foot with 9.5 mm diameter. Max contact area of 71mm²	200g (mass of shoe assembly) 1.96N	Deflection is measured by strain gauges. Signal converted to an average DCOF	(Grönqvist et al., 1999) and (Ricotti et al., 2006)
	The British Pendulum Tester	Gravity-dynamic pendulum impact	4S Rubber with dimension 76 x 25.4 mm. Max	Pendulum mass is 1.50±kg	Energy loss, as the rubber foot slides over the surface is converted to a dynamic COF	(Ricotti et al., 2006)
	Kirchberg Rolling Slider t	Gravity - sled is released at a set ramp height /	Single rubber slider	Mass of sled applies vertical force	DCOF determined from the distance travelled after initial contact with surface	(Kirchberg et al., 1997),(Hallas and Shaw, 2006)

2.7.2 Sport shoe friction/ traction test methodologies

In sports, during dynamic movements such as running, turning and deceleration, it is important to consider the friction developed at the shoe-surface contact, as this is critical to the performance and injury risk of an athlete (Frederick, 1986). The level of friction provided could lead to injuries, therefore, a range of friction for a shoe-surface combination is suggested (Milburn and Barry, 1998). As mentioned in previous literature, poor friction may result in a slip or a fall, which could cause an injury. In contrast, excessive friction could fix the shoe to the surface, and cause injury to the lower extremities (Nigg, 2003). In terms of performance, the friction will have an effect on the effectiveness and control of an athlete's accelerating or decelerating motion. Sports shoe-surface interaction research is of interest to athletes and equipment / surface manufacturers for these reasons. Governing bodies such as the International Tennis Federation (ITF) and The Fédération Internationale de Football Association (FIFA) also examine these issues in order to protect the nature of the game in question.

The majority of the existing shoe friction/traction devices, shown in Table 2-5, attempt to simulate a specific biomechanical movement, and this is typically done by applying loads to a test shoe and measuring frictional resistance to either rotational or translational sliding (Severn et al., 2011, Grund and Senner, 2010, Rosa et al., 2007, Vachon, 2004).

Vachon (2004) used a test apparatus to measure rotational traction. As opposed to taking peak moment force with a torque wrench, he used a load cell to sample the rotational force. This gave an improved understanding of the shoe-surface interaction. In addition, Vachon (2004) measured the translational resistance using a boot fastened to a plate and pulled along a horizontal surface. The boot was loaded with a 15.9 kg mass and the maximum pulling force was recorded visually with a spring scale.

The adidas Traction tester (Adidas 2007) displayed in Table 2-5, utilises a linear actuator driven by servo-motors, capable of applying translational and rotational movements to a shoe oriented to the surface. The vertical loading of the device is constant and provided by masses on top of the device. A testing normal force of 700 N is usually applied, as it is representative of a body mass of a football player. The device was developed to evaluate football shoes in two movements: push-off to full sprint and an internal turn.

Kirk et al., (2008) developed a force-controlled test device, which measures an increasing horizontal force until movement occurs. A hydraulic ram provides a constant vertical load

applied to a stud plate. A pneumatic ram provides an increasing force in the horizontal direction. Load cells in the horizontal and vertical direction and a LDVT provide the necessary data to measure the frictional force resistance to movement.

Grund and Senner (2010) analysed player kinematics from TV footage of real anterior cruciate ligament (ACL) injuries. This information was evaluated and a prototype traction rig was developed which replicates the full range of motion during a real injury situation. This rig consists of a pneumatic control that applies a force to push an artificial leg into the surface, and, at the same time, a rotational force is applied along the longitudinal axis of the leg. The internal loads are measured by a six component load cell.

Rosa et al., (2007) developed a test rig, shown in Table 2-5 capable of reproducing lateral displacements of athletes in their natural movements. It consists of pushing a football boot at constant velocity, 0.4 m/s, and record the horizontal force under a constant vertical force of 150 N.

Although some of this test methodologies have proved to be able to apply higher forces, close to the ones generated by the athletes, they don't represent loads completely. Another disadvantage of some of this equipment is the fact of been very heavy and difficult to move. Transporting this equipment around the world to different venues represents a challenge and high associated costs.

FIFA has used some of these devices to test and classify their football playing surfaces. FIFA has two traction test methods for use in the FIFA Quality Concept for football turf (FIFA, 2016). In order for a surface to be used in official FIFA competitions, it must pass strict limits in each of the tests which classify the player-surface and ball-surface interactions. The first test, showed in Table 2-5 is termed Rotational Resistance. Full details of the procedure and equipment are given in (FIFA 2016). A normal force of 451 N is applied to a circular studded test foot. A handle is turned in order to overcome the initial rotational resistance of the test foot in the surface. A peak torque value during rotation is recorded for evaluation. The second test is the Linear Friction test, which uses a studded plate in combination with a pendulum test (adapted from the rig described in section 2.6.1). This device is shown in Table 2-5. After reaching a maximum swing height, the Stud Sliding Value (SSD) is measured from the scale of the pendulum which is related to the energy lost during the interaction with the surface. The Stud Deceleration

Value (SDV) is also recorded which is the difference between the maximum deceleration and the deceleration just before the impact.

Although these devices provide a simple portable measure of rotational and linear friction /traction, they could be criticised for not replicating loading conditions of athletes and the rate of torque/loading applied may change from operator to another. However, the advantage of these tests rely on their portability and minimal set-up time.

Table 2-5 Summary of portable test methodologies in sport

	Test device	Driving force	Test foot	Loading conditions	Measure	Reference
	Rotational	Hand	Regular football boot	Weight = 529 N	Peak force	(Vachon, 2004)
	Translational	Speed electric motor (max speed = 0.3 m/s)	Regular football boot	Weight = 529 N	Average ratio of horizontal and vertical force	(Vachon, 2004)
	adidas traction tester	Pneumatic Pressure	Regular football boot	Normal Load 700 N	Load Cell. Measures COT for translational and rotational movements	Adidas (2007)
	Translational	Pneumatic	Studded plate	Hydraulic ram (250 – 450 N)	Traction force over 50 mm	(Kirk, 2008)
	Rotational	Pneumatic	Studded shoes	1000 – 2450N axial loading	Peak torque and effective torque	(Grund and Senner, 2010)
	Translational	Pneumatic	Regular football boot	Horizontal displ. At const vel = 0.4 m/s Vertical Force = 150 N,	Traction, Horizontal Force	(Rosa et al., 2007)
	Rotational	Manual	Metal disc 150±2 mm diam. With 6 studs	Total mass wrench, shall be 46kg	Torque measurement, Rotational resistance	FIFA (2016)
	TRL Pendulum	Gravity-dynamic pendulum impact (dynamic friction mechanism)	Spring loaded 4S Rubber with dimension 76 x 25.4 mm. Studded foot.	Pendulum mass is 1.50±kg	Energy loss, as the rubber foot slides over the surface is converted to a dynamic COF	Ricotti et al (2008) ITF CS02/01 FIFA (2016)

2.7.3 Friction test methodologies in tennis

In tennis, standardised dynamic friction tests have been conducted with a portable pendulum device (British Standards Institution, 2011) in different studies (Damm et al., 2013c, Starbuck et al., 2015). However, it has been reported that the average normal loading of the pendulum is 12 N (Lewis et al., 2011), which is significantly lower compared to typical tennis player movements during match play (Dixon et al., 1999, Damm et al., 2014, Stiles and Dixon, 2006). Another mechanical friction test used for tennis is the English XL which was developed to prevent and evaluate slip and fall incidences (Chang et al., 2001a). The English XL applies an average contact load of 37 N, which is very low compared to the loading measured during tennis movements.

More recently a laboratory based mechanical test device was developed at The University of Sheffield capable of measuring the development of friction during shoe-surface contact under loading conditions relevant to the game of tennis (Clarke et al., 2013). During the development of the test device, data from previous studies was analysed with a view to replicating the loads seen during a tennis specific movement (Damm et al., 2013c). The aim of the device was to measure the friction developed at the shoe-surface interaction, when a shear force was gradually increased, using a test shoe under a range of constant normal loads.

The existing test device at The University of Sheffield, shown in Figure 2.17 and fully explained in (Clarke et al., 2013), uses a traditional friction test loading approach, whereby a test shoe is loaded vertically onto a surface and this load is kept constant whilst an increasing horizontal load is applied until a slide occurs and limiting friction effects can be measured. In reality, the vertical and horizontal loads acting on a shoe during a specific movement are not independent of each other and not applied in this way (Starbuck et al., 2015).
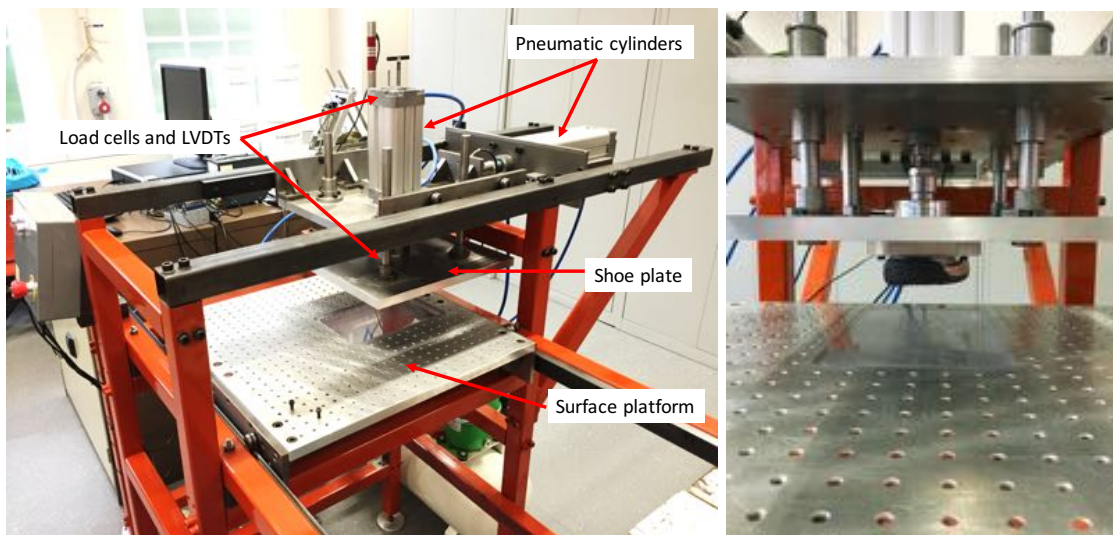
Figure 2.17 Bespoke testing device with a side view of the shoe plate.

Although this device provides peak and average friction measures, the device does not replicate the loading profiles during tennis movements. For example, during dynamic movements as sliding on clay courts, Damm et al., (2014) observed an unloading of the normal force and suggested to be a grip mechanism during this movement. This kind of behaviour is difficult to replicate with current mechanical tests, however, a fixed traction device can provide indicators of the frictional mechanisms during a shoe-surface interaction.

In previous studies, some of these fundamental friction mechanisms have been examined such as the effect of normal force and roughness on friction (Clarke et al., 2012a, Clarke et al., 2012b, Clarke et al., 2013).

In a first study (Clarke et al., 2012a), the effect of a shoe normal force applied to a surface on friction was studied. Via a laboratory based test rig, it was found that friction is dependent on the normal force. As the normal force applied to a surface increases, the COF (referred to in this study as "coefficient of traction", COT) decreases and a power relationship can be fitted as shown in Figure 2.18.
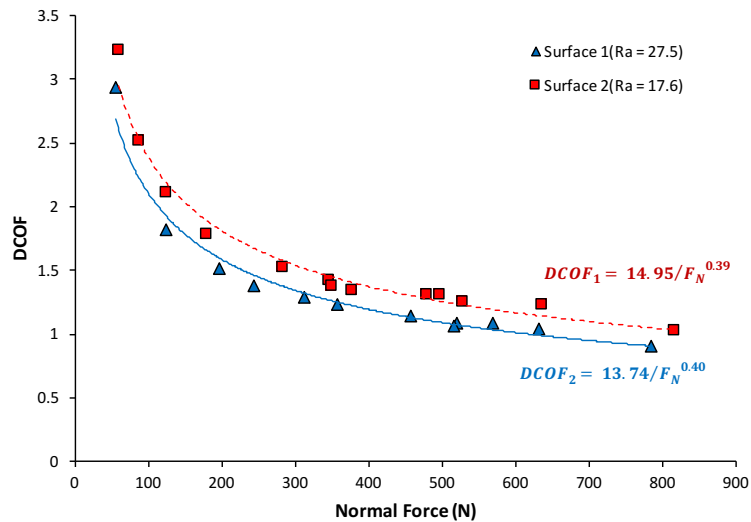
Figure 2.18 Normal force against mean dynamic coefficient of friction (adapted from Clarke et al., (2012a)).

The second study (Clarke et al., 2012b) showed that relationships between roughness and dynamic friction were found to be also dependent on the normal load, as shown in Figure 2.19. Under high normal loads (e.g. 1000 N), the friction decreases with roughness, reaches a minimum and then increases as the roughness increases. The opposite behaviour is observed under low normal loads (e.g. 500 N), and the trend is for friction force to increase with roughness, reach a maximum and then decrease as the roughness increases.
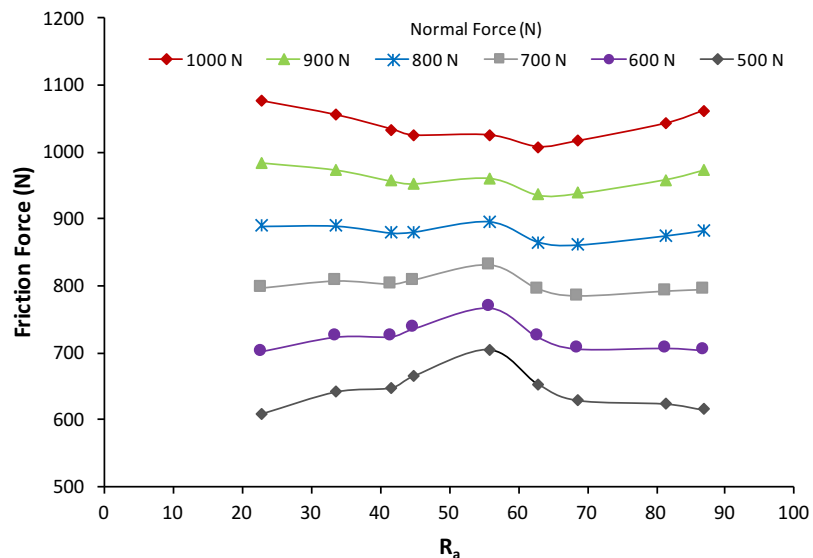
Figure 2.19 Plot of the mean average surface roughness (R_a), against traction force (adapted from Clarke et al., (2012b)).

Clarke et al. (2013) studied the influence of surface characteristics on the shoe-surface friction mechanisms. Linear regression analysis was used to understand the relationship between normal force and initial stiffness, peak traction force and average dynamic traction force. A forefoot segment of a commercial tennis shoe was tested on three surfaces: one acrylic hard court surface and two artificial clay court surfaces.

For the clay surfaces it was found that the infill particle size used significantly influenced the traction developed. The initial stiffness and peak traction depend on the normal force applied. It was stated that surfaces with large sand particles developed lower traction caused by a decrease in shear force between the particles acting individually.

Clarke et al. (2013) describe the traction/friction developed as a measure of the shoe-surface system's opposition to a horizontal force. This traction provided, in combination with tennis specific movements, represents an important part in the performance of the player and injury risk (Frederick 1986, Reinschmidt and Nigg 2000). As stated by Milburn and Barry (1998) there is necessary an optimal range of the tractional properties of the shoe-surface interaction in order to assess this interface.

In tennis, as pointed in different studies (Damm et al. 2011, Stiles and Dixon 2006), the actual loading of the shoe-surface system caused by a tennis player is higher than that replicated by most available mechanical devices.

2.8   Summary and implications for this study

Tennis is a sport which requires players to perform a variety of manoeuvres over several court surface type throughout a year season. These surfaces differ in mechanical properties such as friction, and have been suggested to influence injury risk and performance (Dixon et al., 1999, Stiles and Dixon, 2006, Nigg, 2003). Differences in play-style have been reported between the surfaces, with longer rallies on clay than other surfaces (O'Donoghue and Ingram, 2001). The evolution of tennis shoes, specifically materials and geometry, has proved to be helping and increasing player performance on tennis courts, allowing players to adapt movements common in clay, like sliding, to hard court surfaces (Wilson, 2016).

Shoe-surface friction has been reported to influence player's movements (Damm et al., 2013a) like sliding on clay surfaces or changing direction in hard courts (Pavailler and Horvais, 2014).

Previous studies in tennis friction have shown that both biomechanical studies with subjects and mechanical tests are relevant (Damm et al., 2014, Starbuck et al., 2015). A review of literature has highlighted that a suitable portable test methodology, for measuring the shoe-surface friction (replicating player condition during match play) does not exist. However, test methods used in other sports provide repeatable measurements, eliminating the existing variability when human testing is performed, as well as injury risk to human participants. These devices contain limitations in their weight, portability and capacity of replication of loading conditions.

Ideally, test methodologies should replicate the load-profiles in combination with appropriate and representative shoe and surface materials, as suggested by (Dixon et al., 1999). However, the majority focus their measurements either in the biomechanical aspect or testing the mechanical properties of the materials. The challenge remains to design simple, light and portable test methodologies capable of replicating the load-profiles provided by biomechanical studies. Additionally, there is no approach to design mechanical devices based on the tribological parameters involved in the shoe-surface interaction.

In sports, friction is a property necessary which enables the athlete to perform the movements necessary in sport. The area of Tribology brings an opportunity to study and explain how the traction and friction are generated on sports surfaces. Without these, it would be impossible to play any sport despite the shoe or the surface, as they provide the necessary to make movements without slipping or falling. However, the current understanding of the tribological mechanisms of the shoe-surface interaction remains somewhat limited.

There are few approaches to study and understand the tribological mechanisms involved in friction during a shoe-surface interface in tennis, like the effect of surface roughness and vertical load on friction (Clarke et al., 2012b, Clarke et al., 2012a). Clarke et al., (2013) developed a bespoke rig to help the study of some shoe-surface tribological mechanisms, such as clay particle size, however it is necessary to study others like material properties, contact area, pressure and velocity.

Prior to continuing to develop a portable test methodology, more research needs to be done, to gain a better understanding of the tribological mechanisms involved in the shoe-surface interaction during specific tennis movements.

3. Methodology

3.1 Introduction

Chapter 2 describes previous research studies that have been conducted to investigate the interaction of shoes and surfaces in sport. Based on the arguments presented in the literature review about the importance to replicate biomechanical and material conditions during shoe-surface interactions, further research is needed on some of the tribological parameters of grass, clay and hard courts. Additionally, some biomechanics data will be relevant for the rig design in terms of loading/pressures applied by tennis players. For these reasons, and in order to complete the aim and objectives of this research, this chapter outlines the design process and methodology (lab and field experimental work) of the research based on studying the interaction of the three physical bodies, which are:

1. The player
2. The surface
3. The shoe

The aim of the research project is to develop a robust portable device to assess the friction characteristics of tennis surfaces, as was expanded in the introduction of Chapter 1, therefore, a detailed understanding of the interaction of these three parameters was necessary.

Figure 3.1 presents the overall approach and the grand plan set for this project. This diagram deconstructs the research into the components investigated, and indicates the flow of information (arrows) and the data agreement (double line) between the data sets. As this project is part of a wider study, the "*" indicates the main contributions of this project to the overall approach.

The player section (Chapter 4), which studies the replication of biomechanical conditions, was produced through observational analysis, collection of previous data, and a combination of lab and field based experiments.

Additionally, the shoe and surface sections (Chapter 5 and 6) looked and studied the tribological mechanisms during specific tennis movements, and their effect on the friction generated. These were mainly studied in the laboratory.

Finally, a section linking the three sections together in behalf or the design of the test device, was developed and discussed in Chapter 7.

Arrows indicate flow of information; double lines indicate that agreement between data sets is required.
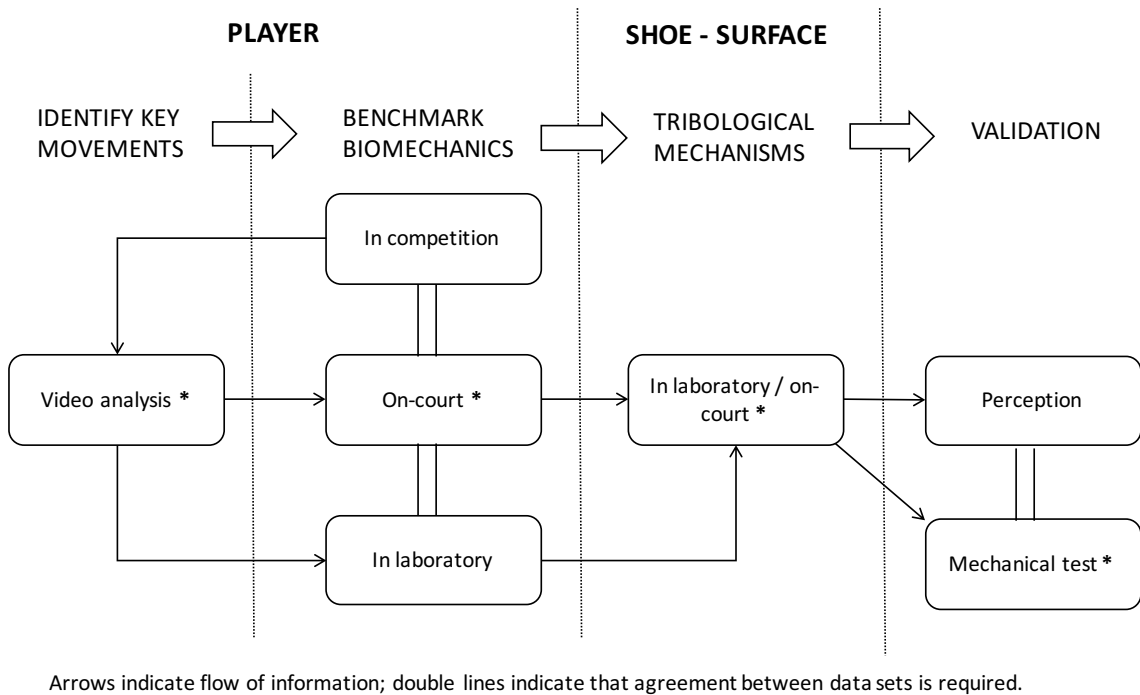
Figure 3.1 Diagram showing the overall approach and grand plan for the project.

3.2   Player

Establishing the characteristics of player-court interaction in tennis is a key challenge. As mentioned by (Redfern et al., 2001), biomechanics can be used, apart from determining required friction during specific movements, to assess frictional instruments, as a calibration or validation.

As discussed previously in the literature review, the replication of player loading using portable light devices in the field, has been a challenge. (Grund et al., 2007) pointed out that many mechanical tests which investigate the shoe-surface interaction do not test shoes under play loading conditions. In the same order of ideas, as suggested by (Dixon et al., 1999), test methodologies should replicate the load-profiles in combination with appropriate and representative shoe and surface materials. Subsequently, studying and investigating the effect of some biomechanical conditions on friction, could be useful to find a feasible solution to this challenge.

Therefore, Chapter 4 shows a series of tests designed to fulfil the following objectives. These were set based on gaps found in the literature and the findings of preliminary results

in order to determine which biomechanical conditions are relevant and need to be considered for the design of the final frictional test device (Chapter 7). These are:

- To determine key movements on a tennis court.
- Benchmark biomechanics of tennis players.

3.2.1 Key movements

With the objective to identify the key movements of elite tennis players under 'match' conditions, an observational analysis of tennis matches was implemented. A video database of several player movements on the three main surfaces (clay, grass and hardcourts) was created in order to perform a wider analysis of common and 'risk' movements. In Chapter 4 the 'risk' movements, are identified and further discussed.

3.2.2 Biomechanics

After identifying the key movements, the next step consisted on benchmarking the biomechanics of these movements. As shown in Figure 3.1, these could be obtained from three different sources: *in competition, on-court* and i*n-laboratory*. Due to the difficulties to obtain data from actual competition, the data used for experiments in Chapter 4 was obtained from previous field and laboratory studies. The data includes forces and pressures applied by tennis players performing common tennis movements. The experiments presented on Chapter 4 focus on the development of a novel loading methodology and, as mentioned previously, due to the difficulty to replicate high vertical loads with a portable equipment, a pilot study was developed to understand the relationships between in-sole pressure, contact area and available friction in order to develop a novel test methodology, as presented in Chapter 7.

3.3   Shoe and surface

To investigate the behaviour of a shoe-surface interaction in tennis, a combination of field and laboratory methods were used. Mainly, the lab work focused on studying the tribological mechanisms of shoes and surfaces involved in this interaction, with the objective to determine their contribution to the friction generated during specific tennis movements. In complement, the fieldwork focused on two main areas: player perception and mechanical testing of tennis courts with the aim to do a first attempt to validate

frictional results from mechanical testing with the perception of the player of a particular tennis court.

3.3.1 Tribological Mechanisms

A first step to find a solution to a certain problem in tribology is to establish a tribological system (ASM, 1992). As previously discussed in the literature review, the tribological system defined to describe the interaction between a tennis shoe and a surface in tennis, is schematically presented in Figure 3.2 and consists of the next structural components: shoe outsole (1), court surface (2), lubrication (3) and environment (4).
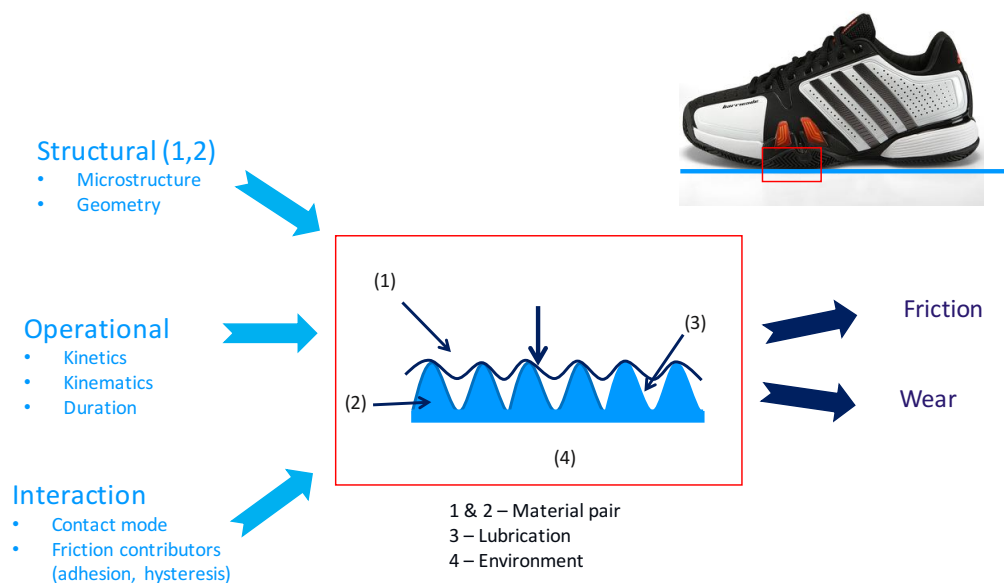
Figure 3.2 Tribological system of a shoe-surface contact.

When these components interact under specific conditions, the system is influenced by some characteristics associated with a group of parameters:

- *Structural parameters,* which characterise the structural components involved in the interaction, such as shoes and surfaces. Shoe outsoles are made from rubber, and tennis surfaces vary, being the main ones, clay, grass and hard courts. In terms of shoes, section 3.5.3 show the results of the material characterisation of different commercial rubbers through a DMTA technique. Additionally, section 3.5.2 show the results obtained for the hardness of shoes and test rubbers. For tennis surfaces, it has been identified that some of the components of this tribological system change according to the playing surface. The identified structural components for each shoe-surface interaction are shown in Table 3-1.

Table 3-1 Structural components of shoe-surface tribosystem

Tribosystem	Triboelement (1)	Triboelement (2)	Interfacial element (3)	Environmental medium (4)
Shoe – Clay court	Shoe rubber	Clay court	Sand particles	Air
Shoe – Grass court	Shoe rubber	Grass blades	Humidity	Air
Shoe – Hard Court	Shoe rubber	Acrylic paint, concrete,	--	Air

Based on the structural components identified, characteristics such as roughness (section 3.5.2), clay particle size (section 5.3), the amount of clay (section 5.4), grass humidity and height (section 5.2) were measured and further utilised in the experiments to determine their effect on the friction between a shoe and a specific tennis surface.

- *Operational parameters,* which characterise the functional conditions of the system. These focus on the player's kinetics, kinematics and their functional duration. In general, for this project these parameters were obtained from previous biomechanical studies. However, to complement these, in Chapter 4 & 6, a combination of lab and field experiments, were implemented in order to measure the effect of different parameters on the friction, such as the shoe velocity (section 4.3) and the temperature of the shoe outsole (section 6.4) both during a sliding movement. Furthermore, a new loading methodology was developed, in order to compare it to a previous one and determine the best option for the final mechanical design (section 4.4).

- *Interaction parameters,* which characterise the action of the operational parameters on the structural components. In chapter 5, the surface parameters, such as the influence of grass height and lubrication (section 5.2), clay particle size (section 5.3), clay sand infill volume (section 5.4), in the friction generated between rubber and tennis surfaces were studied. Additionally, Chapter 6 shows the results of a series of pilot studies which aim to study the effect on shoe-surface friction of interaction parameters such as shoe orientation (section 6.2), contact area and pressure (section 6.3).

3.4   Validation

3.4.1 Player perception

Although the aim of this project is the mechanical design of a portable test device, it was important to make a first comparison of frictional results with player perception. In section 5.4, the friction measurements obtained with a lab based rig were compared to the perception of tennis players with the objective to corroborate and validate the friction measurements.

3.4.2 Mechanical test

Chapter 7 integrates all the findings from the previous experiments with the aim to present a design methodology for the mechanical portable device. The adapted utilised design methodology is shown in Figure 3.3 (Wright, 1998, Cross, 1994), and is composed basically of two main phases, the conceptual and embodiment design with some sub stages. After the design sub stage (2.1 in Figure 3.3), an evaluation and testing phase of a pre-prototype is implemented with the aim to assess and validate the final prototype.
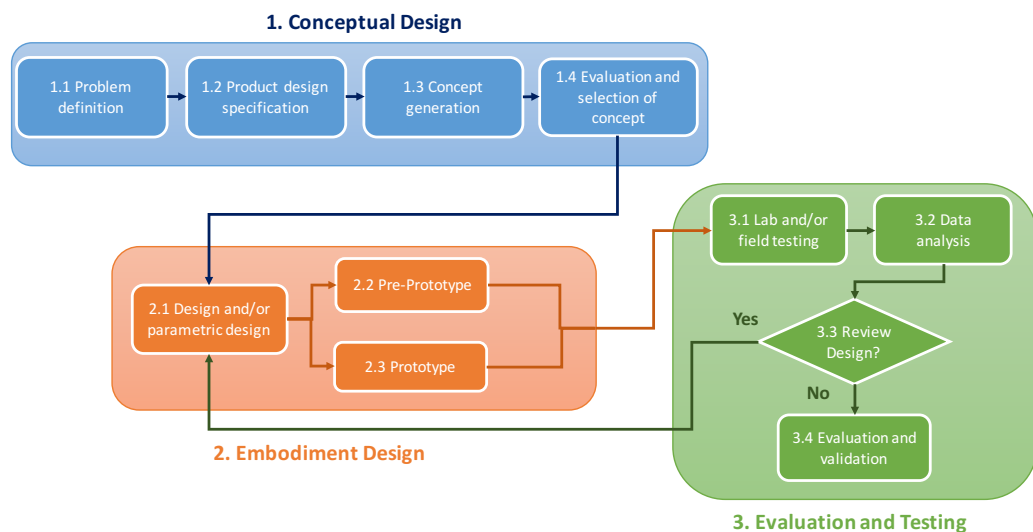
Figure 3.3 Design methodology implemented. Adapted from (Wright, 1998, Cross, 1994)

1. Conceptual design

This phase involves the following stages:

a) **Problem definition:** This is the initial statement of the need and analysis of the problem. It consists on concentrating on what a new design has to achieve rather than how to achieve it. The overall function is identified.

b) ***Product design specification:*** This corresponds to determining the goals, constraints and criteria of the design.

c) ***Concept generation:*** This stage takes the statement of the problem and generates broad solutions to it in the form of schemes. Brainstorming, functional decomposition are typical tools used.

d) ***Evaluation and selection of concept:*** The different concepts are evaluated in this stage in order to select the best one.

2. Embodiment design

In this phase the selected design is worked up in greater detail, throughout the following stages:

a) ***Design:*** The selection of the physical elements with parts modelling and design validation are performed in this stage. Usually the end product is a set of technical drawings, when it can be decided if a pre-prototype, prototype or both need to be produced.

b) ***Pre-prototype***: A mock-up device is fabricated for preliminary testing.

c) ***Prototype***: This normally represents the final version of the design process.

3. Evaluation and testing

This phase comprises four main activities:

a) ***Lab and field testing:*** A series of experiments and pilot studies are implemented to collect the necessary data to verify the reliability and repeatability of the device.

b) ***Data analysis***: A review of data collected with the test device. After analysis, if the data is correct, the evaluation continues, otherwise, the device could be redesigned with the correspondent mechanical modifications. This loop can be repeated as many times as needed.

c) ***Review of design***: A last design stage to develop a robust design from the prototype. Review and definition of final dimensions and tolerances is made, in addition to selection of manufacture processes.

d) ***Evaluation and validation:*** Comparison is made to results from other test devices, and to player perception.

3.5   Test equipment

This section provides details of the equipment and methods used throughout the mechanical testing in the laboratory and tennis courts.

3.5.1 Mechanical test devices

a) Crab Mark III

The Crab Mark III shown in Figure 3.4, was developed by Robert Haines for the ITF (Miller and Capel-Davies, 2006). It is a hand powered device which measures the friction force between a surface and a deformable rubber sphere. The Crab III consists of a metal frame mounted on three wheels. A spring loaded rubber sphere is attached to the frame via a cantilever beam. As the device is pushed along the surface (for a distance of approx. 300 mm) the sphere is loaded normally to the surface and friction forces cause the cantilever beam to be deflected horizontally. The peak beam deflection is measured via an electronic transducer connected to a laptop computer and is related to the static coefficient of friction between the surface and the sphere. The vertical load applied is 1.05 kg and the magnitude of the friction load measured by the transducer is 0.52 kg per millimetre of deflection.
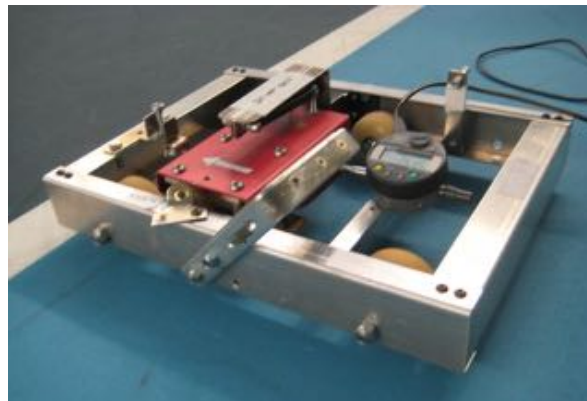
Figure 3.4 The Crab Mark III test device.

b) Sled Test Device

A simple bespoke sled test device, shown in Figure 3.5, was designed the Department of Mechanical Engineering at the University of Sheffield, to simulate contact conditions during footwear-surface interaction in tennis. The device is constituted of a loading plate that supports a set of weights; which is mounted on a test shoe outsole to form a sled. The sled is dragged by hand using a Mecmesin BFG 500 force gauge connected to a laptop

with a Labview acquisition programme. The mass of the device without any weights added is 4.36 kg. The sets of weights added varies through the different experiments in this research.

The testing procedure consists of placing the sled on the test area and dragging it by hand for a distance of 350 mm. The force gauge measures the horizontal force applied during the movement of the sled at a rate of 1000 samples/s. The shoe outsole was brushed before each trial to remove any grass and to maintain the same conditions throughout.

Figure 3.5 The sled test device with a grass outsole attached.

Figure 3.6 shows a typical Horizontal/Vertical force-time curve for a shoe sole dragged across a surface. The procedure to extract the static and dynamic COFs is determined by being able to identify on the H/V graphs two particular regions: (I) a region of increasing initial force during a static regime and (II) a period of dynamic movement over which the force remains relatively constant. The static COF is calculated as the peak force ratio value recorded for each trial during the static regime and occurs when the sled first starts to slide. The dynamic COF is determined as the average value during the dynamic regime when the H/V ratio settles to a consistent value. At the end of the trace, the recorded H/V ratio drops due to the dragging force being reduced to zero.
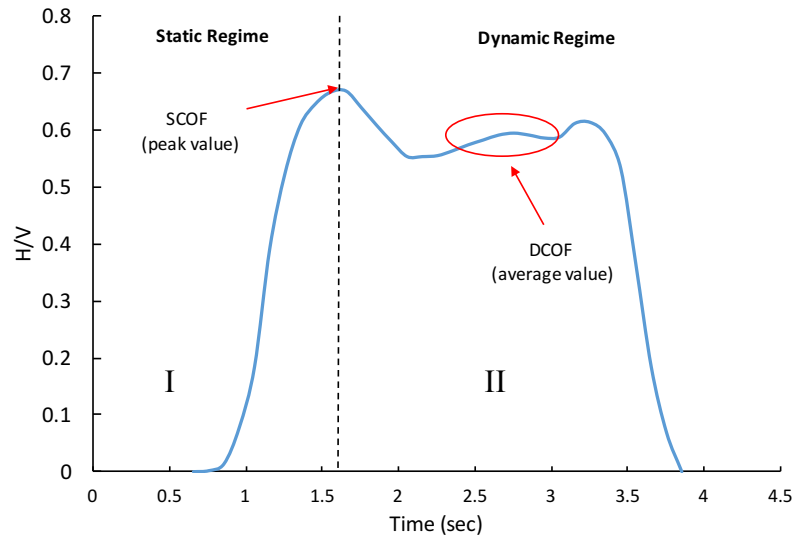
Figure 3.6 Static and dynamic regimes for a typical sled test, showing values of static and dynamic coefficients of friction (SCOF and DCOF).

c) *Pendulum test*

The Pendulum test device, shown in (Figure 3.7), and previously described in the literature review (section 2.7), is a device utilised to measure friction.

Tests were conducted according to the British Standards (British Standards Institution, 2011). The sliders used conformed to the properties for 4S (Standard Simulated Shoe Sole) or Slider 96 rubber specified in (Slip Resistance Group, 2011). The 4S rubber slider was used for court testing, and was prepared conforming to Annex A of (Slip Resistance Group, 2011).

Figure 3.7 The pendulum test device

For each test, the pendulum arm is released, the slider contacts the surface, and the pointer gives a "PTV" (Pendulum test value) to be recorded. The pendulum arm is caught on the return swing before the slider strikes the test surface on its down swing. The procedure is

repeated eight times for each location on a court. The first three readings are ignored, in order to reduce the variability. The mean PTV value is calculated as the mean of the recordings, to the nearest whole number. This PTV value is then converted to a mean coefficient of friction.

d) University of Sheffield lab-test

Figure 3.8 shows a schematic of the laboratory-based traction testing device, developed at The University of Sheffield (*UoSh*) (Clarke et al., 2013) . The mechanical test device was designed to fully replicate the full range of complex dynamic biomechanical loading, focused on the friction/traction developed at the shoe-surface interface. This is achieved when a shear force was gradually increased using a test under a range of normal loads. The objective of this device was to conduct repeatable and reliable friction/traction tests on a range of tennis surfaces. Pneumatic rams were utilised to apply the loads which are measured via electronic transducers.
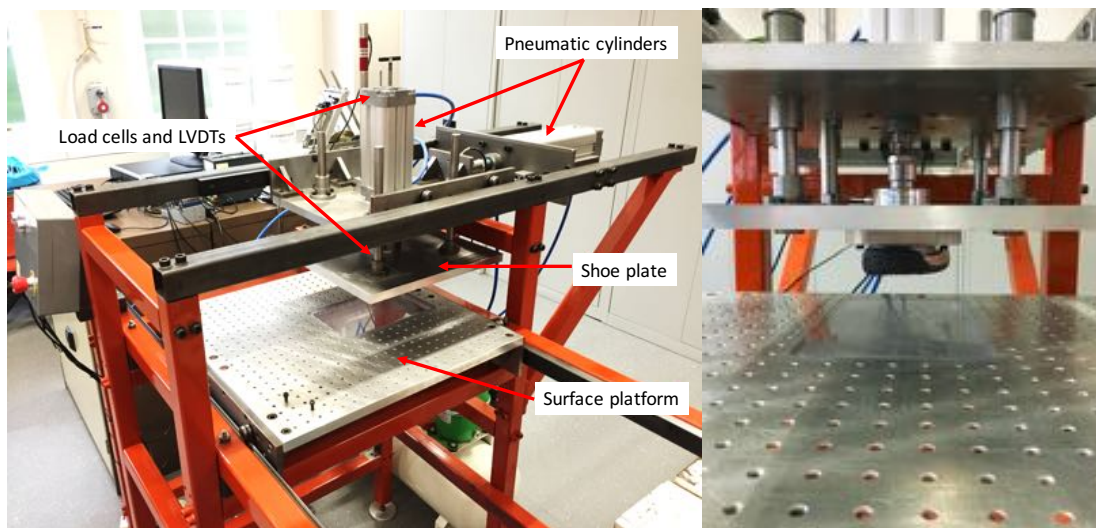
Figure 3.8 Bespoke testing device with a side view of the shoe plate

The testing procedure consists of attaching a section of a shoe sample onto the shoe plate. A surface sample is then secured on the surface platform that is slid into place via a bearing rail system. Subsequently, a pneumatic ram provides a controlled normal force to the shoe plate. A second pneumatic ram provides a controlled driving force in the horizontal direction. The horizontal force is increased until sliding of the shoe is initiated. The shoe plate moves horizontally for a maximum sliding distance of 250 mm. Load cells in the horizontal and vertical direction and two linear variable differential transformers (LVDT) provide the necessary measurements to determine the friction

behaviour. A data acquisition device (National Instruments model number NI9174) samples the load cells and LVDT signals at 2000Hz, which are then transformed into values of force and displacement. The data signals are displayed and saved in real time using LabView (version 13 National Instruments).

Prior to testing, the shoe outsole utilised was prepared in accordance to footwear standards (British Standards Institution, 2012). The outsole was cleaned with an ethanol solution and allowed to dry at ambient temperature. Then, the outsole was lightly sanded by applying P400 silicon carbide paper by hand under minimal pressure. Additionally, any debris was remove using a clean, soft, dry brush.

As fully explained in Clarke et al. (2013), three main parameters are extracted from horizontal displacement and traction/friction force against time plots (shown in Figure 3.9):

1. The initial 'stiffness'.
2. The peak traction/friction force at the transition between the static and dynamic regimes. If this force is achieved, then the shoe-surface system fails and the traction/friction becomes dynamic.
3. The mean dynamic traction/friction measured between 0.05 and 0.20 m sliding distance.
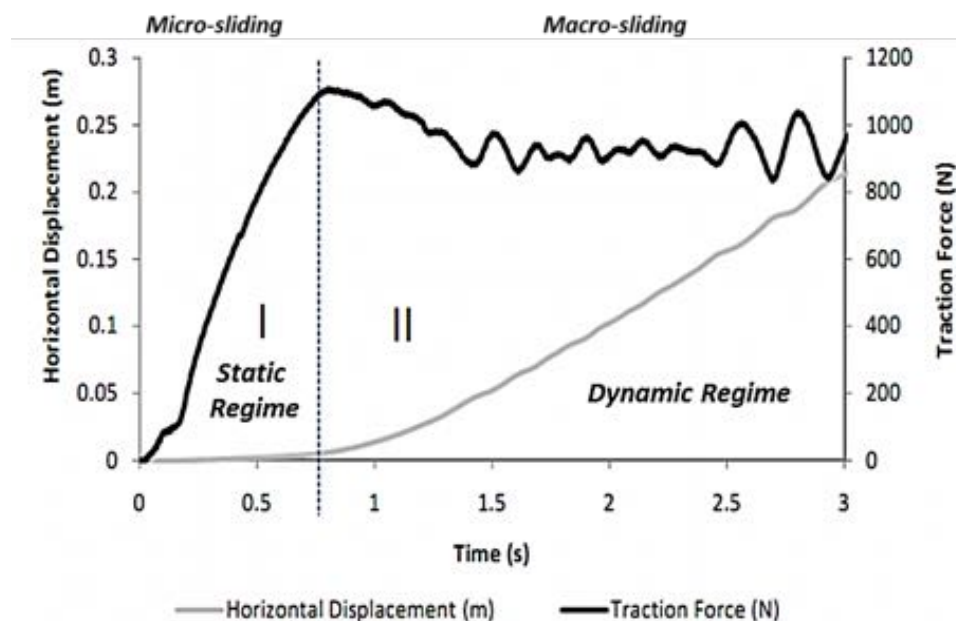
Figure 3.9 Traction (Friction) Force vs Time: Showing Static and Dynamic Regimes for an artificial clay court surface (Adapted from (Clarke et al., 2013)).

e) Profilometer

During this research, the surface roughness was measured with a portable Mitutoyo profilometer (series 178-SJ-401) (Figure 3.10). The profilometer measures surface roughness via a diamond tipped stylus which moves vertically up and down when moving horizontally in contact with the test surface. The R_a of each of the hard court tennis courts surfaces were used for comparison. Firstly, the profilometer was calibrated by measuring five values of R_a on a calibration sample of known profile. For statistical analysis a total of $10 - 15$ R_a values were taken at different regions of the surface tested and in different directions obtaining an average value of R_a.

Figure 3.10 Mitutoyo portable profilometer

f) Hardness - Durometer

Outsole rubber hardness was measured with a portable SATRA digital durometer (model STD 226), shown in Figure 3.11. The durometer had attached an interchangeable Shore A scale module which was selected depending on the 'softness' of the rubber tested. This test method is based in indentation and is used to determine maximum hardness values.

Figure 3.11 SATRA STD 226 Digital durometer

The test specimen preparation and hardness measurements were in accordance to the standard test method for rubber hardness (ASTM International, 2010). The specimen was placed on a flat, hard, horizontal surface. Next, the durometer was positioned in a vertical position with the inventor tip at a distance from the specimen. A sufficient and firm pressure was applied to the durometer for at least 1 second and the indicated reading was recorded. The arithmetic mean was calculated for five measurements at different positions.

3.5.2 Tennis surfaces

Initially, as presented in chapter 4, preliminary tests on natural grass and clay courts were performed, with the objective to evaluate the possibility to include these surfaces in the study. As this study focuses on the interaction of shoes and surfaces at professional level, it was decided to carry out mechanical tests on professional tennis courts (in the field), and a variety of ITF classified surface samples (in the lab). A variety of professional grass and clay courts, maintained to the highest standards were tested during this study.

Future work addressing the difference in mechanical properties of professional and amateur surfaces would be interesting, however it is beyond the scope of this study. Next is the description of the surfaces utilised on the experiments presented later in this thesis.

a) Grass courts used in field testing

The Wimbledon Championships grass courts

Every year, the Wimbledon Qualifiers and Championship takes place in the Bank of England Sports Ground, Roehampton and All England Lawn Tennis Club (AELTC) respectively (Figure 3.12). These courts are prepared and serviced by a full-time team of ground staff who maintain the surfaces to a very high standard. Although the grass composition is not known in detail for the Bank of England tennis courts, the one used during the Wimbledon Championships at the AELTC, is composed by 100% rye grass (changed in Sept 2000 from 70% rye / 30% red fescue) for better wear and tear properties. The grass playing height for both events is 8 mm and the courts maintenance and preparation takes place every morning during the tournament. Grass and soil humidity is controlled according to the groundsmen experience (AELTC, 2016).

Figure 3.12 Left: Bank of England court 7 and right: AELTC court 8, tennis courts.

Three grass tennis courts were tested during this study:

1. *The BoE-7*

(Court No. 7 outdoor, Bank of England Sports Grounds, Roehampton, London, UK)

Testing on this court was carried out during the Junior Wimbledon Championships 2013 qualification, and after the Wimbledon Championships 2013 qualification.

2. *The AELTC-8 and AELTC-9*

 (Court No. 8 & 9 outdoor, AELTC, Wimbledon, UK)

The testing on these courts was carried out 3 weeks after the Wimbledon Championships 2013. The grass height of both courts tested was different: court No. 8 (8 mm grass height), and court No. 9 (10 mm grass height), as court No.9 was not prepared for play conditions. This information was provided by the groundsmen before the testing.

b) Clay courts used in field testing

Two red clay professional tennis courts were tested during this research. These clay courts were constructed to the highest standards. Brief descriptions of both, are presented in the next section.

1. *LTA 4*

(Court No. 4, National Tennis Centre, London, UK)

This is a professional tennis court made from Northern European clay. The court, as shown in Figure 3.13, is characterised as being identical to the courts used at the Bastad ATP Tennis Event in Sweden (LTA, 2016). The courts are characterised by having relatively coarse clay, low maintenance and great ability to resist cold weather conditions.
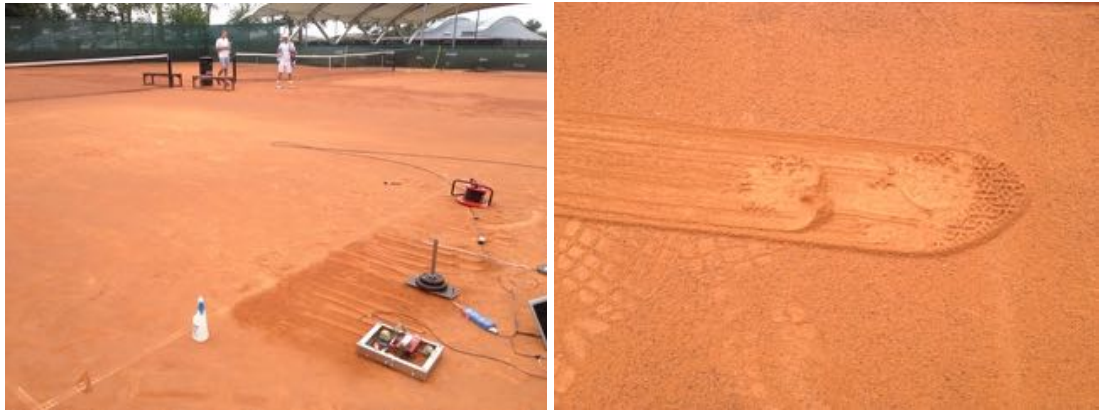
Figure 3.13 Court No. 4 at the National Tennis Centre.

2. RCB 28

(Court No. 28, Real Club de Polo de Barcelona, Spain)

This is a professional tennis clay, shown in Figure 3.14, made of red clay, which is crushed brick of different size and packed to make the court. Over the crushed brick, the surface is topped with a loose layer of smaller crushed particles of different sizes. After passing the clay through different sieves, the particle size distribution was determined by the manufacturer to be approximately 30% less than 0.5 mm and a 70% bigger than 0.5 mm. This court was used for preliminary experiments (Chapter 4) when measuring court surface friction with different mechanical devices.

Figure 3.14 Court No. 28 at the Real Club de Polo de Barcelona, Spain.
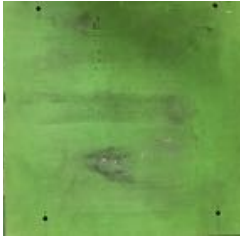
c) Hardcourts used in the lab testing

A range of hardcourt surface samples were tested during the different experiments trough this thesis. These surfaces were provided by the ITF with the objective to cover all the ball-surface pace classifications (slow – fast) previously described in the literature review chapter. The type of hardcourts provided was: acrylic/polyurethane and carpet surfaces

(50 x 50 cm). In addition, the surface roughness was measured with the profilometer and procedure described in section e). Table 3-2 shows a summary of the different surfaces with their ITF classification and roughness values.

Table 3-2 Hardcourt surfaces utilised for testing

Legend	Image	Surface	Type	ITF CPR	Roughness (Ra ± SD) μm
HC1		SPA	Acrylic		18.67 ± 1.66
HC2		Rebound Ace HSA Club	Acrylic		19.84 ± 1.72
HC3		N/A	Acrylic		15.34 ± 2.76
HC4		Courtsol comfort	Acrylic		17.52 ± 1.36
HC5		N/A	Acrylic		12.0 ± 3.19
HC6		Courtsol SP	Acrylic		6.70 ± 0.44
HC7	n/a	Mapecoat TNS	Acrylic		12.20 ± 1.67

HC8		Taraflex	Polyurethane carpet	9.53 ± 1.29
HC9		Synpave Rebound Ace	Acrylic	14 ± 1.54
HC10	n/a	Greenset Cushion	Acrylic	25.30 ± 1.80
HCB1		Bespoke 1	Acrylic	n/a	5.20 ± 0.60
HCB2		Bespoke 2	Acrylic	n/a	19.30 ± 3.0
HCB3		Bespoke 3	Acrylic	n/a	32.60 ± 5.0

d) Synthetic/hybrid courts used in lab testing

Two synthetic systems (clay and grass) and one hybrid clay system were used for mechanical testing (a hybrid clay system is characterised for system that uses a combination of a carpet matrix and real clay particles to provide the play characteristics of a traditional clay court). The synthetic systems are composed of a polypropylene membrane sand-dressed and/or rubber-dressed surface with the appearance of clay/grass. The Figure 3.15 shows the hybrid clay surface and the two synthetic surfaces (grass and clay). Descriptions provided in Table 3-3 .

Figure 3.15 Left: synthetic clay; centre: hybrid clay; right: artificial grass.

Table 3-3 Synthetic/hybrid surfaces description

Legend	Name	Type	Description
AC1	Matchclay	Hybrid clay	Infill = 6 kg/m^2 Total height = 11 mm Pile height = 6 mm
AC2	Acecourt	Artificial clay	Infill: 12 kg/m2 Total height = 13 mm Pile height = 11 mm. Particle size > .060 mm.
AG1	Real Green	Artificial grass	Infill: 14 kg/m^2.

3.5.3 Tennis shoes

While tennis shoe outsole construction varies from brand to brand, for this project it was decided to test a variety of tennis shoes, according to the surface. adidas and Babolat brands have a reputation as leaders in tennis equipment at an elite level. The tennis shoes selected for friction and shoe characterisation studies this study are shown in Table 3-4.

Table 3-4 Description of shoes utilised for testing.

Image	Shoe	Surface	Outsole description
	adidas Barricade 6	Hard court	Herringbone design
	adidas Barricade 7	Hard court	Herringbone design with circular patterns.
	adidas M Barricade 6 OC	Clay	Special dimpled tread design ideal for omni courts.
	adidas grass shoe	Grass	Pimpled tread design to provide traction on grass courts.
	Babolat Propulse 4 all court	All courts	Special "side 2 side" pattern.

a) adidas

The adidas Barricade 6 and 7 shoes, released in 2010 and 2012 respectively, were designed for hard court play. The outsole is herringbone style tread with some circular patterns, which the manufacturer claims to be useful during rotation of the foot on the surface. The adidas grass shoe has a pimpled outsole with a pimple height of 2 mm from the base of the outsole, which helps the players to have more traction on a grass court.

b) Babolat

The Babolat Propulse 4 all court shoe was released in February 2013, and it is still popular with amateurs and professional as it is suitable for hardcourt and clay surfaces. The outsole is a compliant polymer with a special "side 2 side" tread pattern in the forefoot. According to the shoe manufacturer this system, composed of positive and negative relief patterns, shown in Figure 3.16, provides a perfect balance between traction and sliding (Babolat, 2013). The positive relief patterns or "pimples" (Figure 3.16 - left) provide enough traction for quick and clean starts. In contrast, the negative patterns or "dimples" (Figure 3.16 - right) on the outer part of the foot ensure well controlled slides. One of the differences between this two sections rely on the "flat" area, in which for the negative patterns is higher producing higher pressures in contact with a surface. This is confirmed in the parametric tread study (section 7.5). The second difference relies on how the two sections deforms in contact with a surface. For the positive pattern, the pimples fixed into the surface providing a traction effect. In contrast, for the negative pattern, as the relative contact area is higher, then the section is likely to slide on top of the asperities of a tennis court.
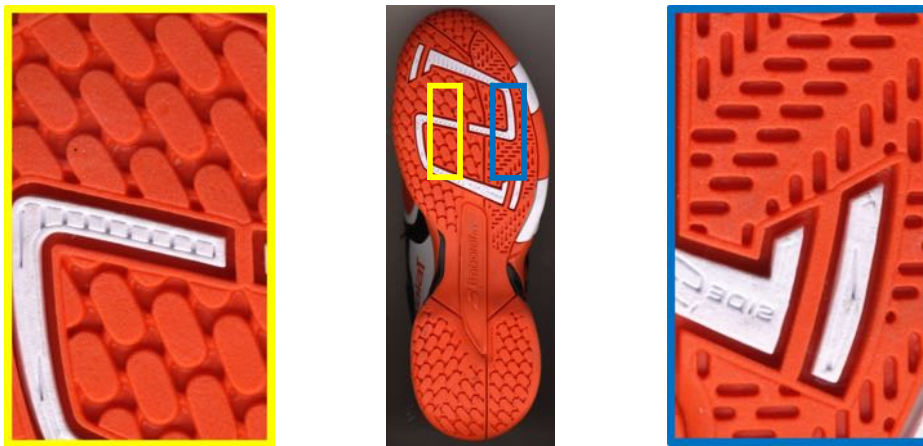
Figure 3.16 Babolat 4 all court shoe outsole, with positive (left) and negative (right) patterns in detail.

Before testing with any of the described shoes, the outsole was cleaned with an ethanol solution and allowed to dry at ambient temperature. Additionally, the outsole was prepared by applying p400 silicon carbide paper by hand under minimal pressure. Any debris from the shoe was removed using a clean, soft, dry brush. These procedures are in

accordance with parts of an international footwear standard (British Standards Institution, 2012).

c) Trends in tennis shoes outsoles

Different tennis shoe treads at a tennis shop were analysed with the objective to have an overview of the actual trends in tread patterns. 100 shoes (hardcourt, grass and clay) of 15 commercial brands were analysed showing the percentage of each tread. The treads were identified into four different groups: Herringbone, Mix, Omni/pimpled and Smooth. Examples of these treads are shown in Figure 3.17 along with descriptions in Table 3-5. Normally, the shoes are sold for the following different types of usage: all court/hardcourt, grass, carpet and clay.

Figure 3.17 Examples of each tread pattern. (a) Herringbone, (b) Mix, (c) Omni/pimpled and (d) Smooth.

Table 3-5 Description of each tennis shoe tread

Type	Description
Herringbone	A tennis shoe tread pattern including many treads lines which can vary 45° clockwise and anticlockwise from the normal.
Mix	A tennis shoe tread pattern which has different tread types on different sections of the forefoot. It includes a combination of concentric circles on the forefoot section.
Omni/pimpled	A tennis shoe tread pattern which mixes small dimples with other geometries to provide traction with the surface. It is used on grass or synthetic surfaces.
Smooth	A tennis shoe outsole consisting of a mostly flat, smooth surface. Used on indoor carpet courts.

The results presented in Figure 3.18 show that the 'all court/hardcourt ' shoe dominates the available tennis shoe market with a 66% compared to a 30% and 4% of clay and grass shoes. Looking in detail by shoe surface, in Figure 3.19 it is shown that the herringbone tread is the pattern most used in tennis outsoles. This pattern, is highly used in clay and 'all court/hardcourt' tennis shoe outsoles.

The 'Smooth' and 'Omni/pimpled' patterns are used mainly for grass/synthetic and indoor carpet surfaces respectively. The dominance of the 'herringbone' pattern in the tennis market suggest that it is very effective. As mentioned previously in Chapter 2, tennis shoes with 'herringbone' pattern have been used in many previous investigations (Damm et al., 2014, Starbuck et al., 2015).
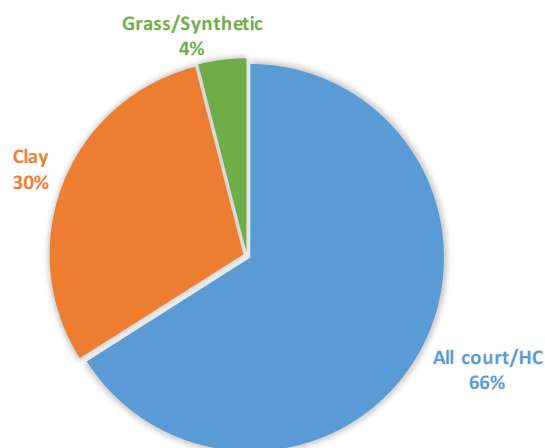
Figure 3.18 Results for the All Court/Hard court tennis shoes (n= 100)

In particular, it is attractive to look in detail into the 'Mix' category of tennis treads (Figure 3.19 (right)). Although the 'herringbone' tread pattern predominates in all court/hardcourt shoes, in contrast to clay, the 'Mix' category has a high 35%. This category is characterised by the visible innovation, in which a lot of the marketing for new tennis shoes focuses. As described in Table 3-5, the fundamental idea of this category is the requirement of several areas of the outsole with different tread patterns to allow the shoe to behave in different ways according to the movement or surface need, and in order to maximise their performance.
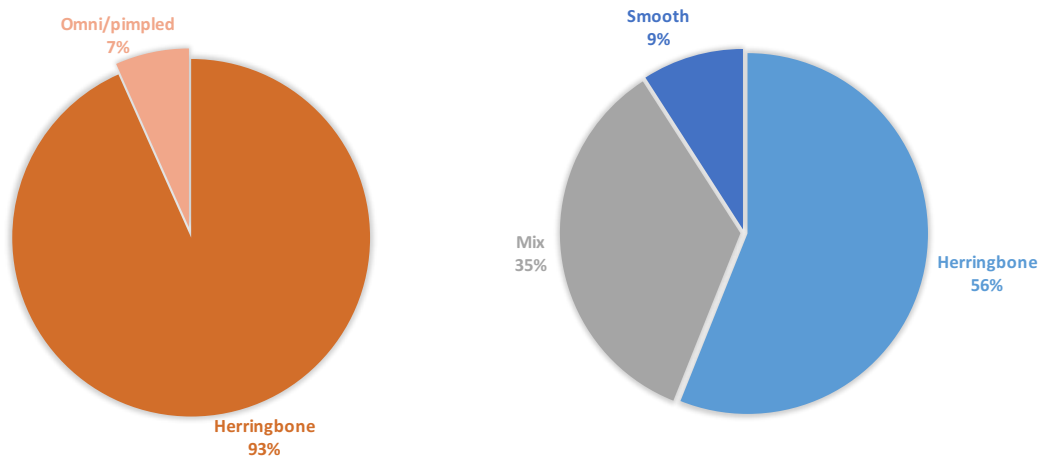
Figure 3.19 Results for clay (Left) and all court (Right) tennis shoes (n= 30 and 66 respectively)

Examples of this 'Mix' tread patterns are mentioned in Chapter 2, where the introduction of 'Glide', a sliding shoe for hard court surfaces, represents a new and innovative trend of shoe manufacturers. A second example is the Babolat Propulse tread pattern, utilised in some testing in this thesis, which is characterised by having two main areas of the forefoot. The inner part of the forefoot is advertised as the area to provide the majority of traction, whilst the outside of the forefoot is the area which enhances the player's ability to slide when turning.

In conclusion, the 'all court' shoe category dominates the tennis shoe market. In terms of outsole treads, the 'Herringbone' is the most used by manufacturers for clay and 'all court' shoes, however, the 'Mix' has started to be more popular due to a specialisation and the introduction of new technologies on the tennis shoes from the manufacturers.

d)   Shoe outsole and rubber characterisation

In order to understand how a shoe outsole behaves in contact with a tennis surface, it is vital to study the mechanical properties of the material. Tennis shoe outsoles are made from elastomers which is the name given to a group of lightly-crosslinked polymers that exhibit elastic or viscoelastic deformation (Werd and Knight, 2010). The experiments and results presented in this section focuses on the material characterisation of typical tennis shoes outsoles. Additionally, these are compared to commercial rubbers, in order to find a representative material of a tennis outsole, that could be used with the final test device.

Material characterisation, such as via Dynamic Mechanical Thermal Analysis (DMTA) and hardness measurements play an important role in the analysis of elastomers (Menard, 2008). They are widely used to characterise raw materials, intermediate products and

vulcanised products. The mechanical properties of elastomers depend on temperature and frequency of loading.

Hardness is one of the most widely measured properties used to characterise rubber. The IRHD (International Rubber Hardness Degree) and Shore, are the most common scales used. Both methods are based on indentation, however differ from geometries, applied forces and procedures. The Shore range of hardness has eight scale types: A, B, C, D, DO, O, OO and M. The A scale is used for soft rubbers and elastomers, type B is used to test moderately hard rubbers and type C for medium hard rubbers and plastics.

The aim of this testing was to measure the mechanical characteristics for a range of actual tennis shoes outsoles and commercial rubbers samples, through hardness measurements and DMTA testing. A comparison between them, and to the commercial test rubbers from other known test methodologies was made, in order to assess the best option for a test shoe. Key results are presented here, particularly those which have been used in future experiments.

Figure 3.20 Left: Tennis shoes tested adidas Barricade 7 and Babolat 4 propulse (small, medium and large). Right: Examples of shoe outsoles.

e) Hardness

Shore A hardness measurements were performed with the durometer and under the procedure described in Chapter 3 (samples of the outsole of five different shoes adidas barricade 6, adidas barricade 7 and Babolat 4 all court (Small, medium, large) were tested. In addition, two standard test rubbers utilised with the Pendulum test (Slider 55 and slider 96) were also tested.

Slider 55 and 96 are standard test rubbers utilised with the pendulum slip resistance test (described in chapter 3) to measure the slip resistance of a floor surface. They are used to replicate barefoot and shoe conditions respectively.
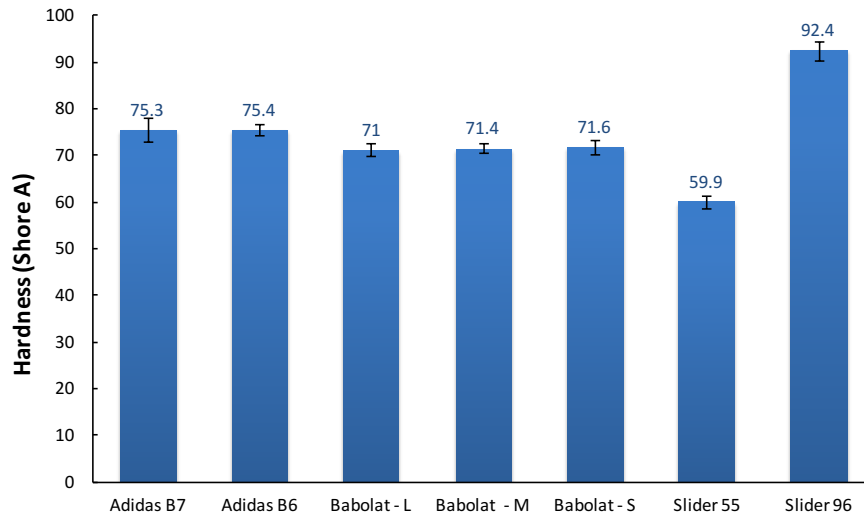
Figure 3.21 Rubber hardness results.

The Shore A results, presented in Figure 3.21, showed a good agreement between the shoes tested and the US Patent US7765720B2 (Yu et al., 2010), where Shore A values between 68-72 are reported as typical values for tennis shoes. The hardness of sliders (55 and 96) are reported in the IRHD scale, being 55 and 96 respectively (James, 1988). In previous literature (Briscoe and Sebastian, 1993) calculated an approximate relationship between IRHD and Shore A ($IRHD = H_A + 4$). For this testing, the shore A hardness results (59.9 ± 1.5 and 92.4 ± 2.0) for both sliders showed to be higher for the slider 55, but in good agreement for the slider 96, compared to the IRHD values.

f)   DMTA- Dynamic Mechanical Thermal Analysis

DMTA can be described as an applied oscillating force applied to a sample whilst analysing the material response to that force (Menard, 2008). It is a technique widely used to characterise a material's properties as a function of temperature, time, frequency, stress or a combination of these parameters.

The test procedure involves a small sample of rubber fixed at both ends whilst it is loaded at a number of required and pre-set frequencies. The sample is inside a small environmental chamber in which the temperature can be changed over a wide range. During a test, the stress and strain are monitored continuously.

Figure 3.22 University of Sheffield DMTA machine.

DMTA works by applying a sinusoidal deformation to a sample of known geometry. When the rubber is loaded in this way, some energy is lost as heat. This loss of energy is resultant from the strain and stress being out of phase. The greater this phase difference, the greater the energy loss. This loss energy is determined as the tangent of the phase between stress and strain (tan δ)(Kime, 1991).

Figure 3.23 shows how the stress is determined into two components, one of which is in phase with the strain and the other 90° out of phase. The ratio of the in-phase component of stress to the strain is called the in-phase or elastic modulus (*E'*)(Kime, 1991). In this way DMTA basically provides measures of stiffness and damping of a material, reported as the storage modulus (*E'*) and loss modulus (tan δ) respectively.

The properties of the rubber vary with frequency and temperature. As the test frequency increases, the stiffness increases until the rubber responds as a glass. A similar effect is observed, if the frequency is kept constant and the temperature is lowered. The temperature at which this occurs is known as the glass transition temperature (T_g). An example of a DMTA trace with the glass transition temperature is shown in Figure 3.24.
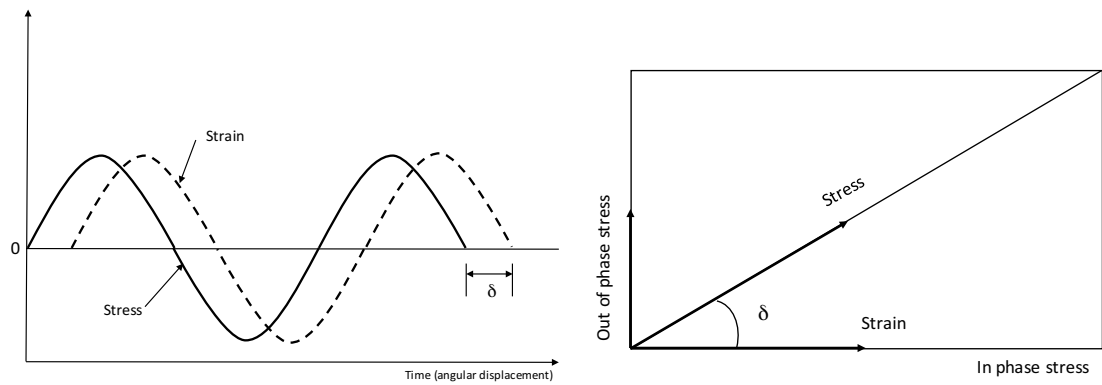
Figure 3.23 Relationship of the applied sinusoidal stress to strain, with the resultant phase lag and deformation
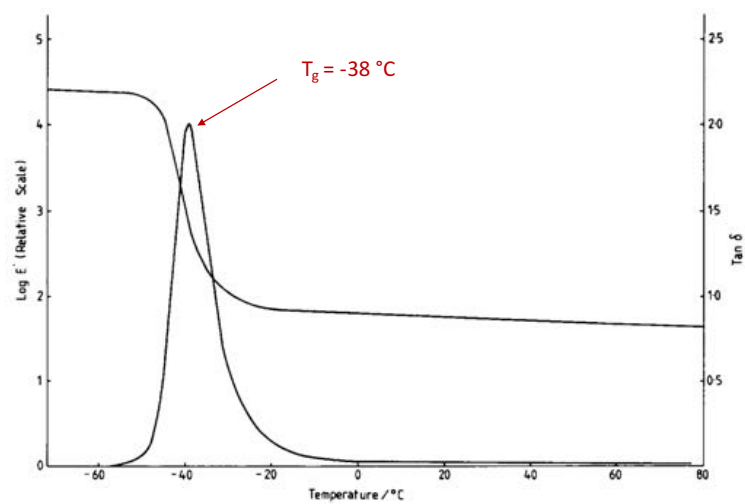
Figure 3.24 Example of DMTA trace for the slider 55 rubber showing the glass transition temperature (adapted from (James, 1986))

The test frequency was 10 Hz and the temperature was varied from -60 °C to 60 °C. Figure 3.25 shows the results obtained for E' and tan δ for both slider 55 and 96 samples from the DMTA tests. The plots show the glass transition points for both rubbers, -42.2 °C for the slider 55 and -50.4 °C for the slider 96. The results are in good agreement with the ones showed in (James, 1988), which reported -38 °C and -50 °C for slider 55 and 96 respectively. These results confirmed the accuracy of the tests in order to compare the shoes samples.
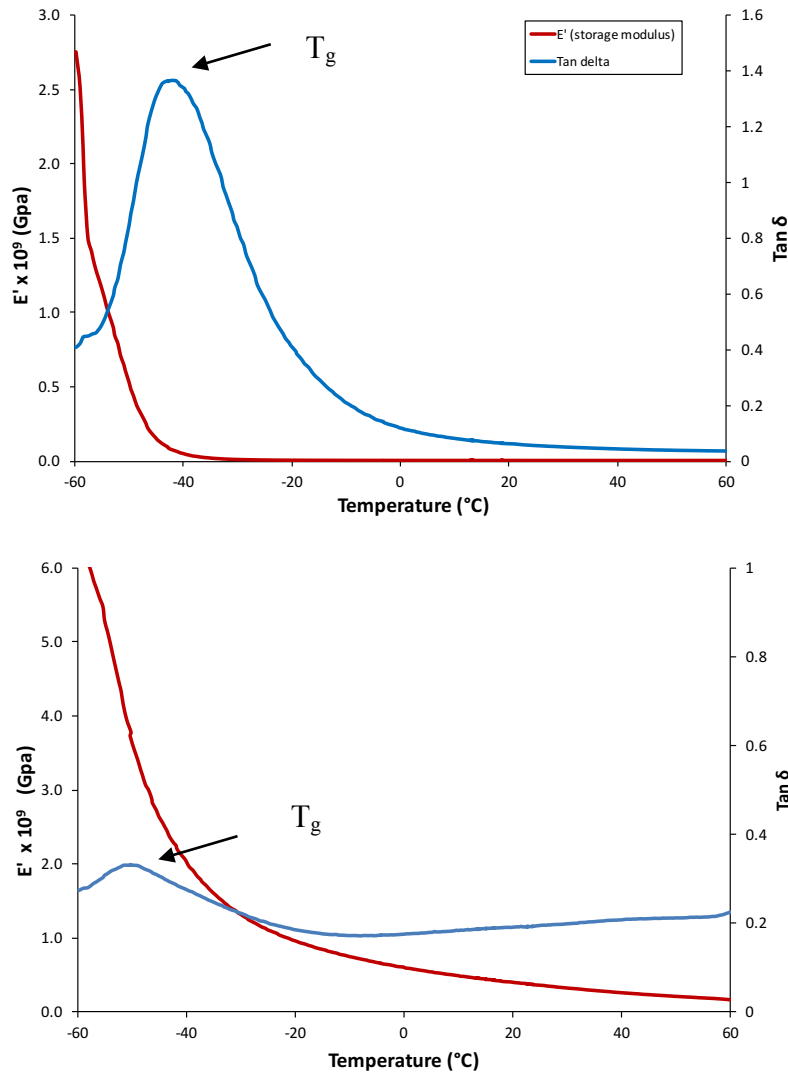
Figure 3.25 DMTA results for the slider 55 (top) and slider 96 (bottom).

In Figure 3.26 and Figure 3.27 the results for the stiffness (E') and damping ($tan \; \delta$) are presented. Although the tests were done at a temperature range from -60 to 60 °C, our range of interest focuses in temperatures from 0 to 60 °C, as most of the tennis tournaments around the globe are played under this range of temperatures.

For the stiffness results (E'), the general tendency for the tennis shoes is to decrease as the temperature increases. It can be seen, as expected from the previous hardness results obtained in the previous section, that the slider 55 rubber is the softest and that slider 96 is the stiffest one, from all the samples tested. Slider 96 plot is significantly higher than the other samples and is not displayed on the stiffness graph. For the tennis shoes samples, it can be seen that for the adidas barricade 6 & 7 shoes, although they are different models, they have similar values, however they are stiffer than the Babolat.
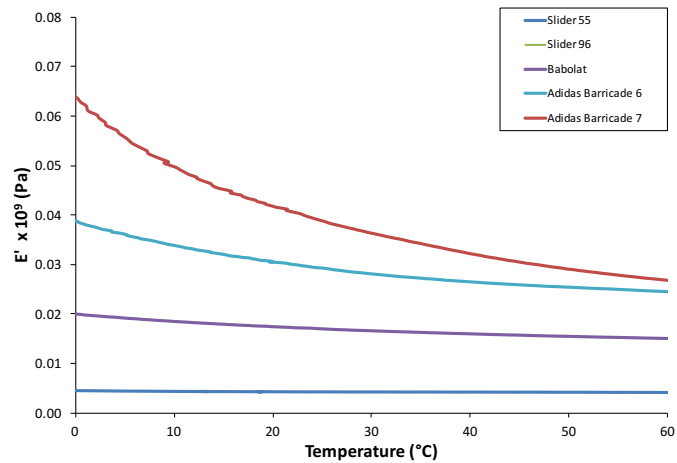
Figure 3.26 DMTA results: stiffness (*E'*) against temperature for the 5 samples tested.

Figure 3.27 shows the results for the damping (*tan δ*) of the five samples tested. The tendency for the tennis shoes and slider 55 sample is to decrease in damping as the temperature increases, however, the slider 96 shows the opposite behaviour. Between the tennis shoes, the behaviour is similar to the stiffness, both adidas shoes presented higher values than the Babolat.
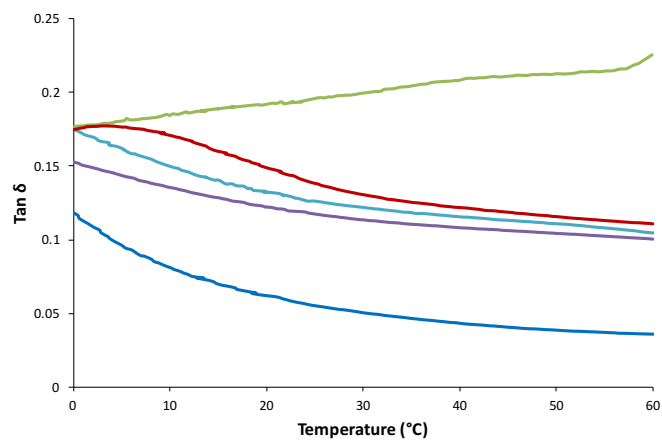
Figure 3.27 DMTA results: Damping (tan δ) against temperature for the 5 samples tested.

3.6   Summary of Chapter

In the first part of this chapter the Methodology utilised within this project is presented. The techniques used during this project were outlined in this Chapter and were developed and selected based on the findings of the Literature Review.

The second part of this chapter presented the test equipment utilised in the experimental chapters (4, 5 and 6), to study and categorise the frictional properties of tennis surfaces. The variety of test equipment was used in lab and field conditions, resulting to be useful to simulate contact conditions between footwear and surface.

In terms of surfaces, a variety of the most common tennis surfaces were presented in this section such as hardcourts, clay, grass and artificial surfaces. With this variety, a good amount of the main surfaces classified by the ITF is covered, helping to study and understand the differences between them.

The shoes selected for this project also represent a sample of the common tennis shoes on the market. Brands such as adidas and Babolat have been in the tennis market for many years, so the study of these shoes, will help develop a standard test shoe, as discussed in the next chapters. Additionally, four main tread categories were identified in the market study of commercial tennis shoes. These are: Herringbone, mix, omni/pimpled and smooth. The Herringbone tread design is the most utilised, used on clay and all-court shoes.

Finally, the first results of rubber characterisation were shown for comparison against tennis shoes. For confidential purposes, it is difficult to get the rubber composition of the shoes outsoles from the shoe's manufacturers, however, rather than knowing the polymers chemistry, it is more important to have an understanding of the mechanical behaviour of the shoe's rubber. It was shown that the mechanical properties of the tennis shoes rubber are highly dependent of the temperature, for this reason is necessary to assess the temperature of a shoe during a contact with a surface. This is further studied in section 6.4.

The shore A values of commercial tennis shoes, were found to be between 71 and 76. These results could be useful as benchmark values in order to find and define the best option for a potential test slider for the final device. It was shown that the standard slider rubbers (slider 55 and 96) normally used with the pendulum device, behave mechanically

different to the rubber shoes, as they are a softer and harder than typical tennis shoes rubber. Slider 96 is used due to its high wear resistance which typically improves with hardness for elastomers. For these reasons, the suitability of these to be used as tests rubber for the final test device, is low, however, results of further testing with these rubbers is presented in section 7.5. These rubbers were developed with the purpose to replicate the tyre-road and shoe-floor interactions under dry and wet conditions. Moreover, despite the manufacturer, shoes behave in a similar way under the same temperature conditions.

The combination of the presented methodology and the test equipment utilised during this project, were chosen to investigate the factors that influence a player-shoe-surface interaction. The results of the data collection are presented in Chapter 4 (biomechanical conditions) and Chapter 5 and 6 (Tribological parameters). In Chapter 7 the design of the new portable device is presented and in Chapter 8 a discussion of the results is presented with focus on the relationships and implications between the player, shoe and surface.

4. Player - Replication of Biomechanical Conditions

4.1 Introduction

As a result of the literature review discussed in Chapter 2, it was established that in the past, obtaining the characteristics of player-court interaction in tennis has been complicated and difficult to determine. As mentioned by (Redfern et al., 2001), biomechanics can be used, apart from determining required friction during specific movements, to assess frictional instruments, as a calibration or validation. Additionally, the replication of player loading using portable light devices in the field, has been a challenge (Grund et al., 2007). As suggested by Dixon et al. (1999), in order to provide a more accurate measurement, test methodologies should replicate the load-profiles in combination with appropriate and representative shoe and surface materials.

Therefore, as explained in the methodology (Chapter 3), this chapter focuses on studying and investigating some biomechanical conditions in tennis, with the objective to determine which are relevant to be considered for the design of the final frictional test device (Chapter 7). To achieve this, a series of experiments were designed to fulfil three main objectives:

1. To determine 'risk' movements of players on a tennis court through video analysis.

2. To study the shoe velocity during a 'sliding' movement on hard courts.

3. To investigate a loading profile more representative to match conditions.

This chapter provides information on how these experiments were planned, the results and analysis, together with relevant findings from previous literature for comparison.

4.2   Video analysis of player movements

4.2.1   'High-risk' tennis movements

With the objective to identify 'high-risk' tennis movements, a series of 45 tennis rally videos available on the internet (15 on each of the three main surfaces: clay, grass and hard courts), were observed and analysed to determine the 'high-risk' movements on a tennis court. A suggested by (Orendurff et al., 2008), it is important to take into account the whole variety of movements in tennis, such as cutting, braking and side jump, at the moment of initiation of likely risk of injury.

In terms of common injuries, the ankle sprain is one of the most common (Hutson and Jackson, 1982). This type of injury is the result of an ankle inversion, and resulting damage to the lateral ligaments (Perkins and Davis, 2006). Hard court surfaces have been associated with two high-risk movements: fixation of the foot to the surface (Newton et al., 2002) and higher pressure on the lateral part of the foot, which could lead to an ankle inversion ((Girard et al., 2007, Damm et al., 2014). A tennis player needs different levels of friction to perform specific movements during a tennis match. However, too high friction could lead the players to slip or fall, and in contrast too low could be reflected on a fixation of a foot with a high potential of injury risk.

This video analysis was performed with the objective to determine possible tennis movements to replicate with the test device, in order to evaluate and assess situations where the player may be exposed to an injury risk.

To evaluate potential 'high-risk' movements, the videos were reviewed to identify incidents where one of the players was involved on a fall-down due to an apparent "frictional" event. This event could be either because of a low or high shoe-surface friction. A series of 'risk' situations on each of the three main surfaces (clay, grass and hard courts) were identified for further analysis.

Three main variables were determined for the analysis: (1) the player movement, (2) a primary mechanism of movement and (3) the frictional mechanism.

1) *Player movement*

This was divided into three main categories:

- **Running**. This movement is defined as the action of the player to run with an acceleration to either side of the court. It could involve hitting the ball (Figure 4.1) .

Figure 4.1 Running backhand. (1) shot preparation, (2) impact with ball, (3) brake movement and (4) push-off.

- **Turning.** This is defined as the movement when a player while running to one side of the court, decelerates and pushes-off on the court to change direction and runs to the other side. This movement is typical after hitting a shot, where the player turns to the centre of the court to be ready for the next shot. An example of this movement is shown in Figure 4.2.

Figure 4.2 Running forehand and backhand. (1) Shot preparation, (2) impact with ball, (3) brake movement and (4) lateral impulse to opposite direction

- **Jumping.** This movement, shown in Figure 4.3, is normally utilised by the player as a 'split step' to start another movement such as running. This involves a knee flexion, a small vertical jump and a landing phase.

Figure 4.3 Jumping movement. (1) knee flexion, (2) small vertical jump, (3) foot landing and a (4) push-off.

2) *Primary mechanism of movement*

Four main categories were identified:

- ***Accelerating.*** This happens regularly at the start of the movement. The player pushes on the surface by applying a specific vertical and shear force.

- ***Sliding***. The player uses this mechanism in two situations. To reach a ball and reduce reposition time, or as a way to stop movement.

- ***Landing***. This occurs during a jump movement, in which either the feet or one foot impacts the surface.

- ***Decelerating***. This happens normally at the end of a running movement. It is used to stop the player movement.

3) *Frictional mechanism*

This was split into two categories:

- ***Slip.*** When the player experiences an uncontrolled slide. It is characterised by a low friction shoe-surface interaction.

- ***Grip.*** The shoe-surface interaction is characterised by a high friction and an extreme fixation of the foot.

Table with overall results, can be seen in Appendix A. The results, shown in Figure 4.4, highlight, besides the surface, 'running' and 'turning' as the movements with higher incidence of a fall. On clay, the majority of these incidents occurred during a 'running' movement and 'turning' was the movement with lowest incidents. In contrast, for grass and hard courts, although 'running' represents the majority, "turning" is the second most important. These results indicate a different playing style on the different surfaces.
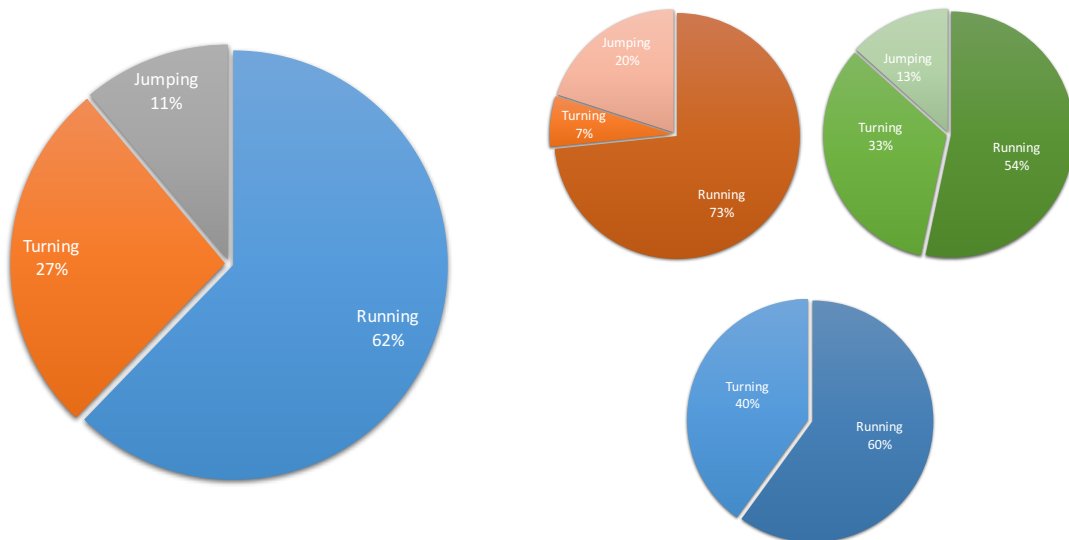
Figure 4.4 Player movement. Left: Overall results. Right: Clay (red); grass (green); hardcourt (blue).

The results for the primary mechanism (Figure 4.5) despite of the surface, show that the main mechanisms involved during the player movement are the 'landing', 'sliding' and 'accelerating'. However, the results by surface show different tendencies. On clay, 'sliding' and 'landing' are the main ones, whilst in grass 'landing' is the main one. For hard courts, the incidents for 'landing' and 'accelerating' are the main ones.
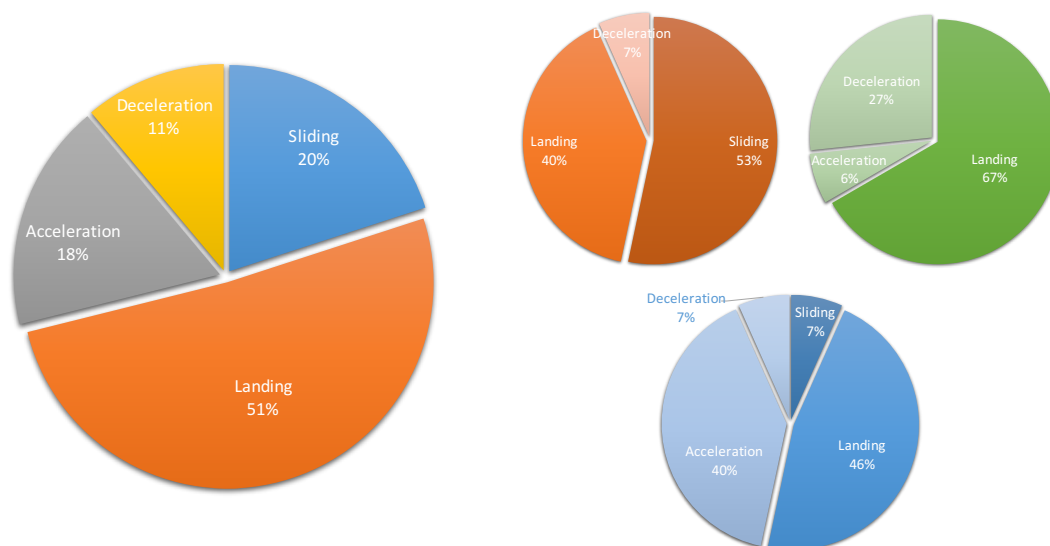
Figure 4.5 Primary mechanism. Left: Overall results. Right: Clay (red); grass (green); hardcourt (blue).

For the frictional mechanism, the results presented in Figure 4.6 show in overall a similar value between 'slip' and 'grip'. If the results are analysed by surface, it is more evident that for clay and hard courts the risk movements occur for an excessive 'grip' suggesting a high friction experienced by players. In contrast, on grass, all of the falling incidents occurred because the players slipped, suggesting a low friction.
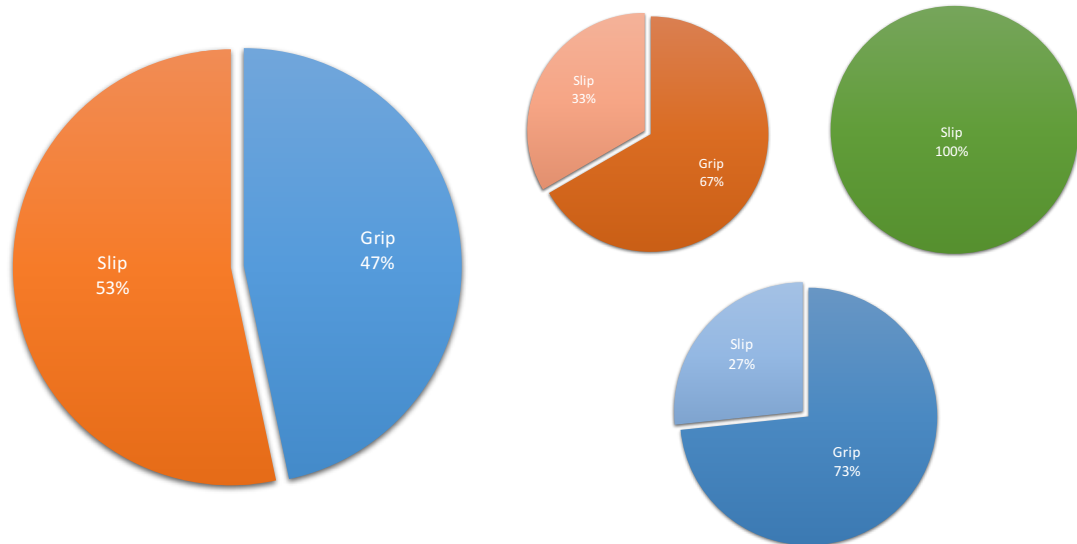
Figure 4.6 Tribological mechanism. Left: Overall results. Right: Clay (red); grass (green); hardcourt (blue).

In conclusion, it is well known that tennis is a sport characterised by high efforts, changeovers, acceleration and decelerations (Fernandez et al., 2006). Although the results from this section shows 'running and 'turning' as 'risky' movements despite the surface, it is important to mention that these are typical movements during a tennis match; and hence increases the frequency of occurrence.

4.2.2 Sliding incidence analysis

Observational video analysis was performed to determine the incidence of sliding movements during a professional tennis match played on hard courts. The results were compared to the incidence of sliding on clay courts, where sliding is well known to be a play style characteristic. The percentage of sliding movements (both players), from the total number of shots in a rally was calculated for a total of 21 videos (11 on hardcourt and 10 on clay).

The criteria to consider a video for analysis, was to have a minimum of 10 shots in total, when combined from two players in a rally. A sliding movement was defined as when, during a player's movement, one of the player's shoes in contact with the surface has a relative horizontal displacement whilst in contact with the surface. As an example, on clay, a player performs sliding movements to reach a ball, change direction or to brake on the court. On hardcourts, as discussed in the literature review in Chapter 2, sliding could possibly be used to reduce the player's reposition time and prepare for the next shot (Pavailler and Horvais, 2014).

Table 4-1 Results of 11 rallies played on hardcourt Grand Slam finals.

Video	Players	Tournaments	Total No. shots in rally	No. sliding movements in rally	% of sliding mov. in rally
1	N. Djokovic vs A. Murray	Australian Open 2011	39	9	23.07
2	N. Djokovic vs R. Nadal	US Open 2011	31	7	22.58
3	N. Djokovic vs R. Nadal	Australian Open 2012	31	10	32.25
4	N. Djokovic vs A. Murray	US Open 2012	30	8	26.66
5	N. Djokovic vs A. Murray	Australian Open 2013	23	7	30.43
6	N. Djokovic vs R. Nadal	US Open 2013	54	11	20.37
7	R. Nadal vs N. Wawrinka	Australian Open 2014	22	7	31.81
8	M. Cilic v K. Nishikori	US Open 2014	10	3	30.00
9	N. Djokovic vs A. Murray	Australian Open 2015	11	4	36.36
10	N. Djokovic vs R. Federer	US Open 2015	13	3	23.07
11	N. Djokovic vs A. Murray	Australian Open 2016	15	4	26.60
		Average (SD)	**25.36 (13.4)**	**6.64 (2.8)**	**27.56 (5.0)**

Table 4-1 and Table 4-2 show the incidence of sliding movements on hard and clay courts respectively. Although the analysis of a rally is a small sample and is not representative of a tennis match, the analysis of 11 rallies, could give us a tendency of how much a tennis player is sliding on a hard court. As expected, the 28% of sliding in a rally on hard courts is lower than the 46% on clay courts. However, this 28% represents a high number compared to the general perception that sliding occurs only on clay.

Table 4-2 Sliding movements on clay

Video	Players	Tournaments	Total No. shots in rally	No. sliding movements in rally	% of sliding mov. in rally
1	N. Djokovic vs R. Nadal	French Open 2014	13	7	53.84
2		French Open 2014	14	6	42.85
3	R. Federer vs Gulbis	French Open 2014	27	11	40.74
4	R. Nadal vs A. Murray	French Open 2014	25	9	36.00
5			29	11	37.93
6	R. Nadal vs D. Ferrer	Madrid Open 2013	12	6	50.00
7			16	8	50.00
8	N. Djokovic vs Gulbis	French Open 2014	17	9	52.94
9			13	6	46.15
10	Wawrinka vs R. Federer	Montecarlo 2014	8	4	50.00
		Average (SD)	**17.4**	**7.70**	**46.4 (6.3)**

Because of the high incidence of sliding on hardcourts, and the 'risk' and implications on tennis players, it was decided in conjunction with the ITF, to review and analyse this movement in more detail.

4.2.3 Sliding shoe-velocity analysis

A further brief video analysis was implemented to determine average shoe-velocity during typical tennis sliding movements on hard courts. Five internet videos from elite players during professional events, were chosen and used for digital tracking analysis. An Open source video analysis and modelling software, *Tracker v4.93* (*Open Source Physics, Douglas Brown*), was utilised for tracking the shoe during sliding movements. The analysed videos were selected in which the camera angle view was fixed, to avoid any error measurement due to the relative motion from the camera. The player moved relatively laterally on the court, which helped to keep the analysis in 2 dimensions. The video resolution was 1920 x 1080 with a frame rate of 25.0 fps. The five videos were selected from the ATP tour final event 2015, with the observation that all the matches being played on a single tennis court. This means that the same surface was constant for all the videos, despite the matches were played on different days over a period of 7 consecutive days.

In order to start the analysis, a calibration factor was calculated by selecting a fixed distance in the horizontal axis. The calibration factor was calculated from the 5.46 m known distance from an official tennis court dimension between the "T" and the doubles line on the baseline (Figure 4.7). With this known distance, 5 calibration factors were calculated on different parts of the image. As shown in Figure 4.7, the origin was at the bottom baseline. From that origin, a distance in pixels was calculated for each of the other reference lines (SL1, Net, SL2 and BL1). Figure 4.8 shows the relationship between the calibration factor against the distance in pixels in the 'Y' axis. The calibration factor for the 'player line', which is the line where the player is moving laterally was extrapolated from the relationship shown in Figure 4.8. As an example, for the video shown in Figure 4.7, the difference from the origin to the player line is 116.4 pixels. After a linear extrapolation based on the data shown in Figure 4.8, the calibration factor was calculated as beings 0.00623 m/pixel.
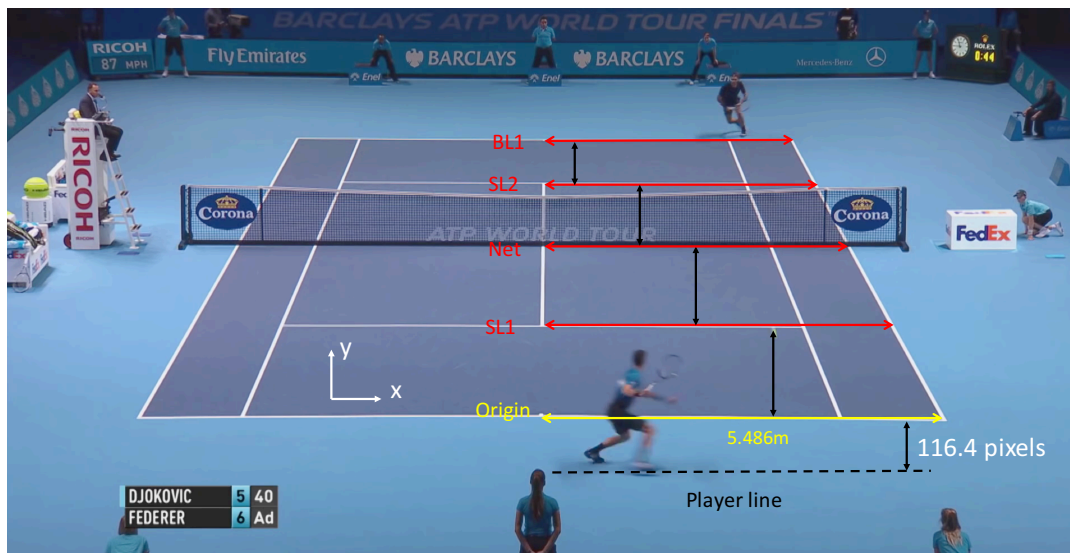
Figure 4.7 Distances utilised to determine a calibration factor.
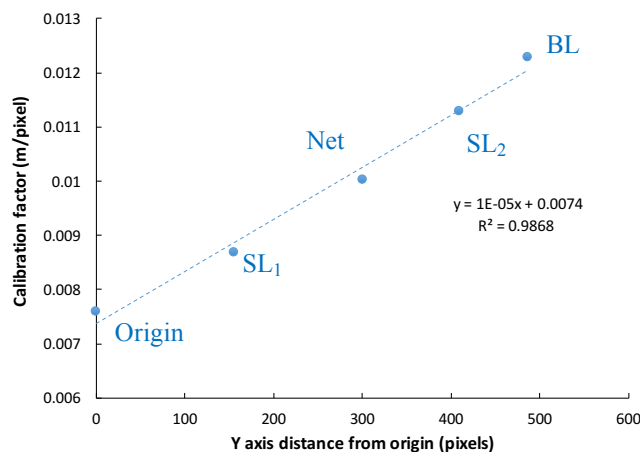
Figure 4.8 Calibration factor against the 'Y' distance from origin with regression line (dotted).

With a calibration factor calculated for each video, the initial shoe velocity and total sliding displacement were extracted. As a reference to extract these parameters, the analysis started from the moment where the player's sliding shoe was totally flat on the surface (No.4 in Figure 4.9) and finished when the shoe was close to stopping or at total rest (No.10 in Figure 4.9). As a validation of the calibration factor, the known tramlines distance (1.37 m) was utilised as a reference. This distance was calculated for each of the reference lines (SL1, Net, SL2 and BL1) with the calculated calibration factor and the distance in pixels. The maximum difference found was 60 mm, overestimating the original value.
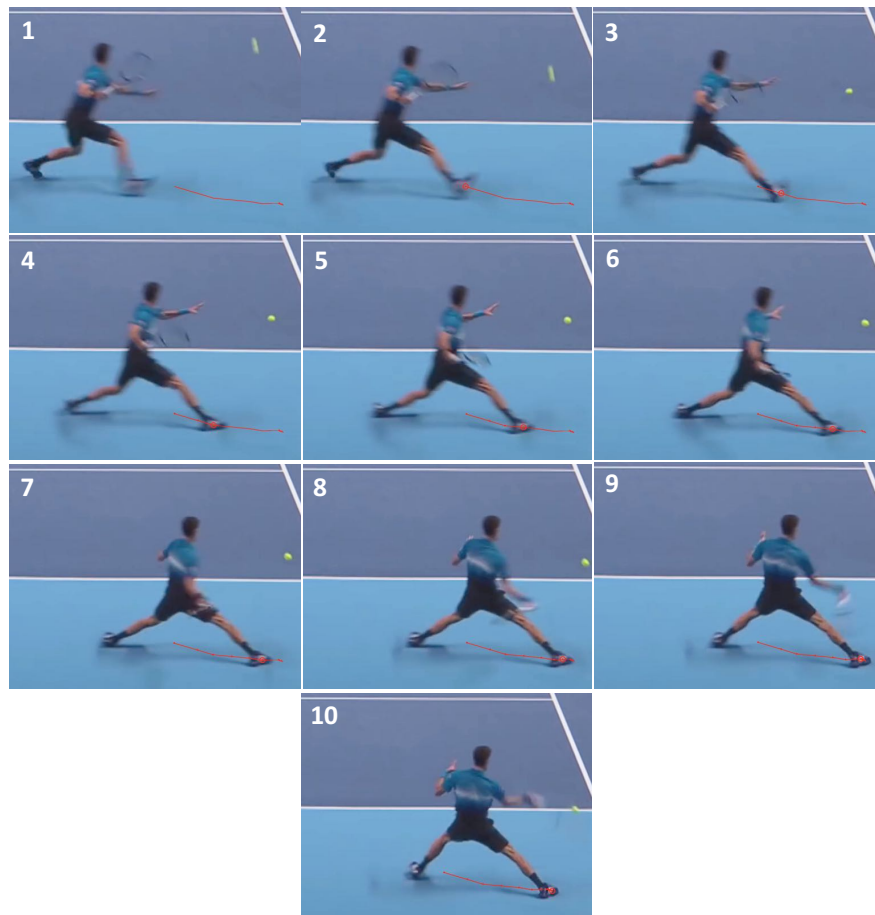
Figure 4.9 10 frames utilised for the measurement of the shoe-velocity. Red line shows the trajectory of the shoe.

Figure 4.10 shows an example of the displacement-time curves for the five videos analysed. In this curve, the four main stages are presented. After the shoe is flat and the sliding starts, the shoe starts to decelerate due to a combination of the friction generated by the shoe and the surface in combination with the biomechanics of the player, then the shoe reaches a stationary stage (No.10 in Figure 4.9) where the player is preparing to turn or to fully stop. The gradient, calculated for the linear part (v = constant), represents the maximum initial shoe velocities during the sliding and shows the ability and effectiveness of the players to brake through sliding.
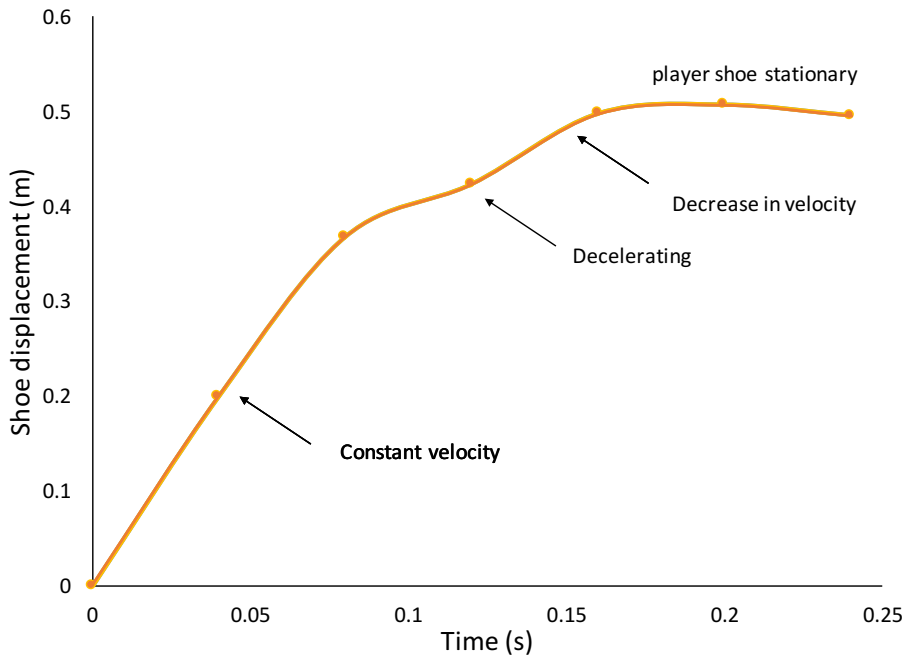
Figure 4.10 Example of a shoe displacement – time graph of one of the videos.

Figure 4.11 shows the various gradients calculated for each of the five videos analysed. The values of velocity extracted range between 2.82 and 4.73 m/s. These values represent a combination of effects of the player technique, the shoe and the surface.
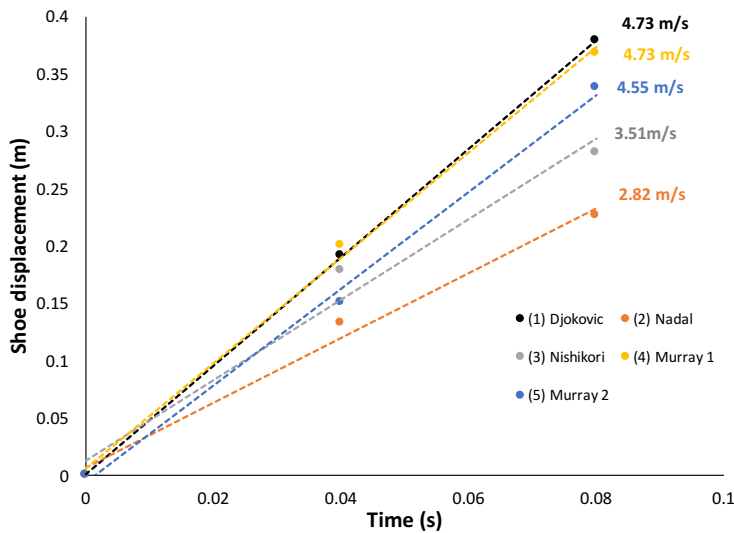
Figure 4.11 Shoe displacement gradients calculated for the 5 videos analysed (linear fit).

Table 4-3 shows the results for the five videos analysed, presenting the initial shoe-velocity (gradient) and the total displacement of the sliding, until the shoe-surface velocity was zero. It can be seen that as the initial sliding velocities increases, the total displacement of the shoe on the surface increases as well.

Table 4-3 Results for the 5 videos analysed with the initial velocity and displacement calculated

Video	Player	Initial Velocity(m/s)	Total Displacement (m) (when v = 0)
1	Djokovic	4.73	0.71
2	Nadal	2.82	0.41
3	Nishikori	3.51	0.42
4	Murray 1	4.55	0.49
5	Murray 2	4.73	0.75
Mean (SD)		*4.06 (0.86)*	*0.56 (0.16)*

The results presented in this section give a good idea of the shoe velocities during a sliding movement, however it will be interesting to assess the friction values, as in section 4.2.1 was suggested sliding as a 'high-risk' movement. The next section tries to validate the results presented here using biomechanics data, and aims to find the behaviour of friction during this movement.

4.3   Study of shoe velocity effects on sliding friction

The purpose of this study was to characterise, in the lab, the dynamic friction during a simulated sliding movement over typical hardcourt surfaces. The second objective was to measure typical sliding velocities. This was a two-part collaborative study with the CSER (Centre of Sports Engineering Research), Sheffield Hallam University.

Our colleagues from CSER developed a biomechanical study in order to understand the relationship between player performance and the amount of available friction on a hardcourt surface. Kinematics and kinetic data were collected during a tennis movement for further comparison.

To complement and for comparison, mechanical friction tests were conducted on the same hardcourts with the UoSh traction device previously described in section 3.5.1.

The main objectives of this testing were:

- Determine typical loading conditions and shoe sliding velocities on hard courts during a typical tennis movement.

- Test the practicality to mechanically achieve high shoe-velocities during a sliding movement.

- Compare the friction from the mechanical testing against biomechanical data.

4.3.1 Biomechanical study

In the next paragraphs, a brief description of the biomechanical study conducted by the colleagues from CSER, is presented. This study was approved by the Ethics Committee of the School of Health and Wellbeing at Sheffield Hallam University. Informed consent forms and pre-test medical questionnaires were acquired before any testing.

Ten athletic male participants, free from any injury (age 23.5 ± 1.2 years; body mass 80.9 ± 7.5 kg) performed a 180 degree turn on three different ITF classified hard acrylic tennis surfaces. The surfaces (HC3, HC5 and HC7) described in section c) varied in their amount of available friction, increasing from low to medium to high. These are surfaces used in competition. Each surface had a pre-determined court pace ranking (CPR) which was relative to a ball bounce suggested by the ITF.

A Klister force platform was used to measure vertical GRF, loading rate and shear force. Kinematic measurements were obtained using a MAC 3D motion capture. Timing gates were used to measure the time for a participant to complete the movement.

Each of the three surfaces were glued to a metal plate, and screwed to the force platform for the respective testing. The test movement performed by participants was a maximum effort 180 degrees turn executed at full speed. Participants started roughly eight metres (approximate width of a tennis court) from the force platform with their feet perpendicular to the running direction. On reaching the force platform, the participants were required to change direction, completing a 180° turn. Participants were asked to perform the movement at maximum effort, running to and from the force platform as quick as possible. Timing gates (Brower Timing Systems, Daper, UT, USA) were placed over four metres from the force platform, recording the time taken to travel to the force platform and return to the four-meter position. Participants wore adidas Barricade 7.0 shoes, described in Chapter 3, supplied by the ITF.

Measurements were taken at a sampling rate of 1000 Hz, and GRF measurements were extracted with Visual 3D Software (C-Motion Research Biomechanics, Germantown, MD, USA). Vertical ground reaction force (GRFy) was provided in the Y-axis of the

force platform. The shear force was calculated as the result of combining the horizontal forces in the X-axis and Z-axis. The utilised coefficient of friction (COFu) was calculated as the ratio between the shear force and the peak vertical ground reaction force.

No instructions were given to the participants to slide on the surface, however, some of the participants used the sliding as a natural way to stop and do the turning movement. Each participant attempted the movement five times on each surface. For our study, only the results from two participants on each surface were utilised, as it was visually confirmed that they slid on the three surfaces. Foot velocity and slide distance were analysed.

Figure 4.12 shows an example of one biomechanical trial for one of the sliding participants. The ground reaction forces plot (GRFy and Fshear) show two loading and one unloading events, suggesting an adjustment from the player to the surface, while sliding, in order to stop and then turn. The magnitudes of the second loading event were higher compared to the first one, suggesting that the player applied higher forces on the surface to stop.
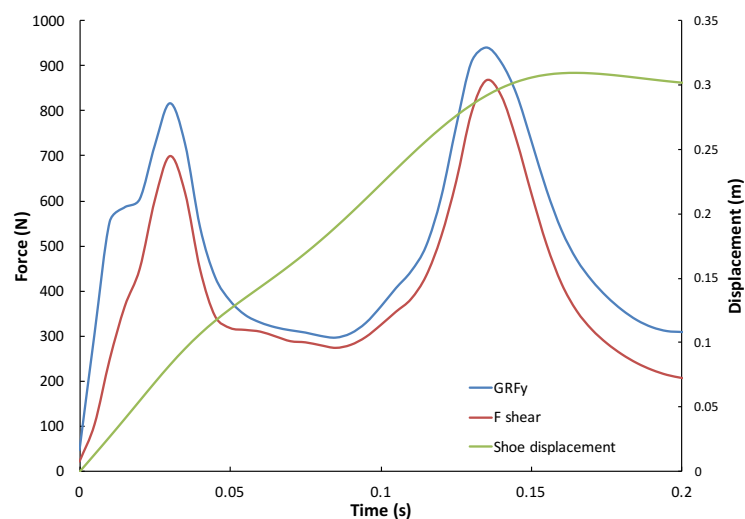
Figure 4.12 Example of the loading conditions and shoe displacement for one biomechanical trial

For comparison purposes, the gradients of the initial displacement on each surface for both participants were analysed. These gradients were defined only for the linear part of the displacement plots, in which the velocity is constant. The results presented in Figure 4.13 show that for both participants the 'slow' surface (HC3) had the lowest gradient value. This is in agreement with the ITF CPR classification, in which HC3 is representative of a surface with the higher friction. However, the results from the

'medium' (HC5) and 'fast' (HC7) surfaces differ from each participant. This difference suggests a small variation on the mechanical properties of the surfaces, and therefore these were investigated in the next section 5.3.2. Table 4-4 show the average results for the forces, and initial velocities of both participants on each surface.
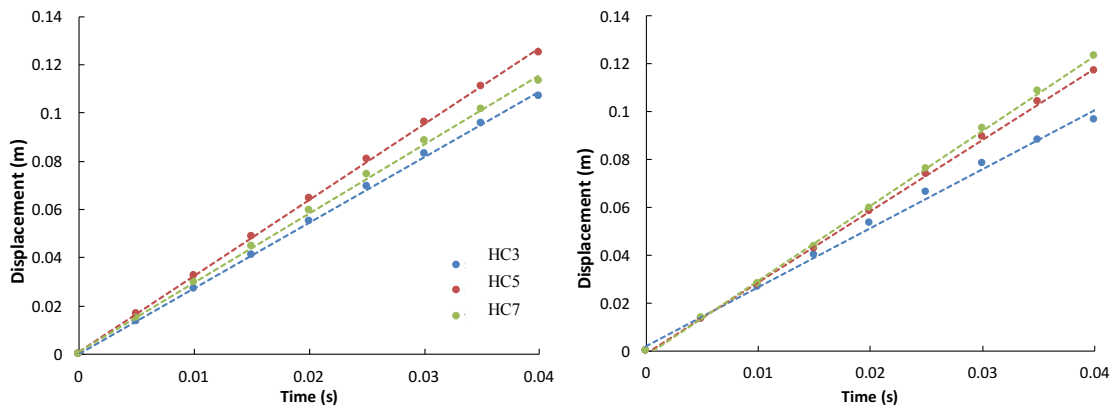
Figure 4.13 Gradients of shoe displacement for both participants.

Table 4-4 Summary of biomechanical results, showing loading conditions, and initial velocities on the three surfaces.

Surface	Peak GRFy (N)	Peak Fshear (N)	Initial velocity (m/s)	Peak COFu
HC3 (slow)	998.84 ± 81.20	907.23 ± 54.63	2.58 ± 0.18	0.92 ± 0.03
HC5 (medium)	890.79 ± 73.87	746.5 ± 91.62	3.05 ± 0.12	0.89 ± 0.02
HC7 (fast)	917.84 ± 196.20	790.59 ± 188.52	2.99 ± 0.18	0.91 ± 0.02

In relationship to the Peak GRFy and Fshear presented in Table 4-4 the highest magnitudes occurred on the slow surface (HC3), which suggest that the player needed to apply more force on the surface to stop, compared to the other surfaces. This is reflected on the initial velocity value, which is the slowest between the three surfaces.

For the calculated peak COFu, presented in Table 4-4, showed no significant difference between the surfaces. In general, the results obtained from this experiment suggest an effect of the surfaces on the shoe velocity during a sliding movement on hard courts. This mentioned effect is suggesting a possible effect of the velocity on the friction, however, the sample size is too small to come with some conclusions. In overall, the analysis presented in this section is helpful to have an idea of what a tennis player is doing in terms of kinematics and kinetics during a sliding movement.

4.3.2 Lab Friction testing

This next stage of studying sliding on hardcourts was to measure friction of the court surfaces under similar conditions as reported by the biomechanical study. The same three hard court surfaces utilised previously (section 4.3.1) and the forefoot of the same adidas barricade shoe 7 from the biomechanics study were used.

The roughness values (R_a) values measured with the Mitutoyo profilometer, described in chapter 3, for the three surfaces tested (presented in section c)), shows a significant difference between HC3 and HC5 and HC7. Table 4-5 shows these differences.

Table 4-5 Roughness values for the three surfaces

Surface	R_a (µm) ± SD
HC3	15.34 ± 2.76 *
HC5	11.9 ± 3.19
HC7	12.20 ± 1.67

*Significant difference compared to the other two surfaces

Friction measurements were carried out with the UoSh test rig and under the test operating procedure described in section d). Due to the capability of the pneumatic cylinders, the measured initial sliding velocities ranged from 0.05 – 0.2 m/s, which were very low compared to the shoe-velocities measured from the video sliding analysis (2 – 3 m/s) and the biomechanical results (2 – 3 m/s). For this reason, an exhaustion valve, shown in Figure 4.14 was installed on the horizontal pneumatic ram, with the purpose to extract the air faster from inside the cylinder, and increase the ram speed. However, the maximum shoe-velocity calculated was 0.8 m/s.
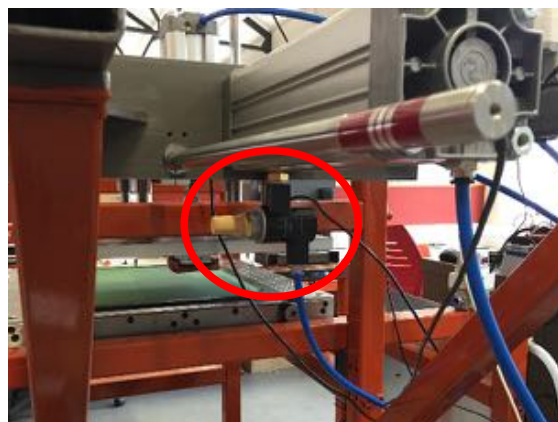
Figure 4.14 Exhaustion valve installed on the horizontal pneumatic ram

Based on the biomechanical results from section 5.3.1, and to recreate similar conditions, it was decided to apply a vertical load of approximately 1000 N and to set the maximum ram pressure possible (6.5 bar) on the horizontal cylinder to aim to achieve the highest shoe velocity.

Figure 4.15 shows a typical graph of one trial. The tendency of the velocity plot is to increase as the 'shear force' increases to a maximum, then as the cylinder reaches its maximum extension, this velocity decreases until it is zero.
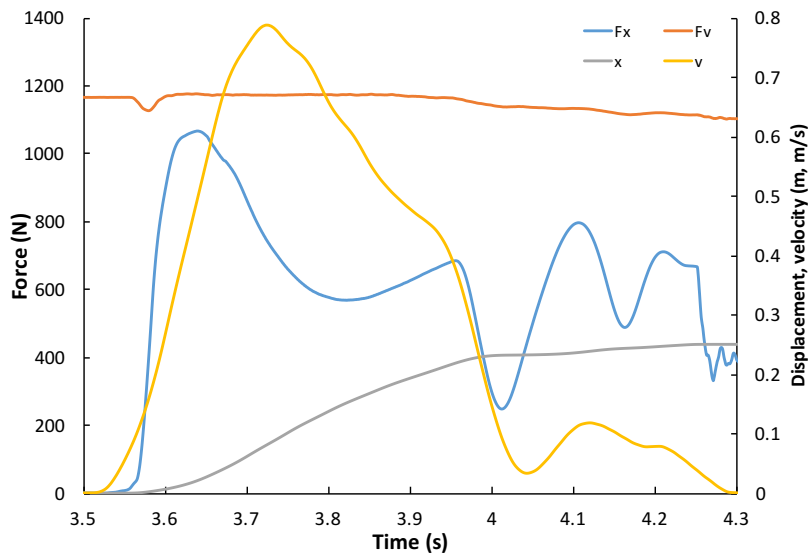
Figure 4.15 Example of graph showing the horizontal and vertical loads, displacement and velocity for one trial.

The difference with this testing compared to the biomechanical results (section 5.3.1) and the previous video analysis (section 5.2.3) is that at the beginning of sliding by players, the shoe has an initial velocity; in contrary, with this rig, the shoe starts from rest, reaches a maximum and then stops.

Table 4-6 shows the frictional results for the three surfaces. Similar to the biomechanical results presented in the previous section, there are no significant differences for the peak COF and horizontal force, between the three surfaces. However, there is a difference in the peak velocities, suggesting that HC3 was the slowest surface. This confirms the roughness data, where HC3 exhibited the highest value.

Table 4-6 Summary of results, showing the peaks of: horizontal force , velocity and COF on the three surfaces.

Surface (Ball pace)	Peak F_x (N)	Peak velocity (m/s)	Peak COF
HC3 (slow)	1057.48 ± 27.95	0.77 ± 0.04	0.92 ± 0.02
HC5 (medium)	1073.55 ± 17.93	0.83 ± 0.04	0.93 ± 0.01
HC7 (fast)	1080.39 ± 33.20	0.85 ± 0.03	0.94 ± 0.04

In conclusion, the series of biomechanical experiments and mechanical testing have been helpful to understand the shoe-surface interaction during a sliding movement on hard courts. Although only a few trials were analysed, for the biomechanical study it can be concluded that:

- Initial velocity calculated on the three surfaces, shows a difference between the 'slow' (HC3) surface and the other two surfaces (HC5 and HC7), which is in good agreement with the roughness data presented in section c).
- Initial shoe-surfaces velocities in the range of 2 - 3 m/s were reported from two participants.

For the lab friction testing, it could be concluded that:

- The loading profile utilised with the test rig, is not representative of typical loading profiles, and hence this could be affecting the friction and velocity measurements.

4.4   Development of a new loading methodology

Dixon et al. (1999) suggested that test devices should ideally replicate the load-profiles of tennis players in combination with appropriate and representative shoe and surface materials providing repeatable measurements. Although some devices, like UoSh developed by (Clarke et al., 2013) has been useful through different studies, the challenge remains specifically in the horizontal and vertical load-profile, which is not completely representative of what an athlete might experience during dynamic movements.

For these reasons, a pilot study was implemented with the objective to develop an alternative method of replicating the loading conditions relevant to sports. Additionally, the results obtained were compared with those obtained using the UoSh.

As explained before in section 3.5.1, the UoSh traction rig uses a traditional friction test loading approach, whereby a test shoe is loaded vertically onto a surface and this load is kept constant whilst an increasing horizontal load is applied until a slide occurs and limiting friction effects can be measured. In reality, the vertical and horizontal loads acting on a shoe during a specific movement are not independent of each other and not applied in this way (Figure 4.16).

In the new approach, the main difference compared to the UoSh traction rig, is that, prior to sliding, the horizontal load is maintained at a constant value and the vertical load is then reduced. In this way, the effective ratio of horizontal to vertical loading (H/V) is still increased until the limiting friction is reached, but the situation leading up to this point replicates more closely a real biomechanical loading. The movement used in this pilot study is a side jump (Figure 4.16 bottom), fully explained in (Damm et al., 2013a) and also used in the study by (Clarke et al., 2013).
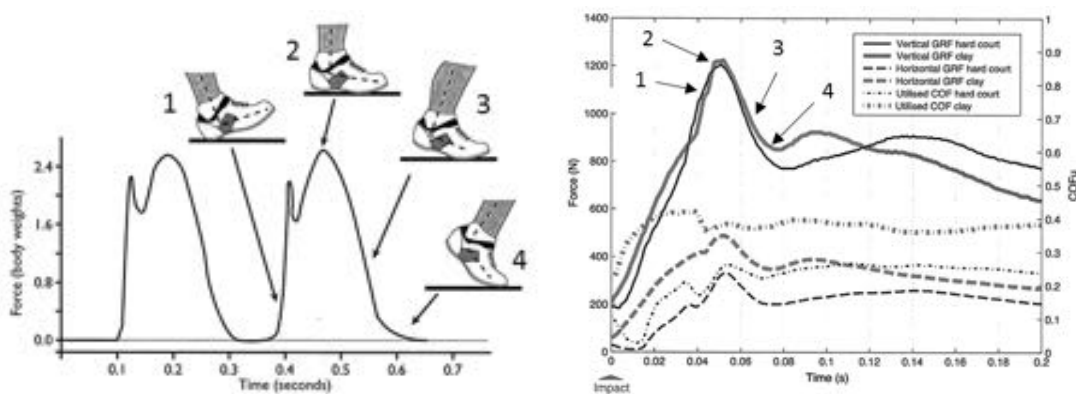
Figure 4.16 Top: Example of heel-toe running action (adapted from (Dixon et al., 2015)); (b) Example of vertical force (GRFz), shear force (F_{shear}) and utilised coefficient of friction (COFu) during a side jump movement on two different surfaces (adapted from Damm et al., 2013 (Damm et al., 2013c)). Both images show the stages of: (1) foot impact, (2) foot flat impact and (3) and (4) forefoot propulsion.

The modified device is shown in Figure 4.17. Two electronic pneumatic regulators were connected to the horizontal and vertical pneumatic rams, in order to allow greater control over the loads applied. In combination with a set of compression springs in the vertical axis, this allowed ascendant and descendant ramp behaviour of the vertical load.
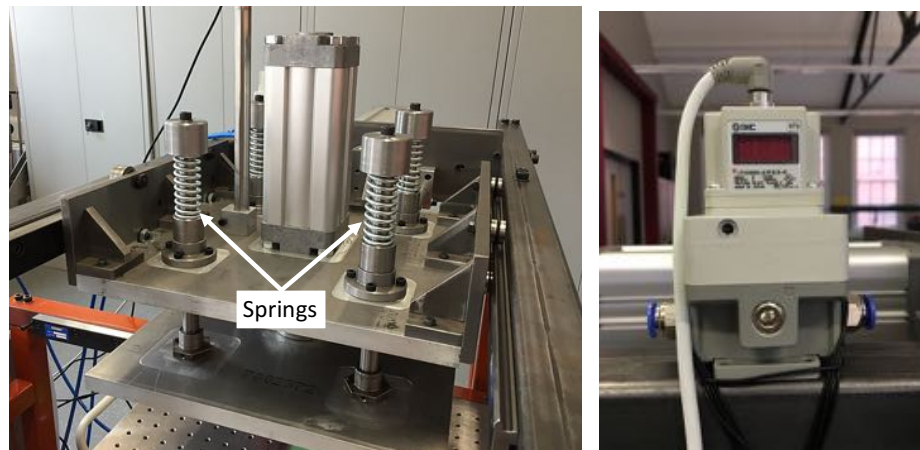
Figure 4.17 Modifications implemented to the UoSh traction rig: four compression springs and two electronic pneumatic regulators.

The shoe and surface sample preparation used was the same as the one developed and detailed in Chapter 3 (Clarke et al., 2013). Prior to testing, the shoe outsole was cleaned with an ethanol solution, and prepared by hand using silicon carbide paper under light pressure. Each test was conducted on a different section of the tennis surface, and any remained debris from the shoe was removed using a clean, soft brush. In a bespoke LabView programme (National Instruments), the load profile for both pneumatic rams was configured. Two analogue voltage signals are sent via signal-conditioning modules (National Instruments) to control the electronic pneumatic regulators. As described previously, the voltage signals from the load cells and the LVDTs are sampled at 5000 Hz simultaneously via signal-conditioning, and displayed in real time using LabView. Examples of these force profiles are presented in Figure 4.18.
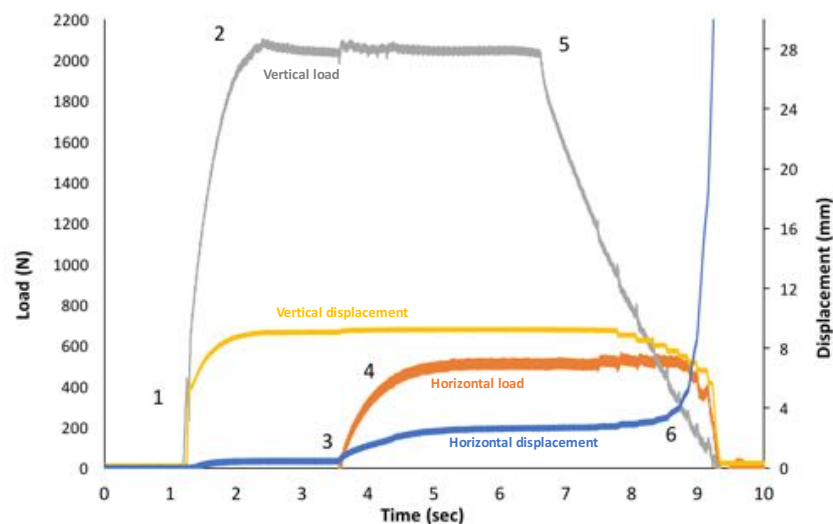
Figure 4.18 Typical plot of the horizontal and vertical load and forces when testing with the TM2 methodology.

The new test protocol is as follows (see Figure 4.18): The electronic pneumatic regulator on the vertical ram is opened (1), increasing the vertical load until a programmed value is reached (2). Due to the application of this vertical force, the springs are mechanically compressed at the same time. When a constant vertical load has been maintained, the electronic regulator on the horizontal ram is opened (3), increasing the horizontal load to a programmed value (4). Now with the horizontal load maintained as constant, the pressure of the vertical ram is reduced gradually using the electronic pneumatic regulator (5), decreasing the vertical load until sliding of the shoe test is initiated (6). The differences between the two methodologies, UoSh (Clarke et al., 2013) and TM2, are highlighted in Table 4-7.

Table 4-7 Description of test methodologies

Test Methodology	Description
UoSh (Clarke et al., 2013)	- Vertical load set to a constant determined value. - Horizontal load increased until test shoe slides. - Horizontal and vertical forces and displacements measured.
TM2	- Vertical load initially maintained at a determined value. - Horizontal load set at a constant determined value. - Vertical load decreased until test shoe slides. - Horizontal, vertical forces and displacements measured.

A series of experiments with both test methodologies (UoSh and TM2) were conducted on the same commercially available hard court sample. Ten profiles of the acrylic surface were measured giving a mean average arithmetic roughness (R_a) determined of 17μm. The same forefoot segment tennis shoe was preconditioned and loaded against the sample surface using the configuration and test protocol described previously. For UoSh, the vertical loads ranged from 400 to 1600 N in intervals of 200 N. This procedure was repeated 3 times for each loading condition. For TM2 the horizontal loads ranged from 450 to 750 in intervals of 50 N. This procedure was repeated 4 times for each loading condition. The limiting ratio of H/V, equal to the static coefficient of friction (SCOF) was calculated for both methodologies.

For the experiments performed with UoSh, the static peak of the ratio between the horizontal and vertical loads, was chosen as the parameter to be utilised for the analysis of the results. A full description of the methodology used to obtain the parameters is explained in section d).

In order to understand the results at the shoe-surface obtained with TM2, plots of forces and displacements in both vertical and horizontal axes were examined. A typical plot from TM2 are presented in Figure 4.19.
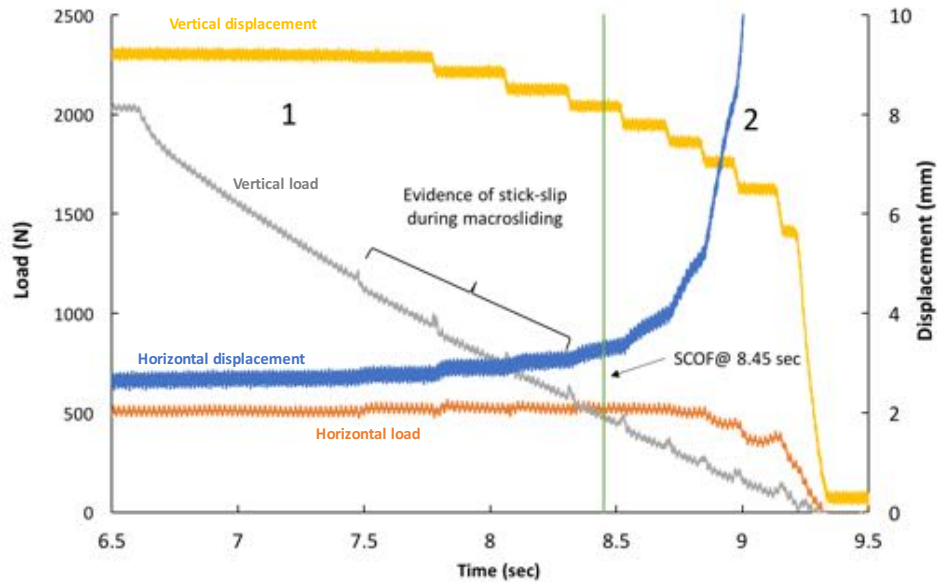
Figure 4.19 Typical plots of load and displacement against time when testing with TM2 for a 550 N of horizontal load test

The plots are characterised by two particular regions: (1) a static region of decreasing vertical load and (2) a period of dynamic movement in which the horizontal displacement, velocity and acceleration of the test shoe increases exponentially (Figure 4.20 and Figure 4.21).

During the static regime, evidence of micro- and macrosliding was observed (Figure 4.20). Microsliding is the period in which the viscoelastic outsole is deformed due to internal shearing (Clarke et al., 2013) and occurs during the application of the horizontal load and manifested by a peak in the horizontal velocity (Figure 4.20).
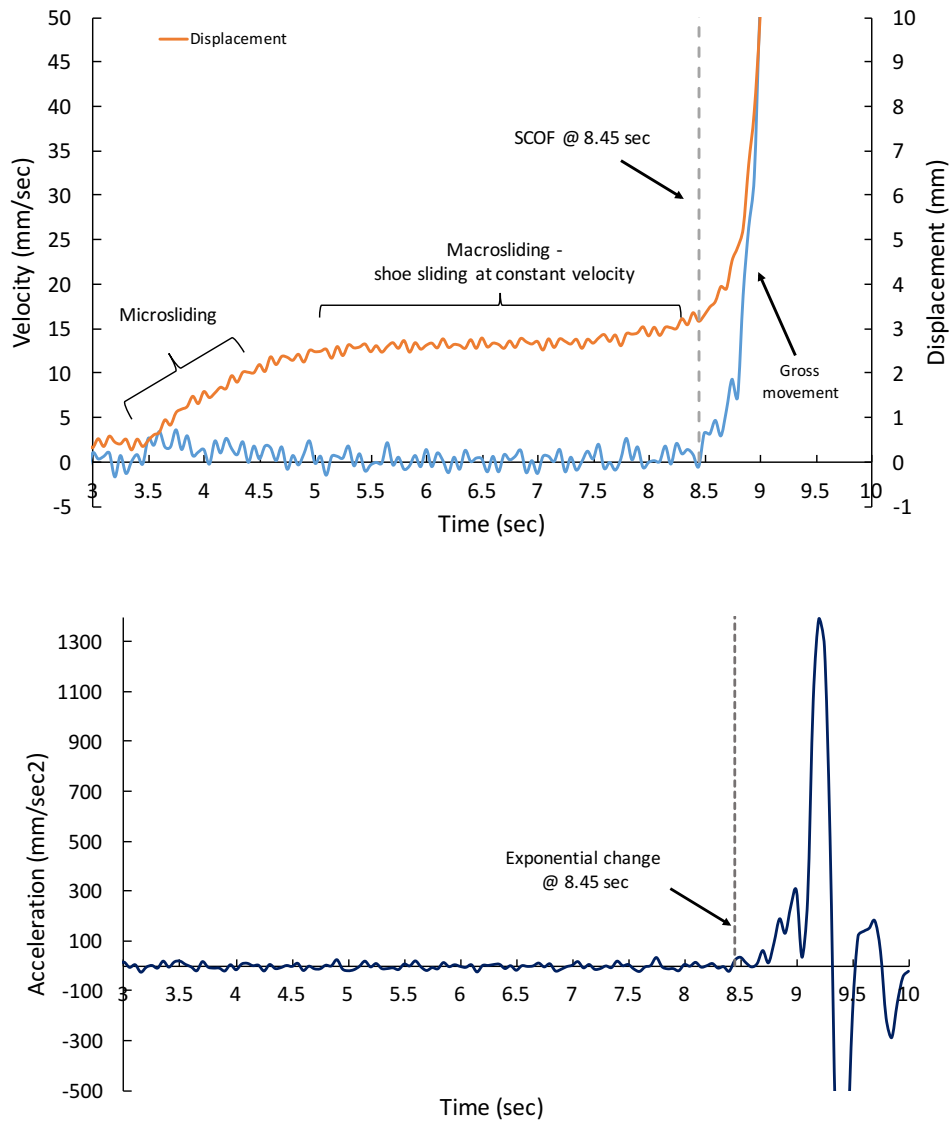
Figure 4.20 Plots of a 550 N of horizontal load test. Top: Velocity and displacement showing the micro and macrosliding during the static regime and the transition point from static to dynamic regime. Bottom: Plot of the shoe acceleration showing an exponential change at 8.45 sec.

Within this period, no sliding between the outsole and the surface occurs. By continuously reducing the vertical load, the test shoe starts to experience macrosliding; which is described as the period of initial relative sliding between the shoe and the surface. During macrosliding the horizontal displacement gradually increases at a relatively constant horizontal velocity (Figure 4.20). In some part of this macrosliding stage, the shoe starts to experience a stick-slip behaviour with the surface, and this can be seen in the velocity data of the vertical load for each test. The example shown in Figure 4.21 shows this stick-slip behaviour as four velocity peaks that occur between the initial decrease of the vertical load and the transition point to gross sliding (SCOF).
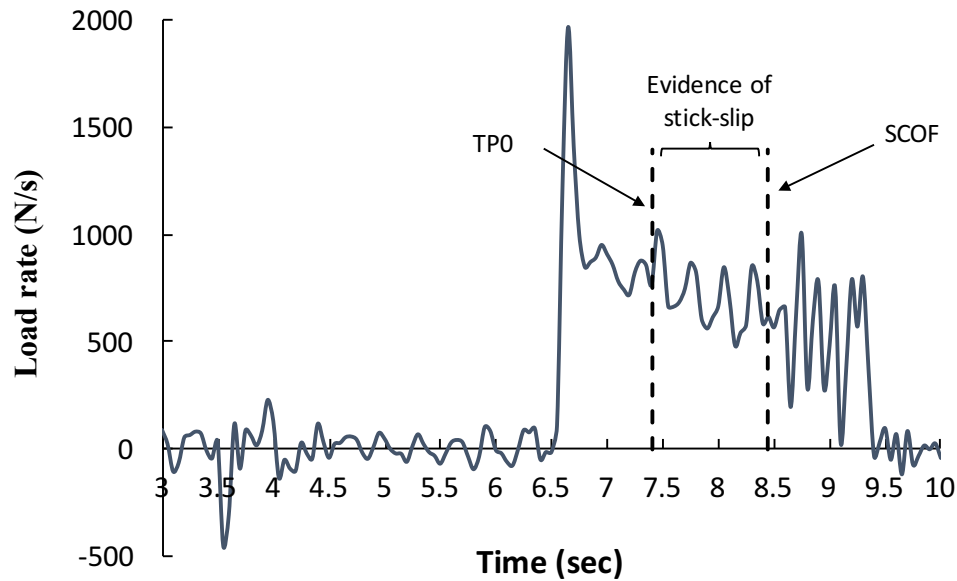
Figure 4.21 Plot of the velocity of the vertical load applied against time for a 550 N of horizontal load test, showing evidence of stick-slip.

By continuing the gradual reduction of the vertical load, the ratio of the horizontal and vertical load (H/V) is increased until the point where the limiting friction is reached and it is equal to the static coefficient of friction. After this point the static regime ends and a period of gross sliding starts, and the velocity increases until the shoe is removed (due to the continued reduction of vertical load due to the action of the springs) and the horizontal load is dramatically reduced.

Two parameters from each plot were extracted, based on the ratio of horizontal and vertical loads (H/V), to understand the particular behaviour at the shoe-surface interface. These were as follows:

1. Transition point 0 (TP0): The H/V ratio value during macrosliding in which the shoe starts to experience a stick-slip effect with the surface.

2. Static coefficient of friction (SCOF): The point just before the shoe velocity increases exponentially and the shoe starts to experience gross sliding. Examples of typical velocity, linear acceleration and horizontal displacement plots are shown in Figure 4.20.

Figure 4.22 shows the relationship of static coefficient of friction (SCOF) with vertical load for UoSh and TM2 respectively. The same tendency for both test methodologies is that as the applied vertical load increases, SCOF decreases.
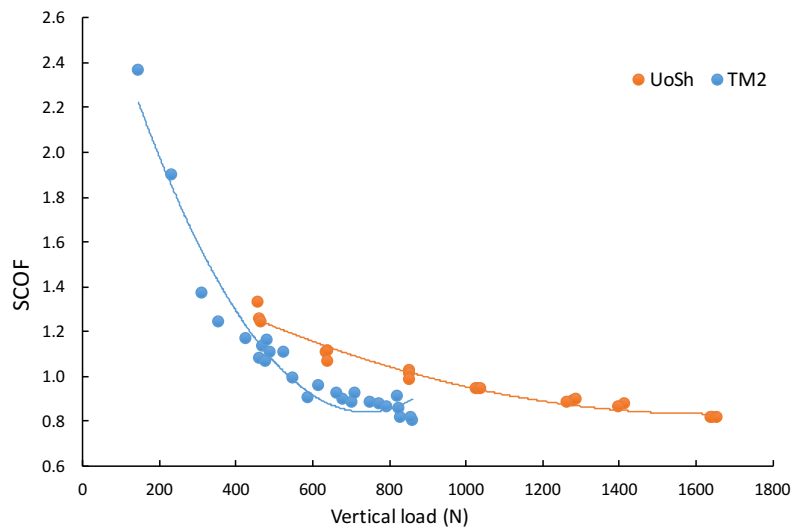
Figure 4.22 Plots of SCOF against the vertical load for each load condition with both methodologies. Best fit 2nd order polynomial shown to illustrate trend.

Figure 4.23 shows the relationship between the horizontal and vertical loads for the calculated SCOF of both methodologies, UOSH and TM2 respectively. In both cases, as the horizontal increases, the tendency of the vertical load increases linearly.
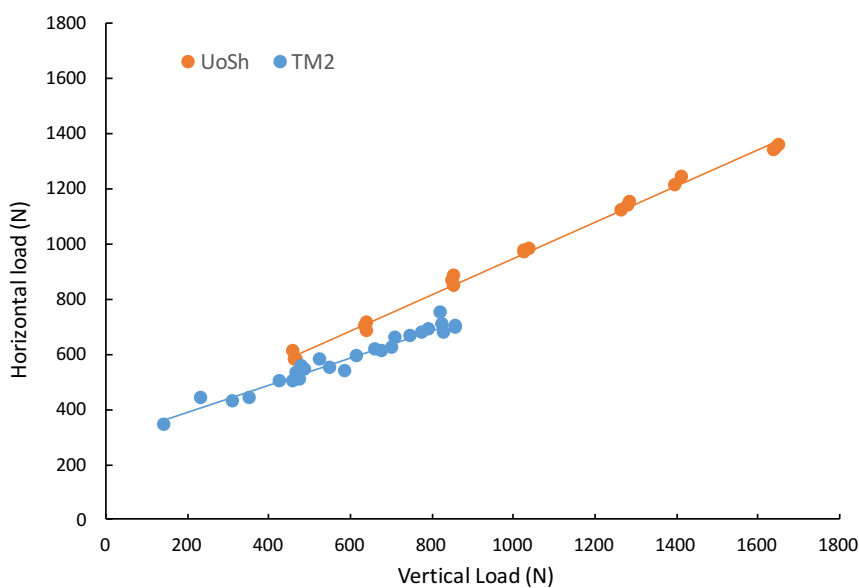
Figure 4.23 Plot of horizontal load against vertical load (with linear regression lines) for both methodologies.

The influence of horizontal loading on the static coefficient of friction (SCOF) is in agreement with previous work done by (Clarke et al., 2013), where it is shown that as the vertical load is increased, SCOF decreases. This suggests that for a particular value of

horizontal load applied, the vertical load needs to be high enough to bring the shoe-surface system closer to the dynamic region to start a gross-sliding of the shoe.

4.5   Discussion of chapter

As discussed at the beginning of this chapter, three main objectives were defined, in order to assess and benchmark the biomechanics of tennis players during specific tennis movements.

Based on the video analysis results of the 'high-risk' movements, rather than focusing on the movements, it is of more interest to analyse the primary and tribological mechanisms (Figure 4.5 and Figure 4.6). 'Sliding' and 'landing' were the primary mechanisms where most of the player's falls occurred. These primary mechanisms are involved during most of the general tennis movements (such as running, turning, turning, etc.) on a tennis court, which support the approach of focusing in more detail on these parameters. In terms of the tribological mechanisms, the results show in general a necessity of the player to reduce or control the amount of shoe-surface friction during the 'sliding' and 'landing' movements. These results also suggest and corroborate the necessity of a friction methodology to measure the level of friction during the shoe-surface interface. This test could be useful to monitor and assess the optimal friction level; and as a result, avoid excessive grip or slipperiness during specific tennis movements.

Additionally, it was identified that tennis players have a tendency to perform sliding movements on hard courts, similar to clay courts. As suggested by (Pavailler and Horvais, 2014) sliding on hard courts nowadays is more common, however there is small literature about the potential increase of performance or the injury risk of this movement. Something to notice from the hardcourt results (Table 4-1) is that most of the final events were played by the same players (top 5), which could be an indication of these players to use the sliding movement more as a strategy rather than a necessity, however this will need to be validated in the future.

A further video analysis presented in Section 4.4, reported sliding shoe velocities of 4 m/s on hard courts. These sliding velocities are in good agreement with the results from the collaborative biomechanical study, validating the video analysis as a useful tool that could be developed in the future to study player movements. Although the biomechanical study represented a good attempt to evaluate and determine the relevant parameters, it only focused on biomechanical parameters such as the loading magnitudes and shoe-surface

velocities. Therefore, there are other intrinsic parameters that need to be studied, such as the orientation of the shoe during this movement, and a more representative loading methodology.

In terms of the development of a new loading methodology, the results presented demonstrate that the novel methodology developed for this study is suitable to determine the transition point from a static to dynamic friction regime of a test shoe in contact with a surface. Additionally, the load-time profile, used with the new methodology (TM2), is closer to replicate sporting foot movements. The slight differences of SCOF calculated and reported from the two methodologies, could be due to how the two methods are subjected to different loading profiles. As described in (Clarke et al., 2013), UoSh focuses its measurements in the peak traction force at a particular constant vertical load, which makes the shoe-surface system to fail. Another possibility could be the effect of the loading on the rubber deformation and contact area. With UoSh, where the vertical load is constant, the contact area and rubber deformation are mainly affected by the increase of shear force. In contrary, for TM2, while the shear force is constant, the contact area and rubber deformation is affected by the vertical load. These interactions have an effect on how the treads of the shoe performs with the profile of the surface tested, and hence will have an effect on the friction experienced.

The evidence of a stick-slip effect during the macrosliding phase in TM2 suggests a loading effect that can be related to what a player might experience during a sport activity. The capability of the new methodology to identify this region could be further explored, to see if this region represents a safe zone in terms of performance and injury risk for an athlete. The evidence of a stick-slip effect during the macrosliding phase in TM2 suggests a loading effect that can be related to what a player might experience during a sport activity. The capability of the new methodology to identify this region could be further explored, to see if this region represents a safe zone in terms of performance and injury risk for an athlete. Although the new methodology was found to more closely replicate the loading profile and allow measurement of the SCOF, it could be concluded that either methodologies could be used to assess shoe-surface interactions. Compared to UoSh, which offer the possibility to take static and dynamic measurements, TM2 offers the possibility to measure the change from static to dynamic only. As a consequence, the choice of methodology, will depend on the sport and the specific movement to be assessed, and the importance of replicating loading conditions.

In general, based on the initial chapter objectives and results obtained in the experiments presented in this section, it is recommended for the new test methodology (Chapter 7), to aim to achieve a shoe velocity close to 4 m/s, in order to simulate realistic player-surface interactions. However, the main challenge remains in replicate high shoe velocities with a light and portable device. Additionally, in terms of the assessment of the loading conditions for the new portable test methodology device, it is more suitable to use the UoSh methodology, as it is more simple and require less components, as one of the restrictions for the new device is to be portable and light. However, any of these methodologies do not solve the challenge of replicating more representative loading conditions with a portable device on tennis courts, and for this reason, it has been proposed to study the relationships between the contact area, pressures and friction (Chapter 6), in order to find a suitable way to apply these high forces.

4.6   Summary of chapter

As a summary, the main conclusions based on the objectives defined at the beginning of this chapter are:

- From the video analysis and due to high incidence, it was decided to focus the development of the new device in two movements: (1) landing and (2) sliding.
- Additionally, a further video analysis measured sliding velocities on hardcourts ranged between 2.8 and 4.5 m/s. Ideally, the values obtained would be useful as foundation for the future test device.
- In terms of loading conditions and with the obtained results, a novel methodology was developed, and validated to a previous one showing to be in good agreement. Having no difference between them, it was decided to use the UoSh approach for the final device.

5. Surface: Tribological mechanisms

5.1   Introduction

Having discussed in the previous chapter about 'high risk' movements of tennis players on the main three different surfaces for tennis (clay, grass and hard courts), and the player's response and adaptability to a tennis court surface, this chapter focuses on the tribological parameters affecting the shoe-surface interaction.

Based on the methodology presented in Chapter 3, this section discusses about the interaction parameters from the surface perspective, which characterise the action of the operational parameters (player's biomechanics) on the structural parameters (shoe and surface). It is well known that on hard court surfaces, roughness is a factor that affects the friction between the shoe-surface interaction in tennis (Clarke et al., 2012a), however, there is small knowledge on clay and grass. For this, this chapter focuses on grass and clay court experimentation. Specifically, on clay, the friction developed by the shoe-surface interface has not been widely studied. There is no regulation on the optimal clay parameters (e.g. particle size, infill volume) used for the preparation of a clay court. In consequence, the variety of clay courts around the world influences, in different ways, the frictional properties of a shoe-surface combination.

As discussed in Chapter 3, this section is composed mainly by field and lab experimentation. Firstly, a series of traction/friction tests with different available test methodologies, were designed on natural grass and clay court surfaces to fulfil the following objectives:

- To measure the traction/friction characteristics of professional tennis courts.
- To compare different traction/friction mechanical devices (Crab Mark III, sled test device, pendulum and lab-based rig), as tools to characterise the frictional properties of tennis surfaces.

Specifically, on grass two main objectives were defined:

- To investigate the influence of humidity and grass height on the shoe-surface traction/friction characteristics.
- To understand the influence of grass tennis shoes on the traction/friction

Subsequently, a field and lab experiments were designed to investigate the influence of two main parameters of clay and artificial clay. These are:

- Clay particle size upon shoe kinematics, friction and player perception.
- To measure the effect of varying the sand infill volume on clay surfaces.

This chapter provides information on how experiments were planned together with results of the friction obtained from the different devices introduced in Chapter 3.

5.2   Grass and clay mechanical testing

The two existing friction test methodologies, the Crab Mark III and the bespoke Sled test devices, shown in Figure 5.1 and described in Chapter 3, were utilised to carry out friction testing on a variety of professional grass and clay tennis courts. The main objectives of this testing was to evaluate existing mechanical test methodologies and its behaviour on different surfaces.

Figure 5.1 The Crab III (top right) and the bespoke sled (left) devices.

The three grass courts (BoE – 7, AELTC-8 and AELTC-9) and the clay court (LTA-4) previously described in section 3.5.2 were tested with the two methodologies in order to compare their results. The court was tested using dry and wet conditions. The water was applied into the surface with a hand sprayer, trying to keep the same conditions before each trial.

The test procedure for both devices previously described in section 3.5.1, was repeated five times for each court location. For the Sled test device, the grass and a omni tennis shoes outsoles, described in section 3.5.3, and shown in Figure 5.2, were mounted and used for the testing.

Figure 5.2 Grass and omni outsoles used with the Sled device.

Six locations on the tennis court were selected for the testing as shown in Figure 5.3 and are referred to as follows:

1. In between the singles and doubles tramlines - *"Tramline"*.

2. Near the net where little activity occurs - *"Net"*.

3. Near the service line where services tend to land - *"Service line"*.

4. Near the baseline where significant player movement occurs - *"Baseline"*.

5. Further back from the baseline where les activity occurs - *"Back baseline"*.

6. On the painted singles tramline - *"Line"*.
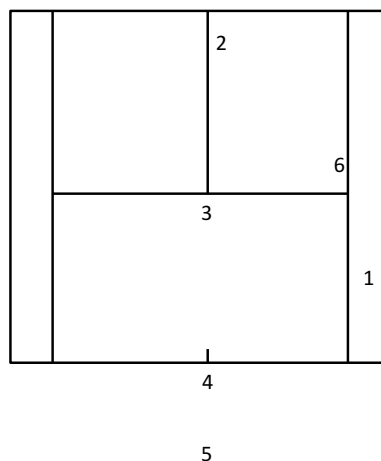
Figure 5.3 Diagram of the six locations tested: 1 – tramline, 2 – net, 3 – service line, 4 – baseline, 5 – back baseline and 6 – line.

Although the test protocols and test devices were the same through this testing, it is important to remark that due to venue availability and permissions, the actual testing was carried on two different stages on different dates, so some of the testing conditions, such as number of test locations on the court (Figure 5.3), moisture conditions and the test outsole varied between the two dates.

The first stage involved the testing of the BoE-7 (grass) and LTA-4 (clay) with both devices. The testing was carried out in the first four court locations (1- 4) (Figure 5.3),

under dry and wet conditions, except for the LTA-4 clay court where, due to time restriction, only the "baseline" location was tested under both moisture conditions. For the sled device on both courts, only the omni shoe was used, and all the testing was carried out with a total sled mass of 11.86 kg (equivalent to a vertical load, V of 116 N). Figure 5.4 and Figure 5.5 show the test locations during the testing.

Figure 5.4 Court No. 7 Bank of England (top left), middle location (top right), tramline location (bottom left) and baseline location (bottom right).

Figure 5.5 Clay testing on LTA-4 court with the sled and Crab III devices.

The second stage of this testing was performed on the AELTC-8 and AELTC-9 grass tennis courts. The six locations were tested with the same test devices, as shown in Figure 5.6. For these particular two courts, and after the first stage testing, in addition to the previous testing protocol, measurements of court temperature and moisture were implemented. The temperature was taken in each location tested, recording average values of 23.6 and 24.8 °C, for dry and wet conditions respectively. Moisture was monitored in each location, using the scale proportioned by a humidity device: dry, dry-, nor, wet-and wet, respectively. For the sled, all testing was done with a total sled mass of 11.71 kg (equivalent to a vertical load, V of 115 N).

Figure 5.6 Court No. 8 AELTC (bottom left), line location (bottom right), net and service line locations (top left) and baseline location (top right).

After all the testing, analysis of variance (ANOVA) tests were performed (using PASW Statistics, version 21) in order to analyse the statistical differences between data sets. ANOVA tests produce a p-value (the probability data sets are significantly different) to assess the statistical significance between two data sets. If $p < 0.05$ then the data sets are significantly different.

5.2.1 Results - grass courts

An example of the results from testing with the Crab III device is shown in Figure 5.7. The COF calculated was very small (less than 0.1), and is not representative of that expected for a shoe/grass court interaction. It is possible that this result was due to the relatively low normal force applied by the Crab III device, allowing the rubber sphere to skid over the slightly flattened grass blades without being in contact with the root/soil system. During testing, this same behaviour was observed in other locations tested. After evaluating the reliability of the data, it was decided to not utilise the device for the rest of the testing.
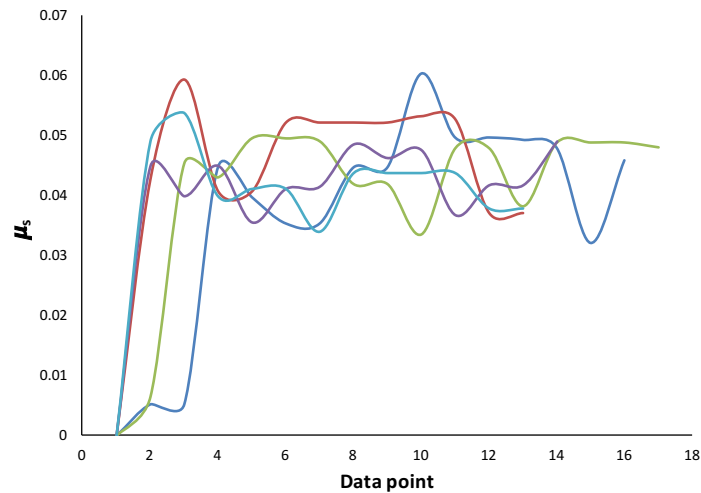
Figure 5.7 Five examples of μ_s traces measured with the Crab III on the BoE -7 court on one location under dry conditions.

BoE – 7 court (8mm grass height)

The mean values of COF measured using the sled are presented in Table 5-1 and Figure 5.8. The dry mean static and dynamic COFs were found to have a statistically higher value than the wet static and dynamic COFs ($p < 0.05$). It is likely that the level of water supplied was sufficient to act as a lubricating layer between the shoe outsole and the grass, in all the locations measured.

For dry conditions, the baseline location was found to have a statistically higher mean static COF than the net location ($p = 0.028$), suggesting that the worn area with low grass cover provides better interlocking friction with the shoe outsole. The mean dynamic COF of the service line location was found to be significantly lower than the tramline ($p = 0.027$), suggesting that once the shoe is moving, a small level of wear, effectively reduces the friction compared with the lusher areas with high grass cover.

For wet conditions, the service line location was found to have a statistically higher mean static COF than the net ($p = 0.043$). In contrast, no significant difference was found for the mean dynamic COF between the different locations, suggesting that the presence of water overrides any effects due to changes in grass cover.

Table 5-1 Mean static and dynamic COF measured with the sled on the four court locations.

Court location	Dry		Wet	
	$\mu_{s\ (1\ SD)}$	$\mu_{k\ (1\ SD)}$	$\mu_{s\ (1\ SD)}$	$\mu_{k\ (1\ SD)}$
Tramline	1.11 (0.07)	1.19 (0.08)	1.02 (0.02)	1.01 (0.02)
Net	1.11 (0.05)	1.31 (0.03)	1.02 (0.02)	1.02 (0.01)
Service line	1.19 (0.04)	1.24 (0.05)	0.96 (0.02)	0.98 (0.02)
Baseline	1.23 (0.04)	n/a	n/a	n/a

Note: the dynamic data for the baseline was not recorded due to a problem with the force gauge
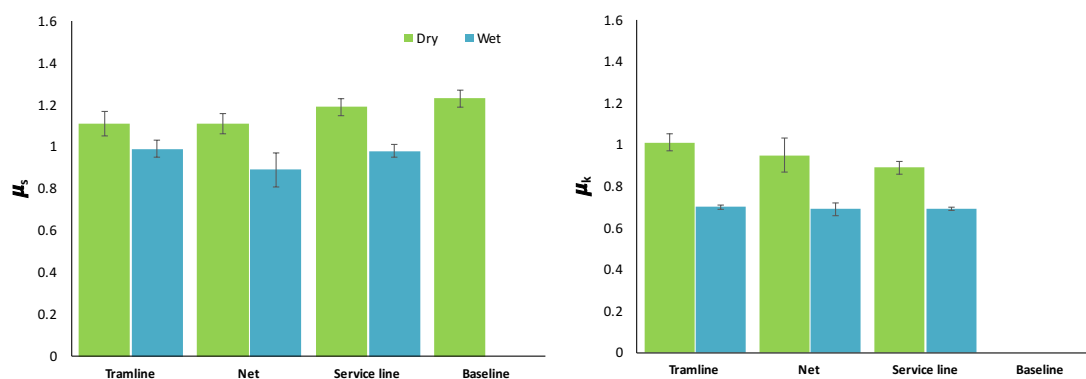
Figure 5.8 Mean COF values measured with the sled on the BoE-7 court under dry and wet conditions with the omni shoe outsole.

AELTC – 8 court (8 mm grass height)

The mean values of COF measured with the sled and grass outsole, are presented in Table 5-2 and Figure 5.9. The dry mean static and dynamic COFs were generally found to have a statistically higher value than the wet static and dynamic COFs ($p < 0.05$) in all the locations measured, except for the baseline location. It is likely that the level of water supplied was sufficient to act as a lubricating layer between the shoe outsole and the grass. It is likely that the relative absence of grass in the baseline region (Figure 5.6) limited the lubricating effect water could have, i.e. it was absorbed by the soil, rather than sitting on the grass blades.

Table 5-2 Mean static and dynamic COF (SD) measured with the grass outsole on the six locations.

Court location	Dry		Wet	
	μ_s (1 SD)	μ_k (1 SD)	μ_s (1 SD)	μ_k (1 SD)
Tramline	1.33 (0.07)	1.02 (0.02)	0.95 (0.04)	0.67 (0.02)
Net	1.30 (0.08)	1.02 (0.02)	1.00 (0.04)	0.70 (0.03)
Service line	1.30 (0.04)	0.96 (0.02)	1.02 (0.03)	0.74 (0.01)
Line	1.11 (0.08)	0.91 (0.02)	0.99 (0.04)	0.75 (0.01)
Baseline	0.81 (0.03)	0.65 (0.05)	0.77 (0.02)	0.64 (0.01)
Back baseline	1.27 (0.06)	1.03 (0.01)	0.96 (0.08)	0.70 (0.02)

For dry conditions (Figure 5.9), the baseline location was found to have a statistically lower mean static COF than the other five locations ($p < 0.05$), suggesting that this worn area with less grass cover provides less grip with the shoe outsole. Further back from the baseline (location 6) where more grass cover was found, higher values of friction were measured. The line location was found to have a statistically higher static COF than the baseline ($p < 0.05$), but significantly lower than the other four locations ($p < 0.05$), suggesting that the paint used for the lines may act as a lubricant layer on dry grass and therefore, reduce the grip of the shoe outsole in contact with the grass.
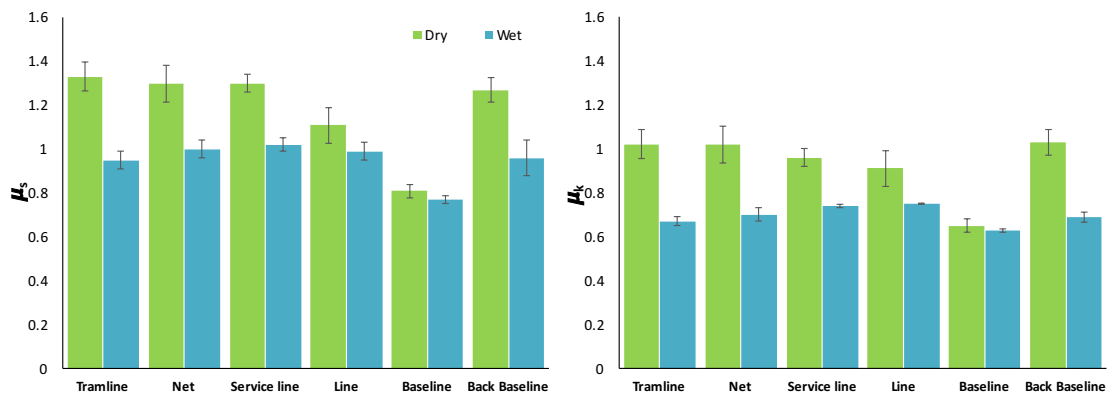
Figure 5.9 Mean static and dynamic COF ($\pm$ 1 standard deviation) measured with the sled on the six court locations (n = 60 for SCOF and DCOF).

A similar pattern of data was found for the mean dynamic COF measurements. The DCOF at the baseline location was found to be significantly lower than the other five locations ($p < 0.05$), suggesting that once the shoe is moving, the worn area with any grass cover provides a sliding effect in contact with the shoe outsole, effectively reducing the friction compared to the lusher grass areas. The line location was found to have a statistically higher mean dynamic COF than the baseline ($p < 0.05$), and was lower than all the other locations (no significance).

For wet conditions (Figure 5.9), the baseline location was again found to have a significantly lower mean static COF than all the other locations ($p < 0.05$) and a significantly lower mean dynamic COF than all the other locations ($p < 0.05$), except the tramline ($p = 0.594$). The line location was now found to have a statistically higher mean dynamic COF than four locations ($p < 0.05$), but not significant higher in comparison with the service line ($p = 0.993$). This suggests that in wet conditions the paint will affect friction differently than in the dry, possibly even repelling water and increasing friction to a degree.

AELTC – 9 court (10 mm grass height)

This court was tested with the grass shoe outsole and only under wet conditions, mainly to measure the possible effect of grass height (8 mm for Court No. 8, 10 mm for Court No. 9). Results are presented in Table 5-3.

Specifically, for static COF, the only location in court No. 9, showing a significant difference compared to the same location in court 8, was the net location. It was found to have a statistically lower mean static COF ($p < 0.05$). The other 5 locations showed no statistical differences between courts. For dynamic COF, the tendency was that 5 of the 6 locations showed a statistically higher mean COF compared to court 8. The only location to show no significant difference is the back baseline location ($p > 0.05$).

These results suggest that increased grass height will effectively act to slow down a player when sliding in wet conditions. However, further testing is required to see if this also happens in dry conditions.

Table 5-3 Court 9 mean static and dynamic COF (SD) measured with the grass sole on the six locations.

Court location	Wet	
	$\mu_{s\ (1\ SD)}$	$\mu_{k\ (1\ SD)}$
Tramline	1.03 (0.03)	0.80 (0.03)
Net	1.10 (0.03)	0.88 (0.01)
Service line	1.08 (0.04)	0.87 (0.03)
Line	0.99 (0.02)	0.85 (0.01)
Baseline	0.77 (0.01)*	0.69 (0.02)
Back baseline	0.99 (0.03)	0.72 (0.01)

5.2.2 Results - Clay court

The results for the clay court LTA–4, presented in Figure 5.10, showed no significant difference for the dry mean static and dynamic COFs between the sled and Crab III devices for all the testing locations. A possible explanation for this could be due to a rolling particle effect that behaves same for both devices, but not same effect with grass. This suggests that either the sled or Crab III devices could be used on clay courts.

A comparison between dry and wet conditions for the 'baseline' location with both devices, showed no significant difference between the dry and wet condition on both static and dynamic COFs. It is likely that the level of water supplied was not sufficient to damp enough the surface, hence increasing the friction.
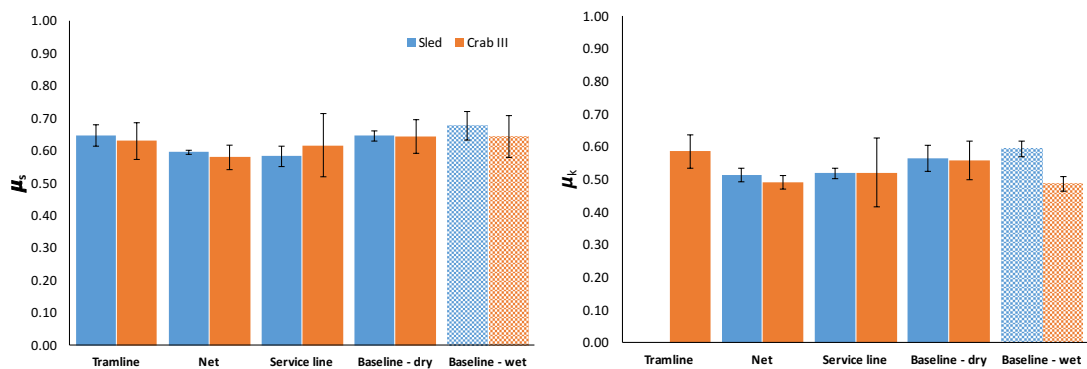
Figure 5.10 Top: SCOF results with ± 1 SD

5.3 Influence of clay particle size on shoe-surface friction

The main aim of this study was to study the influence of certain clay characteristics on the player and shoe interactions. The objectives defined were to identify the kinematics of the shoe during the sliding phase, as it was identified as a 'high risk' movement in Chapter 4; and to mechanically assess the friction of a clay court with different clay particle size.

This section presents the results of a mechanical testing of an elite clay tennis court at the Real Club de Polo in Barcelona, Spain. This was part of a wider and collaborative study between the ITF, The University of Sheffield, INCOTEC (Barcelona, Spain) and the Instituto Biomecánica de Valencia (IBV), Spain. The ITF provided the high speed video cameras, INCOTEC prepared the tennis clay courts for the testing and the biomechanics

and mechanical testing was done in conjunction by The University of Sheffield, INCOTEC and IBV.

The following study was published in the conference proceedings of the 10th International Sports Engineering Association, Sheffield, UK (Ura et al., 2014a).

5.3.1 Biomechanics trial

Velocity and displacement data focusing on one shoe were collected by the University of Sheffield and IBV, on the clay court RCB 28, previously described in section 3.5.2, as part of a biomechanics trial. The data was collected for two movements: a change of direction movement and a sliding forehand. Eight experienced clay players (1 female and 7 male) volunteered to participate in the trial which took place during the Conde de Godó tennis tournament in Barcelona, Spain.

Prior to the testing, the original clay of the two base-line areas of both ends of the clay court was removed and replaced with the clays described in Table 5-4. The base clay used for both ends was the same, only the particle size varied. The preparation, performed by the members of INCOTEC, involved on passing the clay particles through sieves of different grade to allow a controlled mix of particle size.

Table 5-4 Clay court surfaces description

Surface reference name	Description
CC1	Particle size: 30% > 0.5mm and 70% < 0.5mm
CC2	Particle size > 0.5mm

The two dynamic movements were assessed within two separate drills (Figure 5.11). For both drills, the participants began at the one side of the baseline in a ready position (1). In drill (a), the participants were asked to perform a sliding forehand foot plant. The ball was sent to the centre of the baseline and the participant was required to run from point (1) to (2) and then slide whilst simultaneously hitting the ball with the racket. In drill (b) the participants performed a change of direction movement. The participant was required to run at speed from point (1) to point (2) and then a ball was sent to point (3) allowing the player to perform a change of direction movement. Three successful trials for each drill were required. Participants had adequate time to familiarise themselves with the court, drill and warm up before testing.
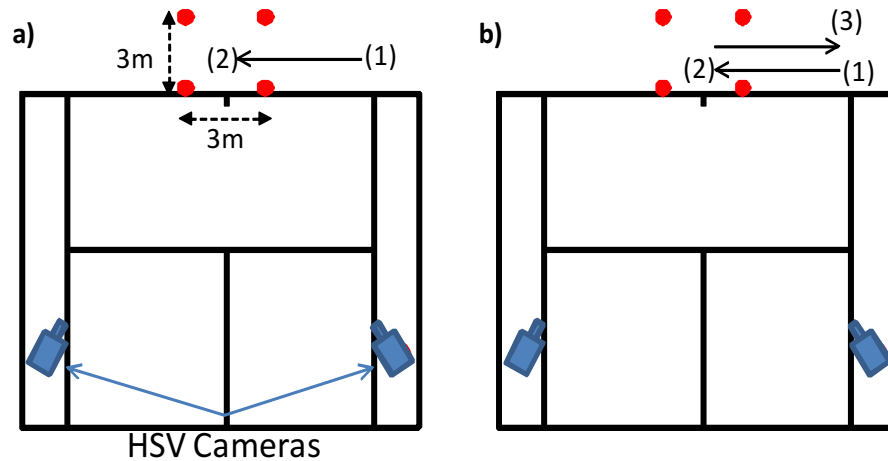
Figure 5.11 A schematic diagram for: a) sliding drill: (1) participants starting position, (2) sliding position; b) turning drill: (1) starting position, (2) turning position, (3) return to starting position.

3D Kinematic data was collected for both movements skills using two synchronised high speed video cameras (*Phantom 4.1*) recording at 300 fps. A 3 x 3 x 1 m calibrated volume was situated at the centre of the baseline (Figure 5.12). The two cameras were positioned close to the net to record within the volume. The footage recorded for each drill was triggered manually when the player made the movement inside the defined volume. One marker was placed upon the tip of the shoe of the dominant leg that carried out the sliding movement. The number of markers was limited to one, to allow quick testing within the short time period allowed with the players. It was felt that this was adequate to gain useful measurements for comparison between the two surfaces. A checkerboard was used to perform the calibration to define the 3D space (Choppin et al., 2005, Choppin et al., 2007) before the players arrived.

All the footage was digitised with the help of the software Check 3D (developed by the Centre for Sports Engineering Research at Sheffield Hallam University, Sheffield, UK). Check 3D allows the calculation of three dimensional positions of markers in a specific volume. Shoe kinematic data, initial velocity, and total displacement during the sliding and change of direction movements, were all obtained from the footage. An absolute test of calibration and digitisation process was assessed by measuring the size of some sample squares of the calibration checkerboard from the footage recorded, and these were compared to the known size of the squares. It was found that the measurement could be reconstructed to within ±2.5 mm on average.
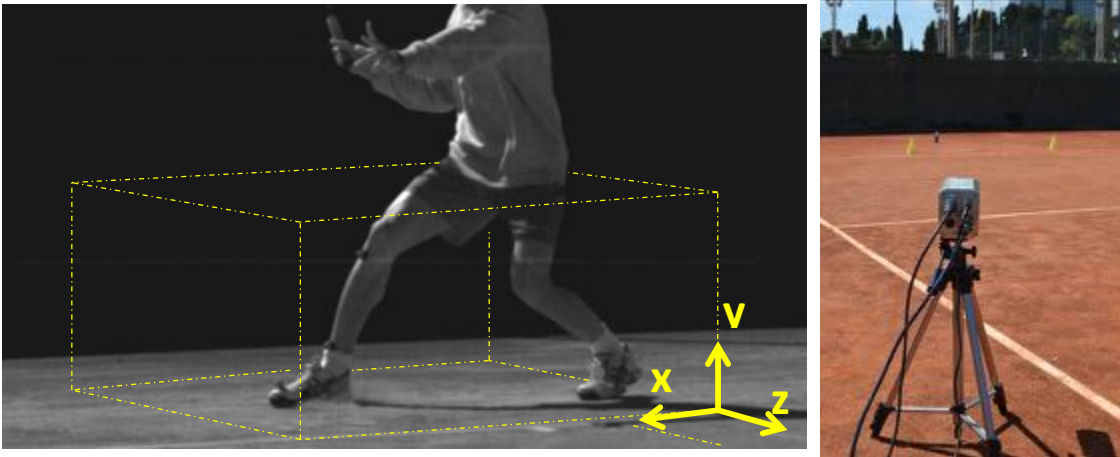
Figure 5.12 Diagram of global axes and volume defined for the 3D filming and high speed camera pointing the defined volume.

5.3.2 Mechanical data

Friction tests were conducted on the surfaces using three different devices: the pendulum test, the Crab Mark III test and the bespoke friction sled (Figure 5.13). These test devices, previously described in Chapter 3, were used to examine static and dynamic friction from the base-line areas of both ends previously described. All data was collected in conjunction with colleagues from INCOTEC and IBV. The sled testing was carried out with a total mass of 13.78 kg. The testing procedure consisted of attaching the force gauge to the sled and dragging the device for an established distance of 350 mm.

Prior to each test with the three devices, the test rubber or shoe outsole were brushed to maintain the same conditions throughout. Each trial repetition was made on a 'fresh' area of the court. The SCOF and DCOF were calculated according to each device procedure described in Chapter 3.

Figure 5.13 Left: The bespoke sled and The Crab III; Right: The pendulum device.

Table 5-5 provides means and standard deviations from the the friction data collected on both base-line areas. A one-way ANOVA with repeated measures was used to examine SCOF and DCOF between the surfaces and the devices.

For the Crab III and the bespoke sled device CC2 had significantly lower static and dynamic coefficients of friction compared to CC1 ($p < 0.05$). In contrast, the pendulum was not able to measure significant differences ($p = 0.529$) between the surfaces. Between devices, the Crab III and the sled device showed no significance ($p = 0.732$) in the measurements for the CC2 surface. However, for the CC1 surface statistical differences ($p < 0.05$) were found.

The same behaviour occurred for the Crab III and the pendulum, with no significant differences ($p = 0.174$) being found between the devices for the CC1 surface. However, for the CC2 surface, statistical differences ($p < 0.05$) were found. As described in section c), the pendulum device only measures dynamic friction, so any SCOF measurements were obtained with this device. For the sled device, due to a problem with the force gauge, no dynamic data was recorded on the two surfaces tested.

Table 5-5 Means and 1SD for mechanical data

Mechanical test	CC1 surface		CC2 surface	
Frictional measures	SCOF	DCOF	SCOF	DCOF
Pendulum	n/a	0.602 ± 0.126	n/a	0.558 ± 0.107^{1}
Crab III	$0.675 \pm 0.116^{*1}$	$0.516 \pm 0.070^{*}$	$0.472 \pm 0.054^{*}$	$0.375 \pm 0.012^{*1}$
Sled Device	$0.462 \pm 0.053^{*1}$	n/a	$0.428 \pm 0.031^{*}$	n/a

*denotes significant difference between surfaces (same device)
[1] denotes significant difference between devices

Table 5-6 shows the shoe-kinematic data for the two drills performed by the players on the two surfaces. A one-way ANOVA with repeated measures was used to examine the differences in data. For the sliding forehand movement, only the total sliding displacement showed a significant difference between the two surfaces ($p < 0.05$). No statistical differences were found for the initial sliding velocities ($p = 0.668$). For the change of direction movement, the initial sliding velocity and total sliding displacement movements showed no statistical difference ($p = 0.399$; $p = 0.195$).

Table 5-6 Means and SD for shoe-kinematic data for the sliding forehand and change of direction movements on both surfaces.

Variable	CC1 surface	CC2 surface
Sliding Forehand		
Initial sliding velocity (m/s)	4.16 ± 1.22	4.09 ± 1.11
Total sliding displacement (m)	0.48 ± 0.16	0.74 ± 0.13*
Change of direction		
Initial sliding velocity (m/s)	3.06 ± 1.08	3.76 ± 0.83
Total sliding displacement (m)	0.51 ± 0.18	0.87 ± 0.44

*denotes significant difference between surfaces

Sliding displacement was 64% further on the CC2 surface compared to the CC1 surface. This suggests that the inclusion of small particles (< 0.5 mm) on the CC1 surface increases the friction during the sliding movement. The mechanical testing performed with the three devices confirms that there is available lower friction on the CC2 surface, compared to the CC1 surface. A study by (Mills et al., 2009), where the effect of size particle on shoe-floor contact friction was analysed, found that particles sizes below 0.06 mm under a compression force, behave as a thin layer to encourage a sliding. However, particles greater than 0.06 mm are less likely to join and act as single entities, encouraging a rolling behaviour. In relationship to our study, this suggests that the CC1 surface with smaller particles included, may allow a balanced behaviour including sliding and rolling particles, whereas the CC2 surface particles may encourage rolling. It is suggested then to compare the mechanical and biomechanical results against player perception in order to find a correlation between the mechanical and biomechanical data with player perception.

5.4   Influence of clay sand infill volume on traction/friction

The aim of this study was to investigate the effect of varying the quantity of infill sand on shoe-surface friction for an artificial clay court. The laboratory-based mechanical test rig (UoSh), described in detail in Chapter 3, and shown in Figure 5.14 was used to measure the friction force developed at the shoe-surface interface. In addition, perception data were collected by our colleagues from the University of Exeter.

The following study was published in the conference proceedings of the 10th International Sports Engineering Association 2015, Sheffield, UK (Ura et al., 2014b).

The artificial clay court surface tested (AC2) is the same one used in the studies by Damm et al., (2011) and Clarke et al., (2013), previously described in section 3.5.2. It was tested under different volumes of infill sand (10, 12, 16 and 20 kg/m^2).

The test procedure was repeated 5 times for each condition, and was designed to best replicate a sliding movement. According to Damm et al., (2011), the peak vertical GRF of a tennis player will exceed 1000 N during specific movements like side jumping and sliding; therefore, the friction tests were conducted under a range of normal forces (1000 – 1500 N in increments of 100 N). First, the forefoot section of the adidas barricade shoe, described in section 3.5.3 , is attached onto a shoe plate Figure 5.14. The synthetic clay surface is then secured on a platform that is slid into place via a bearing and rail system before being secured.

The front shoe attached was rotated 90° to the direction of the movement in order to replicate the likely shoe orientation during a sliding movement. The artificial clay surface was rigidly attached into a polycarbonate tray in order to contain the particles of sand. The sand was brushed by hand into the membrane, and then further particles were added in order to meet the specifications as shown in Figure 5.14. Prior to every test run, the particles were brushed to ensure an approximately even distribution. For wet conditions, the quantity of water used was the same as described by Clarke et al. (2013) which aimed to simulate 24 minutes of play in light rainfall (1 mm of rainfall in total). Water was added with a calibrated sprayer. The water was sprayed by hand, being careful to cover the surface evenly.

Figure 5.14 Left: The laboratory based traction rig; Centre: ACC surface prepared and mounted; Right: Shoe sample attached.

Perception data were collected during a separate trial at the University of Exeter. A group of 16 participants volunteered to participate in this study. Perceptions were collected using visual analogue scales following the trials on each surface. The scales were 100 mm length, being 0 and 100 low and high perception from the player for each

parameter respectively. The perception parameters evaluated by the participants were: (1) predictability, (2) grip, (3) hardness, (4) Qual 1, (ability to change direction), and (5) Qual 2, (ability to slide).

Figure 5.15 Example of participant performing a turning movement on the artificial clay surface

The participants performed a turning movement (180° turn at 3.9 m/s ± 0.20 m/s) on three different volumes of sand 12 kg/m^2, 16 kg/m^2 and 20 kg/m^2 respectively (Figure 5.15) matching three of the samples surfaces tested in the lab at Sheffield. Mixed model ANOVA was used to examine the influence of the group and volume of sand perceptions (significance = $p < 0.05$).

A full description of the methodology used to obtain the parameters from the experiment is explained in chapter 3.3. Linear regression analysis was used to analyse the relationships found for the different conditions. The square of the Pearson correlation coefficient (R^2) was used to determine the strength of the linear correlation between the data sets. The corresponding p-value was used to determine whether the linear relationship was statistically significant. If $p < 0.05$, then a significant relationship between the two data sets is said to exist. Table 5-7 shows strong and significant linear relationships found for each surface condition between friction parameters and the normal applied force ($p < 0.05$).

Table 5-7 Linear relationship coefficients showing effect of normal force applied on each friction parameter

Surface	Peak friction force		Average dynamic friction force	
	R^2	p	R^2	p
10 kg/m^2 dry	0.990	< 0.05	0.992	< 0.05
10 kg/m^2 wet	0.925	< 0.05	0.985	< 0.05
12 kg/m^2 dry	1.000	< 0.05	0.994	< 0.05
12 kg/m^2 wet	0.997	< 0.05	0.994	< 0.05
16 kg/m^2 dry	1.000	< 0.05	0.998	< 0.05
16 kg/m^2 wet	0.997	< 0.05	0.999	< 0.05
20 kg/m^2 dry	0.990	< 0.05	0.984	< 0.05
20 kg/m^2 wet	0.992	< 0.05	0.999	< 0.05

Figure 5.16 shows the relationships between static peak friction force and normal force. For 10 and 12 kg/m^2 sand infill, as normal loading increases, the surfaces were found to lower friction when dry compared to when wet. However, the opposite behaviour was observed with the 16 and 20 kg/m^2, which had a greater peak friction force in dry conditions.

In Figure 5.18-left the effect of the infill volume is shown. For the 10 kg/ m^2, the SCOF under dry and wet conditions is the highest value compared to the other sand volumes, however, as the volume of sand infill increases the friction in general decreases. Something to notice for the lower volumes (10 and 12 kg/ m^2) is that the SCOF under wet conditions is higher than the dry, however as the volume increases, the opposite behaviour occurs.
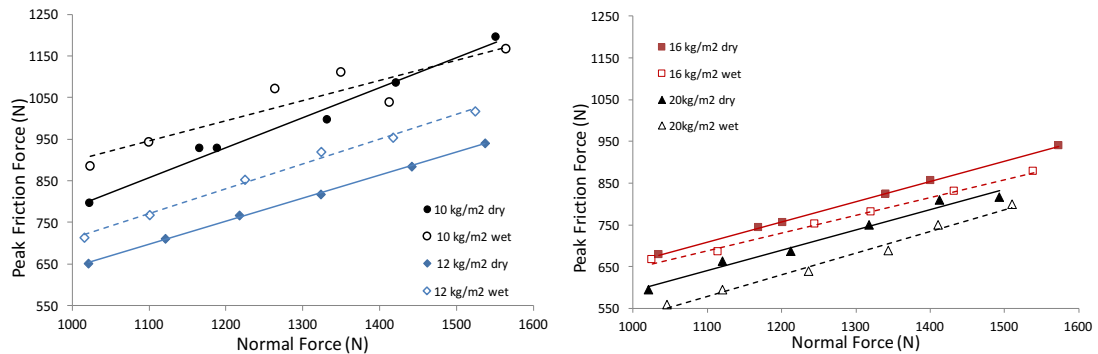
Figure 5.16 Plots of peak friction force against normal force (with linear regression lines).

Figure 5.17 shows the relationship between the average dynamic friction force and normal force. Strong and significant linear relationships were found for each surface condition. For 12 and 20 kg/m^2, the dry conditions exhibit lower average dynamic friction compared to wet. However, in an opposite trend, the 10 kg/m^2 dry condition develops greater dynamic friction as opposed to wet. For the 16 kg/m^2 no differences were found between dry and wet.

In Figure 5.18-right the effect of sand volume on the DCOF is presented. Similar to the SCOF the highest DCOF occurs at the 10kg/ m^2 volume, however as the volume increases to 12 kg/m^2, the DCOF decreases and stays with no variation for the 16 and 20 kg/m^2 conditions. Contrary to the SCOF at 10kg/ m^2 the dry SCOF is higher than the wet, however for the 20kg/ m^2 the opposite behaviour can be observed.
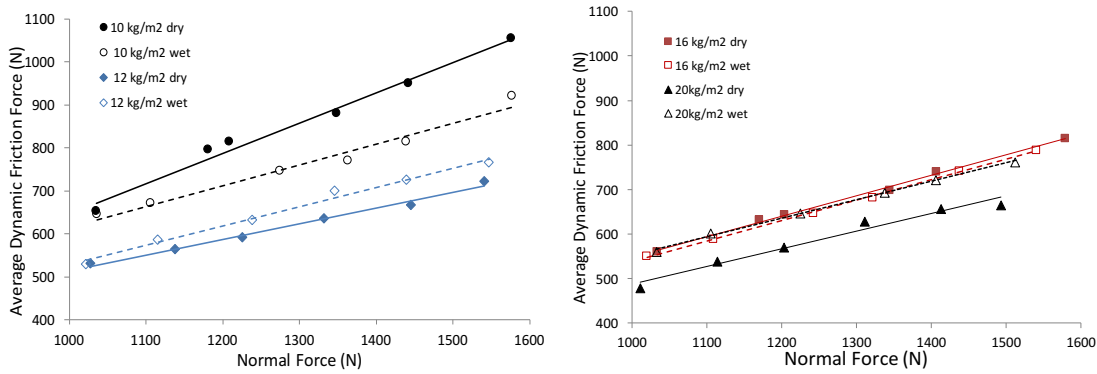
Figure 5.17 Plots of dynamic friction force against normal force (with linear regression lines).
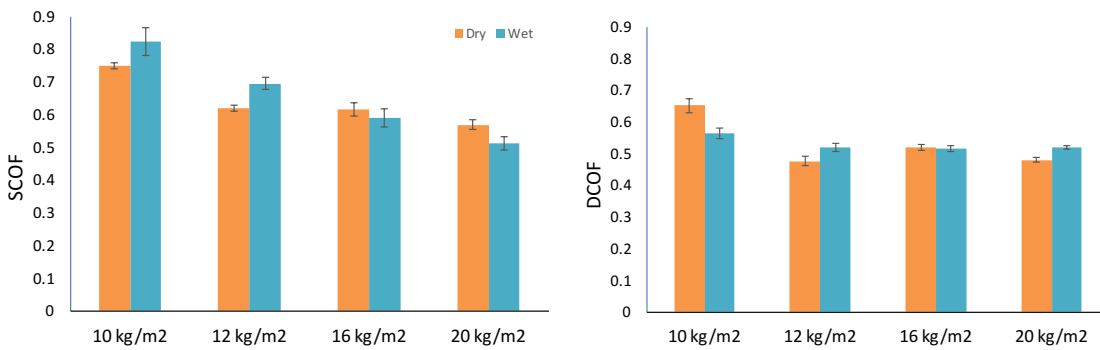
Figure 5.18 Plots of SCOF and DCOF under dry and wet conditions for the 1300 N normal force.

Significant effects were found for three of the five perception conditions reported. Figure 5.19 highlights that the 12 and 16 kg/m^2 volumes are significantly more predictable compared to 20 kg/m^2 ($p = 0.001$). It shows that 16 kg/m^2 is significantly provides more grip compared to 20 kg/m^2 ($p = 0.017$), and that 16 kg/m2 is statistically harder compared to 20 kg/m^2 ($p = 0.011$).
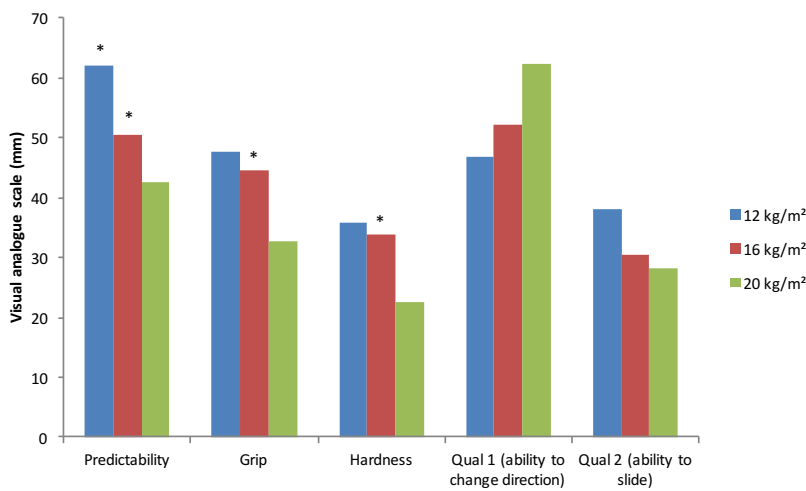
* denotes significant difference against 20 kg.

Figure 5.19 Mean and SD for the perception conditions under dry conditions. Qual1 – lower the number = easier to slide, Qual2 – lower the number = easier to change direction.

The results presented demonstrate that the quantity of artificial clay significantly influences the friction developed at the shoe-surface interface. A study in which the effect of size particle on shoe-floor contact frictions is analysed is the one presented by Mills et al. (2009). In this investigation is reported that the threshold, at which dry particles are less likely to join and act as single entities, is 60 μm. In contrast, dry particles below 50 μm cohere, and act as a thin layer (Mills et al. 2009). In consequence this will affect the mechanical behaviour of the surface.

Clarke et al. (2013) reported that during the dynamic period the moisture of the wet clay is lubricating the shoe-surface contact and inter-particle contact; hence reducing its resistance to dynamic shear. The dynamic period of the shoe sliding on the clay surface can be defined as a stick-slip. It was also observed that during the sliding period, sand particles were built up ahead of the shoe as described by Clarke et al. (2013). The effect of the infill volume on friction when comparing the SCOF and DCOF for 10 and 20 kg/m^2, as the volume increases these decrease, could be explained that at 10 the shoe compresses more the sand, and it may be a contact between the shoe and the surface fibres, making more difficult to move. However, as the sand infill volume increases, the sand starts to have a bigger effect, and therefore, the SCOF and DCOF could be affected by a ploughing effect.

In relation to perception, the 16 kg/m^2 perceived grip by the participants is in good agreement with our mechanical results under dry conditions, which show that this volume is higher in terms of peak friction force and average dynamic friction force compared to the values for the 20 kg/m^2 volume. This suggests that the players experience higher static and dynamic friction on the 16 kg/m^2 during the turning movement, and this is perceived by the participants as more grip compared to the 20 kg/m^2.

5.5   Discussion of chapter

As discussed at the beginning of this chapter, a series of experiments were developed to evaluate and identify the interaction parameters for a shoe-surface interaction with the objective to assess the design of the mechanical test methodology.

The first experiment involved a series of testing, with three different portable test methodologies, on grass and clay tennis courts. These test devices are characterised for their portability and operating simplicity, however, specifically the Crab III, due to its very low normal load applied, showed a lack of capability to measure friction on a grass tennis court. In contrast, based on the results with the bespoke sled, it was proved that it can be an approach to measure the friction between a tennis shoe and a grass tennis court. The results showed an ability to measure a difference in friction under dry and wet conditions. Additionally, thanks to this mechanical testing, further interaction parameters were identified, such as grass height, worn areas of a court, and line paint. In general, these conditions and interaction parameters were found to have an effect on the friction. Therefore, the future test methodology needs to measure the friction and distinguish between these interaction parameters.

In contrast the Crab III and the bespoke sled were found to be useful to measure the friction on a clay tennis court. A comparison between dry and wet results showed no significant differences, however these are specifically for one type of clay and under specific watering conditions. It is likely that the level of water supplied was not sufficient to damp the surface, hence increasing the friction. According to anecdotal comments from groundsmen (Newcomb, 2014), the clay courts at Roland Garros are watered after each match and at the end of the day to help the brick keep its colour and keep from blowing away. It is more about aesthetic rather than a technical reason. Under rain conditions, it is well known that the match should continue, until the umpire decides when to stop. There is no rule and any reference of the effect of watered clay on the friction generated during the shoe-surface interface. For these reasons, the effect of wet conditions on a clay court needs to be further investigated.

Subsequently, field and lab experiments measured the friction for other interaction parameters such as particle size and infill volume for clay/artificial clay were examined. As no regulation of clay particle size or infill volume on a tennis court has been found, the results presented in this section become relevant. Smaller particles size ((< 0.5 mm)

increase the friction during a sliding movement compared to particles bigger than 0.5 mm, affecting the sliding displacement. Moreover, it was found that the amount of artificial clay will significantly decrease the static coefficient of friction, and this could represent a potential injury risk for a tennis player. As mentioned previously, there is no regulation about the clay properties on a tennis court, which could be leading to have different frictional conditions on different clay tennis court around the globe.

Again, the necessity of a test device to monitor and measure these courts is imperative in order to identify and study in detail more tribological parameters, and to try to standardise clay surfaces around the world in terms of friction. In order to get a better understanding of surface characteristics on the friction behaviour, further testing needs to be performed, and once the mechanisms involved are understood, surface properties can be modified to increase performance and reduce injury risk.

The findings presented in this chapter aid the understanding of tennis players' perceived response to a tennis court surface and will assess the design of the final test device. However, shoe characteristics in contact with surfaces, and their effect on friction need to be studied to gain a better understanding of the shoe-surface interaction. Chapter 6 presents a series of experiments with relevant results.

5.6   Summary of chapter

Experimental field and lab-based friction data have provided empirical knowledge into the manner in which surfaces can influence friction forces on grass and clay tennis surfaces during a shoe-surface contact. The main findings in this chapter were:

- In general, the mechanical friction testing performed on two different clay tennis courts with the Crab III and the bespoke sled showed both devices to be useful to measure friction either clay or grass surfaces.

- For the grass testing, based on the results presented in this section over different grass tennis courts, *moisture, wear* and *grass height* were found as parameters, in general, to have a significant influence on the shoe-surface interaction.

- The experiments performed over clay and artificial clay, confirmed a significant effect of *clay particle size* and *sand infill volume* on the shoe-surface friction. The volume results were compared and validated with player perception data, suggesting a player's sensitivity to small changes in sand infill volumes.

6. Tennis shoes: tribological mechanisms

6.1   Introduction

In previous chapters 4 and 5, the biomechanical conditions, surface characteristics and their effect on friction have been studied in order to develop a test to measure the tribological characteristics of the shoe-surface interface. However, the behaviour and the mechanical response of the tennis shoes during dynamic movements are equally important. Tennis shoes are made from elastomers with viscoelastic behaviour, which respond according to the various dynamic movements and frictional demands on different surfaces.

In relation to the design of the portable test methodology, due to the variety of tennis shoes on the market and the evolution of shoe outsoles throughout the years, one of the faced challenges will be to develop a standardise test "shoe". This needs to be able to simulate a tennis shoes on different tennis surfaces. Section 3.5.3 shows the study of some commercial rubbers and the comparison of their mechanical properties to actual tennis shoes.

In this chapter a series of experiments and results are presented with the objective to test some interaction parameters and understand the behaviour of rubber friction under specific conditions and tennis movements. These experiments are complemented with the study and material characterisation of the rubber of some available commercial shoes (section 3.5.3), in order to define their contribution for the final portable test methodology.

Therefore, this chapter starts by studying some tribological parameters identified in the literature review, such as shoe orientation and shoe-surface temperature and their effect on friction. Subsequently it focuses on studying the relationship of contact area, pressure and friction in order to find a solution to the challenge of applying high normal forces with portable devices.

6.2   Effect of shoe-orientation on friction

The following study was published in the conference proceedings of the 11th Footwear Biomechanics Symposium, Natal, Brazil (Ura et al., 2013).

During a sliding on any surface, the shoe orientation angle (Figure 6.1) is different depending on the movement and the player's technique. During dynamic tennis movements, different parts of the shoe sole interact in different ways with the surface asperities. For this pilot study, it is hypothesised that the friction between the shoe and the surface could be influenced by this shoe orientation during tennis movements, e.g. sliding on hard courts.

In a biomechanical tennis study report for the ITF (Damm et al., 2013b) kinematics values of the shoe orientation angle during the sliding phase of a free running forehand and a 180 degree turning manoeuvre were reported. 10 participants performed 5 trials of the mentioned movements over a clay surface. They reported the mean angle values of 33.2 ± 16 ° and 44.6 ± 16 ° for the running forehand and turning movements respectively.
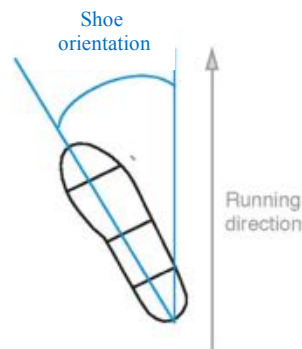
Figure 6.1 Shoe orientation angle in reference to the running direction

The purpose of this pilot study was to investigate the influence of shoe orientation on friction testing over a range of normal loads, with the objective to assess the future test methodology. Friction tests were conducted on an acrylic hard court surface using the UoSh traction rig (section d)).

The forefoot segment of the adidas Barricade 6 EU size 42 (section 3.5.3) tennis shoe was used as the test shoe. Tests were conducted with the test shoe attached in four orientations in relation to horizontal movement (Figure 6.2). Prior to testing under each condition, the sole was prepared in accordance to the protocol previously presented in section 3.2.4.
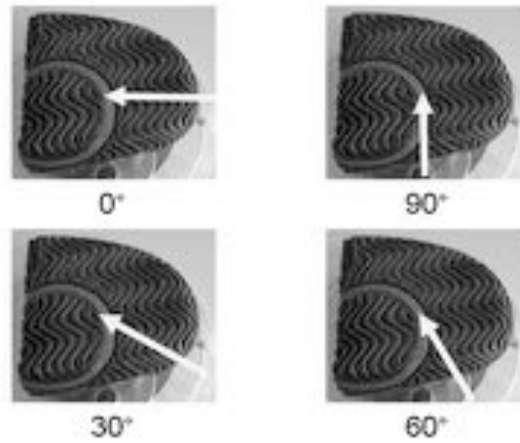
Figure 6.2 Shoe orientation tested (arrows indicate direction of shoe movement).

As discussed in section 3.5.1, the dynamic friction was considered using the mean dynamic friction force in the direction of movement between 10 mm and 30 mm horizontal displacement. Friction force data was collected for a range of normal loads (500 N – 1000 N), to assess the influence of shoe orientation.
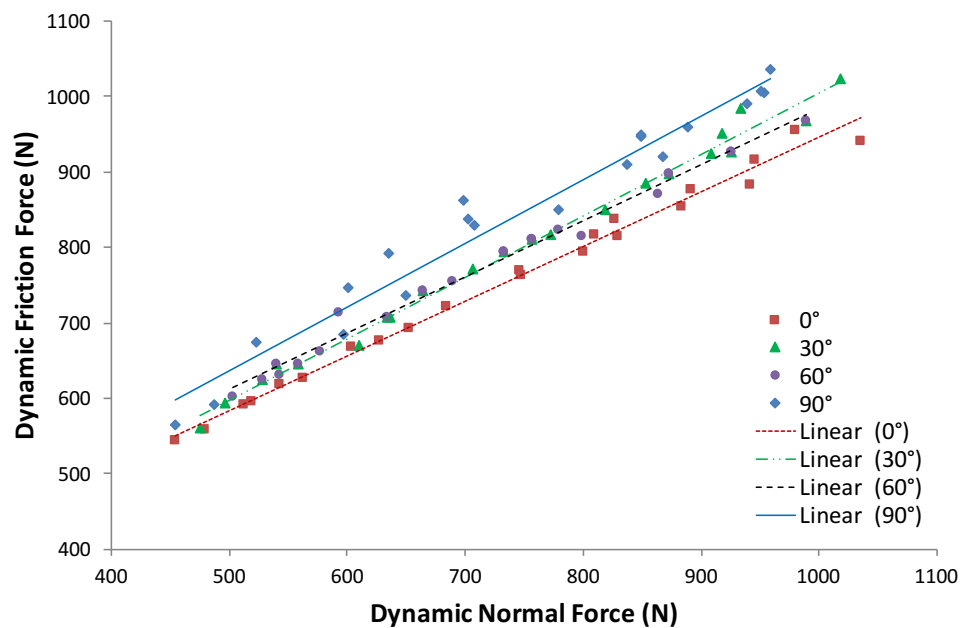
Figure 6.3 Plot of the dynamic force against normal force for each shoe orientation condition.

Figure 6.3 shows the strong and significant linear regressions found between normal force and dynamic friction force ($R^2 > 0.95$, $p < 0.05$, where $n = 22$) for each orientation. Each linear fit has a low root mean squared error with varying gradients (RMS: $0° = \pm 12.22$, $30° = \pm 13.54$, $60° = \pm 11.63$ and $90° = \pm 26.51$ N), showing differences between the orientations. Each relationship was specific to the particular normal force-shoe orientation combination.

6.3   Contact area, pressure and available friction relationships

As mentioned previously in the Literature review section (Chapter 2), in tennis, the complexity of some dynamic movements affect the loading conditions experienced by players. The magnitude of these forces in combination with other variables, e.g. surface roughness (Clarke et al., 2012a) and shoe orientation (section 6.2) affects the friction generated between the shoe and the surface. As discussed in section 2.4.2, the reported peak vertical loads in some studies are above 1000 N on hard and clay tennis courts for specific movements such as side jump and running forehand.

Despite the high loading conditions, lab-based test devices have been developed, however, the challenge remains to replicate these for portable friction test devices. For this reason, pressure insole data collected in previous studies (Damm et al., 2014, Girard et al., 2007, Bloch et al., 1999) could be a key source to develop reliable portable test devices more representative of loading conditions during realistic movements. In this section variables such as shoe-surface contact area, pressure and available friction were assessed in order to examine this further and to possibly use in the development of the final portable test device.

The purpose of this pilot study was to investigate shoe-surface contact area at different vertical loads, relate them to pressures measured in previous biomechanics studies and measure the available dynamic friction force.

The following study was published in the conference proceedings of the 12th Footwear Biomechanics Symposium, Liverpool, UK (Ura et al., 2015a).

Three Babolat Propulse 4 tennis shoes, described in section 3.5.3 were pressed against a surface using the UoSh traction device. The shoes (shown in Figure 6.4), were of the same sole design but ranging in size (EU sizes 31, 39 and 49). The vertical loads applied ranged from 600 to 1600 N in intervals of 200 N.

Figure 6.4 Commercial tennis shoes (EU sizes 31, 39 and 49)

The shoe-surface contact area of the forefoot segments was calculated using an ink print protocol developed previously (Clarke et al., 2012). Blank paper was rigidly attached onto a smooth acrylic sheet under the shoes before they were loaded. The ink prints were digitised and analysed with a bespoke Matlab threshold programme to calculate the ink area. Examples of the ink prints obtained are shown in Figure 6.5. This procedure was repeated 4 times for each condition.

<div align="center">600 N   1000 N   1600 N</div>
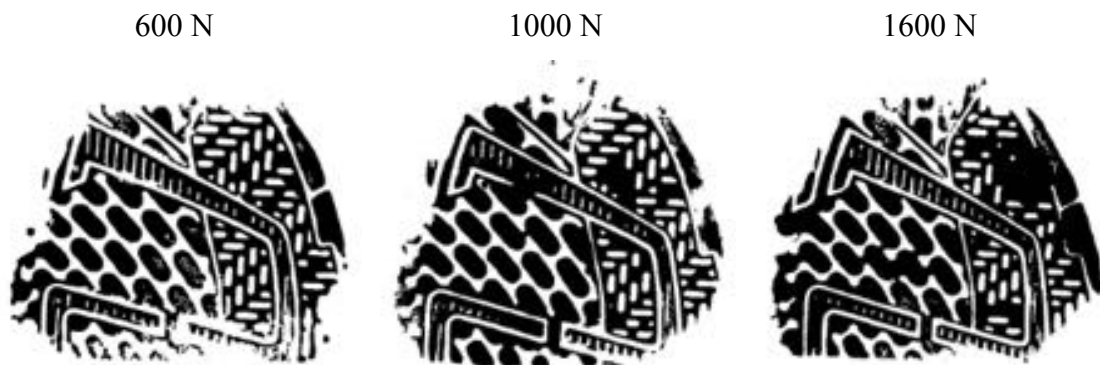
Figure 6.5 Examples of the ink prints for the size EU 31 shoe at 600, 1000 and 1600 N of vertical load

The paper surface was then replaced with a commercial hard court sample (HC9) described in section c), and friction testing was carried out over the same range of vertical loads. The average dynamic coefficient of friction (DCOF) was calculated using the mean dynamic friction force in the direction of movement between 10 mm and 30 mm horizontal displacement (detailed in Clarke et al., 2013).

The results indicated an increase of contact area as the vertical load increases, showing strong and significant linear regressions ($R^2 > 0.81$, $p < 0.05$, where $n = 72$) and differences between each shoe size. Figure 6.6 exhibits the pressure values calculated from the vertical load and contact area for each shoe.
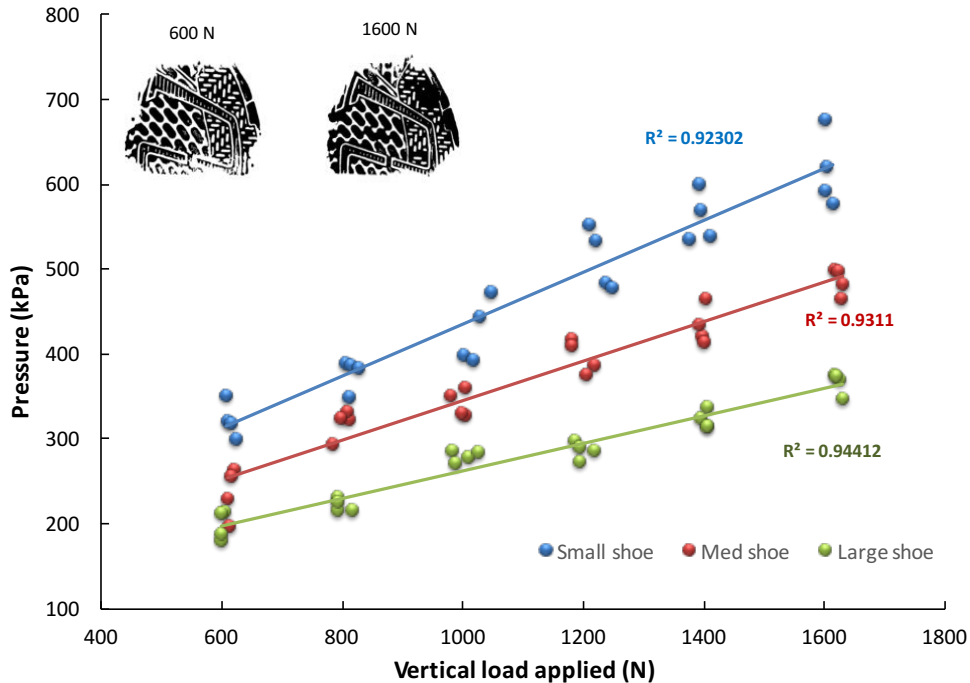
Figure 6.6 Plot of the pressure against vertical load for each shoe tested. Examples of ink prints are shown for the size EU 31 shoe, at 600 and 1600 N of vertical load.

Figure 6.7 shows the results for static and dynamic COF against average applied pressure (as predicted from the linear fits in Figure 6.6). This is assumed to be the average pressure experienced by the shoe before the onset of sliding. As the applied pressure increases, there is a tendency for the static and dynamic COF to decrease. Based on the calculated pressure and despite the size of the shoe and the contact area with the surface, similar friction measurements were obtained.
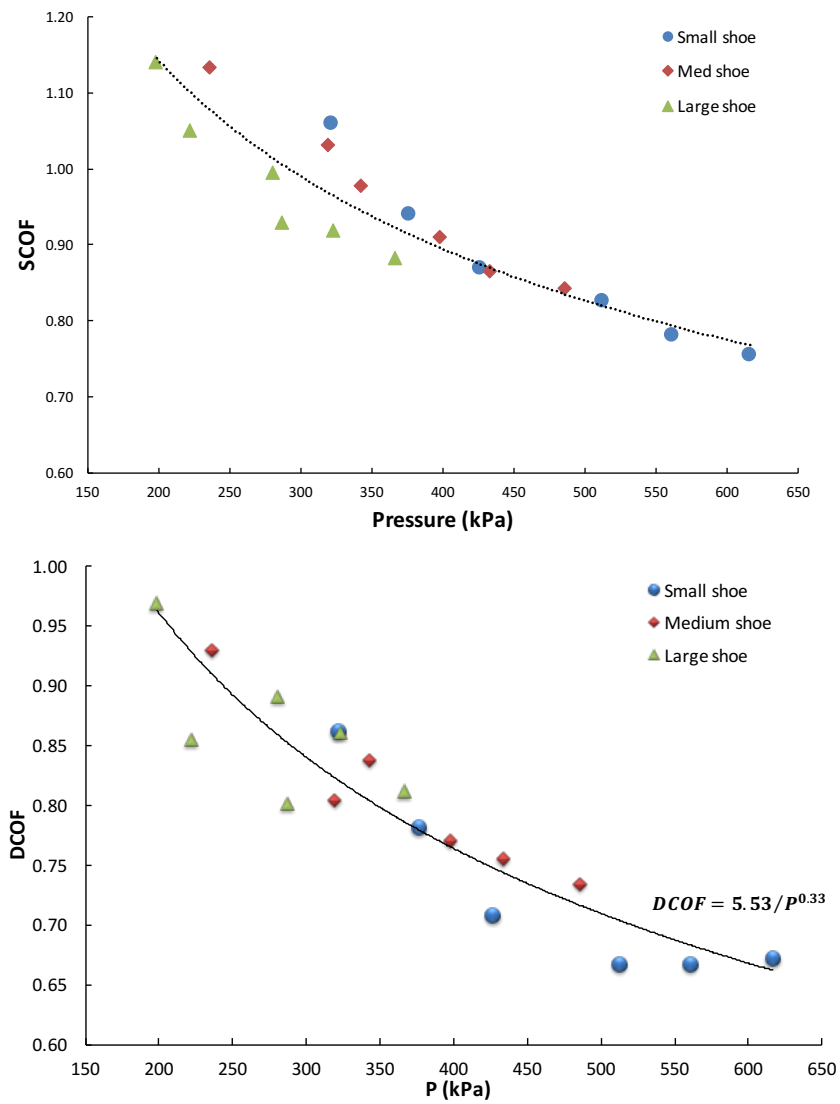
Figure 6.7 Plot of the average SCOF (top) and DCOF (bottom) against average pressure for each shoe. Best fit power shown to illustrate trend (black line).

6.4   Tennis shoe outsole temperature changes during hard court sliding and their effects on friction behaviour.

As pointed in the material characterisation study, temperature variations lead to changes in the material hardness of a viscoelastic material Tennis events played in countries where the court temperature can be very high due to environmental conditions could make these changes in material even greater. For these reasons a tennis shoe outsole temperature study was implemented.

The aim of this pilot study was to evaluate the likely changes in shoe sole temperature during sliding movements on hard courts and the influence of these changes on the tribological mechanisms. This information will be useful for the design stage of the test methodology, however, it could also be useful towards the design and development of footwear and playing surfaces, in order to maximise performance and reduce injury risk. The following study was published in the conference proceedings of the 7th Asia Pacific Sports Technology Conference 2015, Barcelona, Spain (Ura et al., 2015b).

A range of tests, using the UoSh lab-based traction device (described in chapter 3), were implemented to determine the behaviour of the shoe outsole temperature distribution of a commercially available hard court tennis shoe under different conditions during a simulated sliding movement. Figure 6.8 shows the 5 type 'K' thermocouples inserted and attached by an adhesive into the grooves of the forefoot segment, to keep them very close to the shoe surface. The thermocouples were connected to a multiple channel data logger which allowed simultaneously recording of the temperatures on different parts of the shoe segment over a pre-set time. The data logger has a conversion time of 100 ms and an accuracy of $\pm$ 0.2%.

Three bespoke acrylic hard court surfaces (HCB1, HCB2 and HCB3) described in section c) and a commercial tennis surface (HC10) with different roughness values, as provided in Table 6-1, were used for the testing. To best replicate a sliding movement, the shoe orientation was positioned at 30° in relation to the sliding direction. This value was chosen due to the results from section 6.2, where the effect of the shoe orientation was tested.

An initial study was implemented to test the thermocouples and measure a potential change in temperature. The loads tested ranged from 500 N to 2000 N in increments of

300 N. For each load the temperature of the 5 thermocouples was recorded with the data logger, at regular intervals of 0.62 s throughout the sliding motion.
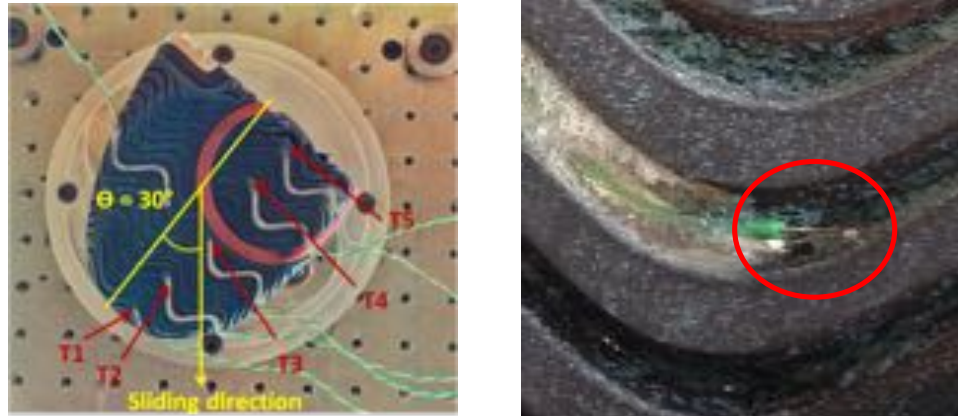
Figure 6.8 Left: the position of the 5 thermocouples on the shoe surface; Right: detail of thermocouple in shoe groove.

The second study involved simulating a repeated sliding during a typical tennis rally and measuring how the temperature changed after a number of slides. In order to replicate this as accurately as possible, the 11 videos of tennis rallies from elite hard court tournaments, utilised in section 4.2.2 for the sliding analysis, were analysed to see the occurrence of sliding motions during a rally and the average time period between them. The average duration of a rally (± 1 SD) was found to be 43.4 ± 8.0 seconds with an average (± 1 SD) of 6.64 ± 2.8 sliding events. It was therefore decided to measure shoe sole temperature during a series of 4 slides of approximately 3 seconds with a rest time period of 10 seconds between each slide at loads of 600, 1200 and 1800 N. The rest time between slides was arbitrary defined with the purpose to allow the rubber to cool down. Additionally, the DCOF was calculated using the mean dynamic friction force in direction of movement between 10 mm and 30 mm horizontal displacement, according to the test protocol described in Chapter 3.

Table 6-1 Average R_a values for a range of surface samples before and after the testing

Surface reference	R_a (µm)	
	Before	After
HCB1	5.2 ± 0.6	1.4 ± 0.2
HCB2	19.3 ± 3.0	18.0 ± 2.5
HC10	25.3 ± 1.8	26.4 ± 1.3
HCB3	32.6 ± 5.0	24.9 ± 2.1

A third study involved a repeated sliding over HC10 surface with an 1800 N vertical load, for 15 minutes with a rest interval of 10 seconds between each slide. The time was arbitrary defined, with the objective to raise the shoe temperature as much as possible. The change in temperature and DCOF were recorded for each of the slides. The shore hardness of the shoe sole was measured before and after the testing to monitor changes in the material properties.

Figure 6.9 shows an example of the results obtained by the first study, and the temperature change of the 5 thermocouples attached to the forefoot segment of the shoe. Although there is a change in temperature for all the thermocouples, T2, T3 and T4 are the positions with the highest difference in temperature and these were used as the focus for the remaining studies.
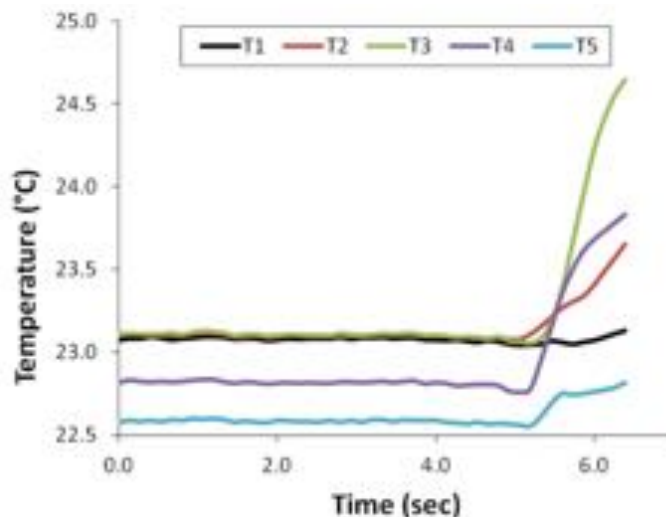
Figure 6.9 Temperature at different positions on the shoe sole against time for surface HCB2 at 1100 N vertical load.

Figure 6.10 shows the relationship between temperature change (± 1 SD), vertical load and thermocouple location. There is a clear effect of the vertical load (1800 > 1200 > 600 N), and at 1800 N vertical load an effect of the sensor location on temperature change (T2 > T3 > T4). However, there is no obvious consistent trend of a surface effect, even though they had different roughness. It is important to note that for HCB1, HCB2 and HCB3 the roughness changed through testing (see Table 6-1).
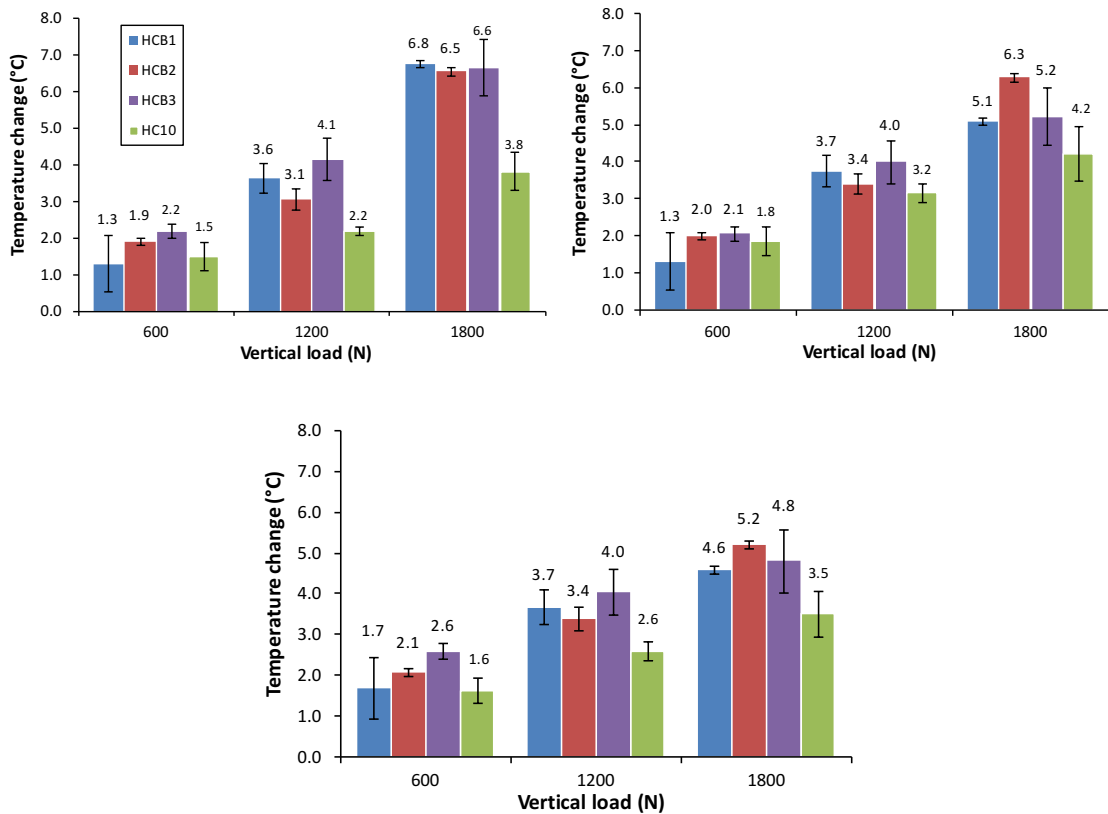
Figure 6.10 Plots of temperature change with SD against the vertical load for T2, T3 (from top left to right) and T4 (bottom) on surfaces HCB1, HCB2 and HCB3.

Figure 6.11 shows the change in temperature of T2, T3 and T4, for four repeated sliding movements, with vertical loads of 600, 1200 and 1800 N on the 4 surfaces tested. The surfaces with the highest temperature change were HCB1 and HCB3. The behaviour of the temperature is to increase during each slide and then decrease between slides, however, it never decreases completely to the previous temperature value, and the overall temperature increases throughout the tests.
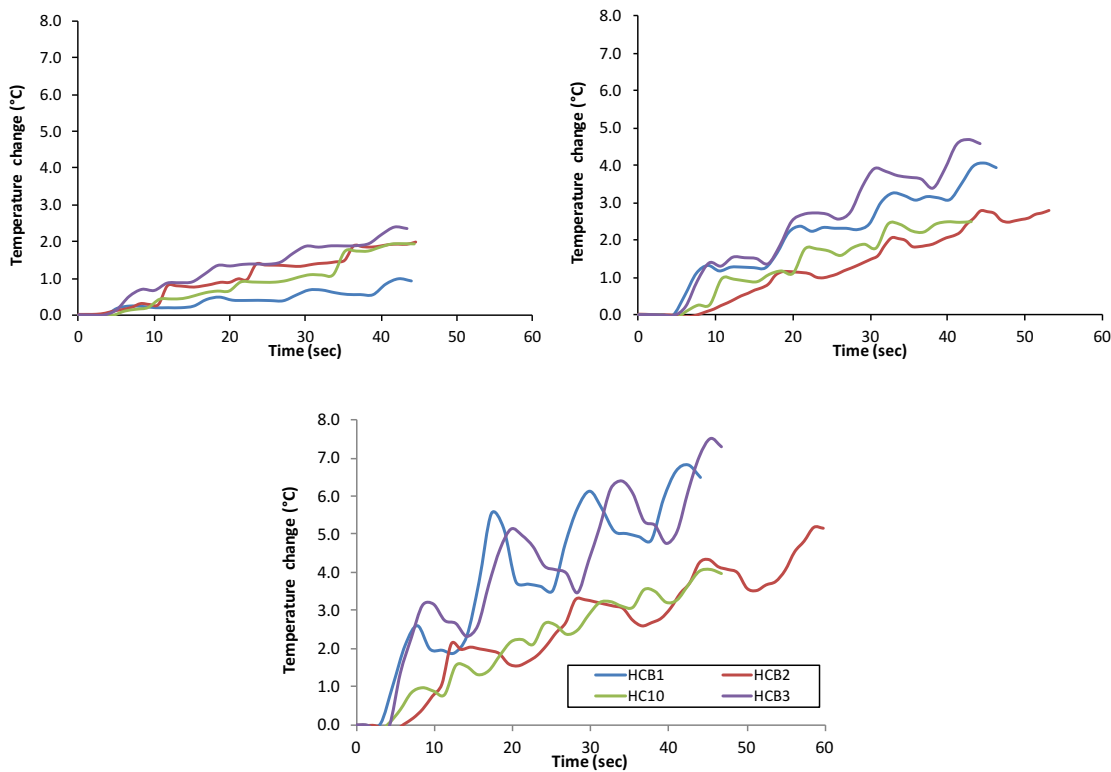
Figure 6.11 Plots of the Temperature change against time for T2, on each surface for 600, 1200 and 1800 N vertical load (top left to right and bottom).

The average DCOF at 600, 1200 and 1800 N of vertical load was calculated for the sets of four repeated slides on the four different surfaces. Figure 6.12 shows that the DCOF from surface HCB1 increases as the vertical load increases. However, surfaces HCB2 and HCB3 have a tendency to decrease in DCOF as the vertical load increases (surface HC10 remains relatively constant).

For most of the tests the general tendency was for DCOF to decrease with increasing numbers of slides. There is a trend for DCOF to initially decrease, however, as shown in Figure 6.13 for the 15 minutes sliding testing, as the number of slides increases (approximately slide number 14), there is a trend for DCOF to increase.
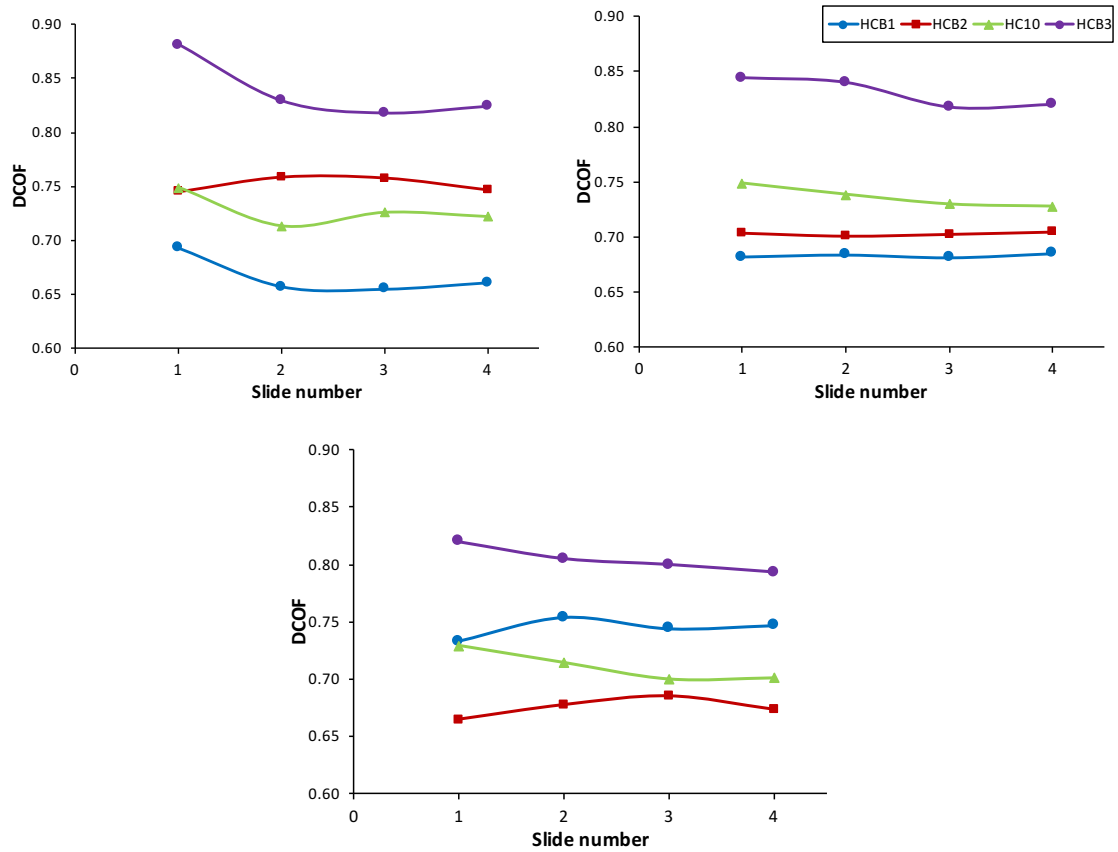
Figure 6.12 Average DCOF against slide number for: 600, 1200 and 1800 N (left to right) of vertical load.

As mentioned in the material characterisation (section 3.5.3), the results from the DMTA testing in the temperature range from 20 to 50 °C (region of interest) for E' and tan δ, suggest a decrease in the damping of the material as the temperature. In this sliding temperature study, the average (±1 SD) hardness value of the rubber before the testing was 75.4 ± 1.1. Immediately after the 15 minutes sliding test, the hardness was 62.1 ± 5.1, confirming a change of the material properties after the testing.
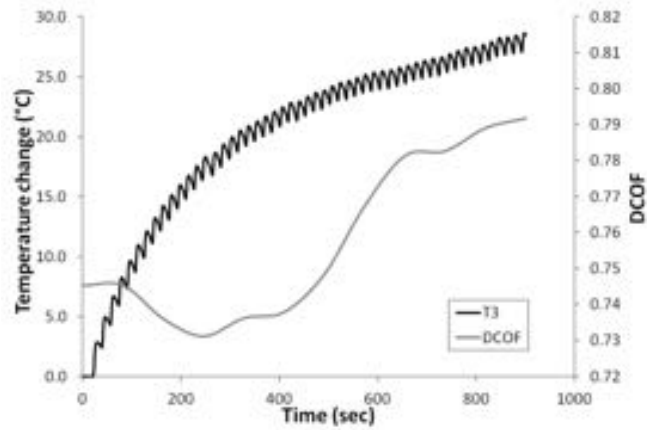
Figure 6.13 Temperature change and DCOF against time for a 1800 N vertical load for 15 minutes sliding test on HC10 surface.
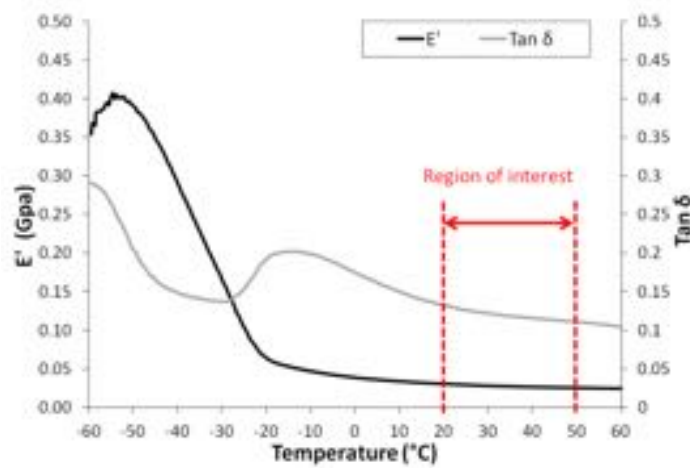
Figure 6.14 DMTA data showing E' and tan δ of the shoe material.

When elastomeric material, such as that tested here, is compressed against a surface with some roughness, there is an interaction between their surface asperities. As the vertical force increases, the shoe sole will deform more, increasing asperity contact and therefore, the adhesion component of friction. During a slide on a hard rough surface, the surface asperities will deform the shoe sole resulting in energy dissipation. This energy will result in local heating and an increase in temperature.

For this experiment, the difference in temperature between the five positions on the shoe sole is dependent of the shoe orientation and the position of the thermocouples relative to the direction of the sliding. For all the tests, T2 is at the front of the shoe during the sliding, experiencing higher deformation and the highest change in temperature in comparison to the other thermocouples. (Persson, 2014) noted that the heat produced in an asperity contact region will result in a 'hot track' on a rubber surface. When this specific region experiences another asperity contact, due to the repeated sliding

movement, it will experience an accumulation of heat, which leads to a temperature increase. Due to the difference in temperature after each slide, positions T2, T3 and T4 could be considered as the 'hottest tracks' in the shoe sole.

The difference in temperature change between low (600 N) and high (1800 N) vertical loads in Figure 6.10 could be explained by the shoe-surface contact area and its asperity contact. In Chapter 5.6, it was reported higher contact areas as the vertical load increases. During sliding, the asperities of the surface deform the shoe sole and the energy dissipation and therefore temperature increases. Under high vertical loads, adhesion dominates the interaction due to an increase of contact area and more elastomeric material inside the cavities of the surface. Under low vertical loads, hysteresis dominates the interaction due to less asperity contact; therefore, there is less deformation of the shoe sole and lower temperature dissipation. Despite the loading conditions, as roughness increases, the sole deforms and recovers, increasing the energy dissipated, which is reflected in an increment of the temperature.

Figure 6.11 shows that for a test of four repeated slides, the temperature increases as the number of slide increases. Persson (2006) stated that in a typical case of a rubber block sliding on a hard rough substrate, the temperature increase results in a decrease in rubber friction. In Figure 6.12 it is shown in general, that after 4 slides the DCOF decreases or stays similar to the first DCOF value, for the three vertical loads on all the surfaces tested. However, comparing the DCOF between the three vertical loads, for the smoothest surface (HCB1) the DCOF increases as the vertical load goes from 600 to 1800 N, suggesting a higher contribution of roughness than temperature change, on the shoe-surface friction. In contrast, for surfaces HCB2 and HCB3, DCOF stays similar or reduces as the vertical load increases, in agreement with (Persson, 2006). This behaviour suggests a bigger influence of temperature change rather than roughness for our study.

Figure 6.13 results are in good agreement with previous tests, after the first few slides, the temperature increases and the friction starts to decrease. However, as the number of slides increases, the friction reaches a minimum and then starts to increase and continues until the end of the 52 slides. This differs from the behaviour suggested by Persson et al. (2006), but the DMTA and hardness data suggest that the sole material tends to reduce its damping and hardness as the temperature increases, in consequence it will deform more, increasing the heat and contact area and hence the temperature and friction measurement.

6.5   Discussion of chapter

As discussed at the beginning of this chapter, three main experiments were developed to evaluate some interaction parameters for a shoe-surface interaction with the objective to assess the design of the mechanical test methodology.

In the first experiment, for the four different shoe orientations tested, significant linear relationships were found between normal force and friction force under the normal loading conditions investigated in this study. Therefore, it is recommended to consider shoe orientation when considering mechanical testing to improve the relevance of the test. Something to take into account is that the variety of tennis shoes in the market have different sole tread designs, that could dictate how the friction behaves depending on the shoe orientation. By varying the shoe orientation, what is really varying is the contact position of the treads in relation to the surface, so after this experiment a closer look to the sole treads geometry and their possible effect on the friction is necessary. This is considered in more detail in Chapter 7.

For the second experiment, significant non-linear relationships exist between contact area, pressures and normal force were found. Similar trends are then observed with friction data. It was demonstrated that by using smaller shoes and scaling down the vertical load applied, it is possible to generate pressures that are comparable to previous biomechanical studies. Damm et al., (2014) reported peak pressure values ranging from 340.4 – 596.6 kPa, which can be achieved by a combination of a specific vertical load in combination with a small test shoe. Therefore, when considering measuring friction with the final portable device on a tennis court, it is highly recommended to consider this approach, as it has been proved to be capable of maintaining levels of applied pressure that are representative to real-match conditions.

For the last experiment, it was found that the vertical force and the location of the thermocouple affected the influence of the temperature and the friction present during a dynamic sliding movement. These effects occurred over a range of surfaces tested; however, the effect of the roughness itself is not consistent as discussed in a previous study (Clarke et al., 2012b). It was found that the mechanical properties of shoe sole rubbers can change over the large temperature ranges measured in this study and these effects could be even greater during tennis matches that take place under extreme ambient temperature conditions. These changes could also occur throughout the duration of a long

rally, set or match. It is therefore recommended to consider the effect of rubber temperature when studying the behaviour of shoe friction on acrylic hard-court tennis surfaces. It will be important to either, monitor temperature of the test shoe over a specific number of tests, or to allow the rubber to "cool down" between a series of tests.

6.6   Summary of chapter

Material characterisation, experimental friction and temperature data have provided empirical knowledge into the manner in which shoe and surfaces can behave. The main findings presented in this chapter were:

1. It was proved that shoe orientation angle affects the friction during a sliding movement, which could be due to the shoe sole tread geometry.

2. It has been demonstrated that measuring friction by the approach to match applied pressures with lower contact areas, is in good agreement with the friction measured by applying high vertical loads.

3. During a sliding movement the rubber temperature of the shoe sole changes due to an effect of the vertical load. It was found that the front part of the shoe experienced the highest temperature change. Additionally, it was reported an effect of the temperature on the friction generated with a hard court surface.

The knowledge obtained in this section, will be useful in the design of a standard test shoe for the final test methodology. This is presented in the next section.

7. Novel portable device – design and development

7.1   Introduction

This chapter pulls together the findings from the previous chapters with the aim to present a design methodology for the mechanical portable device to allow courts to be measured and monitored.

Based on the design methodology for the mechanical portable device, implemented and discussed previously in section 3.4.2, the first stage of the design comprises the conceptual design (Figure 3.3), which involves the problem definition, the definition of product specifications, a concept generation stage and the evaluation and selection of the best concept. This stage is developed presented in detail in Appendix C.

7.2   Design stage - Embodiment design

7.2.1 Pre-prototype design

With the generation and evaluation concept stages completed (Appendix C), a detailed and parametric design stage of the sketches and the solutions selected in the morphological chart was implemented. A final detailed design and technical drawings, based on the components selected from the morphological chart, were formed for the construction of a first pre-prototype (TSSTv1). This pre-prototype was constructed by the Department of Mechanical Engineering, The University of Sheffield, and adapted mainly from available parts in the laboratory were possible, with the objective to quickly evaluate the design concept. As mentioned previously, the design centres around having one device, which could be configured into two configurations: *'Angled-ram'* and *'Sled'*.

In Figure 7.1 the 3-Dimensional representations of both configurations are presented. For the 'Angled-ram' configuration (Figure 7.1 top), the design as can be seen, centres around a "L" shape aluminium framework with a pneumatic cylinder attached to a plate. The plate has some holes that allow the rear end of the pneumatic cylinder to be raised or lowered in order to produce a variety of angles. At the rear of the cylinder there is also a threaded bar which allows the angle to be manually adjusted to a fine degree. At the other end of the cylinder a holder with a bespoke test shoe is attached.
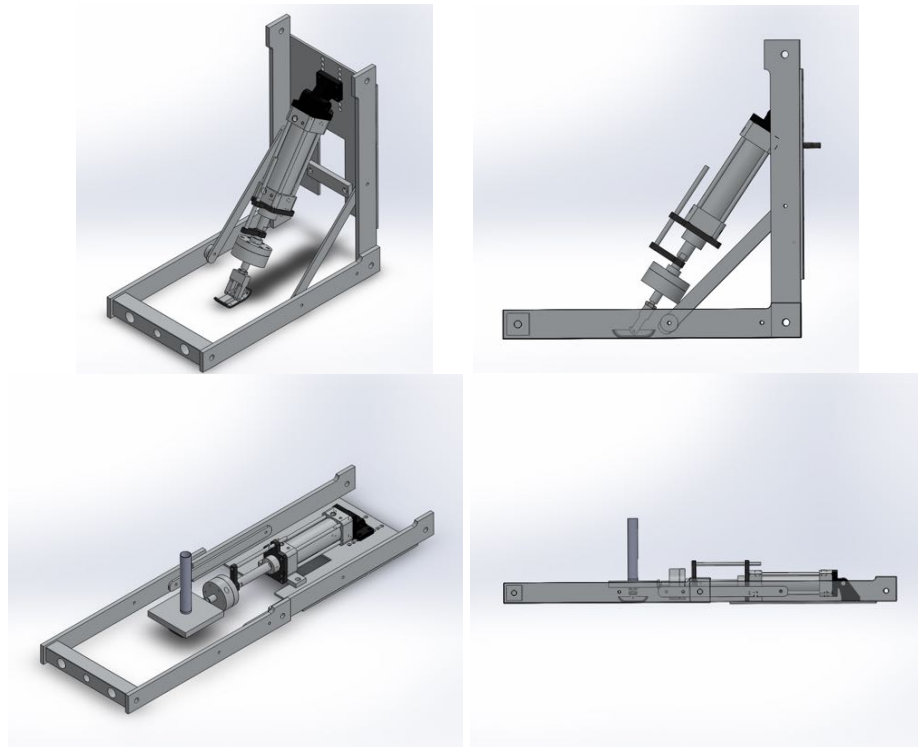
Figure 7.1 TSSTv1 device in angled-ram (Top) and sled (Bottom) configurations.

To change from the "Angled-ram" configuration to the "Sled" (Figure 7.1-bottom), a few adjustments are required. The two lateral supports used to keep the "L" shape need to be disconnected and the threaded bar need to be removed. Subsequently, the pneumatic cylinder is positioned in a horizontal position parallel to the ground. The test shoe is attached to a plate, which supports the desired weights. One side of this plate is attached to the end of the pneumatic cylinder. Figure 7.2 shows the TSSTv1 manufactured device and the two test configurations.
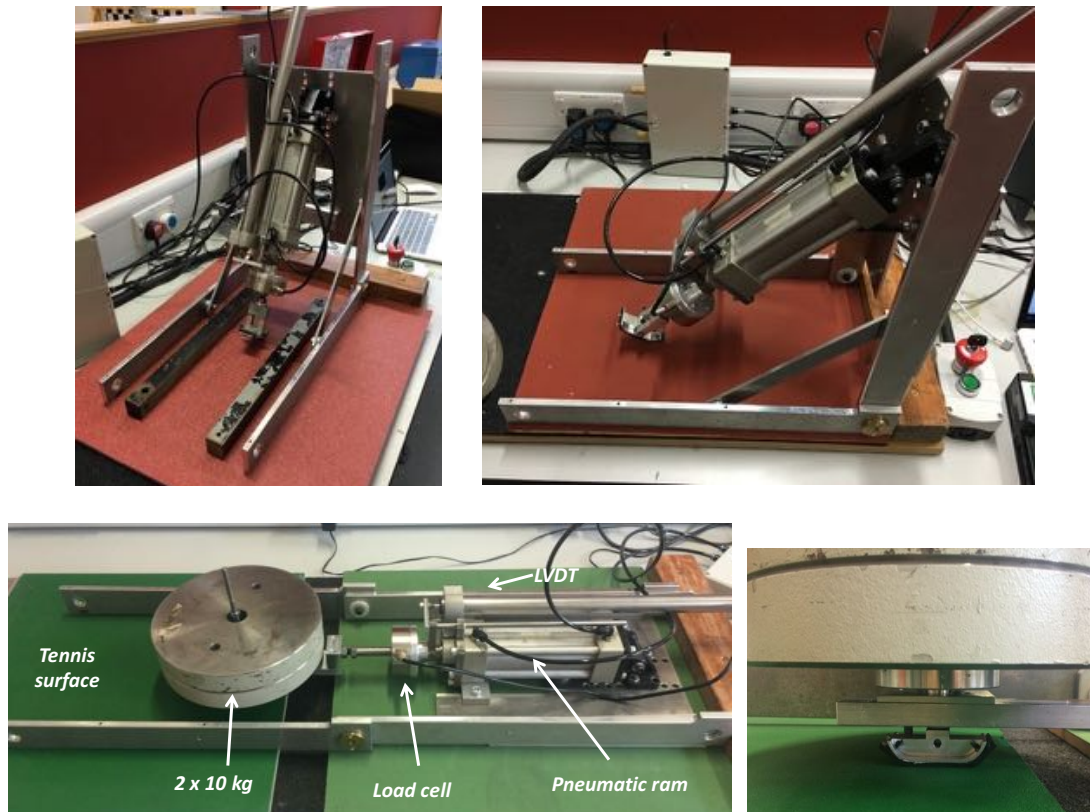
Figure 7.2 The TSSTv1 test device. Angled-ram (top) and sled (bottom) configurations. Sled plate with test shoe (bottom right).

7.2.2 Test shoe design

Additionally, a changeable test shoe slider, shown in Figure 7.3 was designed to mount different test rubbers. A rubber sample is glued on the bottom part of the slider and mechanically secured with four screws. The dimensions of the slider are 63.5 x 31 x 17 mm with a flat area of 961mm^2 (31 x 31 mm). By applying a vertical load of 384 N, a pressure of 400 kPa could be generated (assuming total contact over the area).

Based on the hardness and DMTA results (Chapter 6), and after looking into different commercial rubbers, a Nitrile Butadiene Rubber (N70) was chosen for initial testing, due to its similarities in comparison with the rubber compound of a commercial tennis shoe, as summarised in Table 7-1. Full specifications are presented in Appendix B.

Table 7-1 Comparison of the mechanical properties of the N70 rubber and a typical tennis shoe outsole

Mechanical Properties	N70 Nitrile Butadiene Rubber (NBR)	Tennis shoe outsole (Yu et al., 2010)
Shore Hardness	71	68 - 72
Tensile strength (MPa)	14	13 – 15
Elongation at break (%)	385	350 – 500 %
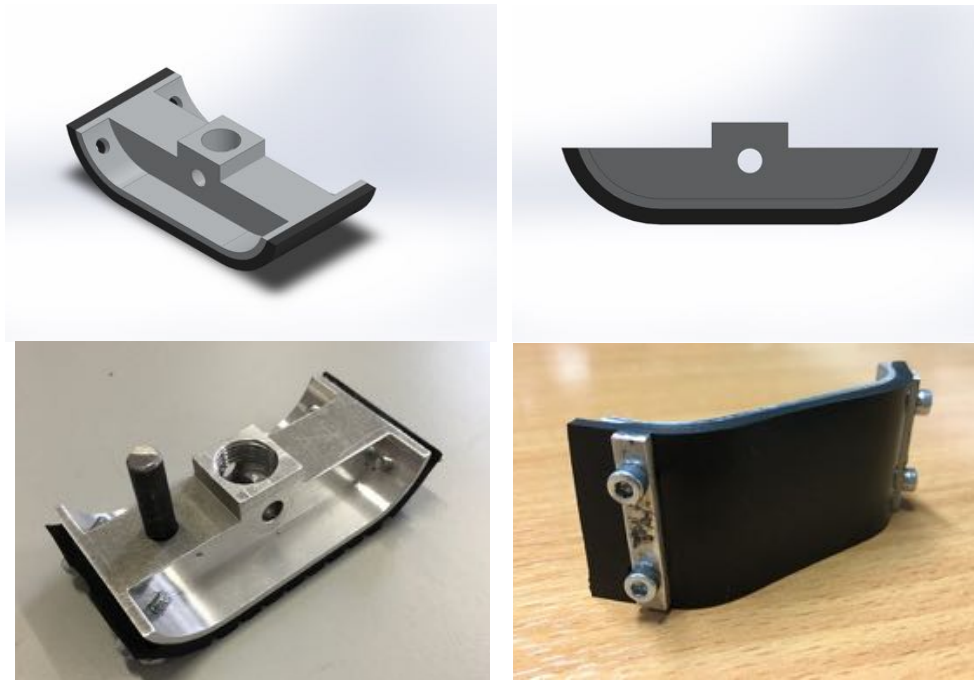
Figure 7.3 Top: CAD model of the test shoe slider. Bottom: Manufactured test shoe slider.

Additionally, to vary the test shoe orientation, a small connecting plate was machined. The orientation could be varied between 0° and 90° in increments of 25° in relation to the direction of movement. The plate with the described graduation is presented in Figure 7.4.
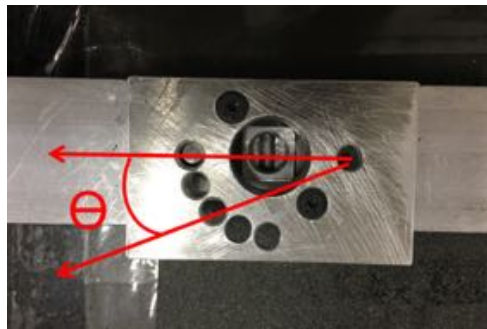
Figure 7.4 Connecting plate for slider orientation adjustment.

Moreover, in order to calculate the friction generated by the shoe-surface interface, the mechanical device was complemented with a load cell (linearity error ± 0.03% full scale.) and a LVDT (linearity error < ± 0.5 / ± 0.25 full scale) to provide the measurements of force applied and the displacement. A data acquisition device (NI9174) with synchronised and signal-conditioning modules (NI9237 and NI9215) samples the signals from the load cell and LVDT (Figure 7.5). These voltage signals, sampled at 1600 Hz, are transformed into force and displacement data and displayed in real time using LabView (version 14 National Instruments).

Figure 7.5 Data acquisition device with signal conditioning modules.

Before beginning any testing, the rig was calibrated, to ensure both the load cell and LVDT provided accurate data. The load cell was positioned vertically on a surface so that weights could be loaded onto it. Two masses of 100 gr and 1000 gr, previously weighed to a resolution of 0.01 grams, were positioned onto the cell. A series of readings were taken from the load cell and were compared to the force from the two masses. With this data, a calibration factor was calculated. Subsequently, this calibration factor was applied to the bespoke LabView data acquisition programme, the masses were reloaded onto the cell and measurements were taken to ensure the calibration factor was correctly calculated. In a similar way as with the load cell, a calibration factor was calculated for the LVDT by extending the LVDT to a specific displacement. Additionally, for all of the subsequent testing, the displacement and horizontal data from the LVDT and load cell were smoothed by applying a moving average algorithm to reduce the noise from the data.

7.2.3 Testing procedure

'Angled-ram'

Initially, the device is positioned on the surface. An initial controlled angle is set, in order to start the testing (Figure 7.6 shows an example of the data obtained from one test). Using a solenoid valve, the pneumatic ram is activated and hence, the test shoe slider initially moves until making contact with the surface. It also applies an increasing force to the surface until it reaches a maximum value (No. 1 in Figure 7.6).

Once the shoe is fixed on the surface, the angle from the vertical, θ, is manually increased (thereby increasing the ratio of horizontal to vertical force) until the test shoe slides on the surface. During the increase of angle θ, controlled by the operator (No. 2 in Figure 7.6), the test shoe experiences a micro-sliding, however, by continuing increasing θ, the

test shoe experience a macro-sliding, which is confirmed by a drop in the resultant force and an increase of the displacement (3 in Figure 7.6). The angle when sliding initiates then is transformed into a value of coefficient of friction.
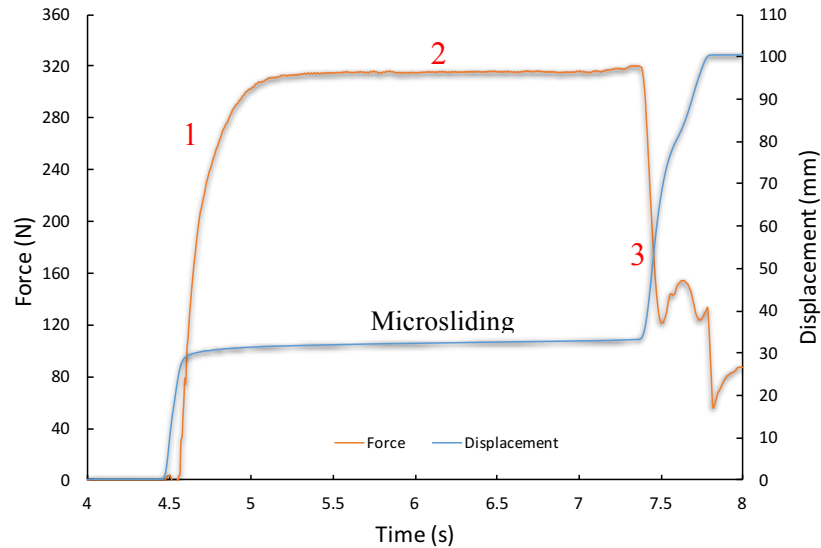
Figure 7.6 Example of the Force and Displacement graphs for the angled-ram configuration.

For this configuration, analysis of the rig's forces can provide the friction needed for the shoe to start movement. Figure 7.7 shows the free body diagram with the forces acting on the test shoe sample.

The force which maintains the body at rest is the friction force (F_f). The force needed to start sliding and overcome static friction is the maximum value of this friction force. The static coefficient of friction (μ_s) can be defined as the tangent of the angle of the inclined force at this point. The body will continue in rest if the angle θ is less than a certain value θ_s and it will start moving if the inclination angle go over θ_s.
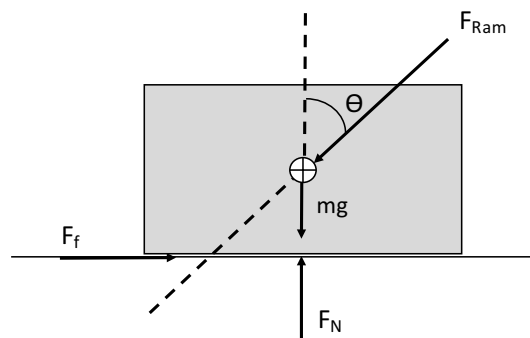
Figure 7.7 angled-ram simplified free-body diagram of the static system, before or at the point of sliding.

$$\sum Fx = 0 \qquad\qquad \sum Fy = 0$$

$$F_f = F_{Ram} \sin\theta \qquad\qquad F_N = mg + F_{Ram} \cos\theta$$

for sliding to be presented:

$$\mu_s > \frac{F_f}{F_N} \quad and \quad \theta < \theta_s$$

Therefore:

$$\mu_s = \frac{F_{Ram} \sin\theta_s}{mg + F_{Ram} \cos\theta_s}$$

mg = 5.88 N, and generally, $F_{Ram} \cos\theta_s$ is much bigger than mg, so if $F_{Ram} \cos\theta \gg mg$ then:

$$\mu_s \approx \tan\theta_s$$

Equation 7-1

Although ideally this configuration would include replication of the shoe landing on the surface, using this approach was found to set up measurement errors due to shock and noise on impact. Previous work with a similar test rig (Keen, 2015) also showed an effect of the ram pressure on the impact velocity and hence the slip angle. Therefore, the approach of using a shoe initially at rest on the surface was selected for further analysis.

'Sled' configuration

In the 'Sled' configuration, the test shoe slider is fixed onto the bottom of the sled plate with the desired orientation set. The system is loaded with a number of weights until the desired normal force is achieved. The pneumatic ram is then set to a desired ram pressure, which for all tests during this research was 2 bar (200 kPa). Then, a solenoid valve is activated, opening the pneumatic cylinder to provide a horizontal force, which increases until the test shoe slider starts to move. The maximum sliding length is 0.1 m. As previously described signals from a load cell and a LVDT deliver the necessary measurements to determine the applied horizontal force and displacement respectively.

In order to understand the friction developed at the shoe-surface interface, typical plots obtained from the 'Sled' configuration at a normal force of 300 N, were analysed. These are presented in Figure 7.8. The force plot is characterised by two regions: a region of increasing initial force during a static regime and a period of dynamic friction during which the force remains relatively constant.
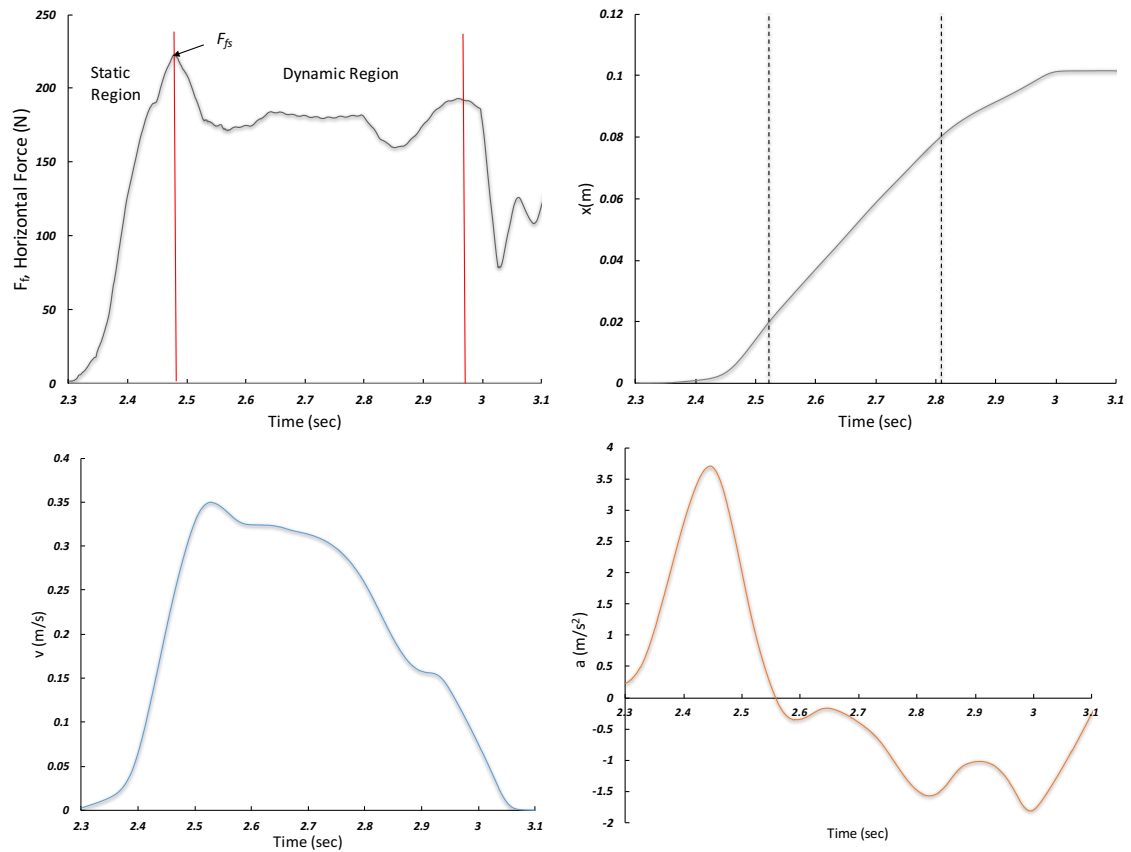
Figure 7.8 Example graphs showing typical data collected using the sled configuration. Top Left: Horizontal force, Top right: horizontal displacement, Bottom left: velocity, Bottom right: acceleration.

As described in Clarke et al., (2013), within the static and dynamic regimes, evidence of micro- and macrosliding is observed (Figure 7.9). Microsliding is described as the shear period in which the rubber is deformed under the initial horizontal force. During this time, no relative sliding between the test shoe and the surface occurs. Macrosliding is the period of initial relative sliding between the test shoe and the surface (Figure 7.9 top). After macrosliding, a peak is reached at which the test shoe-surface fails. After the systems fails, the static region ends and a period of gross sliding begins (Figure 7.9 bottom). During gross sliding, the velocity is not constant, as shown in Figure 7.8 bottom left.
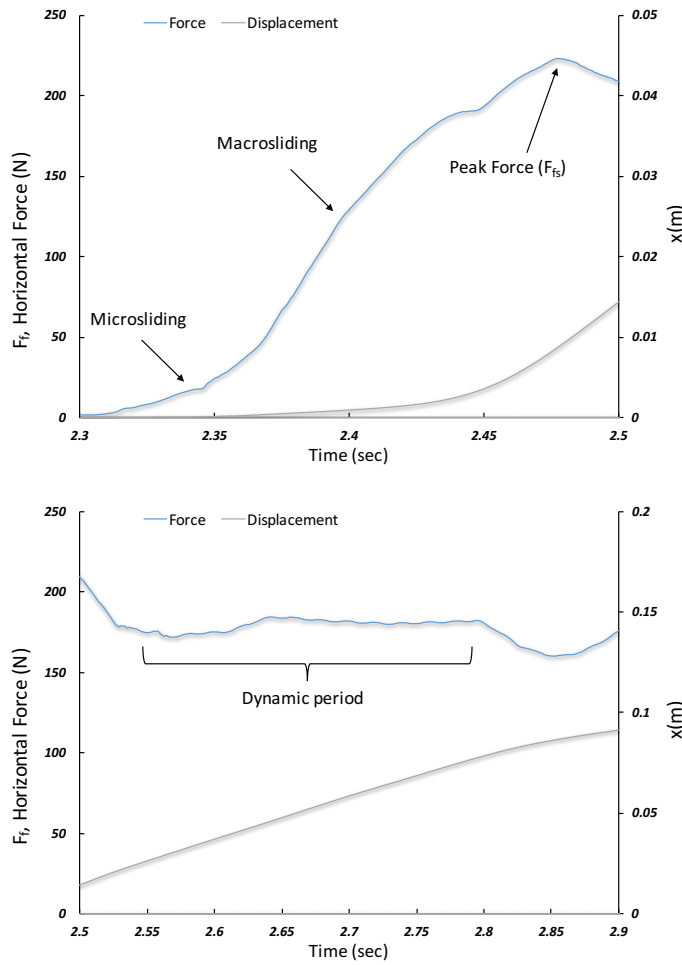
Figure 7.9 Top: static regime, and bottom: dynamic regime of the plot shown in Figure 7.8 top left.

Figure 7.10 shows the free body diagram for this configuration with the forces acting on the test shoe sample.
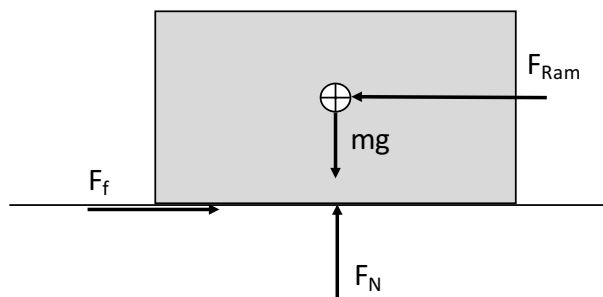
Figure 7.10 Simplified free-body diagram for the sled configuration.

The coefficient of static friction (μ_s), is determined at the moment the test shoe sample moves. At this moment in time, the force ram (F_{ram}), has the same magnitude as the force due to static friction ($F_f = F_{fs}$), just before the sample moves. The normal force (F_N) is determined by the amount of the weight placed above the test sample.

At the instance just before initial sliding:

$$\sum Fx \; = 0 \qquad\qquad\qquad \sum Fy \; = 0$$

$$F_{Ram} = F_f \qquad\qquad\qquad F_N = mg$$

In this case, mg is larger enough (approximately 100N – 400 N), so:

$$\mu_s \; = \frac{F_{fs}}{F_N}$$

<div align="right">**Equation 7-2**</div>

The dynamic coefficient of friction (μ_k), is found from Newton's second law. After the test shoe starts moving, it will come to rest when the horizontal ram is fully extended. Because the test shoe accelerates and decelerates during the motion, the force from the ram, does not match the kinetic friction force. Therefore, as shown in equation 7-3, the measured dynamic coefficient of friction (μ_k) is influenced by the acceleration of the slider. By solving two numerical derivatives of the displacement data, the acceleration of the slider can be found.

$$\sum Fx \; = ma \qquad\qquad\qquad \sum Fy \; = 0$$

$$F_{Ram} - F_f = ma_x \qquad\qquad\qquad F_N = mg$$

$$\mu_k \; = \frac{F_{Ram}}{F_N} - \frac{a}{g}$$

<div align="right">**Equation 7-3**</div>

Figure 7.11 shows an example of a typical graph presenting the relationship between μ_k and velocity. The velocity data is produced by solving one numerical derivative from the smoothed displacement data.
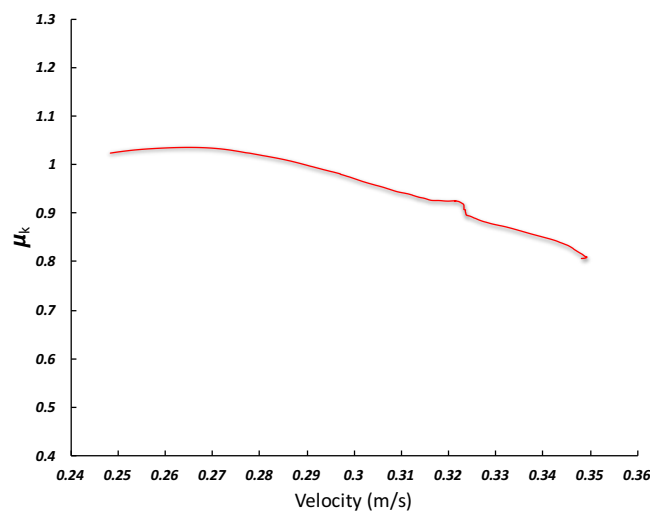
Figure 7.11 Example of μ_k as a function of velocity graph.

7.3   Initial development of test shoe samples

A variety of test shoe bespoke samples were manufactured for the pre-prototype, with the objective to compare the frictional behaviour between them, and to evaluate the feasibility of using commercial rubber for a test shoe. The reason for using bespoke samples instead of actual tennis treads, was because the variability between the different tennis shoe treads, such as tread width, depth and material properties. Furthermore, for testing tennis courts around the world, test shoe samples will need to be provided, making the bespoke treads a more 'future-proof' option. Three main methods for manufacture of the bespoke treads were considered: 3D printing, CNC machining and hole punching.

7.3.1 Manufacture of samples

One advantage of the additive manufacturing process is the new infinite possibility to produce different geometries. However, the disadvantage of this method is the high cost of 3D printing as well the materials available. To test and assess the robustness of this method, a test sample (AM1), shown in Figure 7.13, was produced using an Eden 260VS additive manufacturing machine from a black rubber-like material (Veroblack).

 Figure 7.12 shows a representation of the treads dimensions for each test sample, which are described in Table 7-2.

Figure 7.12 Left: representation of dimensions for total thickness (t), tread height (h), tread width (w) and space between treads (s). Right: representation of hole diameter (ϕ).

Table 7-2 Description of the test samples produced.

Sample	Material	Tread dimensions
AM1	Veroblack	t = 6.5 mm , h = 4.5 mm, w = 3.00 mm and s = 2 mm.
Machined treads	N70	t = 3.5 mm , h = 1.5 mm, w = 3.00 mm and s = 1.5 mm.
Holed rubber	N70	t = 3.55 mm and 2mm diameter.

Upon testing, with the sled configuration and with a vertical load of approximately 100 N, the 3D printed sample, as shown in Figure 7.13, tended to fail in shear. Visibly this sample is not robust enough and makes it difficult to get reliable results. Furthermore, as compared in Table 7-1, the shore hardness of the material is significantly low to that of real tennis, and therefore will exhibit different physical mechanisms.
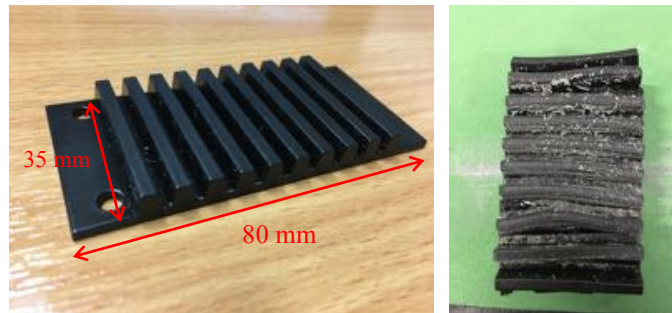
Figure 7.13 Photographs showing the 3D printed sample under 100 N vertical load (left) and the same sample after the testing (right).

In order to assess the feasibility of using CNC machining and hole punching to produce test shoe samples, two N70 samples (35 mm x 80 mm), shown in Figure 7.14,were machined for testing. The tread dimensions (Table 7-2) of both samples were based on the 'Pimples' and 'dimples' main sections of the Babolat 4 Propulse all court shoe described in section 3.5.3. A preliminary testing with the sled configuration, showed that both samples held up well after a series of approximately 45 tests, under different normal load conditions (100 – 300 N). Therefore, more test samples were produced later in this investigation under this method.

Figure 7.14 Top: Actual CNC machined test samples: Machined treads (left); Holed rubber (right).

7.3.2 Test shoe samples developed

Five tennis tread patterns were produced for the preliminary testing phase. Two tread patterns were extracted from the Babolat tennis shoe presented in Figure 7.15 and explained previously in section 3.5.3. The labelled "Babolat pimples" sample was

extracted from the shoe 'grip' section (1) and the second one from the section that is supposed to enhance a player's slide (2), as described previously in section 3.5.3.

In conjunction with these two treads, three rubber samples were manufactured from the N70 nitrile rubber (Table 7-1) for comparison. The "machined treads' sample was produced as a comparison to the "Babolat pimples" and "holed rubber" sample was produced as a comparison to the "Babolat dimples" tread Figure 7.16. Additionally, a "Smooth rubber" tread was produced which featured no tread. Table 7-3 shows a description of the samples with the correspondent dimensions based on Figure 7.12 and Figure 7.16.
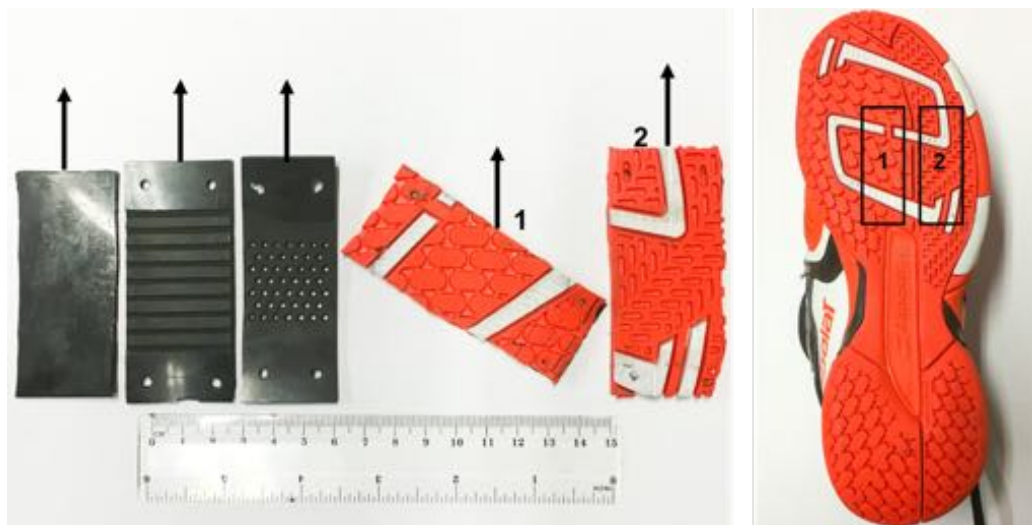
Figure 7.15 From left to right: smooth rubber, machined treads, holed rubber, Babolat pimples, Babolat dimples , complete Babolat shoe.

The dimensions of the bespoke tread samples were designed based on typical in-sole pressures present in real tennis play, as discussed in section 6.3. To ensure this, estimates of the contact area of each sample were calculated. It is necessary to mention that these are estimates and therefore do not necessary represent the real contact area which require additional testing to measure the contact of the rubber onto a tennis surface at a microscopic level. However, the contact area and pressures presented here, show that the bespoke samples in combination with different vertical loads, cover similar pressures to real tennis movements.
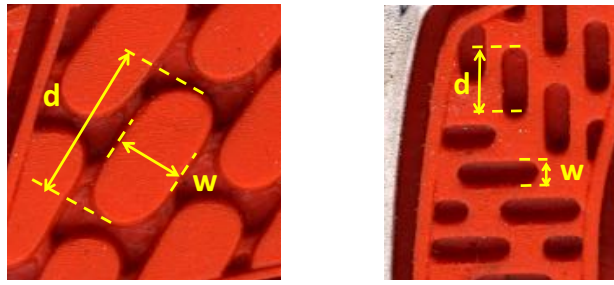
Figure 7.16 Dimensions for Babolat pimples (right) and dimples (left).

Table 7-3 Description of the samples produced for the preliminary testing.

Sample	Material	Description	Area range (mm²)	Pressure range (kPa)
Smooth rubber	N70	t = 3.55 mm	930	109 – 415
Machined treads	N70	t = 3.5 mm , h = 1.5 mm, w = 3.00 mm and s = 1.5 mm.	1133 – 1406	164 – 627
Holed rubber	N70	t = 3.55 mm and 2mm diameter.	636	169 – 644
Babolat pimples	N/A	t = 3.5 mm, w = 6.3 mm and d = 12.1 mm	802 – 1104	93 – 345
Babolat dimples	N/A	w = 2 mm, d = 6.5 mm with a depth of 2.1mm	960 – 982	140 – 417

The area calculation procedure was the same as the one utilised and described in section 6.3. Each test sample was pressed onto a thin layer of black ink under normal loads of 104.5 N, 202.6 N, 300.7 N and 398.8 N. Examples of ink prints used to calculate the pressures are presented in Figure 7.17. Based on the four calculated contact areas, the estimated pressures ranges covered for each sample, shown in Table 7-3, are representative of the pressures mentioned in previous studies. As expected, the measured contact areas increased with increased vertical load for both shoe sizes and the test shoe sliders, in agreement with previous experiments. For the 'Smooth' and 'Holed rubber' samples, the contact area was assumed to be the same for the four normal loads tested.

Figure 7.17 Examples of ink prints used to calculate pressures. Babolat dimples (left), Babolat pimples (centre) and machined treads sample (right).

7.4   Preliminary lab testing of TSSTv1

Two main preliminary studies were implemented with the aim to evaluate and validate the two configurations of the pre-prototype. This preliminary test stage helped to identify the potential improvements or failures in order to complete a final prototype design. The two pilot studies implemented with their respective objectives were:

1. *Comparison against UoSh test methodology*: Initial validation against previous methodology.
2. *Professional tennis surfaces testing*: characterise friction and evaluate the capability of the test devices to distinguish between surfaces.

7.4.1   Comparison against UoSh test methodology

The following study was published in the conference proceedings of the 11th International Sports Engineering Association 2016, Delft, Netherlands (Ura and Carré, 2016).

As a first validation, a comparison of friction measurements was performed between the pre-prototype on the "sled" configuration and the UoSh lab-based device (section d)). The testing took place on one acrylic hardcourt surface HC9, described in section c). Two forefoot segments of the Babolat all court tennis shoe Figure 7.18 of the same design but different size (EU sizes 31 and 39) were tested on the surface with the UoSh device. The vertical loads ranged from 600 – 1600 N in intervals of 200 N.

Additionally, with the sled configuration, two sliders with a "Smooth rubber" and "Babolat pimples" were used as test shoes for this experiment (Figure 7.18). Both sliders were tested over the same surface with a vertical load ranging from 100 – 400 N in intervals of 100 N. The test orientation for both samples was of approximately 50º in relation to horizontal movement. Based on the displacement data, the test shoe slider speed was determined to range from 0.15 to 0.45 m/s. Ambient temperature was monitored throughout the testing. Additionally, after 5 tests with each test shoe slider, they were allowed to cool down for a minute. The μ_s was calculated for both data sets, using the protocols previously described for each test rig.

Figure 7.18 The three test rubber utilised, from left: smooth rubber, Babolat pimples and the Babolat shoe.

Figure 7.19 shows the results for μ_s plotted against average applied pressure calculated and presented in Table 7-3 (assumed to be the average pressure experienced by the shoe immediately before the onset of sliding). All the tests showed the same general pattern with μ_s decreasing with increased applied pressure.
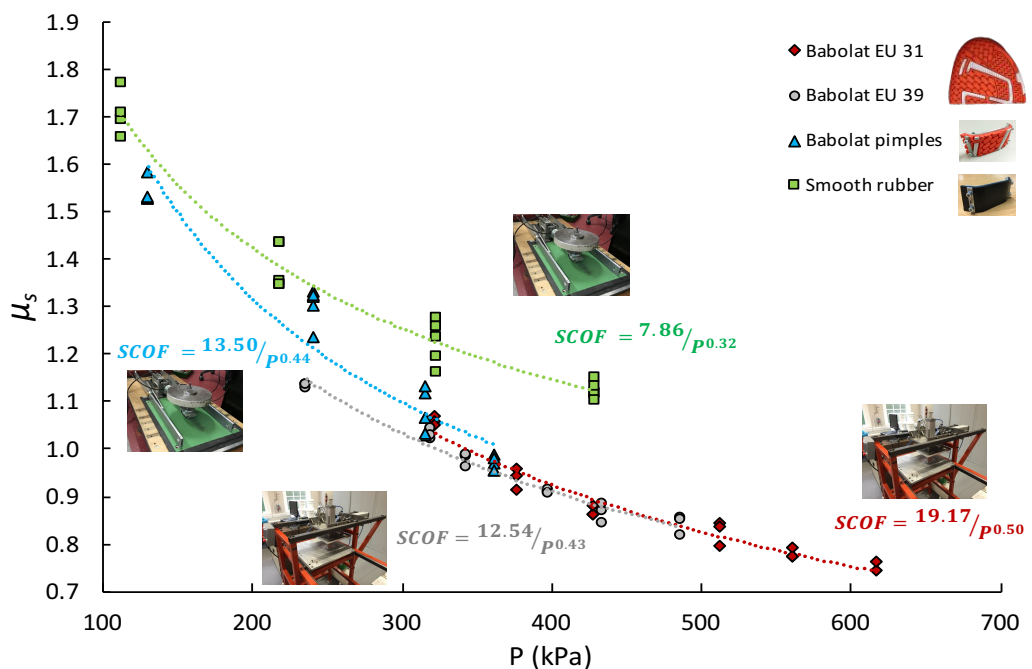
Figure 7.19 (a) Plot of the average SCOF against applied pressure for each shoe and test slider with fitting equations;

The results showed that the principle of matching player insole peak pressures with a small test area and lower vertical loads applied, instead of applying higher vertical loads, has potential to have similar results. Regarding the comparison between the 'Babolat pimples' and the 'smooth rubber' samples with it is clear that sole geometry (e.g. presence of a tread pattern) has a significant effect on friction behaviour. The differences between

these two sliders tested could be due to the different adhesional and hysteretic friction mechanisms generated.

Although further validation of the μ_s *and* μ_k need to be done, this first validation has shown promise to replicate real play conditions, however, in the next sections additional results are compared and analysed.

7.4.2 Professional tennis surfaces testing

One of the main abilities of the new pre-prototype (TSSTv1) is that needs to distinguish between surfaces in terms of the friction measured. For this reason, a number of mechanical tests were conducted with the TSSTv1 test methodology on both configurations (angled-ram and sled) over a range of different classified tennis surfaces.

The testing was in combination with the "smooth rubber", "holed rubber" and "Babolat pimples" test shoe samples, previously described. All the testing was carried out under the operating procedures described in section 7.2.1. For the sled configuration, all the tests were done with a mass of 20 kg on top of the sled.

A variety of seven tennis surfaces, based on the ITF court pace classification, were selected for the testing. The surfaces tested, described in section c) and 3.3.4 were: 4 acrylic hardcourt surfaces (HC1, HC2, HC4, and HC6), one polyurethane carpet (HC8), a hybrid clay surface (AC1) and an artificial grass (AG1). Additionally, a P-150 emery paper and a smooth acrylic surface were tested. 5 trials for each test rubber were carried out for each surface.

The mean values of μ_s obtained with the two configurations on each surface are presented in Figure 7.20 and Figure 7.21. The surfaces in the 'x' axis of the graphs are ranked based on their roughness values (R_a) previously described in section 3.3.3. It is important to note that during the testing with the "Holes" sample in combination with the sled configuration a mechanical problem was present, and no data was collected.

A one-way ANOVA with repeated measures was used to examine the μ_s between the surfaces for each configuration. Significant differences ($p < 0.05$) were found between all the surfaces (acrylics, hybrid clay, artificial grass and polyurethane carpet) for each test tread sample. However, there were a few exceptions of no significant difference:

Angled-ram:

- "Smooth" test shoe - acrylic and polyurethane carpet (*p = 0.97*) and hybrid clay and artificial grass (*p = 0.09*).

- "Holes" test shoe – artificial grass and polyurethane carpet (*p = 0.7*).

Sled:

- Babolat test shoe - acrylic and polyurethane carpet (*p = 1*).

- Smooth test shoe – artificial grass and hybrid clay (*p = 0.52*).

Figure 7.20 shows the μ_s values obtained with the 'angled-ram' and 'sled' configurations. In general the 'angled-ram' measures lower μ_s values compared to the 'sled'. One possible explanation for this could be that, as mentioned in the 'angled-ram' test protocol, by manually increasing the angle, the test shoe starts to experience some 'micro-sliding' before the gross sliding, so possibly, the calculated μ_s could not be considered as a static coefficient of friction, as some movement has already started. Another factor is the angle dependency of the normal and horizontal applied forces. Although the pneumatic ram tries to maintain the resultant force constant as the angle increases (Figure 7.6), the ratio of horizontal to vertical forces also increases, and it may affect the instant of the test shoe sliding on the surface.

For both configurations, the "Babolat pimples" exhibited lower μ_s values compared to the "Smooth" and "Holes" samples. This could be explained by comparing the apparent contact areas of the test samples. As mentioned in section 3.5.3, the contact area measured for the Babolat pimples (843.1 mm^2) is lower than the assumed contact area for the 'Smooth' sample (930 mm^2). This suggest more adhesion between the 'Smooth' sample and the surface and hence higher friction values.

As shown in Figure 7.20, the μ_s values for the three tread samples, with both test configurations (angled-ram and sled) in general presented similar trends between the hardcourt surfaces (HC6, HC8, HC4, HC1 and HC2). However, with the 'angled-ram' configuration, on the synthetic/artificial surfaces, the 'Holed rubber' and 'Smooth' tread samples exhibited the opposite behaviour. For the 'Sled' only the artificial grass (AG1) showed an opposite behaviour. These results could be again explained by the horizontal to vertical ratio. Both synthetic surfaces, as described in section d), are characterised by

having an infill sand, in which the test shoe interacts in a different way compared to hardcourt surfaces. For the 'Angled-ram', as the angle is manually increased, the horizontal to vertical ratio increases, and hence, the friction experienced on the artificial clay (AC1), could be more a 'rolling' friction of the clay particles, rather than a 'sliding' friction. With the 'Sled', the opposite behaviour could be happening, as the vertical force is large enough to compact the clay particles with the test shoe rubber and 'slide' rather than be rolling.
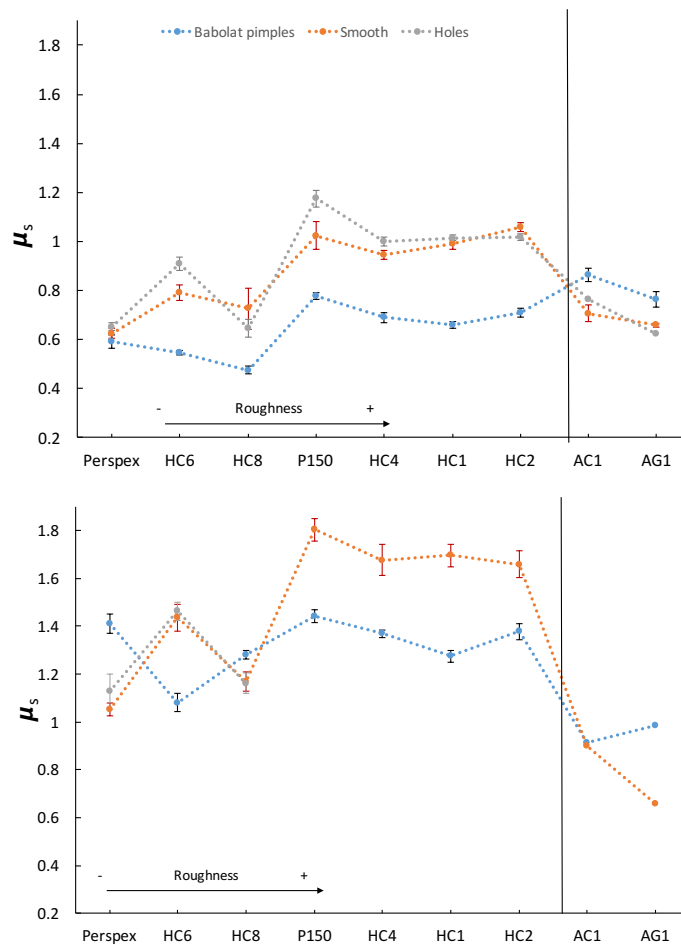
Figure 7.20 Mean values of μ_s obtained with the TSSTv1 angled-ram (top) and sled (bottom).

Figure 7.21 shows the μ_k values for the Babolat pimples and Smooth samples with the sled configuration. For the synthetic surfaces (AC1 and AG1) it is clear that the device is capable to distinguish between surfaces. However, for the rest of the hardcourt surfaces, it is difficult to see differences. By analysing individual plots, the smooth sample results present more peaks within each sample plot, which could be explained by a stick-slip effect. In contrast, the graphs from the Babolat pimples, this effect is less noticeable.
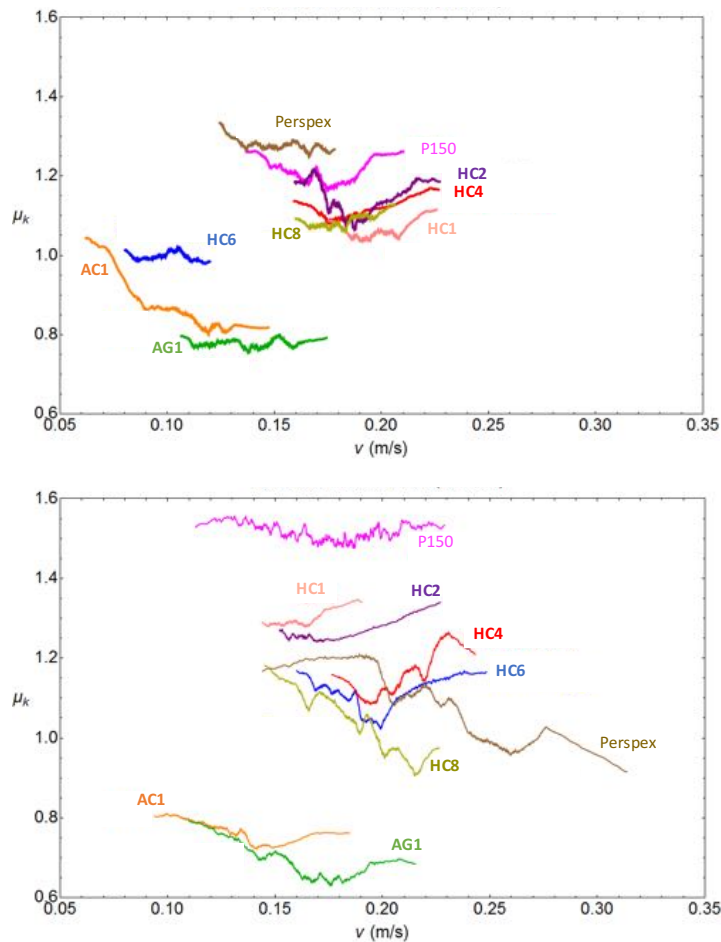
Figure 7.21 μ_k values against sliding velocity obtained with the sled configuration. Babolat pimples (top) and Smooth (bottom).

In terms of roughness except for the HC6 surface the general tendency of friction is to increase as the roughness increases. Looking in more detail to surface HC6, it can be seen that this polyurethane carpet it provides a higher level of cushioning compared to the rest of the surfaces.

In conclusion the two configurations have shown to be capable to measure and differentiate the average μ_s on a range of different tennis surfaces. For the μ_k further testing and analysis need to be done. Additionally, the surface roughness could be used as a parameter to help classify the acrylic hardcourt surfaces. However, for other surfaces with a level of cushioning, or with other characteristics, such as hybrid clay and artificial grass other parameters need to be tested (e.g. cushioning, particle size, etc.).

7.5   Parametric study of simulated tennis treads

The following study was published in the conference proceedings of the 11th International Sports Engineering Association 2016, Delft, Netherlands (Goff et al., 2016b).

The purpose of this pilot study was to investigate and understand the effect of different tread patterns of a tennis shoe on the friction generated during the shoe-surface interaction, in order to decide the best tread pattern to utilise with the final test friction device.

The five tennis treads patterns, shown in Figure 7.15 and described in section 7.5.2 were tested to measure the effect of tread geometry under different vertical load conditions. The experiments were carried out with the TSSTv1 in the sled configuration over the commercially available hard-court tennis surface HC5 sample (R_a = 12 µm), described in section c). The static (μ_s) and dynamic (μ_k) coefficients of friction were determined for each trial under the test protocols defined in section 7.2.1. The testing was carried out over a range of vertical loads and over a range orientation angles. As mentioned in the previous experiment and in the description of the test samples in Table 7-2, the combination of a vertical load and the calculated area of each test sample, generated pressures similar to match conditions. Figure 7.22 shows each tread sample, with the extreme angles utilised for testing, with an arrow depicting the direction the tread samples slide. The angle ranged between 0 and 90°. Each sample was tested at four different normal loads with either a 10, 20, 30 or 40-kg mass placed on top of the test sample. Each load/angle was tested five times to assess the repeatability of each run.
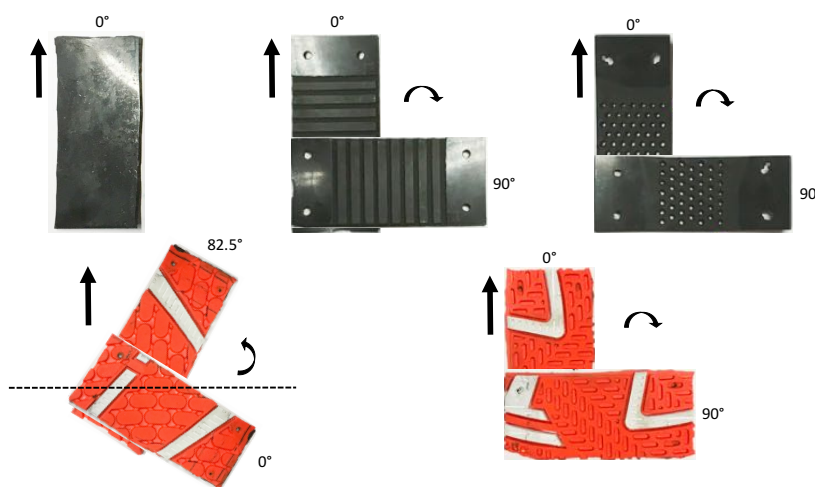
Figure 7.22 The test samples within the initial testing set and the extreme angles at which they were tested.

Figure 7.23 show an example of the results obtained for the smooth rubber sample. It shows μ_s as a function of F_N and μk as a function of v with the fitting equation. These results were calculated for the five test samples.
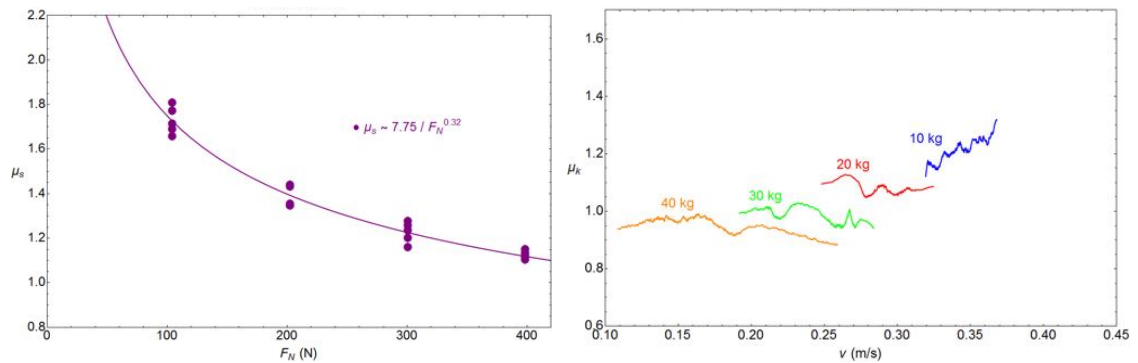
Figure 7.23 Smooth rubber. Left: Coefficient of static friction against Normal Force with fitting equation. Right: Coefficient of dynamic friction against speed.

Some general observations could be made from the obtained results in this study. Despite the spread in data, there is a tendency of the static friction to decrease as the normal force increases for all the cases, it is clear that $\mu_s > \mu_k$, as expected. It was also expected that the sample speed decreases as the normal force increases, due to the larger retarding force due to friction.

For a given angle, the dynamic coefficient of friction decreases with increasing normal force, similar to the coefficient of static friction. For both coefficients as the normal load increases, the data gets more cluttered, revealing less dependence on angle compared to small normal force. For the dynamic coefficient of friction curves, the erratic form is mostly due to an observed stick-slip phenomena and to the linear interpolation used to represent all five repeat test runs.

By observing the impact of tread angle on μ_s, some relationships were identified. For the 'holed rubber' and 'Babolat dimples' graphs, μ_s decreases as the angle increases, particularly at higher normal loads. This is due to the directions of the treads at the different angles. At 0° the treads are perpendicular to the direction of slide and at 90° are parallel to the direction of slide. However, differing to this expectation, μ_s varies in a similar amount with angle for all samples. There is no clear correlation between μ_s and tread angle for the Babolat pimples and machined sample. Comparable results are seen for μ_k at different angles. Both the 'holed rubber' and 'Babolat dimples' show a general

decrease in μ_k with increasing angle, contrary to the 'Babolat pimples' and 'machined sample' where no significant relationship can be seen.

As stated by (Boswell, 2016), a possible reason for these results is due to how the slider changes as the angle is changed. This could have an effect on the measured values of μ_s and μ_k. At 0° the front edge of the slider is curved during the slide. However, at 90°, the front edge is no longer curved and is instead a flat edge as shown in Figure 7.24 . Therefore, there is an impact on μ_s due to the front edge. For the results it is clear that rather than seeing an effect of the change in the tread pattern, there is an effect of the front edge as the angle is increased. This leads to no clear conclusion of how the angle affects the static and dynamic coefficient of friction.
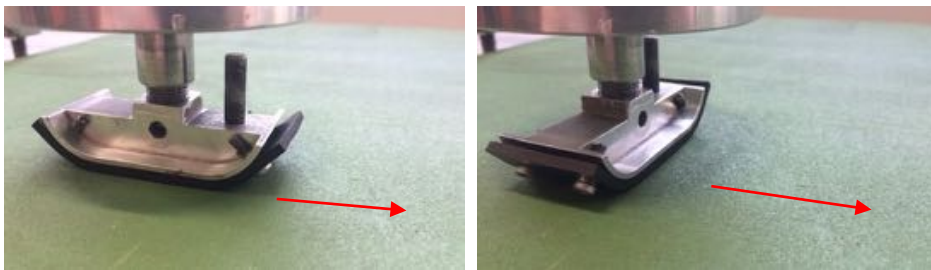
Figure 7.24 Test shoe slider depicting the front edge of the slider at 0° (Left) and 90° (Right). Red arrows indicate direction of slide.

However, it is clear that the data from the three bespoke samples, particularly the 'smooth' and 'holed rubber', exhibit similar frictional effects compared to the two Babolat tennis treads, specifically at higher normal loads. In relationship to the final test prototype, this suggests that these bespoke samples could be utilised with the final test methodology to obtain frictional data characteristic of real tennis treads. The recommendation of which patterned sample to use, based on the feasibility of machining and the results analysed in this section, either the 'smooth rubber' or 'holed rubber' would be suggested. These samples exhibited very similar behaviour at higher loads to the Babolat samples and hence are representative of the friction a tennis player would experience. In the next section a further study on the 'holed rubber' is presented.

7.5.1 Critical shoe contact area ratio

The following study was submitted to the Journal of Sports Engineering and Technology in July 2016 and it is under review (Goff et al., 2016a).

Based on the findings from the parametric tread study presented in the previous section (7.5), and because of the practicality to produce 'holed rubber', further investigation and testing was carried out, with the objective to study the effect of contact area on the frictional interaction between shoe and a court surface.

Seven bespoke samples were manufactured from the N70 Nitrile Butadiene rubber to be tested for this study and are presented in Figure 7.25. All the samples are the same size, and have the same 3mm diameter holes and with the same pattern as the first holed sample presented in Table 7-3. However, changes between the samples rely on the area ratio. The area ratio is defined as the hole area within the contact area divided by the contact area plus hole area. Figure 7.26 shows a typical image of a contact area and its calculation.
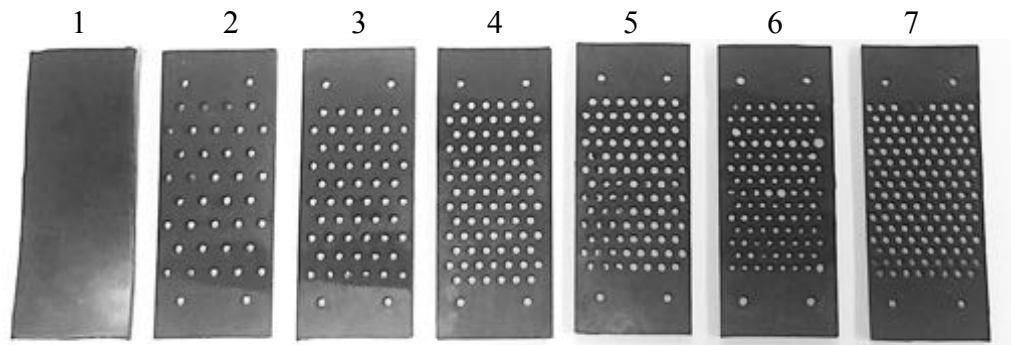
Figure 7.25 Holed-rubber samples. Sample numbers on top
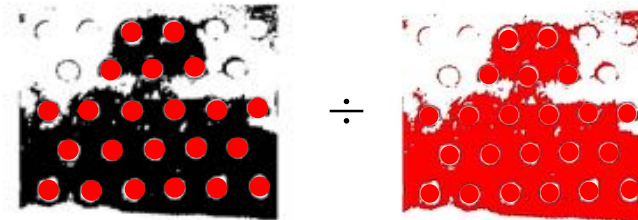
Figure 7.26 Visualisation of calculation of contact area found by dividing the red area on the left by the read area on the right.

To calculate the area ratio, a border of known dimensions was set around the wear regions of each sample after testing. After the testing, each sample was photographed, under appropriate lighting conditions to exhibit contrast between the regions of wear and regions of no wear. Then the images were processed via thresholding. Figure 7.27 shows five of the seven samples tested.
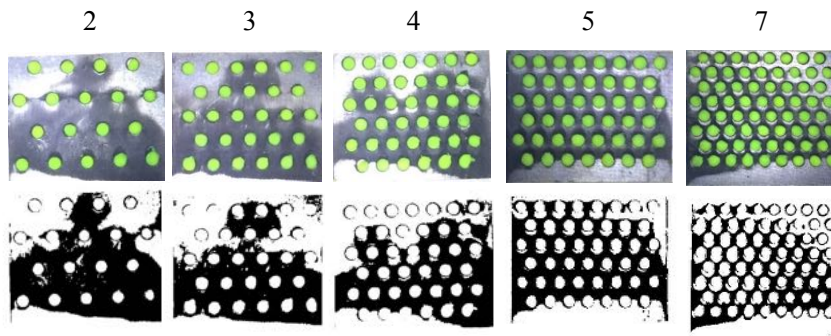
Figure 7.27 Photographs showing wear of the five samples (top) and images processed via thresholding (bottom). Sample numbers are shown above the samples.

The wear region was represented by the black pixels and the area of this region was found by calculating the percentage of black pixels in the overall image. This wear region represents the maximum possible contact area that could occur during testing because of the wear variability between trials. The wear pattern on each sample is the accumulation of all trials. The area ratio was calculated using Equation 7-4 except for samples 1 and 6 could not be assessed using this method, as extra testing took place on these samples before photographs were taken. Therefore, the wear area of sample 1 was assumed to be the same as sample 2, excluding the hole area. For sample 6, the wear area and area ratio were found by interpolating the data across all area ratios. The information regarding the area ratio calculations for each sample is shown in Table 7-16.

$$AR = \frac{Area_{holes}}{Area_{wear\ region} + Area_{holes}}$$

Equation 7-4

The experiments were carried out with the TSSTv1 in the sled configuration on the commercially available hard-court tennis surface HC5 described in section c). The static (μ_s) and dynamic (μ_k) coefficient of friction were determined for each trial using the test protocols defined in section 7.2.1. Each sample was tested at the normal loads of 104.5, 202.6, 300.7 and 398.8 N, achieved by one to four 10-kg masses on top of the test sample. Five tests were done for each condition, having a total of 20 tests for each sample.

Table 7-4 Data used to calculate area ratios for each sample tested. Pressure range calculated with the normal loads (104.5, 202.6, 300.7 and 398.8 N).

Sample	Total area (m²)	Total pixels	Black pixels	Wear area (m²)	No. holes within wear area	Area ratio	Pressure range (kPa)
1	n/a	n/a	n/a	5.57×10^{-4}	0	0	188 – 716
2	8.37×10^{-4}	116022	66401	4.79×10^{-4}	14	0.116	218 – 832
3	8.37×10^{-4}	106876	53650	4.20×10^{-4}	22	0.181	248 – 949
4	7.75×10^{-4}	110960	57811	4.04×10^{-4}	28	0.227	258 – 987
5	7.75×10^{-4}	54080	27490	3.94×10^{-4}	38	0.288	265 – 1012
6	n/a	n/a	n/a	3.68×10^{-4}*	n/a	0.328*	283 - 1083
7	8.37×10^{-4}	60291	24435	3.39×10^{-4}	52	0.373	308 - 1176

denotes values with calculated through interpolation.

Figure 7.28 and Figure 7.29 show coefficient of static friction (μ_s) against the normal force and dynamic coefficient of friction (μ_k) as a function of speed for the seven samples under testing. Raw data are shown on the static friction plots, with best fit curves to the data.
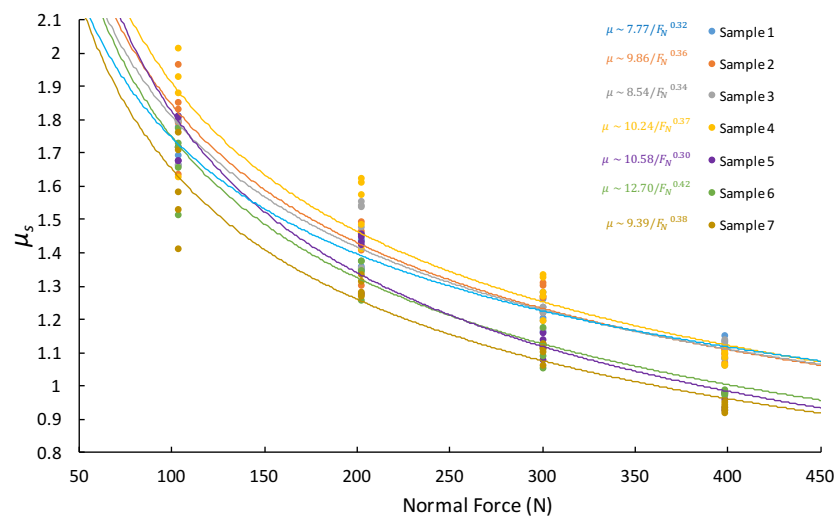
Figure 7.28 Sample 1 results. Left: Coefficient of static friction against Normal Force with fitting equation. Right: Coefficient of dynamic friction against speed.
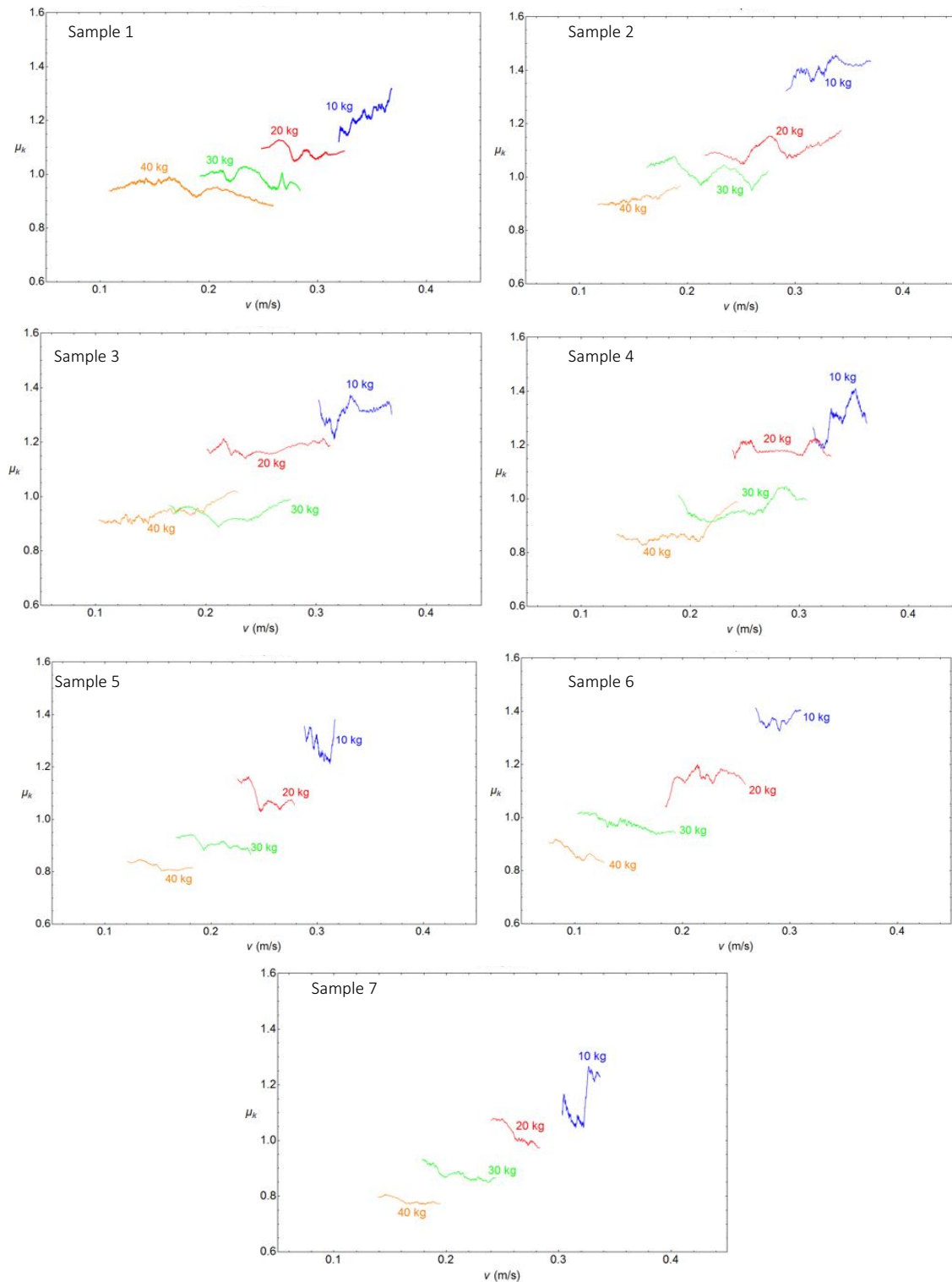
Figure 7.29 Samples 1-7: Coefficient of dynamic friction against velocity results.

For the μ_s graph shown in Figure 7.28, it is clear that samples 2, 3 and 4 exhibited very similar frictional values to sample 1 (smooth), particularly at the higher normal loads of 300 and 398 N. However, the samples with a higher area ratio, samples 5, 6 and 7 showed a clear drop in μ_s at the 398 N normal load. This drop in friction appears to occur at an area ratio between 0.227 (sample 5) and 0.228 (sample 6), and represents a significant difference in friction. This was further confirmed with the average and standard error bars in Figure 7.30. There is no statistical difference of μ_s values for 104 and 200 N normal loads. However, for 300 and 40 kg mass attached, the μ_s values show differences between samples 1 – 4 and 5 – 7. The standard error bars for samples 1 – 4 do not overlap those of samples 5 – 7. Therefore, there is a critical area ratio between 0.227 and 0.228 (sample 4 and 5) where the coefficient of friction drops for higher normal forces. In terms of the player-surface interface, these relationships suggest that at normal loads similar to real tennis movement, the higher area ratios have less frictional resistance than those with a lower area ratio.
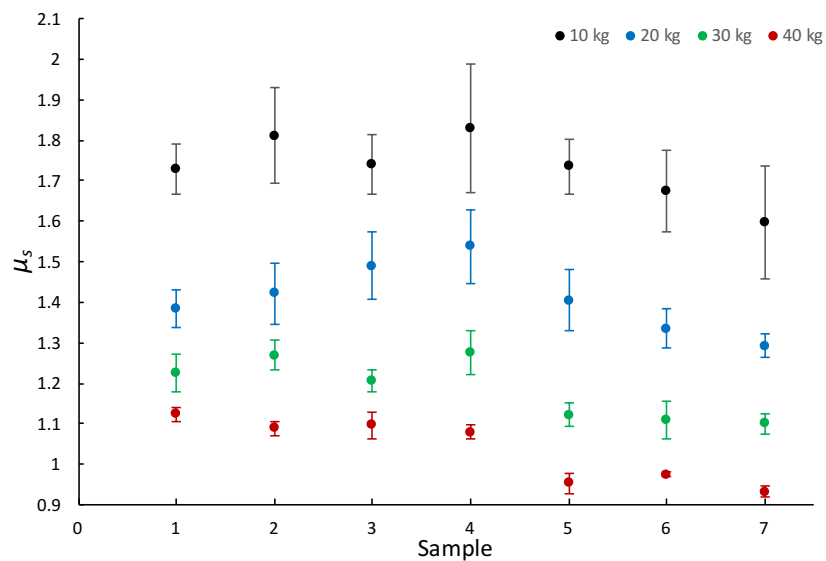
Figure 7.30 Average values of μ_s with standard error (± SD) for the seven samples for the four normal loads applied.

The dynamic friction graphs show a similar behaviour to the static friction graphs. Tread samples 2, 3 and 4 show similar frictional values across all loads. However, unlike the μ_s graphs, sample 1 (smooth) exhibit lower dynamic friction at lower loads 104.5 and 202.6, implying that a smooth rubber will provide less frictional resistance, once sliding compared to a holed sample with a low area ratio. In a similar way, at higher area ratios of samples 5, 6 and 7, dynamic friction falls, particularly at the highest normal load of 398 N, trending towards 0.8.

Furthermore, although normal force was emphasized over pressure in this study, pressures were calculated from the wear areas previously found in Table 7-4. From these estimates, μ_s values showing the frictional change between area ratio was produced in terms of pressure rather than normal force as presented in Figure 7.31. Focusing on the transition region with 30-kg masses attached, pressures on samples 4 and 5 were about 744 kPa and 763 kPa, respectively. With 40 kg attached, those pressures rose to 987 kPa and 1012 kPa.
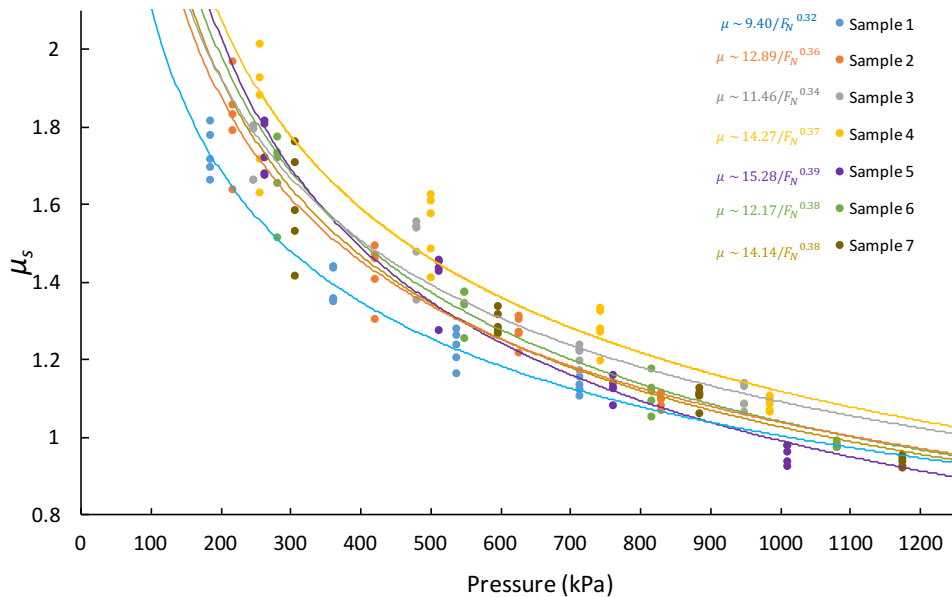
Figure 7.31 Graph depicting μ_s against pressure for the seven rubber samples with a range of area ratios.

As discussed in the previous section 3.5.3, the Babolat Propulse 4 all court tennis shoe, have a 'dimples' section located at the outer part of it outsole. The area ratio of the dimpled portion was calculated under the same procedure previously described giving a value of 0.35, being very close to sample 6 of this study. Figure 7.32 shows the best-fit curve for the Babolat sample tested in the previous study presented in section 7.5. As

expected, based on the Babolat's area ratio, the μ_s curve shows to have a similar behaviour at higher normal loads (from 300 N).
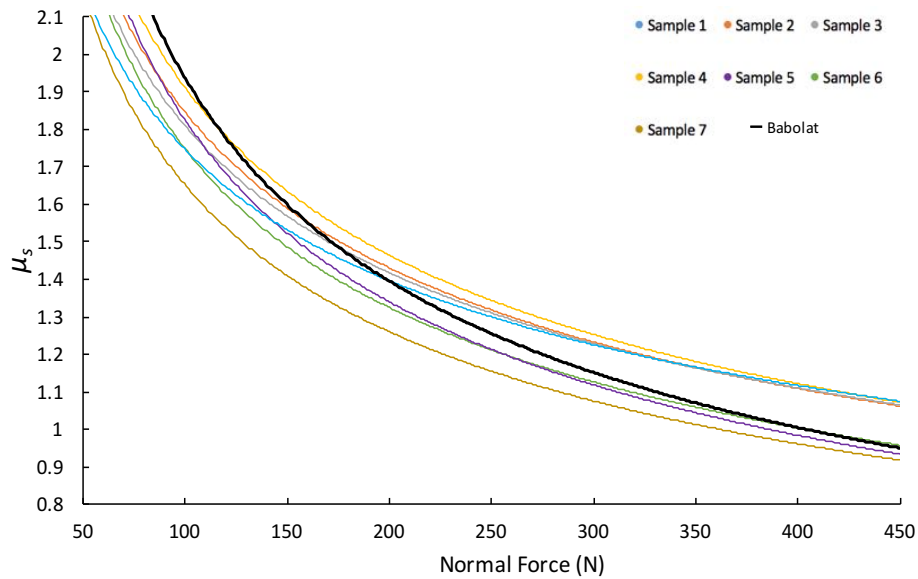
Figure 7.32 Fitting functions for coefficient of static friction. Babolat dimples shoe sample result is shown with a black thick curve.

The results from this study, give a clear insight into how the area ratio parameter can be used to achieve different frictional effects between a tennis shoe and a hardcourt surface. It also highlights the necessity to characterise this relationship through mechanical testing. As discussed in section 4.2.2, with the increasing trend of top tennis players sliding on hardcourt surfaces, tennis shoe manufacturers can utilise the area ratio of a tennis tread to allow players to initiate and continue sliding with less risk of injuries due to friction resistance. Furthermore, a holed tennis tread with an area ratio greater than 0.288 could be used on a tennis shoe outsole as a sliding element, in combination with other elements to give more stability or traction. The position of these elements can be complemented with insole pressure studies, to determine the optimal position depending on the type of movement and frictional needs.

As a conclusion for the final test rig, it is recommended to use a punched hole sample with a minimum area ratio of 0.288, which behaves similar to a part of a tennis shoe, as presented in this section.

7.6 Discussion of chapter

The preliminary tests of the pre-prototype (TSSTv1), showed that the device has the potential of measuring and distinguishing friction between typical tennis surfaces. However, further improvements need to be done to the rig, in order to reach higher test shoe velocities, as it was previously shown (section) an effect of the shoe velocity in the friction generated with the surface.

In addition, some mechanical and component developments have been identified to be required to ensure the rig is working to its full potential.

7.6.1 Rig

In general, a review of materials and mechanical components were identified after the first stage of preliminary tests. These improvements are:

- A more solid and light frame structure.
- Change of material to some specific parts, as aluminium is ductile.
- Implement a solution to easily move around a tennis court.

Angled-ram configuration:

- Improve the interaction between the treaded bar and the pneumatic cylinder.
- An efficient way to adjust the height of the cylinder in order to reach a range of angles.

Sled configuration:

These improvements, previously described, are to enhance the performance of the test device, and to reduce time testing. Therefore, these do not represent a major problem and could not be affecting the results. However, a more serious problem is analysed in the next section.

7.6.2 Slider tipping problem

During the preliminary testing, it became evident that the first slider design had some issues that needed to be reviewed. On both test configurations, after some tests, it was found some marks on some of the tennis surfaces, suspecting that the slider began to tip

to the front edge damaging the surface with the front screws. It was decided to study this phenomenon to understand it and find a solution for the final design.

Angled-ram configuration
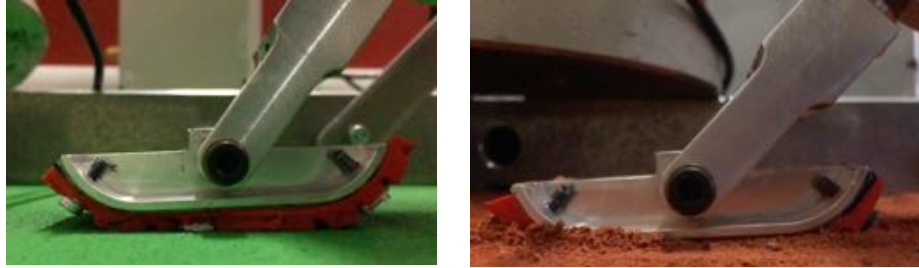
Figure 7.33 Photographs of test shoe slider tipped to the front during two tests on hardcourt (Left) and hybrid clay (Right).

With the help of Solidworks, it was decided to analyse how the forces are transferred into the test slider and onto the surface. Figure 7.34 shows the slider 3D CAD model with a representation of three possible scenarios based on the angle of application. It can be seen that, when the pneumatic ram applies its force at a 20° this force is close to the centre of the slider, however as the angle increases, this force moves to the front of the slider, close to the curve part of the slider and making it tip to the front. These scenarios were observed during high speed videos (240 fps) taken during some testing. Figure 7.33 show two images of the test slider tipping to the front. A possible implication of this could be the reduction of the contact area, and hence the pressure applied to the surface, which could be affecting the friction measurement. Another implication is that, as shown in Figure 7.33, because of this tip to the front, the rubber could be getting fixed on the surface, increasing the adhesion between the two materials, and hence the friction measurement.
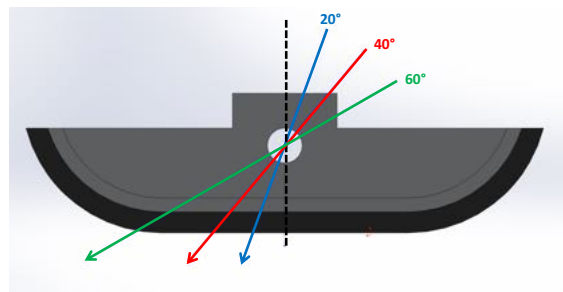
Figure 7.34 Direction of force application.

Sled configuration

For this configuration, Boswell (2016) found similar tipping behaviour to the angled-ram configuration. For the sled, it was evident that at higher normal loads, the slider began to tip to the front edge. This was also manifest on how the rubber sample got worn, as shown in Figure 7.35, in which it can be seen that the rubber sample was worn unevenly. Slow motion videos (240 fps) were taken of the siding motion with the 10 kg and 40kg masses on top, in order to visualise the tipping issue.

Figure 7.35 Example of uneven wear of holes sample.

The 10kg video showed that before and during the slide, the test slider continued parallel to the surface. In contrast the 40kg video showed that, although the slider was parallel at the start of the test, during the slide the test slider tipped onto the front edge and therefore, was no longer horizontal to the surface. In order to analyse this tipping problem for the slider turning, the centre of mass of the rig setup needed to be found. It was obtained with the help of Solidworks CAD software.

$x_{Ram} = 0.123$ m
$y = 0.074$
$b = 0.017$ mm
$c = 0.020$ mm

$x_{Ram} = 0.124\ m$
$y = 0.122$
$b = 0.016\ mm$
$c = 0.068\ mm$
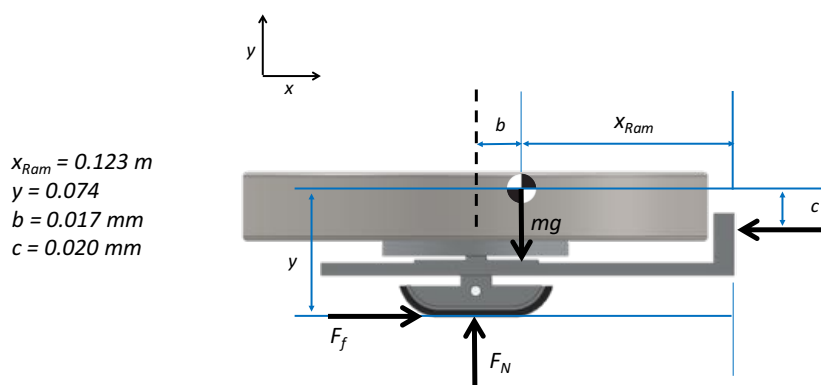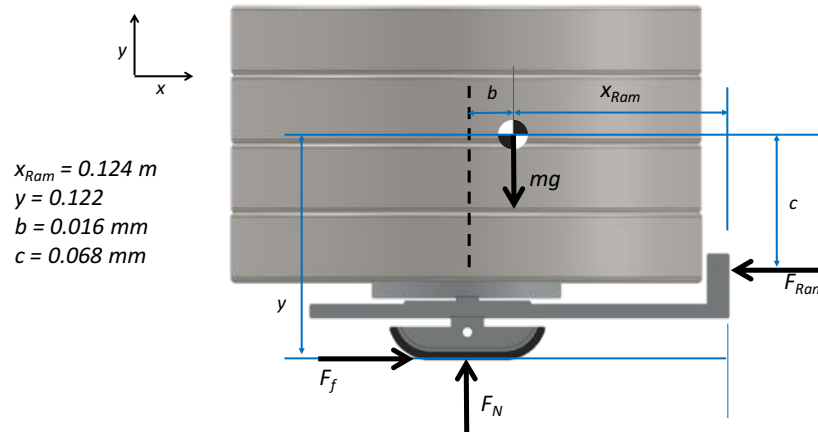
Figure 7.36 Example of force diagrams representing the turning moment problem. Top: 10 kg; Bottom: 40 kg.

Figure 7.36 shows the setups for 10 and 40 kg. These models assume the homogeneity of parts, however, they are useful to analyse the forces which the slider is subject to and try to understand and explain the tipping at higher loads. Although Figure 7.36 only shows the 10 and 40 kg scenarios, the respectively centre of mass, with the forces were calculated also for 20 and 30 kg.

F_{Ram} is is calculated using equation 7.4. The pressure used in the preliminary testing was 2 bar, therefore, F_{Ram} was constant throughout.

$$F = PA \quad where\ A = \pi r^2$$

Equation 7-5

F_N is the reaction force from the surface, and it counters the weight of the rig, therefore is equal to its weight and it is assumed to act at the centre of the slider. Equation 7-5 is used to calculate the frictional force F_f. This is the necessary force for the slider to begin movement, when $F_f = F_{fs}$.

$$F_{fs} = \mu_s F_N$$

Equation 7-6

For this model, μ_s is assumed to be constant for every situation. From Figure 7.19, the values of μ_s are extracted, for a smooth rubber test sample and each loading condition. The values are 1.8, 1.4, 1.2 and 1.1 for the 10, 20, 30 and 40 kg respectively. In a real situation, this μ_s values as well as F_f and acceleration will vary through the slide. Subsequently, the overall counter clockwise turning movement was calculated from equation 7.6 and labelled as M.

$$M = \left(F_f \times y\right) - \left(F_N \times b\right) - \left(F_{Ram} \times c\right)$$

<div align="right">**Equation 7-7**</div>

Table 7-5 shows the respective distances, forces and moment for each situation. It is clear that the 40 kg condition gives a much larger turning moment. At 10 kg, the moment is small around 2.6 Nm and it is not enough to turn the slider onto the front edge. However, the moment at the 40 kg condition, is around 5 times larger, which causes the slider to tip.

Table 7-5 Distances, forces and moments for each loading condition.

Variable	10 kg	20 kg	30 kg	40 kg
X_{Ram} *(m)*	0.123	0.123	0.123	0.124
y (mm)	0.074	0.091	0.106	0.122
b (mm)	0.017	0.016	0.016	0.016
c (mm)	0.020	0.037	0.052	0.068
F_{Ram} *(N)*	475.2	475.2	475.2	475.2
F_N *(N)*	104.5	202.6	300.7	398.8
F_f *(N)*	188.1	283.6	360.8	438.8
M (Nm) CCW	**2.65**	**5.12**	**8.80**	**15.0**

7.7   Summary of chapter

In summary, this chapter describes the design methodology implemented to develop the portable test methodology, a series of preliminary tests and the design refinements for the final device.

1. A rapid pre-prototype test device was designed and manufactured. After some preliminary testing, the device revealed some apparatus limitations, such as slider tipping under the two configurations.

2. After the assessment of three methods, CNC machining and punching of holes was selected as a robust method to produce bespoke test rubber samples. Three types of test sample were then produced: a 'smooth rubber', 'machined treads' and a 'holed rubber' samples.

3. It was found that a commercial available rubber, Nitrile N70, with similar mechanical properties to actual tennis shoes, could be used to produce standard test sliders.

4. After some preliminary tests with the pre-prototype (TSSTv1), the main findings
   obtained identified are:

   a) As a first validation, the comparison of the TSSTv1-sled against the UoSh traction
      rig proved to be promising as the values obtained by matching pressures with the
      regular shoes and a bespoke tread sample.

   b) The ability of the TSSTv1 sled and angled-ram configurations proved to be able
      to distinguish the μ_s between three main surfaces: hardcourts, artificial grass and
      clay, either with commercial tennis shoes samples and bespoke tread samples.
      However, for μ_k further testing and analysis need to be done as a stick-slip
      behaviour was found.

   c) Commercial shoes and bespoke treads exhibited the ability to be used as test
      sliders with the prototype TSSTv2. After some friction testing there is a tendency
      of the static and dynamic friction to decrease as normal force increases, which is
      in good agreement with other studies.

   d) Results from the 'Holed rubber' treads with area ratios from 0 up to 0.227
      exhibited little change in frictional behaviour. However, there is a clear drop in
      friction at area ratios of 0.288 and above at the 400 N normal load condition.
      Samples 5, 6 and 7 showed similar frictional effect to the commercial 'Babolat
      dimples'.

   e) The front edge of the test slider during a slide, showed to have an effect on the μ_s
      and μ_k measured on both configurations. For the 'angled-ram' this was corrected
      by changing the point where the load is transferred to the test slider. For the 'sled'
      the 40 kg condition gives a much larger turning moment. Therefore, it is
      recommended to use smaller loading conditions.

8. General Discussion

8.1   Summary of Findings

The current thesis aimed to take previous existing understanding of the biomechanical parameters and tribological mechanisms that occur during typical tennis player movements, build further on this understanding and develop a robust, portable device to assess the friction characteristics of tennis surfaces. Specific aims were identified in order to achieve the overall aim of the thesis aims. Three experimental chapters (4, 5 and 6) and a design chapter (7) were developed in order to achieve the overall thesis objectives.

Chapter 4 utilised the video analysis in combination with lab and field mechanical testing to specifically inform the main biomechanical parameters that affect the shoe-surface interaction in tennis (Specific objective 1, p. 3). As mentioned in Fernandez et al. (2006), tennis is characterised by dynamic and athletic movements such as running, turning and deceleration on a variety of surfaces. This variety of movements develops different levels of friction during the shoe-surface interaction and it is critical to identify them, as they affect the performance and injury risk of an athlete (Frederick, 1986). The video analysis presented in section 4.2, proved to be helpful as an observational tool to study typical tennis movements and to identify the player's risk-specific movements on tennis courts. After an observational analysis, it was reported that landing and sliding are movements, despite the surface, were more falls occurred. Slip and grip were identified as main contributors to increase the chance of a player's fall, which is in good agreement with Clarke et al., (2013) who stated that poor friction may result in a fall or slip. Additionally, the video analysis was useful to reveal a tendency of players to perform sliding movements on hard courts similar to clay courts. The results showed a sliding occurrence of 28% on hard courts compared to a 46% on clay courts, supporting the statement that the players adapt to the friction characteristics of the playing surface (Damm et al., 2013). The shoe velocities during a slide on hard courts were measured for a small sample through video analysis and were ranging between 2.8 and 4.5 m/s, suggesting that players can adapt to the shoe-surface factors, in order to maintain a slide or stop abruptly. An effect of the shoe velocity during a sliding movements was found and corroborated by lab testing.

Finally, in order to obtain more accurate results in terms of shoe-surface friction, a novel loading methodology was developed in Chapter 4 to replicate more closely a player's

loading profile as suggested by Dixon et al., (1999) and Chang et al., (2001b). One of the main objectives of this new methodology was to be utilised with the final portable test methodology. Although this new methodology opens new possibilities and was useful to measure the static coefficient of friction, it was concluded to use a previous protocol (Clarke et al., 2013) because of its simplicity and less components to implement it.

The current thesis aimed to compare data collected from existent experimental field test methodologies on different tennis surfaces, in order to identify advantages and disadvantages of each one (Specific objective 2, p. 3). From Chapter 5 it was evident that experiments with two bespoke devices (The Crab and a sled), on grass and clay surfaces, were useful to show the practicability on each surface. On clay and grass surfaces, the bespoke sled device was found useful to measure shoe-surface friction. The device showed the ability to exhibit differences in friction depending on characteristics for grass such as: level of wear around a tennis court, moisture level and grass height. For clay, the friction results collected presented differences in friction depending on the particle size and the amount of artificial clay. In a similar way, the second device, The Crab III, showed to be useful on clay surfaces, however, for grass, due to its very low normal load, was found to be skidding on providing no reliable friction measurements. Stiles and Dixon (2006), mentioned that the actual loading of the shoe-surface system caused by a tennis player is higher than that replicated by most mechanical devices. Therefore, the findings suggest to keep normal loads high enough during mechanical testing on tennis courts. However, there is a compromise between the magnitude of a high normal load and the portability of a test methodology. In Chapter 6 it was demonstrated that measuring friction by matching insole peak pressures of match conditions with lower contact areas, is in good agreement with friction measured by applying higher vertical loads, which opens the possibility to design light mechanical devices. Damm et al., (2014) reported peak pressure values ranging from 340.4 – 596.6 kPa, which can be achieved by a combination of a specific vertical load in combination with a small test shoe.

In tennis, as previously showed (section 3.5.3) there is a vast variety of shoes available for tennis. The shoes include a variety of different thread geometries in order to give the enhance the player's performance on clay, grass and hardcourt surfaces. To carry out further laboratory/field based testing as necessary to build on understanding of tribological mechanisms of the shoe-surface interface (Specific objective 3, p. 4).

Chapters 5 and 6 presented the results of some pilot studies in which some of these frictional mechanisms were evaluated.

As demonstrated in section 4.2 sliding is a tennis movement widely used on clay surfaces, however most recently has been utilised on hardcourts to reduce recovery times to reach a ball (Pavailler and Horvais, 2014). During a sliding the player orientates the shoe on different directions in relationship with the movement, to obtain the desired outcome, creating a unique and specific orientation between the treads and the surface. In Chapter 6 the effect of the shoe orientation during a slide on the friction was evaluated as a tribological mechanism. The results showed that the shoe orientation and normal force, were found to affect the friction mechanisms during a sliding movement. Each orientation tested (0°, 30°, 60° and 90°), showed strong and significant linear regressions between normal force and the dynamic coefficient of friction. Damm et al., (2013b), reported values of 33.2 and 44.6 degrees for the shoe orientation angle during a forehand and turning movements respectively. Although the experiments were performed with one specific shoe, the results suggest that the players could experience different levels of friction during a tennis match.

Additionally, it was found that during a slide movement on hardcourts, the front part of the shoe outsole experiences a temperature increase up to 6°C compared to four other positions along the shoe. The results from the shoe-surface temperature study showed a correlation between the vertical load and outsole temperature change. As the load increased from 600 to 1800 N, the temperature change went from 1.3°C to above 6°C on four different surfaces. It was also found that the number of consecutive slides contributes to a change in temperature. As the number of slides increases, the DCOF decreases, however after approximately 14 consecutive slides, the DCOF starts to increase again (for the surface/shoe combination tested).

Chapter 7 aimed to design and develop a bespoke prototype(s) for assessing the friction during shoe-surface interactions in tennis (Specific objective 4, p. 4). After a detailed and parametric design, the construction of a pre-prototype (TSSTv1) and a prototype TSSTv2 was implemented. The main characteristic of these devices is the ability of having two test configurations in order to replicate two tennis movements. In order to measure the friction of the shoe-surface interaction, it was important to closely mimic biomechanical and tribological mechanisms. For this reason, some biomechanical and tribological

conditions were selected from the literature review in conjunction with the results from the experimentation to be used as boundary conditions for the test devices.

Biomechanical conditions

1. In terms of kinematics, two 'high risk' movements were chosen to be replicated with the test device: a shoe landing and a slide (section 4.2.1).
2. Utilise different values of normal loads during friction testing (Clarke et al., 2012a)
3. Target peak pressures for the two movements: a landing (400 – 500 kPa) and slide (200 - 250 kPa).
4. It was found an effect of shoe-velocity on friction during a sliding movement, however due to mechanical components, this needs further reviewing.

Tribological parameters

- The temperature of the shoe and surface need to be monitored through testing. Additionally, a rest time between trials is recommended to cool down the rubber sample (section 6.4).
- A Nitrile commercial rubber (N70) was found to have similar mechanical properties and provide comparable frictional measurements compared to tennis shoe rubber.

In addition to the boundary conditions previously defined, and to aid the process of surface classification, it is recommended to utilise other surface parameters, such as roughness (Clarke et al., 2012b) clay particle size (section 5.3), clay sand infill volume (section 5.4). and grass height (5.2).

Additionally, Chapter 7 aimed to initially evaluate, compare and validate the designed pre-prototype (TSSTv1) against lab established methodologies (Specific objective 5, p. 4). A first preliminary set of lab-tests with the pre-prototype showed the next key findings:

- A comparison of results between the TSSTv1 using the sled configuration with the UoSh test rig showed good agreement for the static friction measured and confirmed the principle of matching player peak pressures in order to replicate play conditions.

- The results of a series of tests over a range of 7 professional tennis surfaces with two bespoke tread samples and a commercial tennis shoe, showed the ability of the pre-prototype to distinguish between surfaces in terms of static friction. These differences

were found with both angled-ram and sled configurations. For the dynamic friction a stick-slip effect was found, making it difficult to distinguish between the surfaces.

- The parametric study of five tennis tread patterns (2 commercial and 3 bespoke) tested under a range of loads (100 – 400) and orientations (0 – 90°) revealed that the static and dynamic friction have a high dependence on normal load rather than angle of orientation. In general, it was found that two bespoke samples (holed and smooth) showed similar frictional effects compared to a commercial tennis shoe.

- The study of the effect of contact area on the friction in contact with a surface revealed how the area ratio parameter can be used to achieved different frictional effects. Samples with an area ratio greater than 0.288, provided less friction compared to other samples and behaved similar to a commercial shoe outsole section.

8.2   Implications of Thesis findings

8.2.1   Player's utilisation of friction during shoe-surface interactions

As previously mentioned, nowadays, tennis is characterised by powerful strokes, high spin and hence more athletic movements (Fernandez et al., 2006). These movements typically consist of an initial split step followed by side steps to reach an incoming ball (Hughes and Meyer, 2005). In tennis there is a wide variety of tennis movements like running, turning, breaking, slipping and sliding. Although it is well known that player movements differ between grass, clay and hardcourt surfaces (O'Donoghue and Ingram, 2001), it has been suggested that the main characteristic affecting the player-surface interaction may be the friction (Girard et al., 2007). Although the results from this thesis confirm it, the factors affecting the generated friction have never been studied for the sport of tennis.

As previously showed in Figure 1.1, a specific tennis movement is determined by the interactions between the three main factors: player biomechanics, the shoe and surface. The sum of these factors (equation 8-1) affect how a player adapts to a tennis court, and hence, increases or reduces the performance or injury risk.

$$Player\ biomechanics + Surface + Shoe = Tennis\ movement$$

The previous equation, shows the factors involved during a tennis movement, however it does not show how these interact. The way a player moves on a tennis court with the correspondent interactions is represented in Figure 8.1. As shown in the diagram, during this process, two main interactions occur in order to perform a particular movement: player-shoe and shoe-surface.
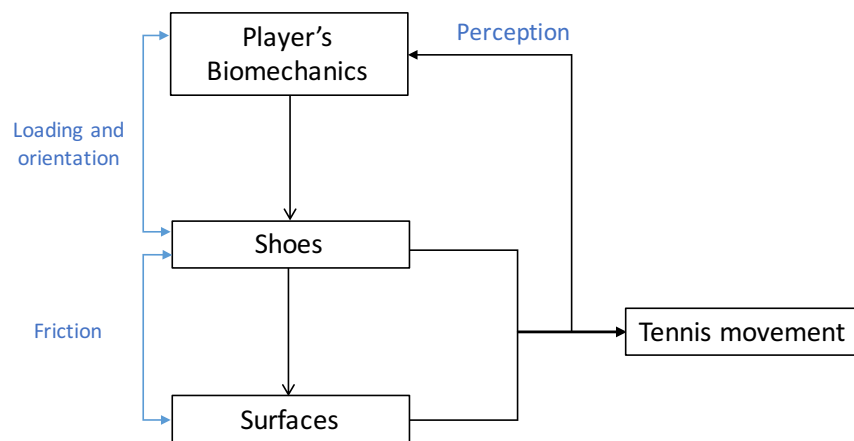
Figure 8.1 Graphic representation of the interactions during a tennis movement.

The first step of this process, in order to perform a movement, is determined by the player-shoe interaction. It involves the player making an instantly decision about the amount of load (horizontal and vertical) to apply into the shoe and how the shoe needs to be oriented in reference to the direction of movement. All of this is based on the type of shoes and playing surface. This interaction is mainly determined by the biomechanics of the player (kinematics and kinetics), which is based on the player's technique and ability. Next, the second step of this process is the interaction between the shoe with the playing surface. This involves a contact between the asperities of both materials producing a friction between them. This friction is ruled mainly by two mechanisms, the adhesion and hysteresis (Persson, 2001, Persson, 2006), which are affected by different factors such as material properties, contact area, pressure, velocity, contact time and other variables (Chang et al., 2001a). Thanks to the specialisation of tennis shoes available in the market, a tennis player could utilise different parts of the tennis shoe to perform a specific movement. (Wilson 2016). The results from the treads analysis (section 7.5) suggest that a player could experience different levels of friction depending on the part of the shoe that utilises.

Finally, during the tennis movement when the shoe and surface are in contact, the player receives a feedback from this interaction which could help deciding if it is necessary to make a change either to the biomechanics or the shoe orientation in order to perform successfully the movement. Players have the ability to regulate the friction experienced with the court surface. A good example is the sliding movement showed in section 4.3.1 and in Figure 5.15, in which the player by modulating the ratio between the vertical and horizontal loads, controls the amount of friction experienced. Damm et al., (2013) reported different utilised COF values for a forehand manoeuvre performed on acrylic and clay tennis courts which confirms that a player could adapt to the tennis court depending on how he perceives the shoe-surface interaction.

The present thesis identified, based on how a player moves on a tennis court (Figure 8.1), and on the results from the experiments presented, other variables that affect the frictional mechanisms for the shoe-surface interaction. These mechanisms depend on the characteristics of the playing surface and treads design. Parameters such as the magnitude of the load applied (Clarke et al., 2012a), shoe orientation (section 6.2), shoe velocity (section 4.3), clay infill volume (section 5.4), clay particle size (section 5.3), level of wear of a grass court, moisture level (section 5.2) and the temperature generated between the shoe with the playing surface (section 6.4) have been proved to affect the friction generated by the player-shoe-surface interaction.

By studying and understanding these variables within this thesis furthers understanding of the influence of player's biomechanics, shoes and surfaces characteristics on the tribological parameters and therefore the implications on each area.

8.2.2 *Implications on characterising tennis surfaces*

As mentioned in Miller (2006), there is little knowledge on how the different court surfaces in tennis impact the player-shoe-surface interactions. Previously, friction measurements between shoes and hard courts have exhibited relationships between surface roughness and dynamic friction (Clarke et al. 2012b). In a similar way, for clay surfaces, it was found that the infill particle size significantly influenced the friction developed (Clarke et al. 2013). The findings from the current thesis confirmed roughness and clay infill particle size as key parameters affecting the friction between a tennis shoe in contact with a surface. Furthermore, the results presented in this thesis suggest other

surface characteristics such as clay infill volume, grass height, moisture level and worn areas as potential contributors.

As pointed in the literature review, there are a few regulations or any standards on the surface parameters for a tennis court. This lack of knowledge suggest that the players could be exposed to different levels of friction within a tennis court. The only one found during this study was the grass height for Wimbledon (AELTC, 2016), which some experimental results confirmed an effect on the friction generated during the shoe-surface interaction. As suggested by Midburn and Barry (1998), there is a necessity of an optimal range of the frictional properties of a tennis shoe with the different tennis surfaces, with the objective to reduce the risk of injuries and to maintain and/or enhance the performance. For these reasons, results from the surface parameters presented in this thesis should be used to, firstly, understand how these affect the friction and then to potentially be used as control measurements to build and classify tennis surfaces.

For surface manufacturers, it could also be of special interest as the surface parameters studied and their effect on friction, could help improving their surfaces based on the implications of shoe-surface characteristics. Additionally, it could help to improve their manufacturing processes to keep consistent the frictional characteristics of a tennis court.

As concluded by Damm et al., (2013), the players adapt to the friction characteristics of the playing surface. Subsequently, by monitoring and controlling the surface parameters of a tennis court, the players could have the necessary information of a particular court and plan their playing strategies based on this. For example, the roughness measurements on hardcourts, clay infill volume (Ura et al., 2014b) or particle size (Ura et al., 2014a) on clay courts, in combination with friction measurements with the TSSTv2, could be used to classify a tennis court. In the same way, for grass, it will be necessary to determine the best parameters to use for this classification.

This approach could be of special interest to the ITF, which could be used to classify and categorise the surfaces around the world based on the type and friction generated during specific tennis movements. In a similar way as the ITF CS 01/02 test method is used to classify the court pace in terms of ball-surface interaction (ITF, 2016a), the TSSTv2 could be used to classify the court friction in terms of shoe-surface interaction.

To help developing this classification, a new test protocol is suggested to be implemented with the TSSTv2. This new test protocol is a combination of the test procedures

previously defined in section 7.2, with some improvements formulated from the conclusions of the four preliminary tests presented in section 7.4.

Although the proposed methodology includes focusing on matching 'play' conditions, the main idea of this test protocol is to perform tests at different vertical loads (e.g. sled: 10, 15 and 20 kg masses on top), in order to generate a wider range of pressures in combination with the test slider.

Once the values of friction are calculated for each normal load condition, the next step will be to calculate the applied pressure based on the estimated test slider contact area at each normal load. With this test data, interpolation can be performed to predict the friction values for real-play pressures. An example of this approach is shown in Figure 8.2, which represents the data collected with the sled configuration and the 'holed rubber' sample number 5 (with a 0.288 area ratio). This test slider as discussed previously, behaves similarly to the Babolat dimples shoe sample. The data was collected with the 10, 20, 30 and 40 kg masses on top of the sled. These results were obtained from section 7.5.1, and the pressures were calculated from the correspondent calculated areas, shown in Table 7-4.
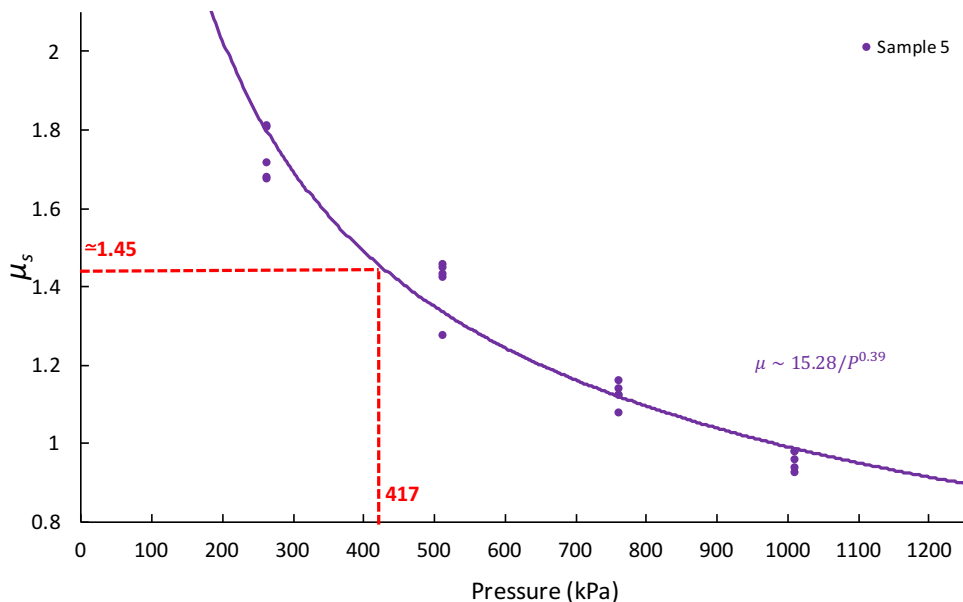
Figure 8.2 Graph depicting μ_s against pressure for sample 5.

With this information, the ITF will be able to assess and classify different surfaces according to a specific movement and under particular real-play pressures. By having the biomechanical data (in-sole pressures) for any particular player movement, a specific

friction value could be obtained from the graph. As an example, if a running forehand on a hard court wants to be evaluated, based on the collated pressure data presented in Table 2-3 in section 2.4.3, a pressure of 417 kPa could be used to interpolate and calculate the static coefficient of friction, which in this case is 1.45 (see * in Figure 8.2). With this approach, a series of tennis movements could be evaluated for each surface for comparison, and then, each surface could be ranked and classified. This represents an initial approach to start classifying the tennis surfaces according to the shoe-surface interface.

8.2.3 Implications for tennis shoes and shoes in general

As mentioned in the literature review, the specialisation of shoes for tennis has evolved according to the player's necessity on a specific surface and thanks to the development of new materials and manufacturing processes. Similar to the surfaces, there is only one official regulation about the shoes used on each surface (AELTC, 2016), and due to the huge variety of tennis shoes in the market, it is difficult to determine the best shoe selection for each surface, in order to enhance performance and/or reduce injury risk.

For these reasons, the knowledge generated in this thesis related to shoe treads (Goff et al., 2016a), could be of interest to manufacturers to improve the design of tennis shoes. The parametric study of treads showed different levels of friction depending on the tread design (Goff et al., 2016b). These could lead to develop a range of tennis shoes for each surface, based on individual player's needs. Eventually, this knowledge could be applied to other areas, such as safety shoes. Additionally, as pointed out in the shoe outsole temperature study (Ura et al., 2015b) the outsole material properties could change with extreme sliding, so this opens the opportunity to develop new materials able to adapt to changes in temperature and extreme environmental conditions, which could affect the shoe-surface friction.

It could also be of interest to the ITF to help standardise and classify the tennis shoes for each surface, in order to reduce injury risk. It is recommended the development and implementation of an in-house shoe testing programme, in order to assess the safety and performance of shoes on each surface. This programme, similar to the ITF Court Pace classification, could be based on some of the results presented in this thesis, such as material characterisation and shoe treads testing; however, a wider study of tread parameters and their effect on friction is recommended. As an example, the study of shoes

like the "Wilson glide" (Wilson, 2016), is relevant to determine their real effect on the player's technique and safety, and to potentially protect the "nature" of the game. The mentioned programme could be developed to assist purchasers or tennis players to determine the best type of shoe for each surface, and to allow or ban specific shoes on specific surfaces.

Additionally, by studying, and designing new shoe treads for each tennis surface, could increase the specialisation of shoes available for any tennis player. Understanding the effect of different treads in contact with a surface could lead a player to utilise a series of tennis shoes during a tournament, or during a tennis match depending on their play strategy (e.g. sliding, more traction, etc.). They could also wear specific shoes depending on the amount of wear of a tennis court (e.g. grass court) or depending on the environmental conditions.

8.2.4 Implications on portable sport test methodologies

Results from the present thesis with the TSSTv1 and TSSTv2 have provided evidence that, based on its portability, lightness and the pressure concept approach, the TSSTv2 could be adapted for the study of shoe-surface interaction in other sports or other areas such as the safety industry (Ura and Carré, 2016). The combination of mechanics, pneumatics and electronics in the design of this novel device, will help to provide repeatable friction measurements, eliminating the variability when human testing is performed, as mentioned by (Clarke et al., 2013).

Additionally, recommendations for future development of portable mechanical tests should attempt to replicate tennis movements (e.g. sliding and landing) with the use of biomechanical data (loading characteristics and foot contact area), and in combination with the assessment of tribological parameters of the shoe-surface interaction. This approach opens new possibilities to other sports and activities in which other type of interactions occurs (e.g. skin-equipment).

8.3 Conclusions

This project has identified some of the tribological mechanisms that occur during typical tennis movements on grass, clay and hardcourts. Experimentally has studied some of these, and based on the results, developed a robust portable device to assess the friction

characteristics of surfaces and provide a better understanding of the shoe-surface interface.

The thesis identified relationships between shoe and surface characteristics such as clay particle size, sand infill volume, shoe-surface temperature, shoe orientation and shoe treads with the main tribological contributors that affects the shoe-surface friction, such as adhesion and hysteresis.

The designed portable test device is based on two tennis movements, landing and sliding, which were identified, through video analysis as key movements on the main tennis surfaces.   This device enables a novel approach to generate pressures that are representative to match-conditions by using a smaller test shoe and scaling the vertical load applied to it.   This improved the problem of replicating the player-surface-shoe interaction under realistic play conditions with portable test devices.

Finally, the findings highlight the necessity to further study more tribological parameters of the shoe-surface interaction, in order to help the International Tennis Federation to identify the main contributors and to start classifying the shoes and surfaces in terms of player's safety and performance.

Finally, the findings highlight the necessity to further study more tribological parameters of the shoe-surface interaction, in order to help the International Tennis Federation to quickly assess tennis shoes and courts around the world and classified them according to expected performance during specific player movements.

8.4   Current and Future Research

When reviewing the results of this research, certain limitations need to be taken into account:

- At the moment of submission of this thesis, based on the results with the TSSTv1, the final prototype design (TSSTv2) was developed and assembled. The final design with a description of the elements incorporated in the new design is presented in the Appendix D.
- Additionally, the TSSTv1 was tested only under lab conditions.

When collecting frictional data of tennis court surfaces with the TSSTv1 and TSSTv2 future experimentation needs to concentrate on both lab and field testing, being field testing the priority, as most of the testing with the pre prototype was under lab conditions.

As identified in the surface experimental results, the friction during a shoe-surface interaction depends on the surface characteristics. Therefore, to continue determining the friction contributors, it is therefore recommended to study other surface characteristics. On grass, further testing is needed to measure the effect of grass properties such as line paint, height, blade direction on friction under dry and wet conditions. On clay, further investigation on the clay particle size effect on friction, and the contribution to friction of a possible ploughing effect would be necessary to understand the interaction between rubber and clay particles. For hardcourts, the study of other surface parameters, such as cushioning (carpets) is necessary. Additionally, the monitoring of shoe-surface friction measurements before, during and after tournaments, is recommended to evaluate any changes in the surface performance and to continue building the knowledge of this area.

When examining the biomechanical conditions, in order to continue improving and exploring new loading methodologies (Chapter 5), further testing needs to be performed to study the effect of different parameters (e.g. different load profiles, surface roughness, contact area, impact velocity and pressure). Supplementary kinetic and kinematic parameters should be obtained from player's tennis movements, in order to better replicate the boundary conditions used in the mechanical test devices. Three dimensional kinematic parameters such as the shoe-surface velocity during specific movements are also important to obtain. Such measurements can be achieved by using motion capture systems or by exploring the video tracking analysis presented in this research.

As presented in this thesis, to obtain reliable results from on-court testing, with elite tennis players represents a challenge, therefore, to aid the study of biomechanical conditions, further development of the video analysis presented in Chapter 5, (sliding incidence analysis and shoe-surface velocity) could be helpful. By increasing the number of video samples analysed, the preliminary results presented in this thesis could be confirmed and other measurements could be determined. As showed from the preliminary video analysis results, further experimental study to measure the effect of shoe-surface velocity on

friction is needed, and could be done by analysing a sliding movement, evaluating different shoe velocities on different tennis surfaces.

The current thesis aimed to examine typical outsoles of tennis shoes, and specifically tread geometries. The results of previous literature were used to determine the main tread characteristics to study, and experimental pilot studies of some treads were implemented. An effect of the tread geometries and dimensions on the shoe-surface friction was found, however, the sample was small compared to the tennis shoes in the market. Therefore, future research performing a wider parametric study of outsole parameters to measure the effects on friction is required. Further assessment of material properties of different rubbers is necessary and the effects of shoe-surface wear on friction. Moreover, an effect of the test shoe velocity on the dynamic friction was found, however due to time, it is necessary to continue studying this phenomena, as the results showed a dependence on the normal force applied (section 7.5).

Additionally, the results from the shoe outsole temperature study, demonstrated an effect of the temperature on the friction generated on the shoe-surface interface, therefore, further testing on a variety of surfaces such as carpets, grass and clay is recommended, to confirm the previous results and to determine further effects on other types of surfaces.

References

adidas. (2006). *Haillet shoe* [Online]. Available: https://www.adidas-archive.org/ - /ourheroes/smith [Accessed 13 June 2016].

AELTC. (2016). *The Grounds* [Online]. Available: http://www.wimbledon.com/en_GB/atoz/grass_courts.html [Accessed 24 Feb 2016].

Anderie, W. (1981). *Sports Shoes*. France patent application.

ASM (1992). *ASM Handbook, Vol. 18: Friction, Lubrication, and Wear Technology*.

ASTM International (2010). D2240-05 Standard Test Method for Rubber Property-Durometer Hardness.

ATP. (2016). *Tournaments* [Online]. Available: http://www.atpworldtour.com/en/tournaments?month=0 [Accessed 5 April 2016].

Babolat. (2013). *OCS* [Online]. Available: http://babolat.kr/wordpress/ocs2/ [Accessed 4 May 2016].

Bharat, B. & Bhushan, B. (2001). *Modern tribology handbook,* Boca Raton, Fla. ; London

Boca Raton, FL ; London, Boca Raton, Fla. ; London : CRC Press, c2001.

Bloch, O., Potthast, W. & Bruggemann, G. (1999). Pressure distribution during sliding on tennis clay court *Symposium on Footwear Biomechanics* Canmore, Canada: Footwear Biomechanics

Boswell, L. (2016). *Interaction Between Tennis Shoes and Surfaces*. Master of Engineering, The University of Sheffield.

Briscoe, B. & Sebastian, K. (1993). An Analysis of the "Durometer" Indentation. *Rubber Chemistry of Technology,* 66**,** 827-836.

British Standards Institution (2011). BS EN 13036 Road and airfield surface characteristics. Test methods . Method for measurement of slip/skid resistance of a surface: The pendulum test. London.

British Standards Institution (2012). BS EN 13287 Personal protective equipment. Footwear. Test method for slip resistance. London, United Kingdom.

Chang, W.-R. (2002). The effects of slip criterion and time on friction measurements. *Safety Science,* 40**,** 593-611.

Chang, W.-R., Grönqvist, R., Leclercq, S., Brungraber, R. J., Mattke, U., Strandberg, L., Thorpe, S. C., Myung, R., Makkonen, L. & Courtney, T. K. (2001a). The role of friction in the measurement of slipperiness, Part 2: Survey of friction measurement devices. *Ergonomics,* 44**,** 1233-1261.

Chang, W.-R., Kim, I.-J., Manning, D. P. & Bunterngchit, Y. (2001b). The role of surface roughness in the measurement of slipperiness. *Ergonomics,* 44**,** 1200-1216.

Choppin, S., Goodwill, S. R., Haake, S. J. & S., M. 3D Player Testing at the Wimbledon Qualifying Tournament. *In:* MILLER, S. & CAPEL-DAVIES, J., eds. Tennis Science and Technology 3, 2007.

Choppin, S., WHYLD, N. M., GOODWILL, S. R. & HAAKE, S. J. 3D Impact Analysis in Tennis. 2005 Tokyo, Japan. Tokyo Institute of Technology, 385-390.

Clarke, J., Carre, M., Damm, L. & Dixon, S. (2012a). Understanding the influence of surface roughness on the tribological interactions at the shoe- surface interface in tennis. *Proceedings of the Institution of Mechanical Engineers, Part J: Journal of Engineering Tribology,* 226**,** 636-636.

Clarke, J., Carré, M., Damm, L. & Dixon, S. (2012b). The influence of surface characteristics on the tribological interactions at the shoe-surface interface in tennis. *Procedia Engineering,* 34**,** 866-871.

Clarke, J., Carre, M. J., Damm, L. & Dixon, S. (2013). The development of an apparatus to understand the traction developed at the shoe-surface interface in tennis. *Proceedings of the Institution of Mechanical Engineers Part P-Journal of Sports Engineering and Technology,* 227**,** 149-160.

Cross, N. (1994). *Engineering design methods : strategies for product design,* Chichester, Chichester : Wiley, c1994.

Damm, L., Clarke, J., Carré, M. & Dixon, S. (2013a). Biomechanical and mechanical testing of non-sliding and sliding tennis surfaces. *Footwear Science,* 5**,** S117-S118.

Damm, L., Clarke, J., Carré, M. & Dixon, S. (2013b). ITF Report: Understanding traction for tennis shoes and surface combination.

Damm, L., Low, D., Richardson, A., Clarke, J., Carre, M. & Dixon, S. (2013c). The effects of surface traction characteristics on frictional demand and kinematics in tennis. *Sports Biomechanics,* 12**,** 389-402.

Damm, L., Low, D., Richardson, A., Clarke, J., Carré, M. J. & Dixon, S. Modulation of tennis players' frictional demand according to

surface traction characteristics. ISB 2011: Proceedings of the International Society of Biomechanics Congress XXIII 2011a Brussels.

Damm, L., Low, D., Richardson, A., Clarke, J., Carré, M. J. & Dixon, S. Modulation of tennis players' frictional demand according to surface traction characteristics. ISB 2011: Proceedings of the International Society of Biomechanics Congress XXIII 2011b Brussels.

Damm, L., Starbuck, C., Stocker, N., Clarke, J., Carré, M. & Dixon, S. (2014). Shoe-surface friction in tennis: influence on plantar pressure and implications for injury. *Footwear Science,* 6**,** 155-164.

Dixon, S., Fleming, P., James, I. & Carré, M. (2015). *The Science and Engineering of Sport Surfaces. Mechanical testing of sport surfaces.,* London and New York, Routledge.

Dixon, S. J., Batt, M. E. & Collop, A. C. (1999). Artificial Playing Surfaces Research: A Review of Medical, Engineering and Biomechanical Aspects. *International Journal of Sports Medicine,* 20**,** 209-218.

Dunlop. (2016). *Dunlop Green Flash History* [Online]. Available: http://www.dunlopgreenflash.co.uk/dunlop-green-flash-history/ [Accessed April 2016].

English, W. (1996). *Pedestrian Slip Resistance. How to measure it and how to improve it.,* Florida, USA, William English, Inc.

Fernandez, J., Mendez-Villanueva, A., Pluim, B. M. & Pearce, A. J. (2006). Intensity of tennis match play. *Br J Sports Med,* 40**,** 387.

FIFA (2016). FIFA Quality Concept, Handbook of test methods for football turf. January 2012 Edition ed.

Frederick, E. C. (1986). Kinematically mediated effects of sport shoe design: a review *J Sports Sci,* 4**,** 169-184.

Girard, O., Eicher, F., Fourchet, F., Micallef, J. P. & Millet, G. P. (2007). Effects of the playing surface on plantar pressures and potential injuries in tennis. *Br J Sports Med,* 41**,** 733.

Goff, J. E., Boswell, L., Ura, D. & Carré, J. M. (2016a). Critical shoe contact area ratio for sliding on a tennis hard court. *Journal of Sports Engineering and Technology*.

Goff, J. E., Ura, D., Boswell, L. & Carré, M. J. (2016b). Parametric Study of Simulated Tennis Shoe Treads. *Procedia Engineering,* 147**,** 443-448.

Grönqvist, R., Hirvonen, M. & Tohv, A. (1999). Evaluation of three portable floor slipperiness testers. *International Journal of Industrial Ergonomics,* 25**,** 85-95.

Grönqvist, R., Matz, S., Hirvonen, M. & Rajamäki, E. (2003). The validity and reliability of a portable slip meter for determining floor slipperiness during simulated heel strike. *Accident Analysis and Prevention,* 35**,** 211-225.

Grund, T. & Senner, V. (2010). Traction behavior of soccer shoe stud designs under different game- relevant loading conditions.

Grund, T., Senner, V. & Grube, K. (2007). Development of a test device for testing soccer boots under gamerelevant highrisk loading conditions. *Sports Eng,* 10**,** 55-63.

Haake, S., Allen, T., Choppin, S. & Goodwill, S. (2007). The evolution of the tennis racket and its effect on serve speed. *Tennis Science and Technology 3,* Roehampton University, London 2007**,** 257-271.

Hallas, K. & Shaw, R. (2006). Evaluation of the Kirchberg rolling slider and slipalert slip resistance meters. Available: http://w.slipalert.com/hse/slipalert-evluation.pdf [Accessed 26 April 2016].

Hickey, J. (2006). *Understanding tennis,* Leeds, United Kingdom, Coachwise.

Hughes, M. & Meyer, R. (2005). Movement pattern in elite men's singles tennis. *International Journal of Performance Analysis in Sport,* 5**,** 110-134.

Hutson, M. A. & Jackson, J. P. (1982). Injuries to the lateral ligament of the ankle: assessment and treatment. *Br J Sports Med,* 16**,** 245.

ITF. (2016a). *Court Pace* [Online]. Available: http://www.itftennis.com/technical/courts/court-testing/court-pace.aspx [Accessed 5 April 2016].

ITF. (2016b). *Court testing* [Online]. Available: http://www.itftennis.com/technical/courts/court-testing/overview.aspx [Accessed 5 April 2016].

ITF. (2016c). *Footwear* [Online]. Available: http://www.itftennis.com/scienceandmedicine/equipment/footwear [Accessed 24 Feb 2016].

ITF. (2016d). *History* [Online]. Available: http://www.itftennis.com/technical/courts/other/history.aspx [Accessed 24 Feb 2016].

ITF. (2016e). *Pro Circuit* [Online]. Available: http://www.itftennis.com/procircuit/about-pro-circuit/overview.aspx [Accessed 5 April 2016].

ITF. (2016f). *Rules of Tennis* [Online]. Available: http://www.itftennis.com/media/221030/221030.pdf [Accessed 24 Feb 2016].

ITF. (2016g). *Surface Descriptions* [Online]. [Accessed].

James, D. I. (1988). A standard slider for slip measurements. *Polymer Testing,* 8**,** 9-17.

James, I. (1986). Measurement of slip-resistance: a modern approach to standardisation. *Road and Buildings Group of the SCI.* London.

Jara, A., Larregain, A. & Perrin, F. (2010). *High-performance sports shoe* US patent application.

Keen, A. (2015). *Development of a New shoe-surface slip resistance test methodology.* The University of Sheffield.

Keyser, A. (2015). *Sneaker Century: A History of Athletic Shoes*, Lerner Publishing Group.

Kime, G. A. (1991). Slip resistance and the UK Slip Resistance Research Group. *Safety Science,* 14**,** 223-229.

Kirchberg, S., Fischer, H. & Rely, H. (1997). *In situ measurement of sliding friction of floors: study for the optimisation of check parameters. Untersuchung zur Optimierung der Prufparameter fur Verfahren zur instationaren Messung der Gleitreibung von Fuβboden. Bundesanstalt furArbeitsschutz und Arbeitsmedizin.* Dortmund.

Kirk, R. (2008). *Traction of Association Football Shoes.* The University of Sheffield.

Lewis, R., Carre´, M. & Abu Kasim, A. (2011). A comparison of pendulum heel slip simulation with actual foot friction measurements. *International conference on slips, trips and falls.* Buxton, UK: Buxton: Health and Safety Laboratory.

Loredana, D. E. (2006). *Static friction in rubber-metal contacts with application to rubber pad forming processes.* Doctor's degree, University of Twente.

LTA. (2016). *National Tennis Centre* [Online]. Available: http://www3.lta.org.uk/Footer/about-us/National-tennis-centre/ [Accessed 5 May 2016].

McNitt, A. S., Landschoot, P. J. & Waddington, D. V. (2004). Effects of turfgrass, cutting height and soil conditions on traction. *Acta Hortic,* 661**,** 39-48.

Menard, K. P. (2008). *Dynamic mechanical analysis : a practical introduction,* Boca Raton, FL, Boca Raton, FL : CRC Press, c2008.

Milburn, P. D. & Barry, E. B. (1998). Shoe-surface interaction and the reduction of injury in rugby union. *Sports Medicine,* 25**,** 319-327.

Miller, S. (2006). Modern tennis rackets, balls, and surfaces. *British Journal of Sports Medicine,* 40**,** 401-405.

Miller, S., & Capel-Davies, J. (2006). *The vertical and horizontal loads acting on a shoe during a specific movement are not independent of each other.* SportSurf 2006.

Mills, R., Dwyer-Joyce, R. S. & Loo-Morrey, M. (2009). The mechanisms of pedestrian slip on flooring contaminated with solid particles. *Tribology International,* 42**,** 403-412.

Moore, D. F. & Geyer, W. (1974). A review of hysteresis theories for elastomers. *Wear,* 30**,** 1-34.

Newcomb, T. (2014). How Roland Garros prepares and maintains the clay for the French Open. Available: http://www.si.com/tennis/beyond-baseline/2014/05/21/how-roland-garros-prepares-clay-courts-french-open [Accessed 9 August 2016].

Newton, R., Doan, B., Meese, M., Conroy, B., Black, K., Sebstianelli, W. & Kramer, W. (2002). Wrestling: Interaction of wrestling shoe and competition surface. *Sports Biomechanics,* 1**,** 157-166.

Nigg, B. (2003). *Injury and performance on tennis surfaces. The effect of tennis surfaces on the game of tennis* [Online]. Available: http://hartru.com/uploads/downloads/Doc_7.pdf [Accessed April 2013].

O'Donoghue, P. & Ingram, B. (2001). A notational analysis of elite tennis strategy. *Journal of Sport Sciences,* 19**,** 107-115.

Orchard, J. W., Chivers, I., Aldous, D., Bennell, K. & Seward, H. (2005). Rye grass is associated with fewer non- contact anterior cruciate ligament injuries than bermuda grass. *Br J Sports Med,* 39**,** 704.

Orendurff, M. S., Rohr, E. S., Segal, A. D., Medley, J. W., Green, J. R. & Kadel, N. J. (2008). Regional foot pressure during running, cutting, jumping, and landing. *The American journal of sports medicine,* 36**,** 566.

Palasantzas, G. (2004). Influence of self- affine roughness on the adhesive friction coefficient of a rubber body sliding on a solid substrate. *Surface Science,* 565**,** 191-196.

Pavailler, S. & Horvais, N. (2014). Sliding allows faster repositioning during tennis specific movements on hard court. *Engineering of Sport 10,* 72**,** 859-864.

Perkins, R. & Davis, D. (2006). Musculoskeletal injuries in tennis. *Phys Med Rehabil Clin N Am. J. Sports Med.***,** 609-631.

Persson, B. (2006). Rubber friction: role of the flash temperature. *J. Phys.-Condes. Matter,* 18**,** 7789-7823.

Persson, B. (2014). Role of Frictional Heating in Rubber Friction. *Tribol. Lett.,* 56**,** 77-92.

Persson, B. N. J. (1998). On the theory of rubber friction. *Surface Science,* 401**,** 445-454.

Persson, B. N. J. (2001). Elastoplastic contact between randomly rough surfaces. *Physical Review Letters,* 87**,** 116101/1-116101/4.

Persson, B. N. J., Tosatti, E., Persson, D., Tosatti, G., Fuhrmann, C., Witte, C. & Wöll, C. (1999). Low- frequency adsorbate vibrational relaxation and sliding friction. *Physical Review B - Condensed Matter and Materials Physics,* 59**,** 11777-11791.

Pluim, B. M., Staal, J. B., Windler, G. E. & Jayanthi, N. (2006). Tennis injuries: occurrence, aetiology, and prevention. *British Journal of Sports Medicine,* 40**,** 415-423.

Redfern, M. S., Cham, R., Gielo-Perczak, K., Grönqvist, R., Hirvonen, M., Lanshammar, H., Marpet, M., Pai, C. Y.-C. & Powers, C. (2001). Biomechanics of slips. *Ergonomics,* 44**,** 1138-1166.

Reinschmidt, C. & Nigg, B. (2000). Current issues in the design of running and court shoes. 14.

Ricotti, R., Delucchi, M. & Cerisola, G. (2008). A comparison of results from portable and laboratory floor slipperiness testers. *International Journal of Industrial Ergonomics,* 39**,** 353-357.

Roland-Garros. (2016). *Clay courts: origin, design and maintenance* [Online]. Available: http://www.rolandgarros.com/en_FR/content/rg_spirit/clay_courts_origins_design_and_ maintenance.html [Accessed 24 Feb 2016].

Rosa, D., Sanchis, J., Gamez, J. & and Alcantara, E. Study on the effect of maintenance operations and season on the traction of natural grass pitches. Technology and Research into Sport Surfaces Conference, 2007 Loughborough University, UK. Proceedings of the Science.

Severn, K., Fleming, P., Clarke, J. D. & Carre, M. (2011). Science of synthetic turf surfaces: investigating traction behaviour. *Proc. Inst. Mech. Eng. Part P-J. Sport. Eng. Technol.,* 225**,** 147-158.

Slip Resistance Group (2011). The assessment of floor slip resistance Issue 4.0. United Kingdom.

Starbuck, C., Damm, L., Clarke, J., Carré, M., Capel-Davis, J., Miller, S., Stiles, V. & Dixon, S. (2015). The influence of tennis court surfaces on player perceptions and biomechanical response. *Journal of Sports Sciences***,** 1-10.

Sterzing, T., Barnes, S., Althoff, K., Determan, L., Liu, H. & Cheung, J. T.-M. (2014). Tennis shoe requirements in China, USA, and Germany. *Footwear Science,* 6**,** 165-176.

Stiles, V. & Dixon, S. (2006). The influence of different playing surfaces on the biomechanics of a tennis running forehand foot plant. *Journal of Applied Biomechanics,* 22**,** 14-24.

Ura, D., Carré, J. M. & Javier, D.-C. (2015a). Tennis shoe-court interactions: Examining relationships between contact area, pressure and available friction.

Ura, D. & Carré, M. (2016). Development of a Novel Portable Test Device to Measure the Tribological Behaviour of Shoe Interactions with Tennis Courts. *Procedia Engineering,* 147**,** 550-555.

Ura, D., Carré, M. J., Charlton, H., Capel-Davies, J., Miller, S., Almenara, M. S., Astiz, J. & Mustienes, A. d. A. (2014a). Influence of Clay Properties on Shoe-kinematics and Friction During Tennis Movements. *Procedia Engineering,* 72**,** 889-894.

Ura, D., Carré, M. J., Starbuck, C. & Dixon, S. J. (2014b). Effect of Varying the Volume Infill Sand on Synthetic Clay Surfaces in Terms of the Shoe-surface Friction. *Procedia Engineering,* 72**,** 877-882.

Ura, D., Clarke, J. & Carré, M. (2013). Effect of shoe orientation on shoe-surface traction in tennis. *Footwear Science,* 5**,** 86-87.

Ura, D., Conway, J., Booth, J. & Carré, M. J. (2015b). Tennis shoe outsole temperature changes during hard court sliding and their effects on friction behaviour.

Vachon, F. (2004). *Football boot sole configurations and their influence upon surface adhesion* [Online]. http://www.isss.de/publications/ArtificialTurf/Vachon Friction.pdf: ISSS Publications. [Accessed 26 April 2015 2015].

Villwock, M. R., Meyer, E. G., Powell, J. W., Fouty, A. J. & Haut, R. C. (2009). Football playing surface and shoe design affect rotational traction. *The American journal of sports medicine,* 37**,** 518.

Wannop, J. W. & Stefanyshyn, D. J. (2012). The effect of normal load, speed and moisture on footwear traction. *Footwear Science,* 4**,** 37-43.

Werd, M. & Knight, L. (2010). *Athletic Footwear and Orthoses in Sports Medicine*, Springer.

Wilson. (2016). *Glide Shoe* [Online]. Available: http://www.wilson.com/dyn/racquet/glide/ [Accessed April 2016].

Wright, I. (1998). *Design methods in engineering and product design,* New York ; London, New York ; London : McGraw-Hill, 1998.

Yu, S., Schiller, D. & Bergmann, M. (2010). *Outsole for an article of footwear*. United States patent application.

Appendix A

Video No.	Player	Surface	Court Location	Player Movement	Primary Mechanism	Frictional Mechanism
1	Bartolli	Clay	Baseline	Running - FH	Sliding	Grip
2	Beneteau	Clay	Baseline	Running - FH	Sliding	Grip
3	Monaco	Clay	Baseline	Running - FH	Landing after shoot	Grip
4	Nadal	Clay	Baseline	Running - BH	Landing after shoot	Slip
5	Petrovic	Clay	Baseline	Running - FH	Sliding	Grip
6	Wozniacki	Clay	Net	Running drop shot	Sliding	Grip
7	Petrovic	Clay	Baseline	Running - FH	Sliding	Grip
8	Mladenovic	Clay	Baseline	Forehand	Landing after shoot	Grip
9	Lisicky	Clay	Baseline	Change direction	Brakeing	Slip
10	Nadal	Clay	Baseline	Running - BH	Landing after shoot	Slip
11	Djokovic	Clay	Baseline	Running - FH	Sliding	Grip
12	Ivanovic	Clay	Baseline	Running - FH	Sliding	Grip
13	Sharapova	Clay	Baseline	Running - FH	Sliding	Grip
14	Jankovic	Clay	Baseline	Return forehand	Landing after shoot	Slip
15	Williams	Clay	Baseline	Return forehand	Landing after shoot	Slip
16	Azarenka	Grass	Baseline	Push-off	Landing	Slip
17	Del Potro	Grass	Baseline	Running - BH	Braking	Slip
18	Hewitt	Grass	Baseline	Running - FH	Braking	Slip
19	Murray	Grass	Serveline	Running - FH	Landing	Slip
20	Nadal	Grass	Net	Running drop shot	Landing after shoot	Slip
21	Sharapova	Grass	Baseline	Running - BH	Landing	Slip
22	Sharapova	Grass	Baseline	Running - BH	Landing	Slip
23	Sharapova	Grass	Baseline	Change direction - Push off	Landing	Slip
24	Djokovic	Grass	Baseline	Change direction	Landing	Slip
25	Veshina	Grass	Baseline	Running- change direction	Braking	Slip
26	Federer	Grass	Baseline	Running - FH	Landing	Slip
27	Federer	Grass	Baseline	Running - FH	Landing after shoot	Slip
28	Federer	Grass	Baseline	Serve - push off	Landing	Slip
29	Djokovic	Grass	Baseline	Change direction - push off	Braking	Slip
30	Del Potro	Grass	Baseline	Change direction - Push off	Brake- push off	Slip
31	Clijsters	HC	Baseline	Running - FH	Landing after shoot	Grip
32	Djokovic	HC	Baseline	Running - BH	Landing after shoot	Grip

33	Dokic	HC	Baseline	Running - BH	Landing after shoot	Grip
34	Federer	HC	Baseline	Change of direction	Push off	Slip
35	Li Na	HC	Baseline	Change of direction	Push off	Grip
36	Li Na	HC	Baseline	Running - BH	Landing after shoot	Grip
37	Sabine	HC	Baseline	Running - FH	Sliding	Grip
38	Serena	HC	Baseline	Running - FH	Landing after shoot	Grip
39	Serena	HC	Baseline	Change direction - Push off	Brake- push off	Grip
40	Tipsarevic	HC	Baseline	Running - FH	Landing after shoot	Grip
41	Djokovic	HC	Baseline	Change direction - Push off	Brake- push off	Slip
42	Nadal	HC	Baseline	Running - BH	Push off	Slip
43	Williams	HC	Baseline	Change direction	Brake- push off	Slip
44	Ivanovic	HC	Baseline	Running - FH	Landing	Grip
45	Sania	HC	Baseline	Change direction	Brake- push off	Grip

Appendix B

POLYMAX
giving you the advantage

Building 90, SEME, Budds Lane,
Bordon, Hampshire
GU35 0JE
Email: sales@polymax.co.uk
Tel: 01420 474123
Web: www.polymax.co.uk

Technical Data Sheet

Compound: N70 - Nitrile (NBR- Butadine Rubber)
Colour: Black

Complies with: ASTM D2000 M2BG714 A14 B14 EA14 EO14 EO34 EF11 EF21 F17

	Required	Tested
Mechanical Properties		
Shore Hardness (Sh.A):	70	71
Tensile Strength (MPa):	14	14
Elongation at Break (%):	250	385
Specific Gravity:	n/a	1.19
Thermal Properties		
Operating Temperature Range (°C):	n/a	- 30 to +120
Compression Set Test @ 100°C for 22 Hours (%):	25	13
Heat Resistance Test @ 100°C X 70 Hours		
Hardness Change Points:	± 15	+3
Tensile Strength Change (%):	± 30	+2
Elongation Change (%):	- 50	-12
Water Resistance Test @ 100°C X 70 Hours		
Hardness Change Points:	±10	-4
Volume Change (%):	±10	+4.3
Fuel A Resistance Test @ 23°C X 70 Hours		
Hardness Change Points:	±10	+2
Tensile Strength Change (%):	-20	-10.84
Elongation Change (%):	-20	-12.61
Volume Change (%):	-5 or +10	+1.2
Fuel B Resistance Test @ 23°C X 70 Hours		
Hardness Change Points:	0 to -30	-7
Tensile Strength Change (%):	-60	-39.61
Elongation Change (%):	-60	-41.29
Volume Change (%):	0 to +40	+16.11
ASTM No.1 Oil Immersion Test @ 100°C X 70 Hours		
Hardness Change Points:	-5 to +10	+3
Tensile Strength Change (%):	-25	+4
Elongation Change (%):	-45	-19
Volume Change (%):	-10 to +5	-1
ASTM IRM 903 Oil Immersion Test @ 100°C X 70 Hours		
Hardness Change Points:	10 to +5	+2
Tensile Strength Change (%):	-45	-21
Elongation Change (%):	-45	-16
Volume Change (%):	0 to +25	+9

Appendix C- Design stage- Conceptual design

Problem definition

As a first step in the design methodology implemented (Figure 3.3), the definition of the problem is vital. In chapter 1, the aim of this project was defined as the design of a portable mechanical test methodology to measure the tribological characteristics of a shoe-surface interaction in tennis. As suggested in previous studies (Dixon et al., 1999, Clarke et al., 2013), a valid mechanical test should ideally replicate the materials and loading of specific human–shoe–surface interactions. However, as mentioned in chapter 5, due to the magnitudes of the vertical forces generated during complex dynamic movements, the replication of the actual biomechanical loading using portable equipment is a challenge.

Therefore, with the objective to design a test device capable to replicate actual 'match-play' conditions and be portable at the same time, it was decided, to analyse the conclusions from the experiments chapters 4, 5 and 6, in order to specify the boundary conditions for the test rig.

As discussed in Chapter 4, and based on the results from the 'player movements' video analysis, it was decided to replicate two shoe movements which represent the majority of risk movements in tennis: a '*landing*' (push-off and running forehand/backhand) and a 'sliding' (forehand/backhand). Figure A - 1 and Figure A - 2 show schematic representations of these two movements in terms of forces and velocities.
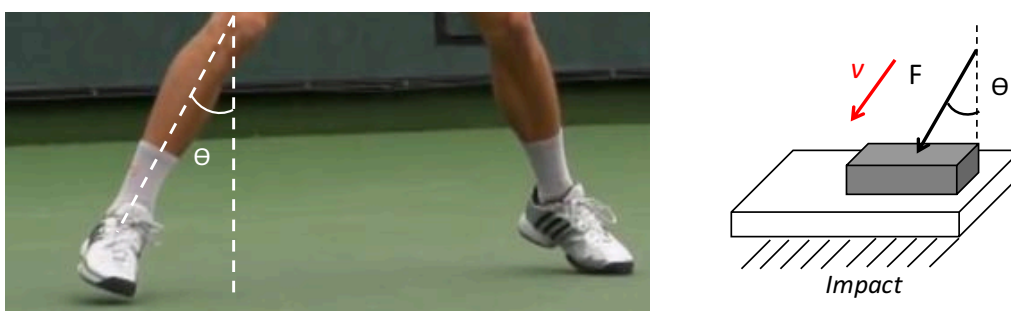
Figure A - 1 Actual (left) and schematic (right) representation of a landing movement (push-off) showing a landing force (F) and an impact velocity (v).

The 'landing' movement shown in Figure A - 1 is characterised by a foot impact with an angle and with a force applied to the surface. The combination of these three parameters

will cause the tennis shoe to initiate a slide on the surface if there is not sufficient friction in the contact.

Figure A - 2 Actual (left) and schematic (right) representation of a sliding movement showing sliding displacement (d), vertical and horizontal forces (F_V and F_H) and sliding velocity (v).

The 'sliding' movement shown in Figure A - 2 is characterised by a shoe displacement with a specific velocity over a surface. Vertical and horizontal forces are applied during the movement.

a) Biomechanical studies

As discussed in the literature review, several lab and field studies (section 2.4, Table 2-3) have reported vertical loading conditions during dynamic tennis movements on hard and clay courts above the 1000 N. Due to the high magnitudes of these forces it represent a challenge to apply these on a tennis court with a portable test device. For this reason, it was decided instead of replicating the forces, to replicate real-play conditions by matching in-sole peak pressures. This approach was validated in part by the previous pilot study on pressure and friction presented in Chapter 4. By the replication of 'match-play' pressures, this allows the use of lower vertical loads by reducing the contact area of the test shoe.

Based on the values reports in previous lab and field experiments in Table 2-3, the target pressures to match with the portable test device, were defined as shown in Table A - 1.

Table A - 1 Pressure range for the two movements

Movement	Pressure (kPa)
Landing	400 – 550
Sliding	200 – 250

b) Tribological mechanisms

As discussed previously in the literature review when tennis shoes outsoles, made from viscoelastic rubber, are compressed against a hard tennis surface with some roughness, there is an interaction between their asperities, and hence a friction between them is generated.

As discussed in previous sections of this work, during dynamic tennis movements, the generated friction is ruled by different parameters such as normal load (Chapter 2) surface roughness (Chapter 2), shoe orientation (Chapter 6) and shoe-surface temperature (Chapter 6). These have proved to be parameters that affect the adhesional and hysteretic components of the friction.

It was shown, in section 6.2, that the shoe orientation also has an effect on friction. For this reason, the design needs to be able to vary the shoe orientation in reference to the movement. This will be covered later in this chapter.

As discussed in section 6.4 it is also necessary to consider the shoe-surface temperature effects during testing. If necessary, it will be important to allow time between trials to cool down the test slider.

To complement the friction measurement, it is recommended to measure the surface roughness, as it has been proved to be a parameter that affects the friction. This measurement will help to have a better understanding of the friction and to help classifying the surface.

It is important to notice that although an effect of the shoe velocity during a sliding movements was found (section 4.3), it was decided to not use this parameter for the design stage, as it has been identified that this needs further examination and analysis, as stated later in this thesis (section 8.4).

Functional analysis

In order to continue with the problem definition and concentrating on what the device needs to achieve rather than how to achieve it, a functional analysis was implemented. The objective of this analysis is the definition of the main function and sub-functions of the designed product.

The simplest way of expressing this is to represent the product or device to be designed as simply a 'black box' which converts certain inputs into desired outputs. Figure A - 3 shows the diagram with the identified overall function, *'Testing device'* in terms of converting the inputs *'shoe'* and *'surface'* interactions into an *'assess friction'* output. These were defined based on the initial objectives, defined in Chapter 1, in combination with the conclusions from Chapter 4, 5 and 6.
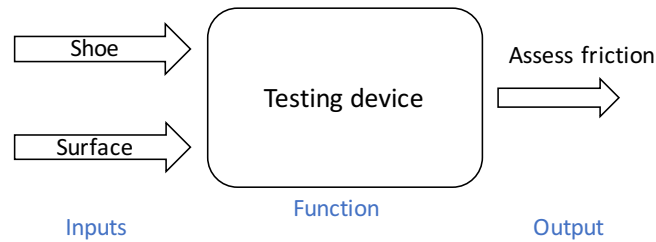
Figure A - 3 The black box model defined for the project, showing inputs, function and output

The next step was the breakdown of the overall function to identify the sub-functions. Three main sub-functions were identified:

1. Replication of play-match pressures (a vertical load with a specific contact area).
2. Replication of two tennis movements (an angled impact and a horizontal slide).
3. Calculation of frictional force (measuring forces and displacements).

The diagram presented in Figure A - 4 shows all the processes needed to go from the inputs to the outputs. After categorising the sub-functions, the player biomechanics were identified and added as a new input for the defined system.
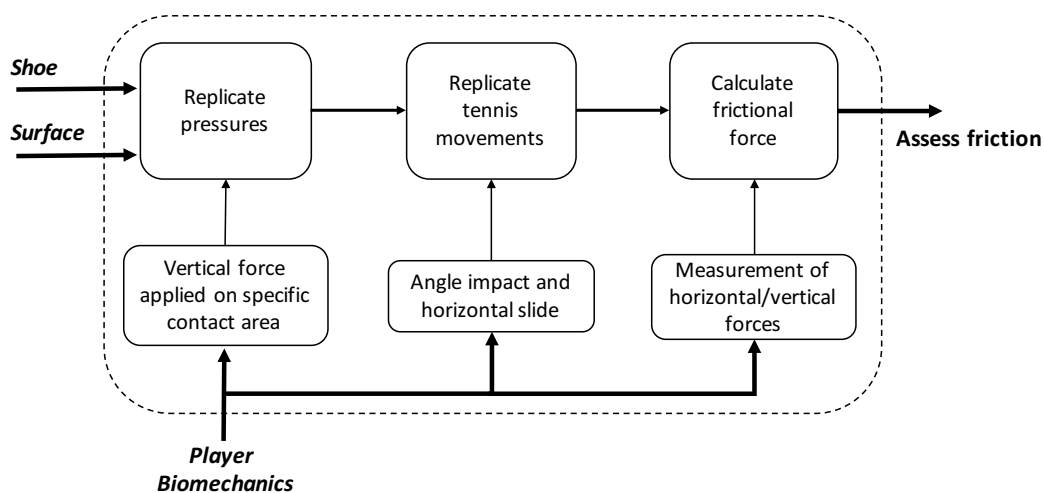
Figure A - 4 Black box model with sub-functions identified.

Product design specifications

Once the inputs, functions, sub-functions and the outputs of the new device are identified, the next phase of the implemented design methodology was to identify the product specifications. This method produces an accurate specification of the performance required by the design solution. It mostly concentrates on setting precise limits within which the design solution must operate. The product specifications were defined in conjunction with the ITF, according to their needs. These are:

- Light weight.
- Portable.
- Simple operation.
- Powered without connection to mains electricity.
- Measure shoe-surface friction.
- Representative of match play conditions.
- Interchangeable test shoe.
- No damage to surface tested.
- Repeatability of results.
- Reliability.

The next steps of this phase are the '*Separation of attributes*' and the '*Definition of limits*' respectively. It consists of separating the specifications identified as '*demands*' from '*wishes*'. The '*demands*' must be achieved, whilst the '*wishes*' would like to be achieved if possible. Table A - 2 shows the performance specification with its demand/wish category and the limits defined. The limits of some of these attributes were defined with the ITF as they were sponsors of this project.

Table A - 2 Product design specifications with the respective defined limits.

	Product specification	Demand/ Wish	Limit
-	Light weight	D	Not to exceed 30kg.
-	Portable size	D	Sum of dimension not more than 158 cm.
-	Simple operation	D	Single person with minimal training.
-	Powered without connection to mains electricity	W	During operation.
-	Measure shoe-surface friction	D	Distinguish between different shoe-surface combinations
-	Representative of match play conditions	D	Apply a range of specific pressures and ability to vary angle.
-	Interchangeable test shoe	D	Quick change of test shoe.
-	No damage to surface tested	D	Any metal contact with surface.
-	Repeatability	D	Low variation of measurements taken.
-	Reliability	D	Consistently produces same results.

Concept generation

Brainstorming

Based on the conclusions of chapter 4 about the replication of the two player's movement, a set of initial ideas were sketched around the design. Only the more representative ones are presented in this section.

The first ideas were around two main objectives:

- To simulate a 'landing' and a 'sliding' movements previously described.
- To determine and design a representative test shoe.

The first sketches, presented in Figure A - 5, were based on a general approach. This involved two main options: human assisted or non-human assisted. Based on the ITF's field testing experience and on the product specifications of 'simple operation' and 'portable and light' it was decided to focus the design on the human assisted option. The main objective of this option was to combine some mechanical or electronic components with an operator, to have a balance between accuracy and portability.
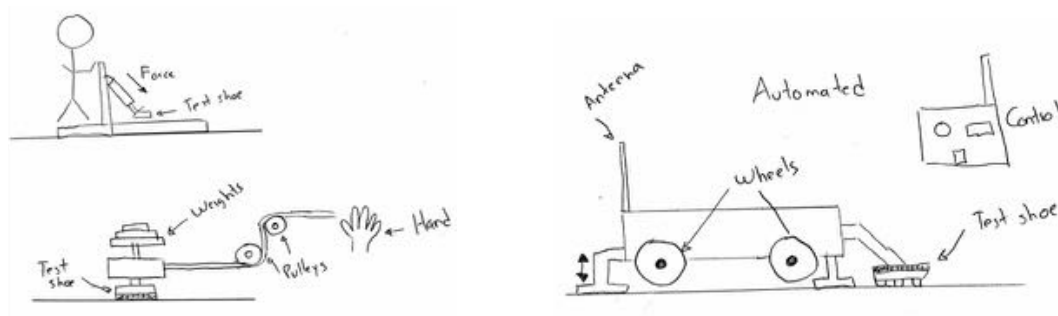
Figure A - 5 Human assisted (left) and automated (right) general ideas.

Focused on the characteristics of the 'landing' and 'sliding' movements previously described in section 4.2, the next step was to determine the best way to replicate the specific player movements. Two main ideas were determined based on the schematic representations presented in Figure A - 1 and Figure A - 2. These ideas focused in reproducing the movements on the basis of how players apply forces on a tennis surface.

For the 'landing' movement, the idea generated was the *'angled-ram'* device (shown in Figure A - 6-left), which is based in the basic inclined plane concept previously discussed in the literature review. This conceptual device is composed by an actuator which applies a force on a test shoe which hits the surface with a controlled angle. The main objective of this device is to find the angle where the test shoe is slides on the surface. The slip angle is related to the static coefficient of friction.

For the 'sliding' movement, the aim is to simulate a sliding shoe on the surface, and it was represented by a simple sled device, shown in Figure A - 6-right. It is composed by a weight loaded test shoe, which, after applying a horizontal load, starts to move on the surface. This concept is based to the UoSh traction rig, (Clarke et al., 2013), whose operation includes in measuring the limiting friction generated when a shear force is gradually increased against a test shoe under a constant vertical load.
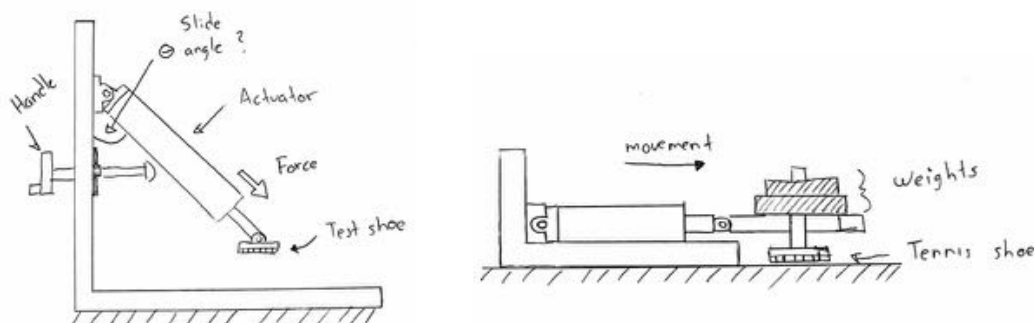
Figure A - 6 The 'angled-ram' (left) and 'sled' (right) devices concept ideas.

A final idea, was to merge both devices from Figure A - 6, into one configurable device capable to be transformed on both *'angled-ram'* and *'sled'*. The main advantage of this idea is in terms of the restriction of portability and dimensions of the device. By having one configurable device, in comparison of two devices, makes easier to travel and/or reduces possible transport costs.

In order to fulfil the second objective of the brainstorming, additional ideas related to the test shoe were developed. Figure A - 7 shows the first main sketched ideas; a circular test shoe (1), a piece of tennis outsole (2) and a slider with rounded ends (3) were the main ones.
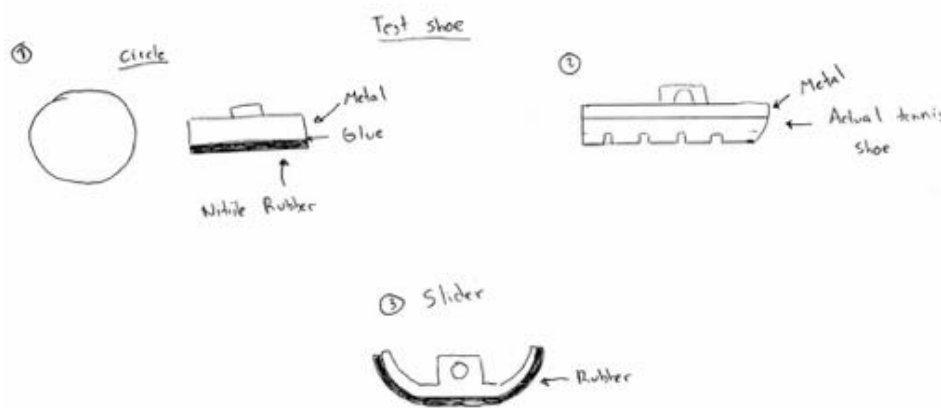
Figure A - 7 Test shoe conceptual design sketches.

Morphological chart

After the brainstorming and generation of the first ideas for the test device, a morphological chart with the essential features or functions determined in the previous was completed. The aim of this morphological chart method was to generate the complete range of alternative design solutions, and hence, to widen the search for potential new solutions. Table A - 3 shows the morphological chart generated with the main features of the portable device with some possible solutions for each function. One of the main criteria to define the solutions was to utilise, as much as possible commercial parts, in order to facilitate the maintenance service of the device.

Table A - 3 Morphological chart

Function	Solution			
	Option 1	Option 2	Option 3	Option 4
1. Application of horizontal force	Pneumatic cylinder	Electric actuator/motor	Human power (pushing or pulling)	Pulleys
2. Application of vertical force	Pneumatic cylinder	Electric actuator/motor	Weights	Human weight
3. Measurement of reaction force	Portable force plate	Load cell		
4. Measurement of displacement	LVDT	Measurement tape	Analog position sensor	
5. Standard Test shoe	Tennis shoe segment	Slider with commercial rubber	Slider with tennis outsole	
6. Calculate static and dynamic friction	Computer + National instrument acquisition cards	Raspberry Pi	Arduino	
7. Move around a tennis court	Lifting by hand	Rolling on wheels	Motorised wheels and remote control	
8. Securing to the ground	Pegs	Weights	Human weight	Weights + human weight

Evaluation and selection of components

To evaluate the different option solutions for each function (Table A - 3), a weighted objectives method was produced. It was based on the functional analysis and product specifications previously defined in section. The aim of this method is to compare the alternative solutions for each function, and select the best one based on the basis of performance.

The first step in this method, is to list the option solutions for each function and evaluate them based on the product specifications. Each solution is scored using values from 1 to 5, evaluating the contribution of the solution to each of the product specifications ('5' represents the highest contribution). After the evaluation, the solution with the highest final sum score is then selected as the optimal and it is utilised for further development.

Table A - 4 to Table A - 11 show the comparison and evaluation of the different solutions, for each function previously defined, proposed in the morphological chart.

For the 'application of horizontal' force function, showed in Table A - 4, the evaluation shows the pneumatic cylinder as the optimal solution for this design. Although human power represents the simplest way to achieve this function, the score in repeatability and reliability were too low compared to 'pneumatic cylinder'.

Table A - 4 Evaluation of 'Application of horizontal force' function.

Product specifications / Solution	Light weight	Portable size	Simple operation	Powered without connections	Measure shoe-surface friction	Representative of match play	Interchangeable test shoe	No damage to surface tested	Repeatability	Reliability	Total	Rank
1. Pneumatic cylinder	3	5	3	3	-	5	-	3	5	5	32	1
2. Electric actuator/motor	3	5	3	1	-	2	-	3	5	5	27	2
3. Human power (pulling or pushing)	5	1	5	5	-	3	-	3	1	1	24	4
4. Pulleys	5	5	3	3	-	1	-	3	3	3	26	3

Table A - 5 shows the evaluation of 'application of vertical force'. The solution with the highest score was the 'weights' options. Although the score value was very close to 'pneumatic cylinder', the difference relied in the highest score of the simple operation and power specifications for the 'weights' solution.

Table A - 5 Evaluation of 'Application of vertical force' function.

Product specifications / Solution	Light weight	Portable size	Simple operation	Powered without connections	Measure shoe-surface friction	Representative of match play	Interchangeable test shoe	No damage to surface tested	Repeatability	Reliability	Total	Rank
1. Pneumatic cylinder	5	5	3	3	-	5	-	4	5	5	35	2
2. Electric actuator/motor	3	5	3	3	-	3	-	4	5	5	31	3
3. Human weight	5	1	4	5	-	5	-	5	3	3	31	4
4. Weights	5	4	5	5	-	5	-	4	5	5	38	1

The evaluation of 'measurement of reaction force' is shown in Table A - 6. Two options were scored, being the load cell the one with the highest score. The contribution of lightness and portability to the device, were the specifications with the highest score.

Table A - 6 Evaluation of 'Measurement of reaction force' function.

Product specifications / Solution	Light weight	Portable size	Simple operation	Powered without connections	Measure shoe-surface friction	Representative of match play	Interchangeable test shoe	No damage to surface tested	Repeatability	Reliability	Total	Rank
1. Portable force plate.	1	2	3	1	-	5	-	3	5	5	25	2
2. Load cell.	4	4	3	1	-	5	-	5	5	5	32	1

Table A - 7 shows the evaluation for the 'measurement of displacement' function. This evaluation showed same scores for the LVDT and analog position sensor, suggesting that any of these devices could be selected. However, the analog position sensor was ranked as number one, as in comparison to the LVDT, requires less or any of extra machined parts for the mounting.

Table A - 7 Evaluation of 'Measurement of displacement' function.

Product specifications \ Solution	Light weight	Portable size	Simple operation	Powered without connections	Measure shoe-surface friction	Representative of match play	Interchangeable test shoe	No damage to surface tested	Repeatability	Reliability	Total	Rank
1. LVDT	4	4	3	1	-	-	-	5	5	5	27	2
2. Measurement tape	4	5	5	5	-	-	-	3	1	1	24	3
3. Analog position sensor	4	4	3	1	-	-	-	5	5	5	27	1

In terms of the 'Standard test shoe' function, Table A - 8 presents the evaluation of three solutions. Here, the best solution focused on designing a bespoke slider with a commercial rubber attached to it as the best solution. Tennis outsoles will be a good option to use as a test rubber, however, because of the variability of tread designs on the market, and the difficult process to remove the outsole of a tennis shoe, the commercial rubber option is ranked with the highest score.

Table A - 8 Evaluation of 'Standard test shoe' function.

Product specifications \ Solution	Light weight	Portable size	Simple operation	Powered without connections	Measure shoe-surface friction	Representative of match play	Interchangeable test shoe	No damage to surface tested	Repeatability	Reliability	Total	Rank
1. Tennis shoe segment	3	4	5	-	5	5	2	5	5	5	39	3
2. Bespoke slider / commercial rubber	5	5	5	-	5	4	5	5	5	4	43	1
3. Bespoke slider/tennis outsole	5	5	5	-	5	5	2	5	5	5	42	2

Table A - 9 shows the evaluation of the possible solutions for the 'Calculate static and dynamic' function. Raspberry Pi and Arduino finished as the highest scored solutions, suggesting that any of these could be used in the final design. The main differences against a computer with acquisition cards were the portability and lightness of the Raspberry and Arduino solutions.

Table A - 9 Evaluation of 'Calculate static and dynamic' function.

Product specifications / Solution	Light weight	Portable size	Simple operation	Powered without connections	Measure shoe-surface friction	Representative of match play	Interchangeable test shoe	No damage to surface tested	Repeatability	Reliability	Total	Rank
1. Computer + acquisition cards	3	3	4	2	5	-	-	-	5	5	27	2
2. Raspberry Pi	5	5	3	4	5	-	-	-	5	5	32	1
3. Arduino	5	5	3	4	5	-	-	-	5	5	32	2

For the 'Move around a tennis court' function, Table A - 10 shows the three solutions evaluated. Although the simplest solution is the lifting by hand option, after many hours of testing, this could represent a disadvantage for the operator. The motorised wheels and remote control represent a good option in terms of effectiveness of moving around a tennis court, however, the implementation and the power specifications, reduced the score of this option. At the end a combination of the human with some rolling wheels incorporated in the final design, make the best solution to solve this function.

Table A - 10 Evaluation of 'Move around a tennis court' function.

Product specifications / Solution	Light weight	Portable size	Simple operation	Powered without connections	Measure shoe-surface friction	Representative of match play	Interchangeable test shoe	No damage to surface tested	Repeatability	Reliability	Total	Rank
1. Lifting by hand	1	5	5	5	-	-	-	4	5	5	30	2
2. Rolling on wheels	5	5	4	5	-	-	-	4	5	5	33	1
3. Motorised wheels and remote control	5	5	4	1	-	-	-	4	5	5	29	3

Table A - 11 presents the evaluation of the 'securing to the ground' function. Although the pins solution was scored with the highest values for lightness and portability compared to the other three options, the main difference was the 'No damage to the surface' specification. After a research, for the pins, it was not found any solution involving no damage to the surface. For this reason, it was considered to utilise the weight of the operator in combination with the weights to apply the vertical force, the best option to secure the device on the surface.

Table A - 11 Evaluation of 'Securing to the ground' function.

Product specifications / Solution	Light weight	Portable size	Simple operation	Powered without connections	Measure shoe-surface friction	Representative of match play	Interchangeable test shoe	No damage to surface tested	Repeatability	Reliability	Total	Rank
1. Pegs	5	5	1	-	-	-	-	1	4	3	**19**	**4**
2. Weights	2	4	5	-	-	-	-	4	3	3	**21**	**2**
3. Human weight	2	3	5	-	-	-	-	4	3	3	**20**	**3**
4. Weights + human weight	3	3	5	-	-	-	-	4	4	4	**23**	**1**

As a summary, Table A - 12, shows with the best scored solutions for each function. These solutions, will be used further in the design process, sections 7.2 and Appendix D, in order to build a robust device. However, during the detailed and parametric design stage, some modifications to the original design components could be implemented, in order to improve the design.

Table A - 12 Summary of the results for the evaluation process

Function	Solution
1. Application of horizontal force	Pneumatic cylinder
2. Application of vertical force	Weights
3. Measurement of reaction force	Load cell
4. Measurement of displacement	Analog position sensor
5. Standard Test shoe	Slider with commercial rubber
6. Calculate static and dynamic friction	Raspberry Pi
7. Move around a tennis court	Rolling on wheels
8. Securing to the ground	Weights + human weight

Appendix D – Current Research-Final prototype design

In order to develop the final prototype, specific improvements and components must be designed and manufactured to improve the accuracy of the device. This section describes the elements and designs for the two main elements of this design: the test rig and the test slider. These were designed based on the product specifications, previously described in detail in the Appendix C.

For this final design stage, a list of new components was selected and incorporated in the new design. These include:

1. *IVAC pneumatic cylinder*

    A light and strong pneumatic cylinder with an integrated solenoid valve, cushion and speed control. By having everything in one unit, space is saved, with less tubing and no need for separate mounting of valves.

2. *Analog positioning sensor*

    A magnetic analog cylinder sensor which gives the linear displacement of the ram. It is mounted straight onto the case of the pneumatic cylinder. It has a sample rate of 1.15 ms.

3. *Castors*

    Two thermoplastic rubber elastomer (TPE) castors with polypropylene wheel centre (low-noise operation with low rolling and swivelling resistance), were included in the design, in order to facilitate the transport of the device around a tennis court.

Additionally, Bosch Rexroth 2016 aluminium extrusion was used in the design of the test device. Figure A - 8 shows the completed Tennis shoe-surface test (TSSTv2) in the folded position with major dimensions shown. The specific features of this configuration are discussed below.
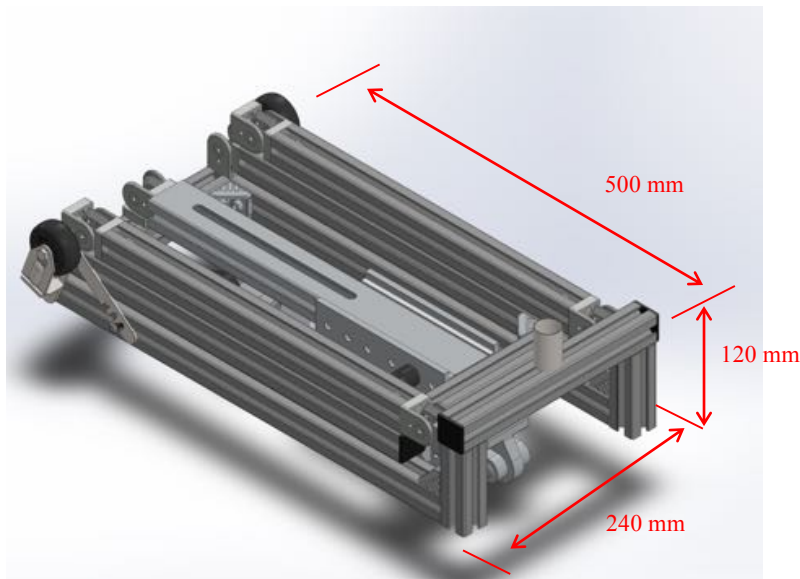
Figure A - 8 Tennis Shoe-Surface Test V2 (TSSTv2) in the folded position.

The size of the TSSTv2 in the folded position is 500 x 240 x 120 mm with a total weight of approximately 10 kg. These dimensions were defined to minimise the space required for transportation. As required by the ITF, the sum of the three dimensions is 860 mm, much less than the 1580 mm as previously specified.

Angled-ram configuration

In order to start the testing, and to move from the folded position to the angled-ram configuration, segment one (*s1*) needs to be lifted and secured at 90° with the horizontal with the "L" supports. Then, segment two (*s2*) is attached to segment one. This procedure is shown in Figure A - 9, and the final assembled TSSTv2 in the angled-ram configuration is presented in Figure A - 10. The dimensions in this configuration are 500 x 240 x 490 mm. To help secure the device on the surface, there is a weight support at the front of the device, in which some weights could be positioned.
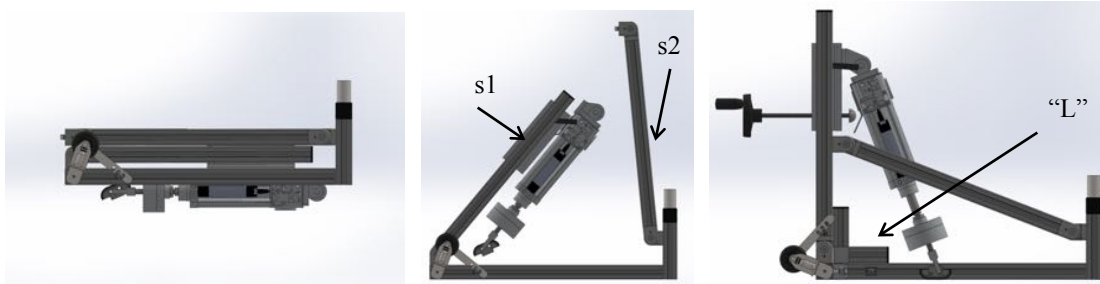

Figure A - 9 Steps to unfold the TSSTv2 for 1st configuration.

As shown in Figure A - 10, one of the main improvements to this configuration design is the carriage in the vertical support, where one of the ends of the pneumatic cylinder is attached. This carriage moves freely in the vertical direction over polypropylene guides helping to reach the necessary test angle. Once the carriage is positioned in the desired position, it is secured by a clamping lever. The second improvement, is the circular indentor attached to the horizontal threaded bar which helps to push the pneumatic cylinder, when the angle is varied through the activation of the hand wheel. The third improvement is a foot plate, which in combination with some weights on the front part of the device, helps to secure it to the ground, by the operator standing on the plate.
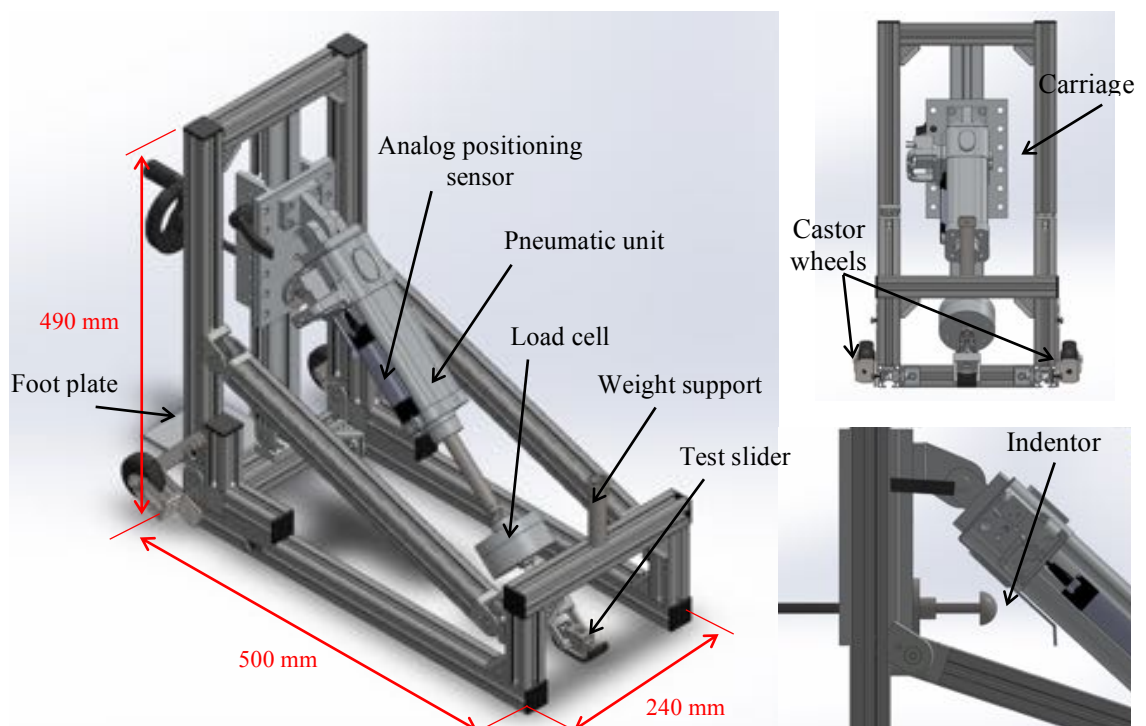

Figure A - 10 The TSSTv2 angled-ram configuration.

Figure A - 11 shows the extreme positions with in this device. In this configuration, the device was designed to be able to reach a range of angles (θ) between 20 – 60° which are equivalent to a range of static coefficient of friction (μ_s) between 0.36 - 1.76.
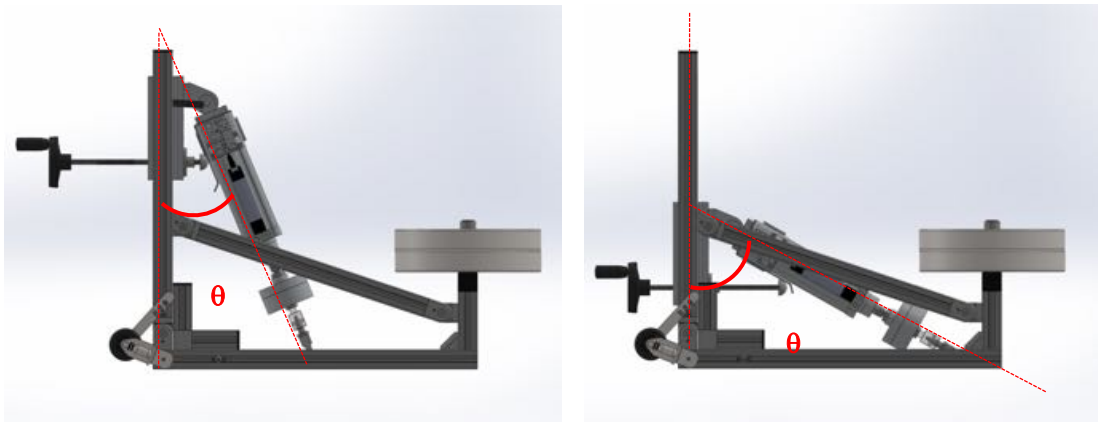
Figure A - 11 The TSSTv2 on a 20° (left) and 60° (right) positions.

As mentioned previously, two wheels were integrated in the final design, which can be activated by tilting the device to the back. Once the wheels are in contact with the surface, the device could be easily moved to a new test position without lifting the entire device. Based on the previous pre-prototype test device, this improvement represents an enormous advantage for the test operator.

Sled configuration

The transition from the angled-ram configuration to the sled one is performed in three steps. These steps are shown in Figure A - 12. The first step consists of removing the handle wheel, threaded bar, foot plate and test indentor from the device. Then, the device is tilted 90°. As the devices rotates, the pneumatic cylinder gets into a flat position, parallel to the test surface. Finally, the third step consists of mounting the test slider on bottom of the sled carriage, and join the sled to the end of the pneumatic ram.
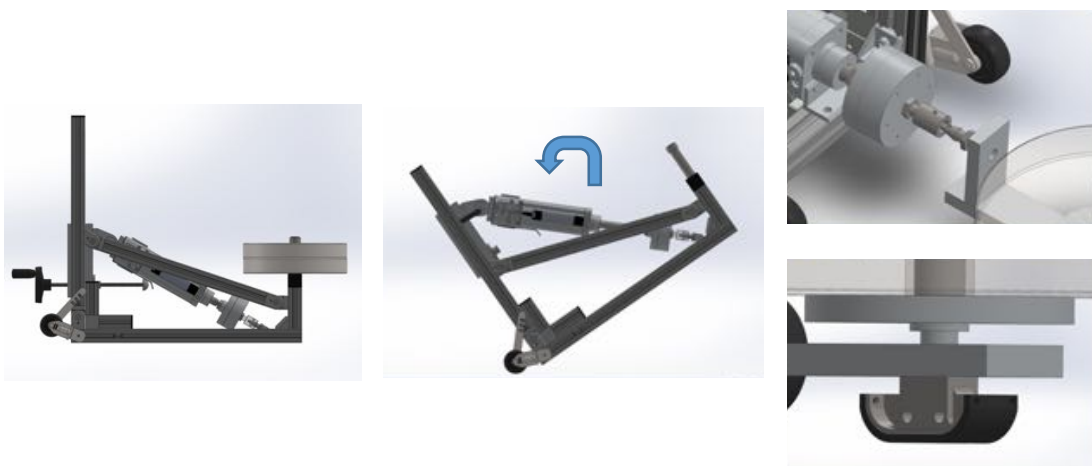

Figure A - 12 Steps to transform from the angled-ram to sled configuration.

Figure A - 13 shows the device in the sled configuration. The dimensions of this configuration are 820 x 24 x 50 mm. The sled with the test slider and weights are equivalent to 200 mm from the total length. A desired number of weights could be attached to the top of the sled in order to match the pressure desired in combination with the test shoe slider.
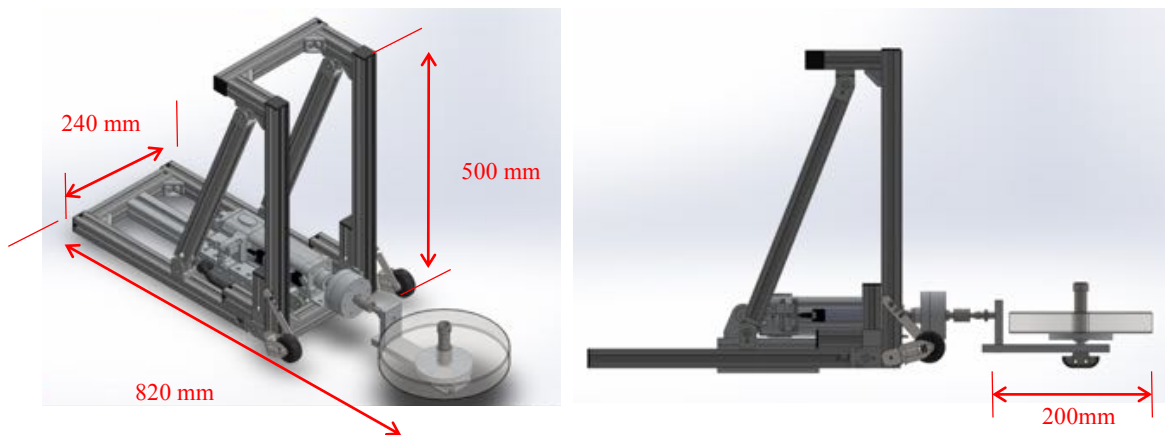

Figure A - 13 The TSSTv2 sled configuration.

Test shoe slider

Based on the preliminary testing conclusions and the problems identified and discussed in the section 7.6.2, a new test shoe slider was designed. The dimensions of the new slider are 51.8 x 25 x 15 mm with a flat area of 625 mm^2 (25 x 25 mm).

To solve the tipping problem in the angled-ram configuration, the joint point between the pneumatic ram and the slider was moved to a position in which the applied force stays on the flat part of the slider, no matter the angle in which the force is applied. The representation of a force applied at the extreme angle positions 20 and 60° is presented in Figure A - 14. Another solution that could be implemented is to punch holes towards the edges of the slider (curve parts). In case the slider tips to the front, then the area ratio could be maintained.

The second improvement implemented is the height of the slider, with new moves positions for the locking screws. In some testing cases previously, represented a problem when the screws came into contact with the test surfaces.
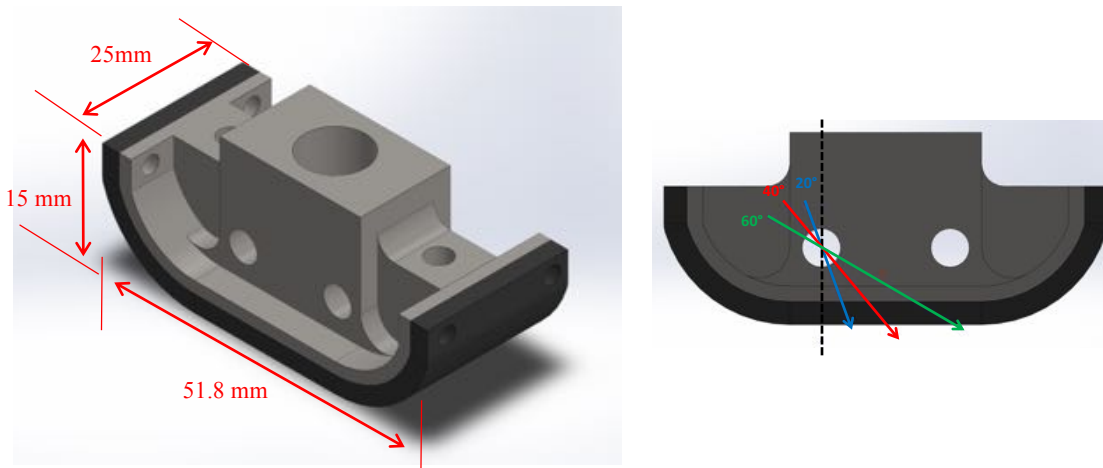
Figure A - 14 Final test shoe device with its dimensions (Left). Direction of force applied on three different angles.

In order to have a more robust test slider and prevent thread jamming problems, the material of the slider was changed from aluminium to stainless steel, which provides a better support for the screws.

TSSTv2 device

As stated in the limitations of this research, section 8.4, at the moment of submission of this thesis, the TSSTv2 assembly stage was still in progress, so it was not evaluated and validated. However, *Figure A - 15* shows some images of the actual TSSTv2 with the new test slider.
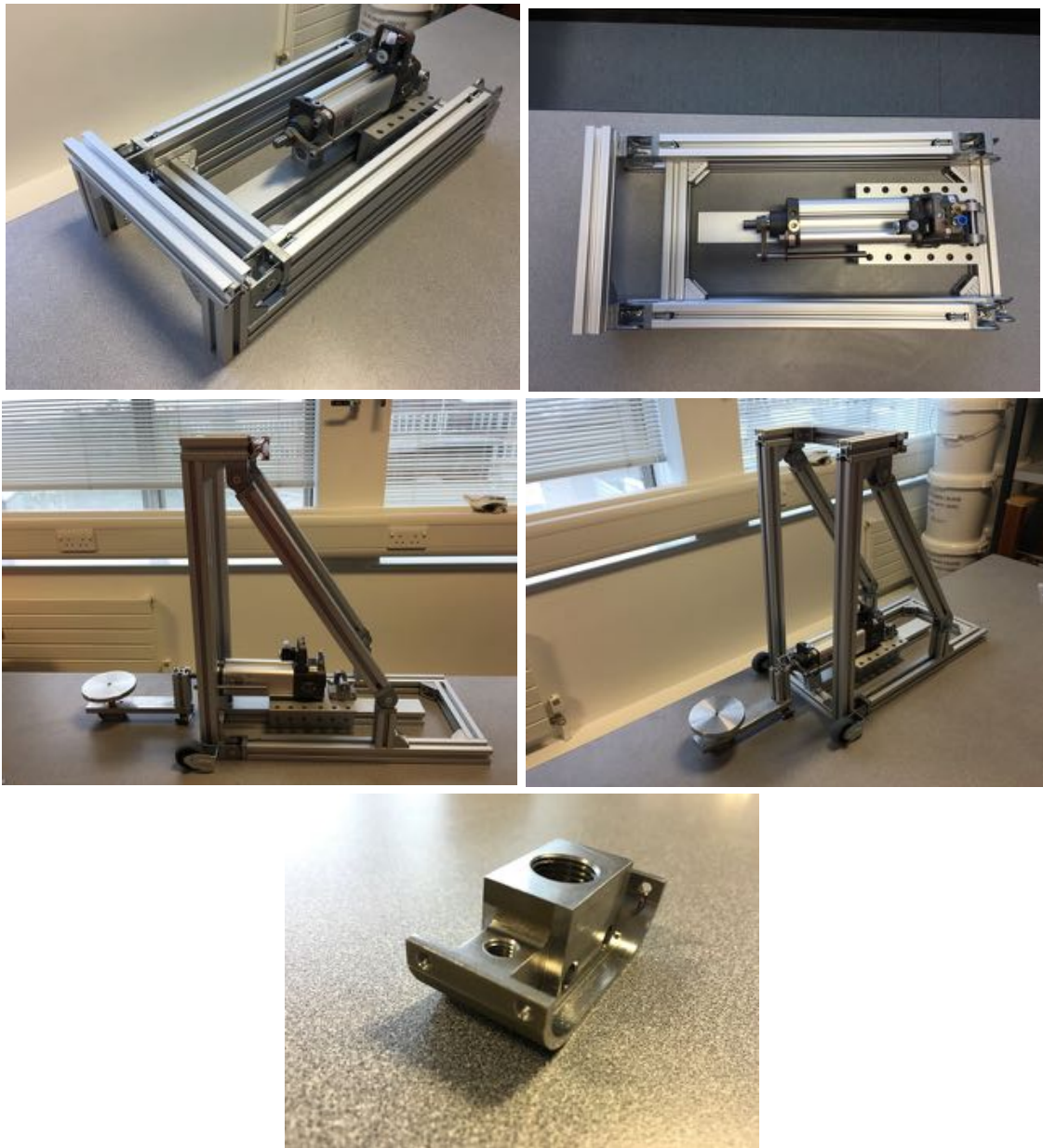
Figure A - 15 TSSTv2 device. Top: folded position; Middle sled position; and Bottom: test slider.